# Polymeric Micelles Loaded with mTHPC for Photodynamic Therapy

from synthesis to *in vitro* and *in vivo* evaluation

**Yanna Liu**

2020

This thesis was (partly) accomplished with financial support from China Scholarship Council.
Printing of this thesis was partially financially supported by Utrecht Institute for Pharmaceutical Sciences (UIPS), Utrecht University, Utrecht, the Netherlands.


Utrecht University

**Polymeric Micelles Loaded with mTHPC for Photodynamic Therapy**
Yanna Liu
Ph.D. thesis, Department of Pharmaceutics, Utrecht Institute for Pharmaceutical Sciences (UIPS), Utrecht University, Utrecht, the Netherlands

Author: Yanna Liu
Layout: ProefschriftMaken || www.proefschriftmaken.nl
Printed by: ProefschriftMaken || www.proefschriftmaken.nl
ISBN: 978-94-6380-794-4

# Polymeric Micelles Loaded with mTHPC for Photodynamic Therapy

from synthesis to *in vitro* and *in vivo* evaluation

# Polymere micellen beladen met mTHPC voor fotodynamische therapie

van synthese tot *in vitro* en *in vivo* evaluatie

(met een samenvatting in het Nederlands)

**Proefschrift**

ter verkrijging van de graad van doctor aan de
Universiteit Utrecht
op gezag van de
rector magnificus, prof.dr. H.R.B.M. Kummeling,
ingevolge het besluit van het college voor promoties
in het openbaar te verdedigen op
maandag 12 oktober 2020 des ochtends te 9.15 uur

door

**Yanna Liu**

geboren op 1 november 1988
te Shandong, China

**Promotor:**
Prof. dr. ir. W.E. Hennink

**Copromotoren:**
Dr. C.F. Van Nostrum
Dr. S. Oliveira

天将降大任于是人也，
必先苦其心志，
劳其筋骨，
饿其体肤，
空乏其身，
行拂乱其所为，
所以动心忍性，
增益其所不能。

——《孟子·告子下》

Whenever heaven invests a person with great responsibilities, it first exercises his mind with suffering, and his muscles and bones with toil. It exposes his body to hunger, and subjects him to extreme poverty. In this way his patience and endurance are developed and his weakness is overcome.

— Mencius

## Contents

# 1

# Chapter 1

## General Introduction

## 1. Photodynamic therapy

Photodynamic therapy (PDT) has been investigated for the last 20 years as a treatment modality for cancers of various types and locations. PDT has been approved by regulatory authorities such as the U.S.A Food and Drug Administration (FDA) and the European Medicine Agency (EMA) for the treatment of head and neck tumors, basal-cell carcinoma, T-cell lymphoma, biliary tract, cervical, endobronchial, esophageal, bladder, and gastric cancers.[1,2] Currently, due to technical advances in interstitial and intra-operative light delivery approaches, clinical trials with PDT are carried out to treat a wide range of solid tumors,[1] such as brain,[3,4] bladder,[5,6] lung,[7-9] pancreas,[10,11] and prostate.[12,13] Besides, PDT has also been exploited for the treatment in many medical disciplines other than oncology among which dermatology, gynecology, urology and cardiology, due to good therapeutic results and the possibility of the parallel application of this treatment modality with other therapeutic protocols.[14,15] For instance, PDT presents a promising alternative for atherosclerosis treatment, where it has been shown to eradicate inflammatory cells and promote plaque stabilization, vascular healing, and debulking of the plaque.[16-18] Compared to conventional treatments such as surgery, radiation and systemic medication, PDT has appealing advantages, including minimal toxicity toward healthy tissues, no long-term systemic toxicity such as immunosuppression, lack of drug resistance mechanisms, and favorable cosmetic outcomes.[19,20]

PDT is based on a photochemical reaction between a light activatable molecule (*i.e.,* photosensitizer, PS), light, and molecular oxygen, which are harmless individually.[1] PDT is a two-stage procedure, which starts with PS administration, followed by a locally directed light exposure.[14,20,21] In this process, the harmless PS is activated by light of the absorbed wavelength, which is locally applied in the pathological tissue by surface illumination or optical fibers.[21] The activated PS subsequently transfers its energy to nearby molecular oxygen, producing oxygen radicals and other reactive oxygen species (ROS). These formed ROS are highly reactive with cellular components such as nucleic acids, proteins and lipids, leading to direct damage to cells and/or vasculature, and/or subsequently inducing inflammatory and immune responses to destroy the obtained abnormal tissue.[21,22]

Photosensitizers (PSs), as the crucial element of PDT, have categorized into different generations based on the time of development and their specific characteristics. A well-known first-generation PS is a water-soluble mixture of porphyrins called hematoporphyrin derivative (HpD). Porfimer sodium (Photofrin®), resulting from partial purification of HpD, was approved for clinical treatment of early- and late-stage lung cancers, esophageal cancer, bladder cancer, malignant and nonmalignant skin diseases and early-stage cervical cancer.[1,23] Although it is still commonly used for cancer PDT, Photofrin® is pharmaceutically a poorly defined product (a mixture

of over 60 molecules [14,23]) with an absorption maximum of 630 nm and a low molar extinction coefficient of 1170 $M^{-1}$ $cm^{-1}$. Its relatively weak absorbance leads to poor tissue penetration. Besides, high Photofrin® dosages are needed for therapeutic effects and its long half-life (~400 h) due to high protein binding after intravenous administration leads to patient skin sensitivity (6–10 weeks after administration).[1,23]

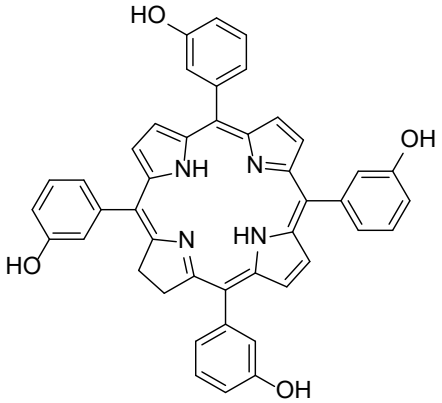


**Generic name: Temoporfin**

**Propietary name: Foscan®, Foslip® and FosPEG®**

**log P: 9.24**

**Absorption for PDT: 652 nm**

**Molar mass: 680.74 g/mol**

**Figure 1.** Chemical structure of meta-tetra(hydroxyphenyl)chlorin (mTHPC, *Left*) and physical data (*Right*).

Taking these limitations into account, a number of second-generation PSs have been developed. In general, the second-generation PSs are characterized by a higher pharmaceutical purity, higher yield of singlet oxygen formation, better penetration of light to deeply located tissues due to their maximum absorption in the wavelength range of 650–800 nm and less skin photosensitization post-treatment. The standard chlorin-based PS, meta-tetra(hydroxyphenyl)chlorin (mTHPC, **Figure 1**), also known by its generic name Temoporfin, is a very potent second-generation PS. Its commercial formulation, Foscan® (solution of mTHPC in ethanol/propylene glycol 40/60 w/w) has been approved by EMA in 2001 for PDT of head and neck squamous cell carcinoma (HNSCC).[24,25] In clinical PDT, mTHPC is applied at both a very low drug dose (0.15 mg/kg) and light intensity (order of 10 $J/cm^2$) resulting in a total PDT dose (light dose × PS dose) >100 times lower when compared to other clinically approved PSs, such as Photofrin®.[2,23] However, like most of the second-generation of PSs, the main drawback of mTHPC is its poor water-solubility due to the high hydrophobicity (logP: ~9 [26]). mTHPC's hydrophobic characteristic promotes non-specific binding to cell membranes, resulting in disposition of PS also in normal healthy tissues (*i.e.,* no selective accumulation of the PS in tumorous tissues), which is responsible for damage to surrounding healthy tissues and the frequently observed and unwanted cutaneous photosensitivity in patients.[22,27-29] Moreover, mTHPC is normally intravenously administrated to the patients as its Foscan® formulation containing 1 mg of mTHPC

in 1 mL of a mixture of ethanol and propylene glycol in order to palliate its high hydrophobic nature.[2] Foscan® should be injected slowly to avoid PS precipitation directly after administration and importantly, even after slow injection, its administration is accompanied with pain.[30] In addition, upon administration, mTHPC is prone to precipitation in biological fluids, leading to lower ROS production, distorting the pharmacokinetics, and causing a decrease of its therapeutic efficacy.[2,31,32] Therefore, the use of nanocarriers such as liposomes and polymeric micelles for delivery of mTHPC provides an opportunity to overcome these mentioned drawbacks.[2]

## 2. Commercially available nanocarriers for delivery of mTHPC used in clinics

Currently, there are two liposomal mTHPC formulations on the market, namely Foslip® and FosPEG®. Foslip® is composed of dipalmitoylphosphatidylcholine (DPPC) and dipalmitoylphosphatidylglycerol (DPPG), while FosPEG® has a similar composition as Foslip® but with the addition of PEGylated lipid (*i.e.,* 1,2-distearoyl-sn-glycero-3-phosphoethanolamine-*N*-[amino (polyethylene glycol)], DSPEG-PEG) on outer surface.[33] The polyethylene glycol (PEG) coating on the surface of the liposomes provides stealth characteristics, avoiding their recognition and rapid uptake by the reticuloendothelial system (RES) and resulting in longer circulation in blood.[29,34-36] Both Foslip® and FosPEG® have hydrodynamic diameters of approximately 110 nm with mTHPC solubilized in their lipid bilayer.[33] Several publications have described some improvements regarding the selective accumulation of mTHPC in tumors compared to Foscan®, due to the enhanced permeability and retention (EPR) effect,[37-39] even though both formulations showed a rapid release of the payload in the first 3 h after injection.[29,33,36] In addition, it is noted that the relatively large hydrodynamic diameters of those liposomes (~110 nm) can cause heterogeneous distribution in the tumor tissues and inability to penetrate the tumor interstitial matrix to reach the interior tumor cells, which can compromise their therapeutic efficacy.[40-44] Therefore, the instability of the liposomal mTHPC formulations in blood and their relatively large sizes leave much room for improvements.

## 3. Polymeric micelles for delivery of mTHPC

As an alternative for liposomes, polymeric micelles are attractive nanocarriers for delivery of mTHPC. Polymeric micelles have been extensively investigated as drug delivery systems for hydrophobic drugs, particularly cytostatic agents. Amphiphilic block polymers self-assemble into polymeric micelles with well-defined core-shell structures in aqueous solutions. The micellar core has a high capacity to accommodate

hydrophobic compounds, including PSs, while the hydrophilic shell, most commonly based on PEG, provides "stealth" properties and thus ensures long circulation time in the blood.[34-36,45] More importantly, polymeric micelles have small hydrodynamic diameters that can be tailored by the composition and molecular weight of the block copolymers that constitute the micelles, as well as by the processing conditions.[46-48] Their small size, generally below 60 nm, is favorable for not only accumulation micellar PS in the tumor through the EPR effect, *i.e.*, so-called passive targeting, but also subsequently penetrating them into the interior of the tumor, being crucial factors for anti-tumoral efficacy of nanomedicines.[40,42,49] In addition, by tailoring the type and characteristics of the micelle-forming block copolymers, polymeric micelles can also be tuned to improve their properties, *e.g., in vivo* stability and PS retention. Also, due to the versatility of polymer chemistry, polymeric micelles can readily be modified to achieve different properties.[50-53] For instance, stimuli-sensitive micelles can be developed, which release their payloads upon a certain physical trigger or by degradation at their site of action.[52,53] Polymeric micelles can also be functionalized with targeting moieties including monoclonal antibodies (mAb), aptamers, antibody fragments, peptides, and/or DNA/RNA fragments.[54] These targeting molecules can specifically bind to receptors overexpressed by tumor cells, leading to enhanced PS internalization and thus improved selectivity and therapeutic response by so-called active targeting.[51,53,55] In the active targeting process, the PS loaded in polymeric micelles is delivered to a specific target tumor site through a molecular recognition process between a receptor overexpressed at the target cell and the matching ligand present on the surface of the micelles.[56]

## 4. Aim and outline of this thesis

As stated above, although mTHPC has improved pharmaceutical characteristics compared to first-generation PSs, some its properties such as low-water solubility, aggregation in biological fluids, limited tumor specificity have to be optimized to fully exploit the therapeutic potential for treatment *e.g.,* cancers. For this purpose, our approach is to load mTHPC in polymeric micelles, which have shown to be attractive drug delivery systems for hydrophobic drugs, particularly cytostatic agents.[57-61] Such PS loaded micelles are suitable for intravenous administration. But importantly, the stability of micelles should be guaranteed to allow the micelles acting as true nanocarriers throughout the body. The aim of this thesis is to develop mTHPC-loaded polymeric micelles and optimize their stability by tailoring the characteristics of the micelle-forming block copolymers. Three strategies were applied to develop stable mTHPC loaded polymeric micelles based on poly(ε-caprolactone)-*b*-poly(ethylene glycol) (PCL-PEG). The exploited strategies included enhanced physical interactions between polymer

chains and/or between polymer and PS molecules by either increasing the chain length of the hydrophobic block or incorporating multiple π-π stacking monomers in PCL-PEG based copolymers. Besides, chemical crosslinking the micellar core by introducing crosslinkable dithiolane units in the PCL-PEG chains was also explored, aiming at preventing the dissociation of micelles and/or slow-down the release in the circulation by creating a covalent network in the micellar core.

In **Chapter 2**, mTHPC was encapsulated in polymeric micelles based on benzyl-poly(ε-caprolactone)-*b*-methoxy-poly(ethylene glycol) (Bz-PCL-PEG) for macrophage selective PDT. We showed that lipoprotein lipase produced in macrophages can provide some selective photo-cytotoxicity as compared to endothelial cells, due to the intracellular enzymatic degradation of the micelles. However, to selectively deliver the micelles to macrophages in the plaques *in vivo*, the micelles should at least be stable and retain their cargo during circulation in the bloodstream. Therefore, we evaluated the *in vitro* stability in blood plasma, the *in vivo* pharmacokinetics and biodistribution of these mTHPC-loaded Bz-PCL-PEG micelles using fluorescence quenching, high performance liquid chromatography and confocal microscopy analysis, respectively.

To demonstrate the proof-of-concept of possible active targeting and the possibility of stabilization of micelles by increased hydrophobic interactions (*i.e.,* the chain length of hydrophobic blocks), in **Chapter 3**, Bz-$PCL_n$-PEG based copolymers with varying chain lengths of $PCL_n$ (n=9, 15, 23) were synthesized. To favor the uptake of the micelles by epidermal growth factor receptor (EGFR) over-expressing cancer cells, mTHPC-loaded micelles, prepared from these copolymers with diameters less than 50 nm, were decorated with EGFR targeted nanobody EGa1. The cellular binding, cellular uptake and photocytotoxicity of these micellar mTHPC formulations were evaluated using EGFR over-expressing A431 cell line and low EGFR expressing HeLa cell line. Finally, the *in vivo* pharmacokinetics of these micellar mTHPC formulations were studied in A431 tumor-bearing mice.

Based on the knowledge and insights described and obtained in **Chapter 2** as well as previous findings of our group,[62,63] in **Chapter 4** we intended to stabilize micelles based on π-π stacking interactions provided by multiple aromatic moieties in the hydrophobic core of PCL-PEG. Thus, the aromatic rings were incorporated along the hydrophobic backbone of the polymer chains by ring-opening polymerization (ROP) of ε-caprolactone (CL) with trimethylene carbonate functionalized by benzyl groups (TMC-Bz), and we compared the behavior of these micelles with those containing a single aromatic unit at the chain end by benzoylation (Bz) of the hydroxyl end groups of PCL-PEG. Therefore, the effect of aromatic π-π stacking interactions on the loading capacity, PS aggregation state and stability of mTHPC loaded micelles were studied. Photocytotoxicity of the micellar PS formulations was evaluated using A431 and HeLa cells by MTS assay. Importantly, the blood circulation kinetics and biodistribution of the micelles as well as the incorporated mTHPC were studied simultaneously and

compared with free mTHPC in A431 tumor-bearing mice.

In **Chapter 5**, we designed micelles that display reversible crosslinking using reduction-sensitive disulfide linkages, to achieve stabilization of micelles in the circulation and triggered PS release by intracellular decrosslinking at the target site. Thus, we introduced pendant dithiolane rings as crosslinkable moieties into PCL-PEG based polymers by ROP of CL with a dithiolane-substituted cyclic carbonate, with or without a flexible diester linker between the dithiolane ring and the cyclic carbonate unit. Three different types of catalysts, *i.e.,* acidic, alkaline or metallic catalysts, were used to investigate the influence of the catalyst on (co)polymerization behaviors of the cyclic ester and carbonate monomers. In addition, comprehensive and detailed exploration of the crosslinking and decrosslinking mechanisms of the dithiolane units were carried out, including potentially influential factors such as monomer sequence, nature of monomer, and reducing agent.

In **Chapter 6**, studies were carried out to evaluate *in vitro* and *in vivo* stability of mTHPC-loaded dithiolane-crosslinked micelles based on poly(ε-caprolactone)-*co*-poly(1,2-dithiolane-carbonate)-*b*-poly(ethylene glycol) (P(CL-*co*-DTC)-PEG) which were explored in **Chapter 5** of this thesis. The *in vitro* release of mTHPC from dithiolane crosslinked P(CL-*co*-DTC)-PEG micelles and the *in vitro* stability of these micelles in human plasma was evaluated by fluorescence spectroscopy and asymmetric flow field-flow fractionation (AF4), respectively, and compared with non (chemically)-crosslinked PCL-PEG based micelles that were explored in **Chapter 3** of this thesis. To validate the *in vitro* findings, the *in vivo* pharmacokinetics including circulation kinetics and tumor accumulation of the crosslinked micelles as well as the loaded mTHPC were studied in A431 tumor-bearing mice and compared with free mTHPC and non (chemically)-crosslinked PCL-PEG based micelles loaded with the same PS.

In **Chapter 7**, the findings of this thesis are summarized, and future research directions and perspectives are discussed.

## References


1. van Straten, D.; Mashayekhi, V.; de Bruijn, H. S.; Oliveira, S.; Robinson, D. J. Oncologic photodynamic therapy: basic principles, current clinical status and future directions. *Cancers* **2017,** *9*, 1-54.
2. Yakavets, I.; Millard, M.; Zorin, V.; Lassalle, H. P.; Bezdetnaya, L. Current state of the nanoscale delivery systems for temoporfin-based photodynamic therapy: Advanced delivery strategies. *J. Control. Release* **2019,** *304*, 268-287.
3. Kostron, H.; Fiegele, T.; Akatuna, E. Combination of FOSCAN® mediated fluorescence guided resection and photodynamic treatment as new therapeutic concept for malignant brain tumors. *Medical Laser Application* **2006,** *21*, 285-290.
4. Muragaki, Y.; Akimoto, J.; Maruyama, T.; Iseki, H.; Ikuta, S.; Nitta, M.; Maebayashi, K.; Saito, T.; Okada, Y.; Kaneko, S.; Matsumura, A.; Kuroiwa, T.; Karasawa, K.; Nakazato, Y.; Kayama, T. Phase II clinical study on intraoperative photodynamic therapy with talaporfin sodium and semiconductor laser in patients with malignant brain tumors Clinical article. *Journal of neurosurgery* **2013,** *119*, 845-852.
5. Bader, M. J.; Stepp, H.; Beyer, W.; Pongratz, T.; Sroka, R.; Kriegmair, M.; Zaak, D.; Welschof, M.; Tilki, D.; Stief, C. G.; Waidelich, R. Photodynamic therapy of bladder cancer – A phase I study using hexaminolevulinate (HAL). *Urologic Oncology: Seminars and Original Investigations* **2013,** *31*, 1178-1183.
6. Lee, J. Y.; Diaz, R. R.; Cho, K. S.; Lim, M. S.; Chung, J. S.; Kim, W. T.; Ham, W. S.; Choi, Y. D. Efficacy and safety of photodynamic therapy for recurrent, high grade nonmuscle invasive bladder cancer refractory or intolerant to bacille calmette-guérin immunotherapy. *The Journal of Urology* **2013,** *190*, 1192-1199.
7. Chen, K.-C.; Hsieh, Y.-S.; Tseng, Y.-F.; Shieh, M.-J.; Chen, J.-S.; Lai, H.-S.; Lee, J.-M. Pleural photodynamic therapy and surgery in lung cancer and thymoma patients with pleural spread. *PLoS One* **2015,** *10*, e0133230.
8. Ji, W.; Yoo, J.-w.; Bae, E. K.; Lee, J. H.; Choi, C.-M. The effect of radachlorin® PDT in advanced NSCLC: A pilot study. *Photodiagnosis and Photodynamic Therapy* **2013,** *10*, 120-126.
9. Kimura, M.; Miyajima, K.; Kojika, M.; Kono, T.; Kato, H. Photodynamic therapy (PDT) with chemotherapy for advanced lung cancer with airway stenosis. *Int J Mol Sci* **2015,** *16*, 25466-25475.
10. Bown, S. G.; Rogowska, A. Z.; Whitelaw, D. E.; Lees, W. R.; Lovat, L. B.; Ripley, P.; Jones, L.; Wyld, P.; Gillams, A.; Hatfield, A. W. R. Photodynamic therapy for cancer of the pancreas. *Gut* **2002,** *50*, 549-557.
11. Huggett, M. T.; Jermyn, M.; Gillams, A.; Illing, R.; Mosse, S.; Novelli, M.; Kent, E.; Bown, S. G.; Hasan, T.; Pogue, B. W.; Pereira, S. P. Phase I/II study of verteporfin photodynamic therapy in locally advanced pancreatic cancer. *British journal of cancer* **2014,** *110*, 1698-1704.
12. Kawczyk-Krupka, A.; Wawrzyniec, K.; Musiol, S. K.; Potempa, M.; Bugaj, A. M.; Sieroń, A. Treatment of localized prostate cancer using WST-09 and WST-11 mediated vascular targeted photodynamic therapy—A review. *Photodiagnosis and Photodynamic Therapy* **2015,** *12*, 567-574.

13. Trachtenberg, J.; Weersink, R. A.; Davidson, S. R. H.; Haider, M. A.; Bogaards, A.; Gertner, M. R.; Evans, A.; Scherz, A.; Savard, J.; Chin, J. L.; Wilson, B. C.; Elhilali, M. Vascular-targeted photodynamic therapy (padoporfin, WST09) for recurrent prostate cancer after failure of external beam radiotherapy: a study of escalating light doses. *BJU International* **2008,** *102*, 556-562.
14. Kwiatkowski, S.; Knap, B.; Przystupski, D.; Saczko, J.; Kedzierska, E.; Knap-Czop, K.; Kotlinska, J.; Michel, O.; Kotowski, K.; Kulbacka, J. Photodynamic therapy - mechanisms, photosensitizers and combinations. *Biomed Pharmacother* **2018,** *106*, 1098-1107.
15. Luo, D.; Carter, K. A.; Miranda, D.; Lovell, J. F. Chemophototherapy: an emerging treatment option for solid tumors. *Adv Sci (Weinh)* **2017,** *4*, 1-24.
16. Drakopoulou, M.; Toutouzas, K.; Michelongona, A.; Tousoulis, D.; Stefanadis, C. Vulnerable plaque and inflammation: potential clinical strategies. *Current pharmaceutical design* **2011,** *17*, 4190-4209.
17. Waksman, R.; McEwan, P. E.; Moore, T. I.; Pakala, R.; Kolodgie, F. D.; Hellinga, D. G.; Seabron, R. C.; Rychnovsky, S. J.; Vasek, J.; Scott, R. W.; Virmani, R. PhotoPoint photodynamic therapy promotes stabilization of atherosclerotic plaques and inhibits plaque progression. *J Am Coll Cardiol* **2008,** *52*, 1024-1032.
18. Jain, M.; Zellweger, M.; Wagnieres, G.; van den Bergh, H.; Cook, S.; Giraud, M. N. Photodynamic therapy for the treatment of atherosclerotic plaque: Lost in translation? *Cardiovasc Ther* **2017,** *35*, 1-14.
19. Naidoo, C.; Kruger, C. A.; Abrahamse, H. Photodynamic therapy for metastatic melanoma treatment: A review. *Technol Cancer Res Treat* **2018,** *17*, 1-15.
20. Dos Santos, A. F.; De Almeida, D. R. Q.; Terra, L. F.; Baptista, M. S.; Labriola, L. Photodynamic therapy in cancer treatment - an update review. *Journal of Cancer Metastasis and Treatment* **2019,** *5*, 1-20.
21. Meulemans, J.; Delaere, P.; Vander Poorten, V. Photodynamic therapy in head and neck cancer: Indications, outcomes, and future prospects. *Curr Opin Otolaryngol Head Neck Surg* **2019,** *27*, 136-141.
22. van Driel, P.; Boonstra, M. C.; Slooter, M. D.; Heukers, R.; Stammes, M. A.; Snoeks, T. J. A.; de Bruijn, H. S.; van Diest, P. J.; Vahrmeijer, A. L.; van Bergen En Henegouwen, P. M. P.; van de Velde, C. J. H.; Lowik, C.; Robinson, D. J.; Oliveira, S. EGFR targeted nanobody-photosensitizer conjugates for photodynamic therapy in a pre-clinical model of head and neck cancer. *J. Control. Release* **2016,** *229*, 93-105.
23. O'Connor, A. E.; Gallagher, W. M.; Byrne, A. T. Porphyrin and nonporphyrin photosensitizers in oncology: preclinical and clinical advances in photodynamic therapy. *Photochemistry and photobiology* **2009,** *85*, 1053-1074.
24. Baskaran, R.; Lee, J.; Yang, S. G. Clinical development of photodynamic agents and therapeutic applications. *Biomater Res* **2018,** *22*, 1-8.
25. Biel, M. A. M. D. Photodynamic therapy of head and neck cancer-what's old and what's new. In handbook of photodynamic therapy: updates on recent applications of porphyrin-based compounds. *World Scientific.* **2016**, pp 439-458.
26. Chen, M.; Liu, X.; Fahr, A. Skin penetration and deposition of carboxyfluorescein and temoporfin from different lipid vesicular systems: In vitro study with finite and infinite dosage application. *International journal of pharmaceutics* **2011,** *408*, 223-234.

27. de Visscher, S. A.; Kascakova, S.; de Bruijn, H. S.; van den Heuvel, A.; Amelink, A.; Sterenborg, H. J.; Robinson, D. J.; Roodenburg, J. L.; Witjes, M. J. Fluorescence localization and kinetics of mTHPC and liposomal formulations of mTHPC in the window-chamber tumor model. *Lasers Surg Med* **2011,** *43*, 528-536.
28. Hopper, C. Photodynamic therapy: a clinical reality in the treatment of cancer. *The Lancet. Oncology* **2000,** *1*, 212-219.
29. Bovis, M. J.; Woodhams, J. H.; Loizidou, M.; Scheglmann, D.; Bown, S. G.; Macrobert, A. J. Improved in vivo delivery of m-THPC via pegylated liposomes for use in photodynamic therapy. *J. Control. Release* **2012,** *157*, 196-205.
30. Senge, M. O.; Brandt, J. C. Temoporfin (Foscan®, 5,10,15,20-tetra(m-hydroxyphenyl)chlorin)--a second-generation photosensitizer. *Photochemistry and photobiology* **2011,** *87*, 1240-1296.
31. Redmond, R. W.; Land, E. J.; Truscott, T. G. Aggregation effects on the photophysical properties of porphyrins in relation to mechanisms involved in photodynamic therapy. *Advances in experimental medicine and biology* **1985,** *193*, 293-302.
32. Triesscheijn, M.; Ruevekamp, M.; Out, R.; Van Berkel, T. J.; Schellens, J.; Baas, P.; Stewart, F. A. The pharmacokinetic behavior of the photosensitizer meso-tetra-hydroxyphenyl-chlorin in mice and men. *Cancer chemotherapy and pharmacology* **2007,** *60*, 113-122.
33. Reshetov, V.; Lassalle, H. P.; Francois, A.; Dumas, D.; Hupont, S.; Grafe, S.; Filipe, V.; Jiskoot, W.; Guillemin, F.; Zorin, V.; Bezdetnaya, L. Photodynamic therapy with conventional and PEGylated liposomal formulations of mTHPC (temoporfin): comparison of treatment efficacy and distribution characteristics in vivo. *Int J Nanomedicine* **2013,** *8*, 3817-3831.
34. Dos Santos, N.; Allen, C.; Doppen, A. M.; Anantha, M.; Cox, K. A.; Gallagher, R. C.; Karlsson, G.; Edwards, K.; Kenner, G.; Samuels, L.; Webb, M. S.; Bally, M. B. Influence of poly(ethylene glycol) grafting density and polymer length on liposomes: relating plasma circulation lifetimes to protein binding. *Biochim Biophys Acta* **2007,** *1768*, 1367-1377.
35. Klibanov, A. L.; Maruyama, K.; Torchilin, V. P.; Huang, L. Amphipathic polyethyleneglycols effectively prolong the circulation time of liposomes. *FEBS letters* **1990,** *268*, 235-237.
36. Torchilin, V. P. Recent advances with liposomes as pharmaceutical carriers. *Nat Rev Drug Discov* **2005,** *4*, 145-160.
37. Maeda, H.; Wu, J.; Sawa, T.; Matsumura, Y.; Hori, K. Tumor vascular permeability and the EPR effect in macromolecular therapeutics: a review. *J. Control. Release* **2000,** *65*, 271-284.
38. Fang, J.; Nakamura, H.; Maeda, H. The EPR effect: Unique features of tumor blood vessels for drug delivery, factors involved, and limitations and augmentation of the effect. *Adv. Drug Deliv. Rev.* **2011,** *63*, 136-151.
39. Maeda, H. Toward a full understanding of the EPR effect in primary and metastatic tumors as well as issues related to its heterogeneity. *Adv. Drug Deliv. Rev.* **2015,** *91*, 3-6.
40. Cabral, H.; Matsumoto, Y.; Mizuno, K.; Chen, Q.; Murakami, M.; Kimura, M.; Terada, Y.; Kano, M. R.; Miyazono, K.; Uesaka, M.; Nishiyama, N.; Kataoka, K. Accumulation of sub-100 nm polymeric micelles in poorly permeable tumours depends on size. *Nat Nanotechnol* **2011,** *6*, 815-823.

41. Danhier, F. To exploit the tumor microenvironment: Since the EPR effect fails in the clinic, what is the future of nanomedicine? *J. Control. Release* **2016,** *244*, 108-121.
42. Jain, R. K.; Stylianopoulos, T. Delivering nanomedicine to solid tumors. *Nat Rev Clin Oncol* **2010,** *7*, 653-664.
43. Jiang, W.; Kim, B. Y.; Rutka, J. T.; Chan, W. C. Nanoparticle-mediated cellular response is size-dependent. *Nat Nanotechnol* **2008,** *3*, 145-150.
44. Yuan, F.; Leunig, M.; Huang, S. K.; Berk, D. A.; Papahadjopoulos, D.; Jain, R. K. Microvascular permeability and interstitial penetration of sterically stabilized (stealth) liposomes in a human tumor xenograft. *Cancer Res* **1994,** *54*, 3352-3356.
45. Tan, C.; Wang, Y.; Fan, W. Exploring polymeric micelles for improved delivery of anticancer agents: recent developments in preclinical studies. *Pharmaceutics* **2013,** *5*, 201-219.
46. Gaucher, G.; Dufresne, M. H.; Sant, V. P.; Kang, N.; Maysinger, D.; Leroux, J. C. Block copolymer micelles: Preparation, characterization and application in drug delivery. *J. Control. Release* **2005,** *109*, 169-188.
47. Park, J. H.; Lee, S.; Kim, J.-H.; Park, K.; Kim, K.; Kwon, I. C. Polymeric nanomedicine for cancer therapy. *Progress in Polymer Science* **2008,** *33*, 113-137.
48. Bagheri, M.; Bresseleers, J.; Varela-Moreira, A.; Sandre, O.; Meeuwissen, S. A.; Schiffelers, R. M.; Metselaar, J. M.; van Nostrum, C. F.; van Hest, J. C. M.; Hennink, W. E. Effect of formulation and processing parameters on the size of mPEG- b-p(HPMA-Bz) polymeric micelles. *Langmuir* **2018,** *34*, 15495-15506.
49. Danhier, F.; Feron, O.; Preat, V. To exploit the tumor microenvironment: Passive and active tumor targeting of nanocarriers for anti-cancer drug delivery. *J. Control. Release* **2010,** *148*, 135-146.
50. Talelli, M.; Iman, M.; Varkouhi, A. K.; Rijcken, C. J.; Schiffelers, R. M.; Etrych, T.; Ulbrich, K.; van Nostrum, C. F.; Lammers, T.; Storm, G.; Hennink, W. E. Core-crosslinked polymeric micelles with controlled release of covalently entrapped doxorubicin. *Biomaterials* **2010,** *31*, 7797-7804.
51. Talelli, M.; Rijcken, C. J.; Oliveira, S.; van der Meel, R.; van Bergen En Henegouwen, P. M.; Lammers, T.; van Nostrum, C. F.; Storm, G.; Hennink, W. E. Nanobody-shell functionalized thermosensitive core-crosslinked polymeric micelles for active drug targeting. *J. Control. Release* **2011,** *151*, 183-192.
52. Lee, E. S.; Kim, J. H.; Sim, T.; Youn, Y. S.; Lee, B.-J.; Oh, Y. T.; Oh, K. T. A feasibility study of a pH sensitive nanomedicine using doxorubicin loaded poly(aspartic acid-graft-imidazole)-block-poly(ethylene glycol) micelles. *Journal of materials chemistry B* **2014,** *2*, 1152-1159.
53. Xin, Y.; Yin, M.; Zhao, L.; Meng, F.; Luo, L. Recent progress on nanoparticle-based drug delivery systems for cancer therapy. *Cancer biology & medicine* **2017,** *14*, 228-241.
54. Yu, B.; Tai, H. C.; Xue, W.; Lee, L. J.; Lee, R. J. Receptor-targeted nanocarriers for therapeutic delivery to cancer. *Molecular membrane biology* **2010,** *27*, 286-298.
55. Nicolas, J.; Mura, S.; Brambilla, D.; Mackiewicz, N.; Couvreur, P. Design, functionalization strategies and biomedical applications of targeted biodegradable/biocompatible polymer-based nanocarriers for drug delivery. *Chemical Society reviews* **2013,** *42*, 1147-1235.

56. Naves, L. B.; Dhand, C.; Venugopal, J. R.; Rajamani, L.; Ramakrishna, S.; Almeida, L. Nanotechnology for the treatment of melanoma skin cancer. *Prog Biomater* **2017,** *6*, 13-26.
57. Deng, C.; Jiang, Y.; Cheng, R.; Meng, F.; Zhong, Z. Biodegradable polymeric micelles for targeted and controlled anticancer drug delivery: Promises, progress and prospects. *Nano Today* **2012,** *7*, 467-480.
58. Varela-Moreira, A.; Shi, Y.; Fens, M. H. A. M.; Lammers, T.; Hennink, W. E.; Schiffelers, R. M. Clinical application of polymeric micelles for the treatment of cancer. *Materials Chemistry Frontiers* **2017,** *1*, 1485-1501.
59. Cabral, H.; Kataoka, K. Progress of drug-loaded polymeric micelles into clinical studies. *J. Control. Release* **2014,** *190*, 465-476.
60. Houdaihed, L.; Evans, J. C.; Allen, C. Overcoming the road blocks: advancement of block copolymer micelles for cancer therapy in the clinic. *Mol. Pharmaceutics* **2017,** *14*, 2503-2517.
61. Hofman, J. W.; Carstens, M. G.; van Zeeland, F.; Helwig, C.; Flesch, F. M.; Hennink, W. E.; van Nostrum, C. F. Photocytotoxicity of mTHPC (temoporfin) loaded polymeric micelles mediated by lipase catalyzed degradation. *Pharm Res* **2008,** *25*, 2065-2073.
62. Shi, Y.; van der Meel, R.; Theek, B.; Oude Blenke, E.; Pieters, E. H.; Fens, M. H.; Ehling, J.; Schiffelers, R. M.; Storm, G.; van Nostrum, C. F.; Lammers, T.; Hennink, W. E. Complete regression of xenograft tumors upon targeted delivery of paclitaxel via π-π stacking stabilized polymeric micelles. *ACS Nano* **2015,** *9*, 3740-3752.
63. Shi, Y.; van Steenbergen, M. J.; Teunissen, E. A.; Novo, L.; Gradmann, S.; Baldus, M.; van Nostrum, C. F.; Hennink, W. E. π-π stacking increases the stability and loading capacity of thermosensitive polymeric micelles for chemotherapeutic drugs. *Biomacromolecules* **2013,** *14*, 1826-1837.

# 2

# Chapter 2

## Macrophage Selective Photodynamic Therapy by Meta-Tetra(hydroxyphenyl) chlorin Loaded Polymeric Micelles: a Possible Treatment for Cardiovascular Diseases

Jos W.H. Wennink [1,#], Yanna Liu [1,#], Petri I. Mäkinen [2], Francesca Setaro [3], Andrès de la Escosura [3], Meriem Bourajjaj [1], Jari P. Lappalainen [2], Lari P. Holappa [2], Joep B. van den Dikkenberg [1], Mina al Fartousi [1], Panagiotis N. Trohopoulos [4], Seppo Yla-Herttuala [2], Tomas Torres [3], Wim E. Hennink [1], Cornelus F. van Nostrum [1,*]

[1] Department of Pharmaceutics, Utrecht Institute for Pharmaceutical Sciences (UIPS), Utrecht University, Universiteitsweg 99, 3508 TB Utrecht, Netherlands.
[2] Department of Biotechnology and Molecular Medicine, A.I. Virtanen Institute for Molecular Sciences, University of Eastern Finland, Neulaniementie 2, Kuopio FIN-70211, Finland
[3] Departamento de Química Orgánica (C-I), Universidad Autónoma de Madrid/IMDEA Nanociencia (TT), Cantoblanco 28049, Madrid, Spain
[4] CosmoPHOS Ltd, 77 Tsimiski str. , GR – 54622, Thessaloniki , Greece
[#] Both authors contributed equally to this paper

*European Journal of Pharmaceutical Sciences 2017, 107, 112–125*

**Abstract**

Selective elimination of macrophages by photodynamic therapy (PDT) is a new and promising therapeutic modality for the reduction of atherosclerotic plaques. m-Tetra(hydroxyphenyl) chlorin (mTHPC, or Temoporfin) may be suitable as photosensitizer for this application, as it is currently used in the clinic for cancer PDT. In the present study, mTHPC was encapsulated in polymeric micelles based on benzyl-poly(ε-caprolactone)-*b*-methoxy poly(ethyleneglycol) (Ben-PCL-mPEG) using a film hydration method, with loading capacity of 17%. Because of higher lipase activity in RAW264.7 macrophages than in C166 endothelial cells, the former cells degraded the polymers faster, resulting in faster photosensitizer release and higher *in vitro* photocytotoxicity of mTHPC-loaded micelles in those macrophages. However, we observed release of mTHPC from the micelles in 30 min in blood plasma *in vitro* which explains the observed similar *in vivo* pharmacokinetics of the mTHPC micellar formulation and free mTHPC. Therefore, we could not translate the beneficial macrophage selectivity from *in vitro* to *in vivo*. Nevertheless, we observed accumulation of mTHPC in atherosclerotic lesions of mice aorta which is probably the result of binding to lipoproteins upon release from the micelles. Therefore, future experiments will be dedicated to increase the stability and thus allow accumulation of intact mTHPC-loaded Ben-PCL-mPEG micelles to macrophages of atherosclerotic lesions.

**Keywords**: polymer micelles; photodynamic therapy; atherosclerosis; drug targeting; drug release

## 1. Introduction

At present the world population encounters increase in age, obesity and lack of physical activity.[1] This can give imbalance in the human physiology leading to among others high blood pressure, diabetes and unhealthy cholesterol levels, which eventually cause cardiovascular diseases being the number one cause of death in the western world. The prevalent contributor to cardiovascular morbidity is atherosclerosis, a chronic inflammation with slow progressive buildup of lipids and macrophages within the arterial wall.[2] Lipid build up can start in the early thirties of a human's life and cause signs and symptoms 20 years later. Atherosclerosis is the main cause of myocardial infarctions and atherosclerotic plaque rupture.

When atherosclerosis is detected in an early phase, administration of hypolipidemic agents has mostly been applied as a therapy for the last two decades.[3] More recently, novel therapeutic strategies involving treating vessel wall inflammation have emerged. [4] However, after administration of anti-inflammatory drugs, there is a chance on the occurrence of side effects, primarily systemic immunosuppression and other off-target effects.[5] When atherosclerosis is detected in a later phase it is mainly due to myocardial infarctions. In this stage the options are more rigorous and are mainly focused on opening the vessel by balloon angioplasty [6] with or without stenting [7] and in the most severe cases a bypass vessel [8] will be installed. Currently much research is directed to repairing affected vessels by tissue engineered vessels that lack the drawbacks (unfavorable compliance and high stiffness) of current bypass vessels.[9,10] Until now none of these methods are actually treating or removing the inflammation and reoccurrence of myocardial infarctions in atherosclerotic patients is high.[11,12]

A new and promising combination therapy for the treatment of atherosclerotic plaques is photodynamic therapy (PDT).[13] A pivotal component of PDT in promoting plaque stabilization is sustained macrophage removal. Waksman et al. showed that PDT can reduce plaque formation and promotes smooth muscle cell repopulation if the macrophages are properly targeted.[14] PDT is based on three interacting elements: 1) a non-aggregated photosensitizer (PS); 2) light of appropriate wavelength to activate the PS and 3) tissue oxygen.[15] When the PS is activated by light to the excited state and returns to the ground state, it releases energy, which is transferred to the surrounding tissue oxygen to generate singlet oxygen which in turn causes cell death.[16] However, aggregation of PS molecules must be prevented, since the quantum yield of PS emission is highly dependent on its aggregation state.[17] Selective exposure of the plaque regions by light can be accomplished using an intra-arterial light emitting catheter.[18] However, illumination of endothelial cell lining of the arteries that have possibly taken up PS can lead to atherosclerotic plaque rupture,[19] which should by all means be avoided. Therefore, selectively targeting the neo-vessels inside the plaques and/or the macrophages located in the plaques is highly desired. Importantly, most effective PS

have low water solubility, therefore a simple intravenous injection is complicated and a safe solubilizing excipient or carrier system is necessary.
If one aims for PDT to become the future treatment of atherosclerosis, the problems stated above have to be overcome.[20] A method to circumvent these problems is by encapsulating the hydrophobic PS in nanoparticles. Besides enabling intravenous injection, nanoparticles are also known for enhancing therapeutic efficacy and safety of encapsulated drugs by improving solubility, ability of combining multiple drugs, protecting against metabolism, and controlling release.[20,21] Furthermore, the formation of leaky vessels from the vasa vasorum in atherosclerotic plaques allows for accumulation of nanoparticles by the enhanced permeability and retention (EPR) effect inside the plaque and avoids uptake by the endothelium layer.[22] Current research in atherosclerosis and nanoparticles primarily focuses on the targeted delivery of anti-inflammatory drugs,[23-25] however such drugs usually only delay progression of atherosclerosis [26] thereby becoming a reoccurring medication during the lifetime of patients. In the present study, we therefore combine the advantages of PDT and nanomedicine to develop a curative treatment for atherosclerosis.
Meta-tetra(hydroxyphenyl)chlorine (mTHPC) is a photosensitizer currently used in the PDT treatment of squamous-cell carcinoma [27] and available in a variety of commercial and EMA approved formulations including liposomes (Foscan®, FosLip®, FosPEG®). Previous research in our group showed that benzyl-functionalized micelles based on poly(ε-caprolactone)-*b*-methoxy poly(ethylene glycol) (Ben-PCL-mPEG) block copolymers can encapsulate mTHPC with very high loadings and remarkable stability.[28-30] Most interestingly, it was shown that the release and subsequent photocytotoxic activity of mTHPC are controlled by lipase induced enzymatic degradation of the micelles.[30] This can be advantageous since it is known that macrophages present in the plaque synthesize lipoprotein lipase (LPL),[31] and therefore we hypothesized that it could thus potentially promote local release and activation of the photosensitizer once the loaded micelles are delivered to and internalized by the macrophages.
In this paper, mTHPC-loaded micelles were conveniently prepared by a film hydration method. We investigated if the LPL produced in macrophages can provide some cell specificity as compared to endothelial cells due to the enzymatic degradation of the micelles. The small size of the micelles might be advantageous for plaque penetration by the EPR effect. However, to selectively deliver the micelles to macrophages in the plaques, the micelles should at least be stable and retain their cargo during circulation. Therefore, we evaluated the *in vitro* stability in blood plasma and the *in vivo* pharmacokinetics of the mTHPC-loaded Ben-PCL-mPEG micelles.

## 2. Materials and Methods

### *2.1. Materials*

Acetonitrile, dimethyl sulfoxide (DMSO), trifluoroacetic acid, hydrogen peroxide, fetal bovine serum (FBS), trypsin, EDTA, PBS, ethanol, propylene glycol and high glucose Dubecco modified eagle medium (DMEM) were obtained from Sigma-Aldrich (Zwijndrecht, the Netherlands). 384-Well plates were purchased from Fisher scientific GmbH (German). Optimem phenol red free was purchased at Invitrogen (Bleiswijk, the Netherlands). CellTiter 96® $AQ_{ueous}$ One Solution was obtained from Promega (Leiden, the Netherlands). Human plasma and mice plasma were purchased from Seralab (UK) and mTHPC was purchased from Molekula (Germany). Foslip® (mTHPC liposomal formulation) and Foscan® (mTHPC in ethanol: propylene glycol 40/60 w/w) was kindly provided by Biolitec AG (Jena, Germany). Foslip® is composed of Phospholipids, glucose, and mTHPC with a dye: lipid ratio of ca. 1:13. Foslip® was reconstituted from lyophilized powder in distilled water. Foscan diluent is referred to a mixture of ethanol: propylene glycol (40/60 w/w).

### *2.2. Micelle formation*

Micelles with and without mTHPC loading were formed by the film hydration method. [28] In short, 10 mg of Ben–PCL-mPEG block copolymer was dissolved in 1 mL of dichloromethane. Next, 5 mg of mTHPC was dissolved in 1 mL THF and different amounts corresponding to the desired polymer/photosensitizer ratios were mixed with the dichloromethane block copolymer solution. After evaporation of dichloromethane and THF in a vacuum oven, a thin solid film was formed. The formed film contained both block copolymers and photosensitizer that was visually distributed in a homogeneous way. The block copolymer (+ photosensitizer) film was subsequently hydrated in 1 mL PBS solution by gentle shaking and after 1 hour subsequently filtered through a 0.2 μm syringe filter to remove non-encapsulated and thus precipitated photosensitizer. This procedure results in empty micelles or photosensitizer loaded micellar dispersions of 10 mg/mL Ben-$PCL_n$-$mPEG_{45}$. Size of micelles (by DLS) and critical micelle concentration were determined as described in Supplementary Material.

### *2.3. Loading efficiency and capacity of micelles*

The concentration of mTHPC in micellar dispersions was determined by UV/Vis spectroscopy. The dispersions were diluted in DMF to dissolve the micelles. A spectrum between 300 and 800 nm was recorded by a Shimadzu UV-2450 spectrophotometer (Shimadzu, Japan). The absorbance at 650 nm was analyzed against a calibration curve of mTHPC in DMF, which was linear between 0.1 and 6 μg/mL. The loading efficiency and loading capacity were calculated by equations 1 and 2, respectively.

$$LE\ (\%) = \frac{mTHPC\ loaded\ (mg)}{mTHPC\ fed\ (mg)} x100\% \quad (1)$$

$$LC\ (\%) = \frac{mTHPC\ loaded\ (mg)}{polymer\ \ used\ (mg) + mTHPC\ loaded\ (mg)} x100\% \quad (2)$$

### *2.4. Aggregation state of mTHPC*

Absorption spectra were measured to determine the aggregation state of the mTHPC in the polymeric micelles. mTHPC loaded micelles were 20 fold diluted in PBS and analyzed with UV/Vis spectrophotometry (Shimadzu UV-2450 spectrophotometer) from 300 to 800 nm. The recorded samples were compared to free mTHPC dissolved in DMF. If the mTHPC aggregates, the 650 nm peak shows a distinctive red or blue shift.

### *2.5. Singlet oxygen production of mTHPC loaded micelles*

$^1O_2$ quantum yields ($\phi_\Delta$) were measured in DMSO (for the non-encapsulated mTHPC) and $D_2O$ (for the mTHPC-loaded micelles), following the *relative method*, based on the photoinduced decomposition of a chemical (*i.e.*, 1,3-diphenylisobenzofuran (DPBF) in DMSO, and α,α'-(anthracene-9,10-diyl)bimethylmalonate (ADMA) in $D_2O$) that reacts readily with $^1O_2$.[32,33] Non-substituted ZnPc ($\phi_{\Delta\ (DMSO)}$ = 0.67) [34] and eosin Y ($\phi_{\Delta\ (D2O)}$ = 0.60) [35] were used as the respective reference compounds.

A stock solution of scavenger (DPBF in DMSO or ADMA in $D_2O$, volume was 2.5 mL with an absorbance of ca. 1) was transferred into a 1 x 1 cm quartz optical cell and flushed with oxygen for 1 min. A concentrated stock solution of the mTHPC (non-encapsulated or loaded in micelles) in the corresponding solvent was then added in a defined amount to reach a final Q-band absorbance value of about 0.1 (λ=650 nm). The solution was stirred and irradiated for defined time intervals, using a halogen lamp (typically, 300 W). The duration of these intervals is tuned in each experiment, in order to get a decrease in scavenger absorption of about 3-4% per irradiation interval. Incident light was filtered through a water filter (6 cm) and an additional filter to remove light under 455 nm (Newport filter 20CGA-455). The decrease of scavenger concentration with irradiation time was monitored at 414 and 379 nm, respectively. For quantum yield determination, the experiment was performed three times and the obtained data represent mean values of those three experiments. The estimated error is ± 10%. Singlet oxygen quantum yield ($\phi_\Delta$) was calculated using the following equation:

$$\phi_\Delta^S = \phi_\Delta^R \frac{k^S I_{aT}^R}{k^R I_{aT}^S}$$

Where $k$ is the slope of a plot of ln ($A_0/A_t$) *versus* irradiation time t, with $A_0$ and $A_t$ being the absorbance of scavenger at the monitoring wavelength before and after irradiation time t, respectively. $I_{aT}$ is the total amount of light absorbed by the dye. Superscripts $R$

and *S* indicate reference and sample, respectively. $I_{aT}$ is calculated as a sum of intensities of the absorbed light $I_a$ at wavelengths from the filter cutoff to 800 nm (step 0.5 nm). $I_a$ at given wavelength is calculated using Beer's law:

$$I_a = I_0(1 - e^{-2.3A})$$

Where transmittance of the filter at a given wavelength stays for $I_0$ and the absorbance of the dye at this wavelength stays for *A*.

### *2.6. Cell culture*

#### *2.6.1. RAW264.7 macrophages*

Vials of RAW264.7 macrophages (passage 4) were thawed and taken into culture in a T75 flask. The cells were harvested by washing with 12 mL PBS. After washing, 2 mL of PBS was added and a cell scraper was used to detach RAW264.7 macrophages from the T75 flask. Next, 4 mL high glucose (4500 mg/L) DMEM medium containing 10% FBS was added and the cell suspensions were transferred into a sterile 12 mL tube and centrifuged at 200 relative centrifugal force (rcf) for 3 minutes at 4 °C. The supernatant was discarded and the cells were suspended in 1 mL of the same medium by repeatedly pipetting using a 200 µL pipette to remove cell lumps. Subsequently, 9 mL of the same medium was added to yield a final volume of 10 mL. Accordingly, the cell density and viability were determined by counting the cells with a Burker Turk cell counter after staining with trypan blue.

#### *2.6.2. C166 endothelial cells*

Vials of C166 endothelial cells (passage 27) were thawed and taken into culture in a T75 flask. The cells were harvested by washing with 12 mL PBS followed by detaching the cells from the flask with 2 mL of 0.25% (w/v) trypsin / 0.53 mM EDTA solution. Next, 4 mL high glucose DMEM medium containing 10% FBS was added and the cell suspensions were transferred into a sterile 12 mL tube and centrifuged at 200 rcf for 3 minutes at 4 °C. The supernatant was discarded and the cells were resuspended in 10 mL of the same medium. Finally, the cell density and viability were determined by counting the cells with a Burker Turk cell counter after staining with trypan blue.

#### *2.6.3. Dark toxicity and photocytotoxicity*

Cell viability was determined with a CellTiter 96® $AQ_{ueous}$ One Solution (Promega) containing 3-(4,5-dimethylthiazol-2-yl)-5-(3-carboxymethoxyphenyl)-2-(4-sulfophenyl)-2*H*-tetrazolium (MTS). The MTS is converted by enzymes present in the mitochondria of the living cells to form formazan. The quantity of formazan produced is proportional to the amount of living cells and is detected by measuring absorbance at 490 nm.

In short, 10,000 cells/well murine RAW264.7 macrophages or 4,000 cells/well murine endothelial C166 cells were seeded into 96 well plates and incubated overnight in 100 µL

high glucose DMEM medium containing 10% FBS per well. After overnight incubation at 37 °C and 5% $CO_2$, the medium was aspirated and replaced by 50 µL high glucose DMEM medium containing 10% FBS and 50 µL mTHPC micelles formulations in PBS. The incubation time for the uptake of the mTHPC micelles was varied between 1 and 24 hours. For dark toxicity, the cells loaded in the wells were kept in the dark for 24 hours. For photocytotoxicity experiments, after the chosen incubation time, the cells were illuminated for 10 minutes with 3.5 mW/cm$^2$ light intensity, using a homemade device consisting of 96 LED lamps (670±10 nm, 1 LED per well).
To give time for the dead cells to detach from the surface of the wells, the illuminated plate was placed in an incubator for 1 hour at 37 °C and 5% $CO_2$. Next, the medium was aspirated and to each well 100 µL high glucose DMEM medium containing 10% FBS and 20 µL of CellTiter 96® $AQ_{ueous}$ One Solution was added. Subsequently, the well plate was incubated for 4 hours at 37 °C and 5% $CO_2$ and the absorbance at 490 nm was measured with a 96 well plate reader (Biochrom EZ Read 400 Microplate reader, Biochrom, U.K.).

### *2.7. Colorimetric lipase activity assay*

RAW264.7 macrophages or endothelial C166 cells (both 4,000 cells/well) were seeded into 96 well plates and incubated overnight in 100 µL high glucose DMEM medium containing 10% FBS for each well at 37 °C and 5% $CO_2$. The medium was aspirated and the protocol according to the colorimetric lipase activity assay kit II from Sigma-Aldrich was used to determine the lipase activity. Hundred µL of Master mix (Sigma Aldrich, 85 µL lipase assay buffer, 10 µL DTNB and 5 µL lipase substrate) were added to the wells. Subsequently, the plate was placed in a well plate reader (SPECTROstar$^{nano}$, BMG labtech, Germany) at 37 °C and the absorbance was measured at 412 nm ($A_{412, initial}$). Subsequently, every 2 minutes the absorbance was measured for 30 minutes or until the values exceeded the TNB calibration curve ($A_{412, final}$). The change in absorbance was calculated by subtracting $A_{412, initial}$ from $A_{412, final}$ and the resulting $\Delta A_{412}$ was compared with the absorbance of the TNB calibration curve to determine the amount of TNB produced. The formed amount TNB is proportional to the amount of enzyme present. One unit of lipase is the amount of enzyme that generates 1.0 µmole of TNB per minute at 37 °C. From this, the lipase activity was calculated in milliunits/mL (abbreviated as mU/mL).

### *2.8. Fluorescence microscopy*

RAW264.7 macrophages or C166 endothelial cells were seeded in uncoated six channel µ-Slides (µ-slide IV 0.4 ibitreat, Ibidi, Germany) with 20,000 or 8,000 cells per channel, respectively. The slides were incubated for 1 hour at 37 °C and 5% $CO_2$ and the medium was refreshed with high glucose DMEM medium containing 10% FBS. After overnight incubation at 37 °C and 5% $CO_2$, the medium was refreshed again and replaced with the same medium and the mTHPC formulation (500 µg/mL Ben-$PCL_7$-$mPEG_{45}$ and 4 µg/mL mTHPC). After incubation times of 1, 2, 4, 8 and 24 hours, the slides were

washed with PBS. After washing, 150 µL Optimem Phenol red free was added to the cells. The slides were imaged with a Deltavision Elite Microscope equipped with an incubation chamber set at 37 °C and a mCherry filter. The exposure time was 600 ms.

### *2.9. In vitro stability of micelles in serum and blood plasma*

The *in vitro* stability of mTHPC-loaded micelles based on Ben-$PCL_7$-$mPEG_{45}$ and containing different mTHPC loadings was studied in FBS, mouse plasma and human plasma dilutions with various concentrations of plasma proteins at 37 °C, by monitoring the change of fluorescence intensity of mTHPC using a Jasco FP8300 spectrofluorimeter (Japan). Foslip® (a liposomal formulation of mTHPC) and Foscan® (free mTHPC) were used as reference.

Foscan® with different concentrations of mTHPC was prepared by adding certain amounts of Foscan diluent (ethanol: propylene glycol, 40/60 w/w) to a stock solution of 3 mg/mL Foscan®. mTHPC loaded micelles with different photosensitizer loadings (0.1% to 20% w/w) were prepared in PBS as described in section 2.2 (polymer concentration was fixed at 10 mg/mL). Foslip® solutions were prepared at different mTHPC concentrations by preparing a 3 mg/mL stock solution in PBS and diluting this with PBS. FBS, human or mouse plasma were diluted in different amounts of PBS to get 10, 50 and 90% serum or plasma solutions. mTHPC samples were added to the different serum/plasma solutions with the ratio of 1:9 (v/v). As controls, samples were mixed with PBS (1:9 v/v). After incubation at 37 °C, samples were taken at different time points (5, 15, 35 min, and 1, 1.5, 2, 3, 4, 6, 8 h) and added in a 384-Well plate. After taking the samples, the fluorescence intensity was recorded using a Jasco FP8300 spectrofluorimeter at 655 nm after excitation at 420 nm. All fluorescence measurements were carried out in duplicate.

### *2.10. In vivo studies*

#### *2.10.1. Pharmacokinetics in healthy mice*

All animal experiments were approved by local and national regulatory authorities and by an animal ethics welfare committee. All procedures involving animals were performed under general anesthesia with inhaled isoflurane using a Univentor 400 anesthesia unit (Genestil, Royaucourt, France), with every effort made to minimize suffering.

For *in vivo* pharmacokinetic study, female Balb/c nude mice of 6–8 weeks age, weighing 16-22 g were purchased from Envigo. Mice were housed in ventilated cages at 25 °C and 55% humidity under natural light/dark conditions and allowed free access to standard food and water. Mice were divided into two groups (n = 3 per group), which were intravenously injected via the tail vein with 100 µL mTHPC loaded micelles in PBS at 5% (w/w) loading (high mTHPC dose) and 0.6% (w/w) loading (low mTHPC dose), respectively (solutions containing 1 mg Ben-$PCL_7$-$mPEG_{45}$ and 50 µg mTHPC for the high dose group or 6 µg mTHPC in PBS for the low dose group). About 50 µL of

blood samples were taken and collected in heparinized tubes at different time points post injection via cheek puncture. Each collected blood sample was centrifuged for 15 min at 1000 ×g at 4 °C. Afterwards, the clear supernatant was collected and vortex-mixed with acetonitrile: DMSO (4:1 v/v) for 1 min. The mixture was centrifuged at 15,000 ×g for 10 min and the clear supernatant was analyzed by high performance liquid chromatography (HPLC). The HPLC system consisted of a Waters X Select CSH C18 3.5 μm 4.6 x 150 mm column with 0.1 % trifluoroacetic acid in acetonitrile (60:40, v/v) as a mobile phase, using a flow rate of 1 mL/min. The injection volume was 20 μL and mTHPC was detected by a UV-Vis detector set at 423 nm at a retention time of about 3 min. The measuring range was from 0.05 μg/mL to 25 μg/mL and the detection limit was about 10 ng/mL. A calibration curve was obtained from a series of standard solutions of mTHPC in Foscan diluent to which 60 μL of Balb/c mice plasma was added. Acetonitrile: DMSO (4:1 v/v) was used to extract mTHPC and the collected supernatant was analyzed by HPLC as described above.
Data are presented as the percentage injected mTHPC dose in blood (%ID) over time. On average, Balb/c nude mice have around 58.5 mL of blood per kg of bodyweight. Therefore, the total blood volume (1-1.5 mL) of each individual mouse was calculated by multiplying its bodyweight by 58.5 mL/kg.

### *2.10.2. Biodistribution in atherosclerotic mice*

$LDLR^{-/-}ApoB^{100/100}$ mice were kept on high cholesterol diet (42% of calories from fat and 0.15% from cholesterol, no sodium cholate; TD 88173 Harlan Teklad, Boxmeer, NL) for 5 months to develop atherosclerotic lesions. Food and water were provided *ad libitum* during the entire study. All animal experiments were approved by National Experimental Animal Board of Finland and carried out in accordance with guidelines of the Finnish Act on Animal Experimentation. For the micelle injections, mice were anaesthetized with isoflurane (induction: 4.5% isoflurane, 450 mL air, maintenance: 2.0% isoflurane, 200 mL air; Baxter International, Helsinki, Finland). Hundred μL of each solution was injected into the tail vein. After 4 hours, mice were sacrificed using carbon dioxide anesthesia, perfused with PBS and 1% PFA solution, and aortas and other organs were collected for microscopy analysis. The fluorescence was analyzed from longitudinal sections from aortas or cryo-sections from other tissues with LSM 700 confocal microscope (Carl Zeiss, Jena, Germany).

## 3. Results

### *3.1. Micelle preparation*

The synthesis and characterization of poly(ε-caprolactone)-*b*-methoxypoly(ethyleneglycol) block copolymers are described in Supplementary

Material. Micelles were conveniently prepared by hydration of a solid polymer film in phosphate buffered saline pH 7.4. The size and size distribution of empty micelles made from Ben-$PCL_7$-$mPEG_{45}$, Ben-$PCL_{11}$-$mPEG_{45}$, Ben-$PCL_{14}$-$mPEG_{45}$ and Ben-$PCL_{19}$-$mPEG_{45}$ are summarized in Table S2 (Suppl. Mater.). Ben-$PCL_7$-$mPEG_{45}$ micelles prepared at 10 mg/mL polymer concentration had a size of 16 nm and a narrow size distribution (low PDI), while the size increased to 57 nm for the largest Ben-$PCL_{19}$-$mPEG_{45}$ copolymers. At the same time, an increase is seen in the polydispersity of the micelles, suggesting the formation of larger aggregates with increasing CL block length. DSC data of Table S2 shows that the $T_m$ of the PCL block in Ben-$PCL_7$-$mPEG_{45}$ copolymer is 13.0 °C and increases to 42.7 °C in Ben-$PCL_{14}$-$mPEG_{45}$ (for Ben-$PCL_{19}$-$mPEG_{45}$ the PCL $T_m$ overlapped with the PEG $T_m$ at 45.7 °C). Also, the $\Delta H_m$ of the PCL block increases from 5.1 J/g in Ben-$PCL_7$-$mPEG_{45}$ to 14.7 J/g in Ben-$PCL_{14}$-$mPEG_{45}$. Both the increase in $T_m$ and $\Delta H_m$ of the PCL block demonstrates that the degree of crystallinity increases with increasing PCL block length.

Due to the small and uniform size and low $T_m$, Ben-$PCL_7$-$mPEG_{45}$ was selected for the preparation of mTHPC loaded micelles and for *in vitro* experiments. The critical micelle concentration of Ben-$PCL_7$-$mPEG_{45}$, determined by the pendant drop method was 0.04 mg/mL (Fig. S2), which is comparable to other Ben-PCL-PEG block copolymers with a similar PCL/PEG ratio.[28]

### *3.2. Preparation and characterization of mTHPC loaded micelles*

Micelles of Ben-$PCL_7$-$mPEG_{45}$ loaded with mTHPC (Fig. 1A) were prepared using the same film hydration method as for the empty micelles.[28] Fig. 1B shows micellar dispersions obtained with different feed ratios from 0.05 to 20% of mTHPC. Loading efficiencies of these dispersions were approximately 90% for these feed ratios (Fig. 1C) and a loading capacity of 17% could be obtained at a feed ratio of 20% (Fig. 1D). Fig. 1D shows that a higher feed ratio of 30% did not result in further increased loading, corresponding with a drop in the loading efficiency (Fig. 1C). This indicates that Ben-$PCL_7$-$mPEG_{45}$ micelles have a maximum loading capacity of 17% for mTHPC based on polymer-PS weight ratio. Most importantly, Fig. S3 shows that the absorbance spectrum of the loaded micelles at 20% feed ratio resembles the spectrum of an mTHPC solution in DMF, from which it can be concluded that no aggregation occurred of the mTHPC that is encapsulated in the micelles, even at such high loadings.

For demonstration of the photosensitizing ability of the mTHPC-loaded micelles, $^1O_2$ generation was studied upon illumination of the micellar dispersion with broadband light of >455 nm. As one of the main reactive species in PDT, the rate of $^1O_2$ production is a critical parameter when characterizing new photosensitizers. $^1O_2$ quantum yields ($\phi_\Delta$) were determined in $D_2O$ using the relative method as described by Nombona et al.[33] Fig. S4 (see Supplementary Material) shows an example of the decay of the scavenger absorption during these experiments. Neither decrease in Q-band intensity

nor appearance of new bands were observed, confirming the photochemical integrity of the sensitizer during illumination and subsequent formation of $^1O_2$. Plotting the dependence of $\ln(A_0/A_t)$ against irradiation time ($t$) affords a straight line whose slope reflects the photosensitizer efficacy to generate $^1O_2$, and from which $\phi_\Delta$ can be calculated. Fig. 2A-B represents the scavenger photo-degradation profiles induced by two series of samples obtained from stock solutions with varying ratios of Ben-$PCL_7$-$mPEG_{45}$ or mTHPC, respectively, and the other component´s concentration remaining constant. The corresponding $\phi_\Delta$ (%) values are summarized in Fig. 2C. Before measurement, all micelle samples were diluted with PBS in $D_2O$ to a similar mTHPC concentration with an absorption of around 0.1 at the Q-band.

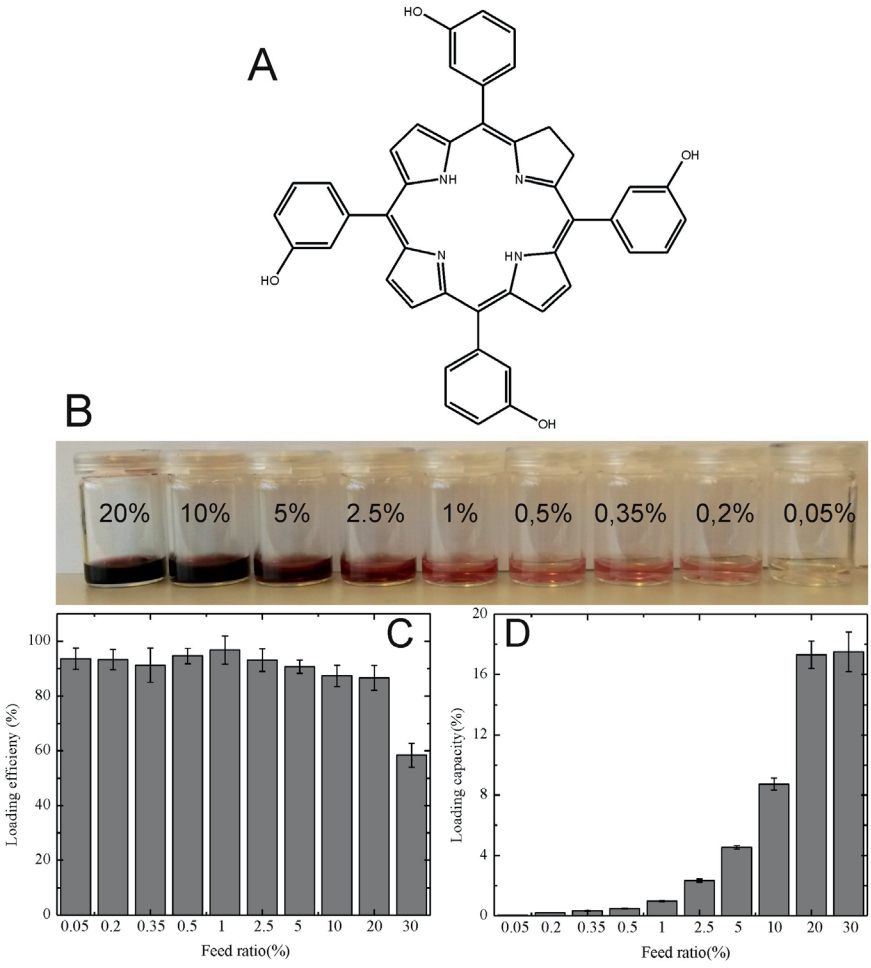


**Figure 1.** A) Structural formula of mTHPC. B) 10 mg/mL micellar dispersions of Ben-$PCL_7$-$mPEG_{45}$ in PBS, loaded with different feed ratios of mTHPC (weight%). C) Loading efficiency of Ben-$PCL_7$-$mPEG_{45}$ (10 mg/mL dispersions) for mTHPC at different feed ratios (weight%) in in PBS. D) Loading capacity of 10 mg/mL Ben-$PCL_7$-$mPEG_{45}$ micelles for mTHPC at different feed ratios in PBS dispersions. N=3.

First, stock solutions with a fixed amount of mTHPC (0.4 mg/mL) and varying Ben-$PCL_7$-$mPEG_{45}$ concentrations (2-10 mg/mL, i.e. relatively high feed ratio of 4-20%) were used. These samples were approx. diluted in 100 times $D_2O$. Fig. 2C (open triangles) shows that with increasing polymer to mTHPC ratio, i.e. with decreasing photosensitizer loading per micelle, an increasing quantum yield was obtained. When the polymer amount was fixed at 10 mg/mL and the amount of encapsulated mTHPC was decreased over a broader feed ratio (0.05-20 %), the $\phi_\Delta$ value showed an optimum at a ratio of 200:1 Ben-$PCL_7$-$mPEG_{45}$:mTHPC (w:w) or 0.5% loading ( $\phi_\Delta$ = 0.46, see Fig. 2C, closed triangles, and Table S3 in the supplemental materials).

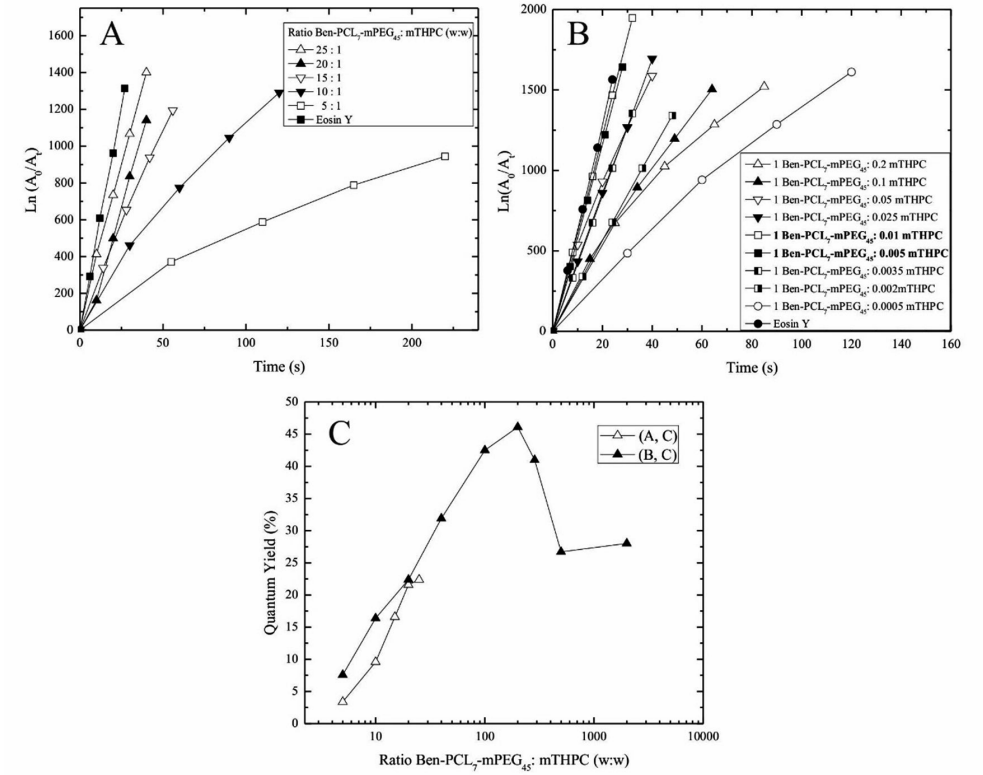


**Figure 2.** (A,B) Plot of the decrease in ADMA absorption induced by mTHPC-loaded micelles with varying ratios and (C) corresponding singlet oxygen quantum yield (QY) values obtained from the slope of lines represented in (A,B), of: (A,C) Ben-$PCL_7$-$mPEG_{45}$:mTHPC (w:w) ratios where the amount of Ben-$PCL_7$-$mPEG_{45}$ was changed (2-10 mg/mL) and the amount of mTHPC remained constant (0.4 mg/mL); (B,C) Ben-$PCL_7$-$mPEG_{45}$:mTHPC (w:w) ratios where the amount of mTHPC was changed (0.005-2 mg/mL) and the concentration of Ben-$PCL_7$-$mPEG_{45}$ was kept constant (10 mg/mL).

### *3.3. In vitro cellular uptake and photo-cytotoxicity of mTHPC loaded micelles*

A micellar photosensitizer formulation composed of 0.5 mg/mL Ben-$PCL_7$-$mPEG_{45}$ and 0.1 mg/mL mTHPC (20% loading) showed no dark toxicity on murine RAW264.7

macrophage cells and C166 endothelial cells after an incubation time of 24 hours (MTS assay, see Fig. S5). For photocytotoxicity measurements, the cells were not washed for removal of non-internalized micelles but directly illuminated for 10 minutes after predetermined incubation times (1, 2, 4, 8 or 24 hours) with micellar photosensitizer formulations composed of 0.5 mg/mL Ben-$PCL_7$-$mPEG_{45}$ polymer and 2.5 μg/mL mTHPC (0.5% loading). Fig. 3 shows an increase in photo-cytotoxicity in time for the RAW264.7 macrophages. After 24 hours incubation with the photosensitizer formulation, the macrophages were almost completely killed by the generated $^1O_2$, while the C166 endothelial cells hardly showed cell death under the same conditions.

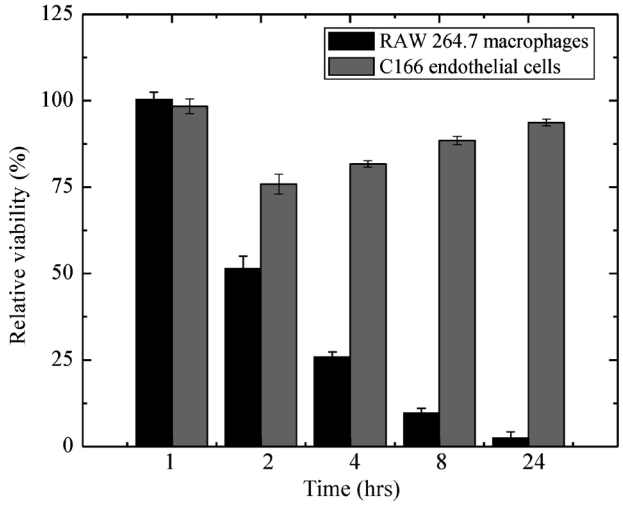


**Figure 3.** Photo-cytotoxicity by MTS assay of RAW264.7 macrophages and C166 endothelial cells incubated with micelles composed of 0.5 mg/mL Ben-$PCL_7$-$mPEG_{45}$ and 2.5 μg/mL mTHPC. After 1, 2, 4, 8 and 24 hours of incubation, the cells were illuminated for 10 minutes, 3.04 mW/cm$^2$ (n=3).

To investigate the rate of uptake of mTHPC in its micellar form by RAW264.7 macrophages and C166 endothelial cells, fluorescence microscopy was performed at several time points (Fig. 4). Because the low photosensitizer concentration used for photocytotoxicity (2.5 μg/mL of mTHPC) gave minimal fluorescence, a higher concentration of 25 μg/mL mTHPC was taken. The pictures clearly show that the fluorescent photosensitizer is associated with both the macrophage and endothelial cells. The darker cores in the cells represent the cell nuclei which are not stained by the mTHPC because it cannot penetrate to the nucleus. From this, it can be concluded that the photosensitizer is in the cytosol and not associated with the cell surface.

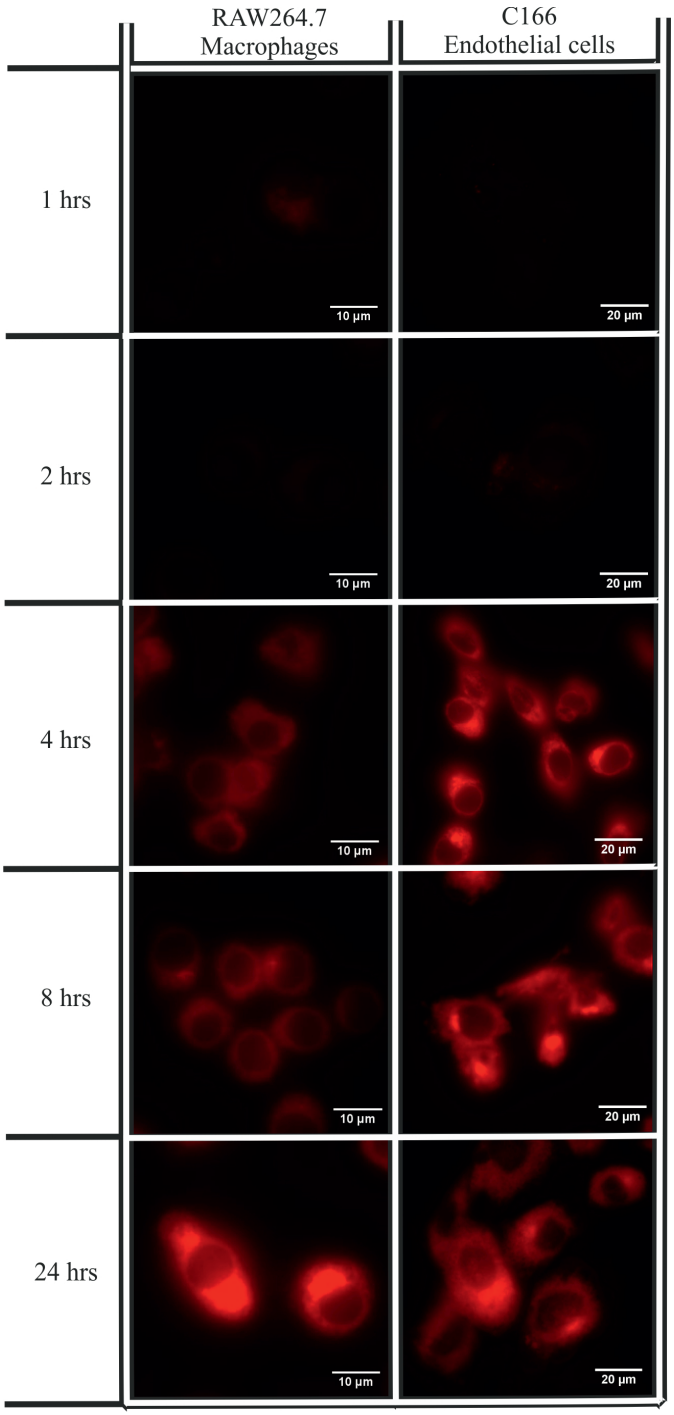


**Figure 4.** Fluorescence image of RAW264.7 macrophages and C166 endothelial cells incubated with micelles composed of 0.5 mg/mL Ben-$PCL_7$-$mPEG_{45}$ polymer and 25 µg/mL mTHPC after 1, 2, 4, 8 and 24 hours. The cells were not illuminated to preserve cell morphology for the microscope pictures.

To obtain more information about the mechanism of photoinduced cell killing, and which formulation factors play a major role in that, both polymer concentration and mTHPC concentration were systematically varied and photo-cytotoxicity was studied using RAW264.7 macrophages and C166 endothelial cells. According to Fig. S6 and S7 (supplementary material), when the polymer concentrations were fixed below the CMC (i.e. 0.04 mg/mL) the IC50 is hardly dependent on the polymer concentration. As expected, this indicates that the micelles dissociated and the PDT effect is caused by the released photosensitizer. Those IC50 values were a bit higher for C166 endothelial cells (approximately 0.3 μg/mL mTHPC) as compared to RAW264.7 macrophages, which had an IC50 of 0.08 μg/mL. This indicates that C166 endothelial cells are less sensitive to singlet oxygen generation or have a lower uptake rate of the free mTHPC. Surprisingly, however, above the CMC, i.e. in the presence of intact micelles, not only the mTHPC but also the polymer concentration plays an important factor in the cell killing potential, i.e. the IC50 values increased with increasing polymer concentration. For example, in Fig. 5 it can be seen that 0.1 mg/mL polymer and 0.35 μg/mL mTHPC gave major cell killing after illumination (cell viability of only 26%), while the same mTHPC concentration but with a higher polymer concentration of 0.5 mg/mL did not kill the RAW264.7 cells at all under these conditions (i.e. 125% cell viability). Most importantly, the IC50 values were also cell type dependent. A similar polymer concentration dependency was observed for the C166 endothelial cells, but above the CMC (0.04 mg/mL) the amount of mTHPC that is needed to give similar photo-cytotoxicity (i.e. IC50 value) is approximately one order of magnitude higher (Fig. 5).

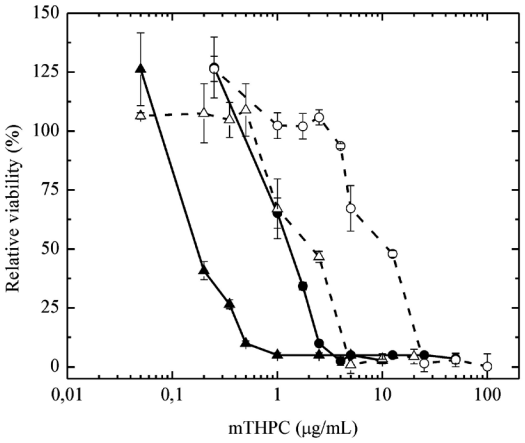


**Figure 5.** Photocytotoxicity by MTS assay at fixed polymer concentrations above the CMC and varying mTHPC loadings on RAW264.7 macrophages and C166 endothelial cells after 24 hours of incubation. The cells were illuminated for 10 minutes, 3.04 mW/cm$^2$. ●— RAW264.7 Macrophages, 0.5 mg/mL Ben-PCL$_7$-mPEG$_{45}$, —○— C166 endothelial cells, 0.5 mg/mL Ben-PCL$_7$-mPEG$_{45}$, ▲— RAW264.7 Macrophages, 0.1 mg/mL Ben-PCL$_7$-mPEG$_{45}$, —△— C166 endothelial cells, 0.1 mg/mL Ben-PCL$_7$-mPEG$_{45}$. N=3

Photocytotoxicity for RAW264.7 macrophages was also investigated with micelles composed of Ben-$PCL_n$-$mPEG_{45}$ with increasing PCL blocks lengths (*n*) of 7, 11, 14 or 19 units. The concentration of the micelles was kept at 0.5 mg/mL, the concentration of mTHPC was 1.75 μg/mL and incubation time was 24 hrs. In Fig. 6 it is clearly seen that upon increasing the PCL block length, the relative viability of the macrophages also increased and thereby increasing the IC50 value of mTHPC.

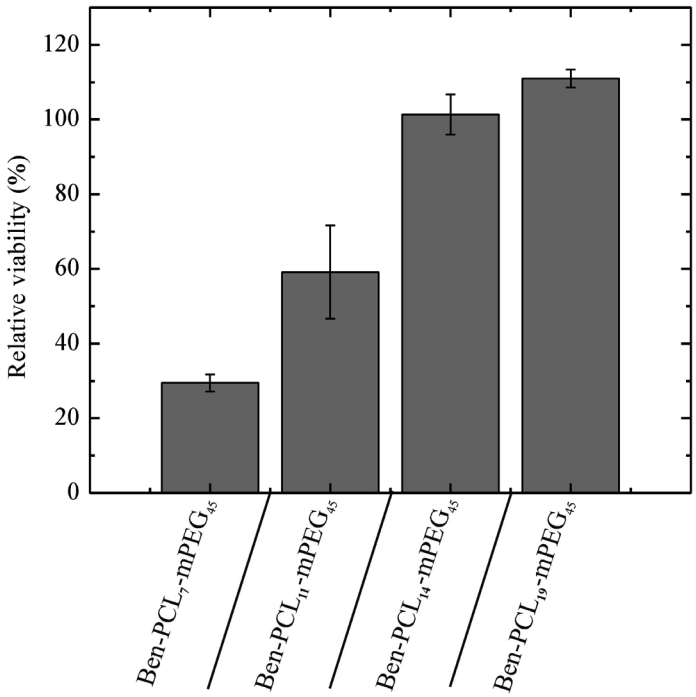


**Figure 6.** Photo-cytotoxicity by MTS assay of 0.5 mg/mL polymer with varying PCL block lengths, and 1.75 mg/mL mTHPC, on RAW264.7 macrophages after 24 hours of incubation. The cells were illuminated for 10 minutes, 3.04 mW/cm$^2$. N=3

Previous results have shown that mTHPC-loaded PCL-based micelles can be degraded by lipases, thus releasing the photosensitizer and induce cell killing upon illumination. [30] In Fig. 7, the lipase activity of both RAW264.7 macrophages and C166 was investigated using a colorimetric assay. It is seen that the RAW macrophages have a lipase activity of 12 milliunits/mL while the C166 cells display a lipase activity of 6.6 milliunits/mL.

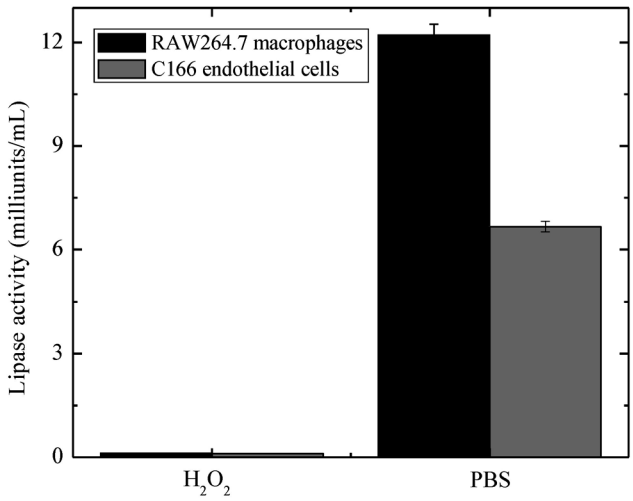


**Figure 7.** Lipase activity in RAW264.7 macrophages and C166 endothelial cells measured in PBS. $H_2O_2$ treated cells were used as a negative control. N=3

### *3.4 In vitro stability of mTHPC–loaded micelles in serum and plasma*

Fluorescence properties of micellar and liposomal formulations of mTHPC were evaluated in PBS and compared with Foscan® (free mTHPC in solvent). Figure 8A shows the intensity of fluorescence of mTHPC in these samples as a function of mTHPC concentration. For the micelles, the range of concentrations was obtained by varying the loading % of mTHPC at a fixed polymer concentration (10 mg/mL), while for the liposomes a dilution series in PBS was obtained from a stock solution of Foslip®, thus keeping the loading % (i.e. mTHPC/lipid ratio) constant upon dilution. The fluorescence of mTHPC loaded micelles increased almost linearly with increasing mTHPC concentration ranging from 0.001 to 0.005 mg/mL (loading from 0.1 to 0.5% w/w), with similar intensity as for free mTHPC in Foscan® at the same concentrations. At higher loading %, the fluorescence of mTHPC loaded micelles showed a rapid decrease with increasing mTHPC loading, while the fluorescence intensity of Foscan® showed a gradual upward trend until it levelled off at 0.1 mg/mL. The fluorescence from Foslip® is lower than that of Foscan® in the whole mTHPC concentration range. The fluorescence of Foslip® did hardly change when diluted in PBS from 0.2 to 0.025 mg/mL of mTHPC (Fig. 8A). However, only with further dilution of Foslip® in PBS, mTHPC fluorescence started to decrease. The fluorescence of mTHPC loaded micelles at different loadings and Foslip® dilutions in PBS was stable in time over 8 h at 37 ℃ (see Supplementary Figure S8). When Foscan diluent (ethanol/propylene glycol, 40/60 w/w%) was added to the micelles or to Foslip® at mTHPC concentration of 0.2 mg/mL to destroy the particles, the fluorescence was restored to almost the same level as Foscan® (data not shown).

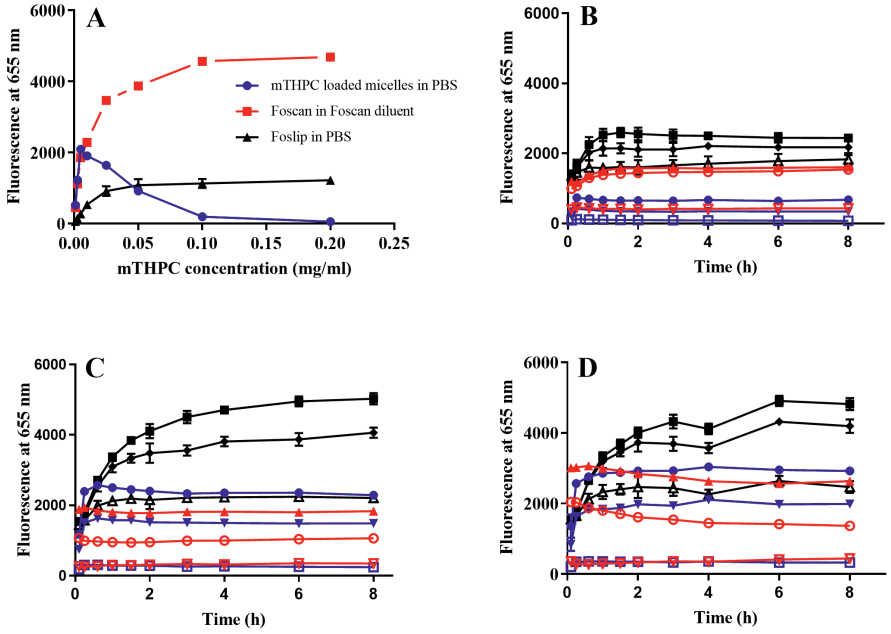


**Figure 8.** A) Fluorescence intensity ($\lambda_{ex}$ 420 nm, $\lambda_{em}$ 655 nm) as a function of mTHPC concentration; Foscan® and Foslip® stock solutions were diluted in ethanol/propylene glycol (40:60 w/w%) and PBS (pH 7.4), respectively, while micelles of 10 mg/mL with different loading amounts (0.1-20% w/w) were individually prepared and each diluted 10× in PBS to obtain the corresponding mTHPC concentrations. B)-D) Fluorescence intensity as a function of time at mTHPC concentration of 0.2 mg/mL in FBS (B), mouse plasma (C), human plasma (D); Foscan®, Foslip® and mTHPC loaded micelles were 10× diluted with FBS or plasma solutions and incubated while the mTHPC fluorescence was recorded at 37 ℃ over a period of 8 h (in duplicate). In B)-D) black lines, red lines and blue lines represent Foslip®, Foscan® and mTHPC loaded micelles, respectively. Squares, triangles and open dots are for all samples in 90, 50 and 10% FBS or plasma, respectively.

The stability of the three formulations (Foscan®, Foslip® and micelles) at 0.2 mg/mL mTHPC was assessed in diluted serum (FBS), mouse plasma and human plasma by the change in fluorescence over time at 37 °C (Figures 8 B-D). Upon addition to plasma or serum, the fluorescence of Foscan® was lower than in organic solvent (ethanol/propylene glycol, 40/60 w/w%) (compare Fig. 8A with Fig 8B-D) but remained quite constant in time in different amounts of mouse and human plasma (Fig. 8, red lines). Only a slight increase of the Foscan® fluorescence was observed in the first 1 h incubation in FBS solutions and then remained stable. The fluorescence of Foslip® (black lines in Fig. 8 B-D) increased gradually in FBS, human plasma and mice plasma in the first 2 or 3 hours of incubation, which was more pronounced with higher serum or plasma concentrations, and then remained stable. For the micellar formulation with 20% loading (blue lines in Fig. 8 B-D), a rapid increase of fluorescence was observed within the first 30 min of incubation and then levelled off, which was more significant with

increasing serum or plasma concentration from 10% to 90%, reflecting a burst release of mTHPC from the micelles.

The changes of fluorescence in time at lower mTHPC concentrations (0.025, 0.05 and 0.1 mg/mL) for the micelles, liposomes and free mTHPC in 10, 50 and 90% of FBS, human plasma and mouse plasma are shown in Supplementary Fig. S9. The trends are similar as for the higher mTHPC concentration shown in Fig. 8: the constant fluorescence of Foscan® (Fig. S9 red lines), the progressive increase of fluorescence from Foslip® in the first 2 or 3 hours of incubation (black lines in Fig. S9), and a rapid increase of fluorescence for the micellar formulations at the first 30 min incubation (blue lines in Fig. S9), were all independent of the mTHPC concentration.

The final fluorescence intensities of the three formulations with a series of mTHPC concentrations after 8 h incubation in the different media are summarized in Table 1. The fluorescence of free mTHPC (Foscan®, Table 1A) increased with increasing FBS concentration, and was more significant in mouse plasma and even slightly more in human plasma, except for the lowest mTHPC concentrations. Fluorescence generally increased when Foscan® was more diluted at a fixed serum or plasma concentration. When the lowest concentration (0.025 mg/mL) was added to the highest amount of mouse or human plasma (90%), fluorescence intensity levelled off to a maximum value of 3,400 a.u., similar to that of free mTHPC in organic solvent (3,500 a.u.: see red line in Fig. 8A at this concentration), which was also the case with 0.05 mg/mL in 90% human plasma (3,800 a.u. versus 4,100 a.u. in organic solvent).

For Foslip® with different mTHPC concentrations (Table 1B), the increase of fluorescence with increasing serum or plasmas concentrations was observed as well, again following the order in human plasma > mouse plasma > FBS. Also here, the values levelled off at 50 to 90% serum or plasmas at the lower mTHPC concentrations. Overall, the intensities of Foslip® at given mTHPC concentrations were higher than that of Foscan®.

**Table 1**. Fluorescence intensities (FI, a.u. × $10^3$) ($\lambda_{ex}$ 420 nm, $\lambda_{em}$ 655 nm) of Foscan® (A), Foslip® (B) and mTHPC loaded micelles (C) with various mTHPC concentrations after 8 h incubation in diluted (0, 10, 50 and 90% in PBS) fetal bovine serum (FBS), mouse plasma (MP) and human plasma (HP).

**A**

| | Foscan® FI in FBS | | | | Foscan® FI in MP | | | Foscan® FI in HP | | |
|---|---|---|---|---|---|---|---|---|---|---|
| [mTHPC] (mg/mL) | 0%* | 10% | 50% | 90% | 10% | 50% | 90% | 10% | 50% | 90% |
| 0.025 | 0 | 1.1 | 1.6 | 2.2 | 1.0 | 3.3 | 3.4 | 1.7 | 3.3 | 3.4 |
| 0.050 | 0 | 1.3 | 1.5 | 1.8 | 0.8 | 2.6 | 3.2 | 1.1 | 3.2 | 3.8 |
| 0.100 | 0 | 0.8 | 1.6 | 1.6 | 0.6 | 1.7 | 3.0 | 0.7 | 2.8 | 3.6 |
| 0.200 | 0 | 0.4 | 1.5 | 1.6 | 0.4 | 1.1 | 1.8 | 0.4 | 1.4 | 2.6 |

**B**

| | Foslip® FI in FBS | | | | Foslip® FI in MP | | | Foslip® FI in HP | | |
|---|---|---|---|---|---|---|---|---|---|---|
| [mTHPC] (mg/mL) | 0%* | 10% | 50% | 90% | 10% | 50% | 90% | 10% | 50% | 90% |
| 0.025 | 1.0 | 1.8 | 2.8 | 2.7 | 2.5 | 3.3 | 3.3 | 3.5 | 4.2 | 4.1 |
| 0.050 | 1.1 | 1.7 | 2.6 | 2.8 | 2.4 | 3.7 | 3.9 | 3.7 | 4.9 | 4.9 |
| 0.100 | 1.1 | 1.9 | 2.6 | 3.0 | 2.2 | 4.8 | 5.2 | 2.8 | 4.6 | 4.9 |
| 0.200 | 1.2 | 1.8 | 2.2 | 2.4 | 2.2 | 4.0 | 5.0 | 2.5 | 4.2 | 4.8 |

**C**

| | Micelles FI in FBS | | | | Micelles FI in MP | | | Micelles FI in HP | | |
|---|---|---|---|---|---|---|---|---|---|---|
| [mTHPC] (mg/mL) | 0%* | 10% | 50% | 90% | 10% | 50% | 90% | 10% | 50% | 90% |
| 0.025 | 1.6 | 1.4 | 1.7 | 1.9 | 1.3 | 3.2 | 3.3 | 1.7 | 3.3 | 3.4 |
| 0.050 | 0.9 | 0.6 | 0.8 | 1.3 | 0.6 | 2.6 | 3.2 | 0.6 | 3.2 | 3.7 |
| 0.100 | 0.1 | 0.1 | 0.5 | 1.0 | 0.3 | 1.7 | 2.6 | 0.5 | 2.6 | 3.5 |
| 0.200 | 0.0 | 0.0 | 0.3 | 0.7 | 0.2 | 1.5 | 2.3 | 0.3 | 2.0 | 2.9 |



As shown in Table 1C, decreasing the loading % of mTHPC loaded micelles led to increase of the fluorescence intensity from 0 to 1.600 a.u. in 0% plasma or serum (pure PBS, same data as in Figure 8A). Remarkably, addition of micelles to plasma or serum resulted in similar FI as for free mTHPC (compare Table 1C with 1A). As for free mTHPC, the fluorescence from mTHPC loaded micelles increased with increasing FBS concentration and was more significant in mouse and human plasma. For all loading%, fluorescence intensity increased around 300 units from 10 to 50% FBS and another 400 units from 50 to 90% FBS. In mouse plasma, FI of micelles with 0.2 mg/mL (20% loading) and 0.1 mg/mL mTHPC (10% loading) increased 4-7 times from 10 to 50% plasma and then increased another 1.5 times when increasing to 90% plasma. The lower loadings seemed to level off at around 3,200 a.u. when mouse plasma concentrations were increased. Similar trends were observed in human plasma but with slightly higher absolute fluorescence intensities compared to that in mouse plasma.

*3.5. In vivo pharmacokinetics and biodistribution of mTHPC loaded micelles in mice*

The pharmacokinetic profiles of mTHPC loaded micelles were determined from blood samples after intravenously administering micelles with 5.0 and 0.6% mTHPC loading (w/w) to Balb/c nude mice via tail vein (Figure 9). The "low dose" formulation with 0.6% mTHPC loading was chosen to give a systemic concentration upon *i.v.* injection in mice of approx. 0.6 mg/mL Ben-$PCL_7$-$mPEG_{45}$ and 4 μg/mL mTHPC, which were the similar concentrations that gave the highest macrophage selectivity *in vitro*. The "high dose" formulation with 5% mTHPC loading would give the same systemic concentration of polymer (around 0.6 mg/mL Ben-$PCL_7$-$mPEG_{45}$) but 8 times higher concentration of mTHPC (approx. 32 μg/mL). mTHPC loaded micelles in low dose group exhibited slightly higher mTHPC levels in the circulation for the first 5 min as compared to the high dose group, but decay profiles were similar for both mTHPC formulations. According to the semi-logarithmic plot (insert Fig. 9), these profiles followed first order kinetics, the slope corresponding with half-life times ($t_{1/2}$ values) of 1.5 h. The corresponding mTHPC plasma concentrations at low and high dose were 4.9 and 32.4 μg/mL, respectively, at 5 min, which decreased to 0.74 and 4.74 μg/mL at 4 h.

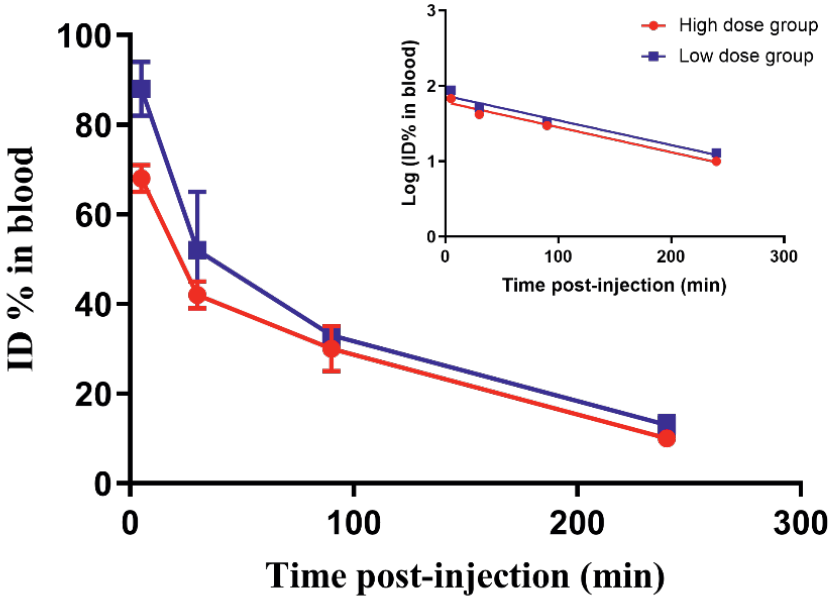


**Figure 9**. *In vivo* pharmacokinetics of mTHPC loaded in micelles based on Ben-$PCL_7$-$mPEG_{45}$ upon tail vein administration in healthy nude Balb/c mice (mTHPC dosage in high (5% loading) and low (0.6% loading) dose group is 50 μg and 6 μg mTHPC, respectively). Blood samples taken at different time points were used to quantify the percentage of mTHPC injected dose (%ID) present in systemic circulation. The total blood volume of the mice is assumed to be around 1-1.5 mL, depending on bodyweight. The inset shows the log-concentration versus time. Data are presented as mean ± SD, N = 3.

Similar two samples (high and low dose) as used in pharmacokinetic study were selected for determination of the biodistribution in atherosclerotic $LDLR^{-/-}ApoB^{100/100}$ mice *in vivo*. Directly after *i.v.* injection, the "low dose" formulation gives a systemic concentration in mice of 0.5 mg/mL Ben-$PCL_7$-$mPEG_{45}$ and 4 μg/mL mTHPC, while the "high dose" formulation would give the same systemic concentration of polymer (0.5 mg/mL Ben-$PCL_7$-$mPEG_{45}$) and 25 μg/mL mTHPC. The mice were kept on a high fat diet to develop an atherosclerotic lesions for 5 months. 4 hours after tail vein injection, the mice were sacrificed, and organs were analyzed with confocal microscopy. mTHPC was present in liver, spleen, kidney and lung in varying degrees (Supplementary Figure S11). The most interesting result obtained is depicted in Fig. 10. The high dose formulation clearly preferentially located in the atherosclerotic plaque. In the low dose the mTHPC is probably present but the amount of mTHPC is too low to observe any fluorescence, similar as with the fluorescence microscope described earlier.

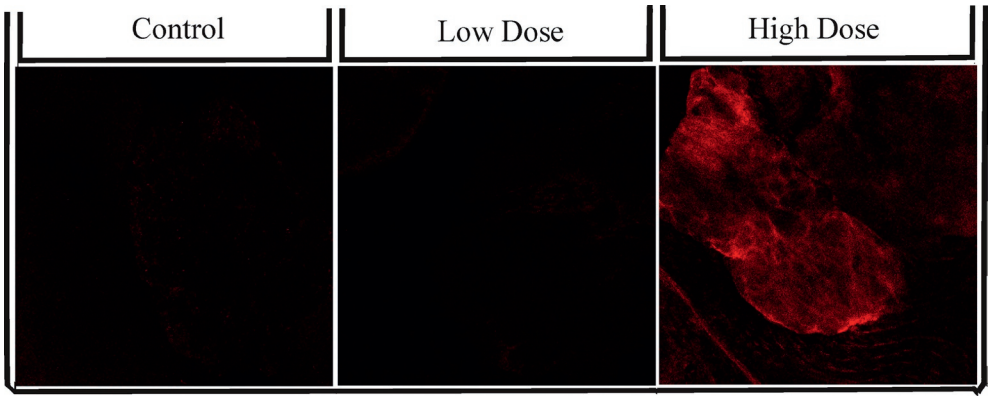


**Figure 10.** Confocal fluorescence images of atherosclerotic lesions in LDLR$^{-/-}$ApoB$^{100/100}$ mice aorta's, taken 4 hrs post injection of formulations in the tail vein. The control group was injected with PBS. In the low mTHPC dose, 100 µL of a solution containing 1 mg Ben-PCL$_7$-mPEG$_{45}$ and 8 µg mTHPC in PBS was injected, resulting in a systemic concentration of 0.5 mg/mL Ben-PCL$_7$-mPEG$_{45}$ and 4 µg/mL mTHPC. In the high mTHPC dose, 100 µL of solution containing 1 mg Ben-PCL$_7$-mPEG$_{45}$ and 50 µg mTHPC in PBS was injected, resulting in a systemic concentration of 0.5 mg/mL Ben-PCL$_7$-mPEG$_{45}$ and 25 µg/mL mTHPC. The total blood volume of the mice is assumed to be 2 mL.

## 4. Discussion

We have shown previously that PCL based micelles can be used to encapsulate very high amounts of the photosensitizer mTHPC.[30] Encapsulation reduced the uptake and photocytotoxicity with 14C head and neck cancer cells as compared to free mTHPC, which was recovered by dilution of the micelles below the CMC or after enzymatic degradation of the micelles by lipase. Since macrophages generally show elevated lipase activity,[31] these findings triggered us to investigate these formulations for its applicability in the PDT of atherosclerosis, an inflammatory disease. As opposed to our previous work, for simplicity, we did not fractionate the polymers to obtain monodisperse polymers, but just took the polydisperse ones as prepared. Also the length of the PEG block was increased from 750 to 2000 Da and the synthesis route was modified. Despite that, the size of the empty micelles with average number of 7 caprolactone units (16 nm) was very similar to the micelles of the monodisperse polymers with the same (exact) number of CL units.[28] Also the melting temperature of the polymer (13 °C) was in accordance with the previously obtained results; block copolymers of Ben-PCL$_4$-PEG$_{17}$ with monodisperse PCL blocks had a PCL melting temperature at -25 °C which increased upon an increase of the PCL block to 10 °C for 6 CL units. The observed increase in PDI when the PCL chain length increased beyond 7 correlated with the increased $T_m$ and $\Delta H_m$ (table S2), and can therefore be attributed to the higher tendency to form crystals and thus larger aggregates for the larger block copolymers.

The maximum loading capacity of the micelles for mTHPC (17 w%) was again similar to Hofman et al. for the loading capacity of Ben-$PCL_5$-$PEG_{17}$ with monodisperse PCL blocks at 20% feed ratio of mTHPC.[30] As opposed to our new results, loading capacity in those micelles based on Ben-$PCL_5$-$PEG_{17}$ could be further increased to 30 wt%, at 30% feed ratio of mTHPC. A possible explanation for this difference is the ratio of PCL/PEG. The Ben-$PCl_5$-$PEG_{17}$ of Hofman et al. has 43 wt% PCL and the current Ben-$PCL_7$-$mPEG_{45}$ copolymer has only on average 28 wt% PCL. Due to lower hydrophobicity in the Ben-$PCL_7$-$mPEG_{45}$ system, the extremely high loading capacities such as in Ben-$PCL_5$-$PEG_{17}$ were not obtained. In any case, the absence of aggregation of mTHPC inside the micelles (see Fig. S3) is very important and promising, since aggregation of photosensitizers often hampers singlet oxygen generation.[36] Despite the fact that even at the highest loading (20% w/w) we observed no aggregation by UV-Vis spectroscopy, quenching of the fluorescence of the mTHPC in the micelles was observed above 0.5% w/w loading (Fig. 8A: 0.005 mg/mL mTHPC in 1 mg/mL polymer dispersion). The fluorescence intensity nicely correlates to the singlet oxygen quantum yield: both show their highest values at a loading of 0.5% w/w (200:1 polymer to mTHPC ratio) (compare Fig. 8A and 2C). In those best conditions, the singlet oxygen quantum yield values obtained approached those of the best PDT photosensitizers in the literature,[37] encouraging us to further study the use of mTHPC-loaded micelles for PDT treatment of atherosclerosis.

Photocytotoxicity experiments revealed a much larger sensitivity of the macrophages as compared to the endothelial cells. After the incubation with the mTHPC loaded micelles, the cells were not washed for removal of non-internalized micelles but directly illuminated for 10 minutes in the presence of the micellar dispersions. In other words, total mTHPC concentration (extracellular plus intracellular) was the same in all experiments. Therefore, if the singlet oxygen generated by the photosensitizer is similarly active outside and inside the cells, the photo-cytotoxicity would be independent of the incubation time. However, Fig. 3 clearly shows an increase in photo-cytotoxicity in time for the RAW264.7 macrophages, most likely related to the increasing extend of internalization. This indicates that the uptake of the photosensitizer plays an important role in the cell killing of RAW264.7 macrophages. Interestingly, in Fig. 3 it is clearly visible that RAW264.7 macrophages are efficiently killed after 24 hours incubation by the generated singlet oxygen, while the C166 endothelial cells hardly show cell death under the same conditions. Nevertheless, the fluorescence microscopy pictures, especially after 4 and 8 hours, suggest that the uptake rate by C166 endothelial cells is even slightly faster than by RAW264.7 macrophages, which is not in accordance to the photocytotoxicity results. This suggests that after uptake of loaded micelles another process is active inside macrophage cells, and not in C166 cells, which results in the observed selective cell killing after illumination. Because in our previous work we have seen that the mTHPC only became photoactive after degradation of the micelles by lipase, [30] we measured

the lipase activity of both cell lines and corroborated that macrophages indeed showed higher lipase activity (Fig. 6). This process could therefore very well explain the selective killing of macrophages as compared to the endothelial cells. The lipase-dependent activation of the photosensitizer was further indicated by the observed dependency on the polymer concentration and molecular weight at a fixed mTHPC amount (i.e. the higher the relative polymer amount and the longer the PCL blocks, the longer it takes for the micelles to fully degrade and release the photosensitizer), and by the fact that the polymer concentration and the cell type dependency of the IC50 values were only observed above the polymer's CMC.

This selectivity in cell killing potential is most interesting for the targeting because we want the endothelial layer of atherosclerotic plaques to stay alive. It gives us an opportunity to select a window where it is possible to kill the RAW264.7 macrophages and keep the endothelial layer alive: for example at 0.5 mg/mL polymer concentration and 4 mg/mL mTHPC, 94% of the endothelial cells survived while 95% of the macrophage cells were killed. The same was true for 0.1 mg/mL polymer but then at a lower mTHPC concentration of 0.5 mg/mL (Fig. 5). If the selectivity towards macrophages could be translated to the *in vivo* situation, it could become a very interesting intervention treatment in the inflammation process of atherosclerosis,[14] without harming the endothelial layer.

Before moving to *in vivo* studies, we first investigated the *in vitro* stability of the mTHPC micellar formulations in serum and plasma, and compared this with a known commercial liposomal formulation of mTHPC (Foslip®). As shown in Figure 8A, mTHPC loaded micelles exhibited linear increase in fluorescence intensity with increasing mTHPC loading from 0.1 to 0.5% w/w. However, above 0.5% w/w loading, the sudden decrease in the fluorescence of mTHPC loaded micelles can be attributed to fluorescence quenching resulting from high mTHPC local concentration in micelles. In such case, fluorescence can be restored after destroying the micelles by addition of a surfactant or an organic solvent.[38] Indeed, this was the case when the micelles or Foslip® were dissolved in Foscan® diluent. As opposed to the loaded micelles, where mTHPC to polymer ratio was varied in Figure 8A, the liposomes of a Foslip® stock solution were diluted in their entirety keeping a constant mTHPC to lipid ratio. Therefore the fluorescence quenching of mTHPC in Foslip® did not change in PBS (Fig. 8A) because dilution of both mTHPC and lipids does not have an effect of the local concentration inside each liposome. Only when significantly diluted (below 0.025 mg/ml of mTHPC), liposomes may become unstable, thus leading to the decrease of mTHPC fluorescence.

When mTHPC dissolved in an organic solvent (Foscan®) was added to PBS, severe precipitation occurred and fluorescence intensity was completely diminished. However, when added to plasma or serum, part of the mTHPC associated to proteins and remained fluorescent, its intensity depending on the ratio of mTHPC to plasma or serum (Table

1A). When the amount of protein was sufficient to solubilize the amount of mTHPC that was added, the fluorescence intensity coincided with similar concentrations of free mTHPC in organic solvent. The amount of plasma or serum to fully solubilize a certain amount of mTHPC was medium dependent and reflects the order of solubilisation power for mTHPC. The solubilisation power of human plasma > mouse plasma >> FBS is probably due to the different amount of proteins in these media.

For the stability studies of micelles and liposomes in serum and plasma, we made use of the quenched state of the fluorescence when mTHPC is present in the micelles (above 0.5% w/w loading) or in the liposomes. Therefore, the observed increase in fluorescence upon incubation in serum or plasma can be attributed to release from the micelles or liposomes and binding to serum or plasma proteins. Foslip® showed a steady increase in fluorescence when incubated for 8 h in serum or plasma regardless of mTHPC concentrations, indicating slow-release. This is consistent with previous studies, where a slow-release of m-THPC from liposomes in 5% human serum was observed.[39] The release of mTHPC from Foslip® is medium and medium concentration dependent (Table 1B). The fluorescence at low mTHPC concentrations (0.025 and 0.01 mg/mL) levelled off at 50 and 90% serum or plasma solutions, indicating release of mTHPC from liposome was complete. The higher intensities of Foslip® compared to Foscan® at corresponding mTHPC concentrations are due to the presence of liposomes which aid in the solubilization of mTHPC.

All mTHPC loaded micelles, irrespective of the loading%, exhibited a rapid increase in fluorescence intensity in the first 30 min and then remained stable (Fig 8B-D and Fig S9). This dequenching process indicates burst release. Like Foslip®, the amount of release of mTHPC from micelles is dependent on medium and medium concentration. At lower mTHPC loading, 2.5% (w/w) for instance, the release is almost complete in 50% FBS or plasmas because fluorescence was similar to that of Foscan® and did not increase significantly more at 90% serum or plasma.

In the pharmacokinetic study, after *i.v.* administration of the mTHPC loaded micelles, the $t_{1/2}$ value is 1.5 h, regardless of mTHPC to polymer ratio (high dose at 5% loading or low dose at 0.6% loading). This is very much consistent with data reported by Cramers et al. after administration of Foscan® (*i.e.* $t_{1/2}$ is 1.3 h in Balb/c mice),[40] indicating rapid release of mTHPC from the micelles in circulation. This rapid release *in vivo* is in line with the *in vitro* release in serum and plasmas, suggesting the importance of pre-testing the *in vitro* release behavior in plasma for predicting the fate of a delivery system *in vivo*. This fast release behaviour can be caused by high binding affinity of mTHPC with serum and plasma (lipo)proteins leading to mTHPC redistribution from intact micelles to lipoproteins.[41-43] Also protein binding of polymer unimers can play a role, which in combination with dilution upon injection causes an adverse shift of the micel-unimer equilibrium and the destruction of micelles.[43,44]

Combined with premature release and concomitant pharmacokinetic profile of

mTHPC loaded micelles, the observed fluorescence of the atherosclerotic lesions in mice by accumulated mTHPC (see Fig. 10) is probably due to released mTHPC that subsequently binds to lipoproteins, particularly in low-density lipoprotein (LDL). [45,46] LDL as an endogenous carrier can be rapidly transported across an intact endothelium and then ingested by macrophages in the form of oxidized LDL particles. [41,47,48] Indeed, it has been reported that the association of photosensitizers with lipoproteins promotes selective accumulation into tumour tissues and atherosclerotic plaques, thus enhancing their therapeutic potential.[47,49-51]

## 5. Conclusions

The photosensitizer mTHPC was loaded in Ben-PCL-mPEG micelles with high efficiency and capacity and without any aggregation of the photosensitizer. mTHPC-loaded micelles' photo-cytotoxicity is induced by the degradation of the PCL block of Ben-PCL-mPEG micelles by lipases. In accordance with their higher lipase activity, RAW264.7 macrophages degrade the micelles faster and thus activate the photosensitizer earlier than C166 endothelial cells, thus creating a window for selective killing of the RAW264.7 macrophages. Despite the selective accumulation of mTHPC in atherosclerotic plaques of mice aorta, likely due to the proposed binding to lipoproteins, translation from *in vitro* to *in vivo* of the beneficial selective macrophage photocytotoxicity was not possible due to the premature release from the micelles. Therefore, our current aim is to improve the stability of mTHPC-loaded PEG-PCL based micelles (e.g. by chemical crosslinking [52] to fully take advantage of the macrophage selectivity and passive targeting to atherosclerotic plaques. If this aim is achieved, the Ben-PCL-mPEG micelles might be a very interesting delivery system with dual targeting effect, *i.e.* passive targeting to atherosclerotic lesions and faster degradation by macrophages and thus higher selectivity to PDT compared to healthy endothelial tissue.

## Acknowledgements

The research leading to these results has received funding from the European Union Seventh Framework Programme (FP7/2007–2013) under the CosmoPHOS-nano Project, grant agreement no 310337. Financial support from Spanish MINECO (CTQ-2014-52869-P (TT) and CTQ-2014-53673-P (AdlE)) is acknowledged. YL is supported by China Scholarship Council, grant number 201506220178.

## References


1. Roger, V. L.; Go, A. S.; Lloyd-Jones, D. M.; Benjamin, E. J.; Berry, J. D.; Borden, W. B.; Bravata, D. M.; Dai, S.; Ford, E. S.; Fox, C. S.; Fullerton, H. J.; Gillespie, C.; Hailpern, S. M.; Heit, J. A.; Howard, V. J.; Kissela, B. M.; Kittner, S. J.; Lackland, D. T.; Lichtman, J. H.; Lisabeth, L. D.; Makuc, D. M.; Marcus, G. M.; Marelli, A.; Matchar, D. B.; Moy, C. S.; Mozaffarian, D.; Mussolino, M. E.; Nichol, G.; Paynter, N. P.; Soliman, E. Z.; Sorlie, P. D.; Sotoodehnia, N.; Turan, T. N.; Virani, S. S.; Wong, N. D.; Woo, D.; Turner, M. B.; American Heart Association Statistics, C.; Stroke Statistics, S. Heart disease and stroke statistics--2012 update: a report from the American Heart Association. *Circulation* **2012,** *125*, e2-e220.
2. Libby, P.; Ridker, P. M.; Maseri, A. Inflammation and atherosclerosis. *Circulation* **2002,** *105*, 1135-1143.
3. Gotto, A. M.; Pownall, H. J., Prevention and treatment of atherosclerotic vascular disease: hypolipidemic agents. In *Pathophysiology and Pharmacotherapy of Cardiovascular Disease*. Springer International Publishing AG **2015**, pp 589-611.
4. Tabas, I.; Glass, C. K. Anti-inflammatory therapy in chronic disease: challenges and opportunities. *Science* **2013,** *339*, 166-172.
5. John, H.; Kitas, G. Inflammatory arthritis as a novel risk factor for cardiovascular disease. *European journal of internal medicine* **2012,** *23*, 575-579.
6. Gray, B. H.; Sullivan, T. The treatment of iliac artery atherosclerosis with angioplasty and intravascular stents. *Vascular medicine* **1996,** *1*, 287-291.
7. Farb, A.; Sangiorgi, G.; Carter, A. J.; Walley, V. M.; Edwards, W. D.; Schwartz, R. S.; Virmani, R. Pathology of acute and chronic coronary stenting in humans. *Circulation* **1999,** *99*, 44-52.
8. Sarjeant, J. M.; Rabinovitch, M. Understanding and treating vein graft atherosclerosis. *Cardiovascular pathology* **2002,** *11*, 263-271.
9. Song, Y.; Wennink, J. W.; Kamphuis, M. M.; Sterk, L. M.; Vermes, I.; Poot, A. A.; Feijen, J.; Grijpma, D. W. Dynamic culturing of smooth muscle cells in tubular poly(trimethylene carbonate) scaffolds for vascular tissue engineering. *Tissue Eng. Part A* **2011,** *17*, 381-387.
10. Song, Y.; Wennink, J. W.; Poot, A. A.; Vermes, I.; Feijen, J.; Grijpma, D. W. Evaluation of tubular poly(trimethylene carbonate) tissue engineering scaffolds in a circulating pulsatile flow system. *The International journal of artificial organs* **2011,** *34*, 161-171.
11. Davidsen, M.; Bronnum-Hansen, H.; Jorgensen, T.; Madsen, M.; Gerdes, L. U.; Osler, M.; Schroll, M. Trends in incidence, case-fatality and recurrence of myocardial infarction in the Danish MONICA population 1982-1991. *European journal of epidemiology* **2001,** *17*, 1139-1145.
12. Smolina, K.; Wright, F. L.; Rayner, M.; Goldacre, M. J. Long-term survival and recurrence after acute myocardial infarction in England, 2004 to 2010. *Circulation. Cardiovascular quality and outcomes* **2012,** *5*, 532-540.
13. Drakopoulou, M.; Toutouzas, K.; Michelongona, A.; Tousoulis, D.; Stefanadis, C. Vulnerable plaque and inflammation: potential clinical strategies. *Current Pharmaceutical Design* **2011,** *17*, 4190-4209.

14. Waksman, R.; McEwan, P. E.; Moore, T. I.; Pakala, R.; Kolodgie, F. D.; Hellinga, D. G.; Seabron, R. C.; Rychnovsky, S. J.; Vasek, J.; Scott, R. W.; Virmani, R. PhotoPoint photodynamic therapy promotes stabilization of atherosclerotic plaques and inhibits plaque progression. *Journal of the American College of Cardiology* **2008,** *52*, 1024-1032.
15. Henderson, B. W.; Dougherty, T. J. How does photodynamic therapy work? *Photochemistry and photobiology* **1992,** *55*, 145-157.
16. Guo, H.; Qian, H.; Idris, N. M.; Zhang, Y. Singlet oxygen-induced apoptosis of cancer cells using upconversion fluorescent nanoparticles as a carrier of photosensitizer. *Nanomedicine : nanotechnology, biology, and medicine* **2010,** *6*, 486-495.
17. Ozoemena, K.; Kuznetsova, N.; Nyokong, T. Photosensitized transformation of 4-chlorophenol in the presence of aggregated and non-aggregated metallophthalocyanines. *Journal of Photochemistry and Photobiology A: Chemistry* **2001,** *139*, 217-224.
18. Jenkins, M. P.; Buonaccorsi, G. A.; Raphael, M.; Nyamekye, I.; McEwan, J. R.; Bown, S. G.; Bishop, C. C. Clinical study of adjuvant photodynamic therapy to reduce restenosis following femoral angioplasty. *The British journal of surgery* **1999,** *86*, 1258-1263.
19. Demidova, T. N.; Hamblin, M. R. Macrophage-targeted photodynamic therapy. *International journal of immunopathology and pharmacology* **2004,** *17*, 117-126.
20. Mulder, W. J.; Jaffer, F. A.; Fayad, Z. A.; Nahrendorf, M. Imaging and nanomedicine in inflammatory atherosclerosis. *Science translational medicine* **2014,** *6*, 239sr1.
21. Szelenyi, I. Nanomedicine: evolutionary and revolutionary developments in the treatment of certain inflammatory diseases. *Inflammation research* **2012,** *61*, 1-9.
22. Fang, J.; Nakamura, H.; Maeda, H. The EPR effect: Unique features of tumor blood vessels for drug delivery, factors involved, and limitations and augmentation of the effect. *Advanced drug delivery reviews* **2011,** *63*, 136-151.
23. Lobatto, M. E.; Calcagno, C.; Millon, A.; Senders, M. L.; Fay, F.; Robson, P. M.; Ramachandran, S.; Binderup, T.; Paridaans, M. P.; Sensarn, S.; Rogalla, S.; Gordon, R. E.; Cardoso, L.; Storm, G.; Metselaar, J. M.; Contag, C. H.; Stroes, E. S.; Fayad, Z. A.; Mulder, W. J. Atherosclerotic plaque targeting mechanism of long-circulating nanoparticles established by multimodal imaging. *ACS Nano* **2015,** *9*, 1837-1847.
24. Sanchez-Gaytan, B. L.; Fay, F.; Lobatto, M. E.; Tang, J.; Ouimet, M.; Kim, Y.; van der Staay, S. E.; van Rijs, S. M.; Priem, B.; Zhang, L.; Fisher, E. A.; Moore, K. J.; Langer, R.; Fayad, Z. A.; Mulder, W. J. HDL-mimetic PLGA nanoparticle to target atherosclerosis plaque macrophages. *Bioconjugate chemistry* **2015,** *26*, 443-451.
25. van der Valk, F. M.; van Wijk, D. F.; Lobatto, M. E.; Verberne, H. J.; Storm, G.; Willems, M. C.; Legemate, D. A.; Nederveen, A. J.; Calcagno, C.; Mani, V.; Ramachandran, S.; Paridaans, M. P.; Otten, M. J.; Dallinga-Thie, G. M.; Fayad, Z. A.; Nieuwdorp, M.; Schulte, D. M.; Metselaar, J. M.; Mulder, W. J.; Stroes, E. S. Prednisolone-containing liposomes accumulate in human atherosclerotic macrophages upon intravenous administration. *Nanomedicine : nanotechnology, biology, and medicine* **2015,** *11*, 1039-1046.

26. Berman, J. P.; Farkouh, M. E.; Rosenson, R. S. Emerging anti-inflammatory drugs for atherosclerosis. *Expert opinion on emerging drugs* **2013,** *18*, 193-205.
27. Lorenz, K. J.; Maier, H. Plattenepithelkarzinome im Kopf-Hals-Bereich. *HNO* **2008,** *56*, 402-409.
28. Carstens, M. G.; Bevernage, J. J. L.; van Nostrum, C. F.; van Steenbergen, M. J.; Flesch, F. M.; Verrijk, R.; de Leede, L. G. J.; Crommelin, D. J. A.; Hennink, W. E. Small oligomeric micelles based on end group modified mPEG–oligocaprolactone with monodisperse hydrophobic blocks. *Macromolecules* **2007,** *40*, 116-122.
29. Carstens, M. G.; van Nostrum, C. F.; Verrijk, R.; de Leede, L. G.; Crommelin, D. J.; Hennink, W. E. A mechanistic study on the chemical and enzymatic degradation of PEG-Oligo(epsilon-caprolactone) micelles. *J. Pharm. Sci.* **2008,** *97*, 506-518.
30. Hofman, E. G.; Ruonala, M. O.; Bader, A. N.; van den Heuvel, D.; Voortman, J.; Roovers, R. C.; Verkleij, A. J.; Gerritsen, H. C.; van Bergen En Henegouwen, P. M. EGF induces coalescence of different lipid rafts. *J Cell Sci.* **2008,** *121*, 2519-2528.
31. O'Brien, K. D.; Gordon, D.; Deeb, S.; Ferguson, M.; Chait, A. Lipoprotein lipase is synthesized by macrophage-derived foam cells in human coronary atherosclerotic plaques. *J. Clin. Invest.* **1992,** *89*, 1544-1550.
32. Makhseed, S.; Tuhl, A.; Samuel, J.; Zimcik, P.; Al-Awadi, N.; Novakova, V. New highly soluble phenoxy-substituted phthalocyanine and azaphthalocyanine derivatives: Synthesis, photochemical and photophysical studies and atypical aggregation behavior. *Dyes and Pigments* **2012,** *95*, 351-357.
33. Nombona, N.; Maduray, K.; Antunes, E.; Karsten, A.; Nyokong, T. Synthesis of phthalocyanine conjugates with gold nanoparticles and liposomes for photodynamic therapy. *Journal of photochemistry and photobiology. B, Biology* **2012,** *107*, 35-44.
34. Kuznetsova, N.; Gretsova, N. S.; Kalmykova, E. A.; Makarova, E.; Dashkevich, S. N.; Negrimovsky, V.; Kaliya, O.; Lukyanets, E. Relationship between the photochemical properties and structure of pophyrins and related compounds. *Russian Journal of General Chemistry* **2000,** *70*, 133-140.
35. Ma, J.; Chen, J.-Y.; Idowu, M.; Nyokong, T. Generation of singlet oxygen via the composites of water-soluble thiol-capped CdTe quantum dotssulfonated aluminum Phthalocyanines. *The Journal of Physical Chemistry B* **2008,** *112*, 4465-4469.
36. Tanielian, C.; Schweitzer, C.; Mechin, R.; Wolff, C. Quantum yield of singlet oxygen production by monomeric and aggregated forms of hematoporphyrin derivative. *Free radical biology & medicine* **2001,** *30*, 208-212.
37. Zhu, T. C.; Liu, B.; Kim, M. M.; McMillan, D.; Liang, X.; Finlay, J. C.; Busch, T. M. Comparison of singlet oxygen threshold dose for PDT. *SPIE Int. Soc. Opt. Eng.* **2014,** *8931*, 893101-893118.
38. Kachatkou, D.; Sasnouski, S.; Zorin, V.; Zorina, T.; D'Hallewin, M. A.; Guillemin, F.; Bezdetnaya, L. Unusual photoinduced response of mTHPC liposomal formulation (Foslip). *Photochemistry and photobiology* **2009,** *85*, 719-724.
39. Reshetov, V.; Kachatkou, D.; Shmigol, T.; Zorin, V.; D'Hallewin, M. A.; Guillemin, F.; Bezdetnaya, L. Redistribution of meta-tetra(hydroxyphenyl)chlorin (m-THPC) from conventional and PEGylated liposomes to biological substrates. *Photochemical & photobiological sciences* **2011,** *10*, 911-919.

40. Cramers, P.; Ruevekamp, M.; Oppelaar, H.; Dalesio, O.; Baas, P.; Stewart, F. A. Foscan® uptake and tissue distribution in relation to photodynamic efficacy. *British Journal of Cancer* **2003,** *88*, 283-290.
41. Polo, L.; Valduga, G.; Jori, G.; Reddi, E. Low-density lipoprotein receptors in the uptake of tumour photosensitizers by human and rat transformed fibroblasts. *The international journal of biochemistry & cell biology* **2002,** *34*, 10-23.
42. Chowdhary, R. K.; Sharif, I.; Chansarkar, N.; Dolphin, D.; Ratkay, L.; Delaney, S.; Meadows, H. Correlation of photosensitizer delivery to lipoproteins and efficacy in tumor and arthritis mouse models; comparison of lipid-based and Pluronic P123 formulations. *J. pharm. pharm. sci.* **2003,** *6*, 198-204.
43. Sasnouski, S.; Zorin, V.; Khludeyev, I.; D'Hallewin, M. A.; Guillemin, F.; Bezdetnaya, L. Investigation of Foscan interactions with plasma proteins. *Biochimica et biophysica acta* **2005,** *1725*, 394-402.
44. Talelli, M.; Barz, M.; Rijcken, C. J.; Kiessling, F.; Hennink, W. E.; Lammers, T. Core-crosslinked polymeric micelles: principles, preparation, biomedical applications and clinical translation. *Nano Today* **2015,** *10*, 93-117.
45. Michael-Titus, A. T.; Whelpton, R.; Yaqub, Z. Binding of temoporfin to the lipoprotein fractions of human serum. *British journal of clinical pharmacology* **1995,** *40*, 594-597.
46. Reshetov, V.; Zorin, V.; Siupa, A.; D'Hallewin, M. A.; Guillemin, F.; Bezdetnaya, L. Interaction of liposomal formulations of meta-tetra(hydroxyphenyl)chlorin (temoporfin) with serum proteins: protein binding and liposome destruction. *Photochemistry and photobiology* **2012,** *88*, 1256-1264.
47. Jori, G.; Reddi, E. The role of lipoproteins in the delivery of tumour-targeting photosensitizers. *The International journal of biochemistry* **1993,** *25*, 1369-1375.
48. Berliner, J. A.; Navab, M.; Fogelman, A. M.; Frank, J. S.; Demer, L. L.; Edwards, P. A.; Watson, A. D.; Lusis, A. J. Atherosclerosis: basic mechanisms, oxidation, inflammation, and genetics. *Circulation* **1995,** *91*, 2488-2496.
49. Allison, B. A.; Crespo, M. T.; Jain, A. K.; Richter, A. M.; Hsiang, Y. N.; Levy, J. G. Delivery of benzoporphyrin derivative, a photosensitizer, into atherosclerotic plaque of Watanabe heritable hyperlipidemic rabbits and balloon-injured New Zealand rabbits. *Photochemistry and photobiology* **1997,** *65*, 877-883.
50. Konan, Y. N.; Gurny, R.; Allemann, E. State of the art in the delivery of photosensitizers for photodynamic therapy. *Journal of photochemistry and photobiology. B, Biology* **2002,** *66*, 89-106.
51. Svensson, J.; Johansson, A.; Grafe, S.; Gitter, B.; Trebst, T.; Bendsoe, N.; Andersson-Engels, S.; Svanberg, K. Tumor selectivity at short times following systemic administration of a liposomal temoporfin formulation in a murine tumor model. *Photochemistry and photobiology* **2007,** *83*, 1211-1219.
52. van Nostrum, C. F. Covalently cross-linked amphiphilic block copolymer micelles. *Soft Matter* **2011,** *7*, 3246-3259.

## Supporting information

### S1. Synthesis and characterization of block copolymers

*S1.1. Materials for synthesis*

ε-Caprolactone (ε-CL), Tin (II) 2-ethylhexanoate ($Sn(Oct)_2$), deuterated chloroform ($CDCl_3$) and *p*-nitrophenyl chloroformate (PNC), triethylamine (TEA), $mPEG_{45}$-OH (2000 g/mol), 1-pentanol, benzyl alcohol, naphthalene alcohol, mesyl chloride, aqueous ammonia (25%), sodium hydroxide and dichloromethane were obtained from Sigma-Aldrich (Zwijndrecht, the Netherlands). Other solvents were obtained from Biosolve (Valkenswaard, the Netherlands). Toluene was dried over 4Â molecular sieves (Aldrich) prior to use. All other chemicals were used as received.

*S1.2. Synthesis*

*S1.2.1. Benzoyl-$PCL_n$-OH*

A typical procedure for the synthesis of a benzoyl-$PCL_n$-OH polymer with an average degree of polymerization of 8.0 was done as follows. To ε-CL (25.00 g, 0.21 mol), benzyl alcohol (2.96 g, 0.027 mol) and stannous octoate (1 drop) were added. The melt polymerization was allowed to proceed overnight at 130 °C in a nitrogen atmosphere. The product was dissolved in 50 mL dichloromethane and purified by precipitation in a 20-fold excess of cold (-20 °C) diethyl ether. The Benzoyl-$PCL_8$-OH was filtered and dried overnight *in vacuo* at room temperature to give a white powder (yield: 96%). $^1$H NMR ($CDCl_3$): δ = 7.3 (bs, aromatic protons, benzyl alcohol), 5.1 (s, $CCH_2O$), 4.05 (m, $CH_2CH_2O$), 3.6 (t, $CH_2CH_2OH$), 2.3 (m, $OC(O)CH_2$), 1.6 (m, $CH_2CH_2CH_2CH_2CH_2$), 1.3 (m, $CH_2CH_2CH_2CH_2CH_2$).

*S.1.2.2. Benzoyl-$PCL_n$-PNC*

In a typical procedure, benzoyl-$PCL_8$-OH (4.00 g, 3.6 mmol) was dissolved in 20 mL dry toluene in a nitrogen atmosphere. The solution was cooled to 0 °C and triethylamine (TEA, 0.70 g, 7.2 mmol) and subsequently *p*-nitrophenyl chloroformate (PNC) (1.45 g, 7.2 mmol) was added to the solution while stirring. After 24 h the mixture was filtered to remove the triethylamine HCl salt and the product was precipitated into cold (-20 °C) diethyl ether. The solid fraction was filtered and carefully washed with a small amount of cold (-20 °C) diethyl ether. The resulting product, benzoyl-$PCL_8$-PNC, was dried in a vacuum oven and obtained as a white powder (yield: 95%). $^1$H NMR ($CDCl_3$): δ = 8.3 (d, aromatic protons, PNC), 7.3 (m, aromatic protons, benzyl alcohol and PNC), 5.1 (s, $CCH_2O$), 4.2 (m, $CH_2CH_2OC(O)O$), 4.05 (m, $CH_2CH_2O$), 2.3 (m, $OC(O)CH_2$), 1.6 (m, $CH_2CH_2CH_2CH_2CH_2$), 1.3 (m, $CH_2CH_2CH_2CH_2CH_2$).

### *S.1.2.3. mPEG-$NH_2$*

mPEG-$NH_2$ was synthesized according to a previous procedure (Elbert and Hubbell, 2001). mPEG$_{45}$-OH (50.0 g, 25 mmol) was dissolved in 700 mL of dry toluene and dried by removal of 350 mL of the solvent by azeotropic distillation. After the solution was cooled in an ice-bath, 25 mL of dichloromethane and TEA (14.5 mL, 100 mmol) were added. Subsequently, mesyl chloride (7.73 mL, 100 mmol) was added drop-wise under stirring and allowed to react overnight at room temperature. The solution was filtered and the product was precipitated in a large excess of cold diethyl ether. After drying, the formed mPEG$_{45}$-mesylate was reacted with 100 mL of an aqueous ammonia solution (25%) for 4 days at room temperature. Subsequently the ammonia was allowed to evaporate and the pH of the solution was raised to 13, using 1 M NaOH. The solution was extracted 3 times with 200 mL dichloromethane. The dichloromethane extracts were combined and the solution was concentrated. The mPEG$_{45}$-$NH_2$ was isolated by precipitation in cold diethyl ether, and dried *in vacuo* (yield: 76%). $^1$H NMR ($CDCl_3$): $\delta$ = 3.65 (m, PEG protons), 3.37 (s, $CH_2OCH_3$), 2.94 (t, $CH_2CH_2NH_2$).

### *S1.2.4. Benzoyl-PCL$_n$-PEG$_{45}$*

Benzoyl-PCL$_8$-PNC (1.00 g, 0.707 mmol) was dissolved in 20 mL of dry toluene. mPEG$_{45}$-$NH_2$ (1.41 g, 0.707 mmol) was added and the reaction mixture was stirred for 24 h at room temperature under a nitrogen atmosphere. The mixture was poured into 400 mL of diethyl ether, filtered and carefully washed at least 6 times with diethyl ether to remove p-nitrophenol. The product was dried in a vacuum oven and obtained as a white powder (yield: 97%). $^1$H NMR ($CDCl_3$): $\delta$ = 7.3 (m, aromatic protons, benzyl alcohol), 5.1 (s, $CCH_2O$), 4.05 (m, $CH_2CH_2O$), 3.64 (m, PEG protons), 3.38 (s, $OCH_3$), 2.3 (m, $OC(O)CH_2$), 1.6 (m, $CH_2CH_2CH_2CH_2CH_2$), 1.3 (m, $CH_2CH_2CH_2CH_2CH_2$).

## *S1.3. Polymer characterization*

### *S1.3.1. $^1$H-NMR*

$^1$H NMR spectra were recorded using a Gemini NMR spectrometer (300 MHz, Varian Associates Inc. NMR instruments, Palo Alto, CA). Polymers were dissolved in $CDCl_3$ at a concentration of 0.015 g.mL$^{-1}$. Peak multiplicity was denoted as s (singlet), d (doublet), dd (double doublet), t (triplet), q (quartet), m (multiplet), and b (broad signal).

### *S1.3.2. Gel permeation chromatography*

Relative number average and weight average molecular weights ($M_n$ and $M_w$, respectively), and molecular weight distributions of purified Ben-PCL-PEG copolymers were determined by gel permeation chromatography (GPC, Viscotek, USA) equipped with a PLgel OligoPore column (300x7.5 mm, including a guard column, 50x7.5 mm). Data were obtained from the refractometer. Narrow poly(ethylene glycol) standards ranging from 200 to 5000 g/mol were used for calibration and relative molecular weights were

calculated using the OmniSEC 5.02 software. DMF with LiCl was used as an eluent at a flow rate of 1 mL/min at 30 °C, sample concentrations ranged from 3-5 mg/mL with 100 µL injection volume.



*S1.3.3. Differential scanning calorimetry (DSC)*

Thermal analysis of the Ben-PCL$_n$-PEG$_{45}$ copolymers was carried out using a TA instruments differential scanning calorimeter (TA Discovery series), calibrated with indium. First, the sample (5-10 mg) was cooled to -80 °C and kept at this temperature for 5 min. The sample was then heated to 150 °C at 3 °C/min, annealed for 1 min and subsequently cooled to -80 °C at 3 °C/min. Melting temperatures ($T_m$) were obtained from the peak maxima. The melt enthalpies ($\Delta H_m$) were determined from the area under the curve.

**Results**

A library of poly(ε-caprolactone)-*b*-methoxypoly(ethyleneglycol) block copolymers with benzoyl ester units at the PCL terminus (Ben-PCL-mPEG) was prepared by a modular synthetic approach (Scheme S1). First, Ben-PCL-OH precursors of different chain lengths were synthesized by ring opening polymerization of ε-caprolactone (CL) using benzyl alcohol as initiator and tin(II) 2-ethylhexanoate ($Sn(Oct)_2$) as catalyst (Scheme S1A). The monomer-to-initiator ratios were chosen in such a way that the average degrees of polymerization were between 7 and 19 CL units. After dissolution in dichloromethane and precipitation in cold diethyl ether, the average degree of polymerization of the obtained polymers was calculated by $^1$H NMR spectroscopy from the integral ratios of the $CH_2$ protons of the caprolactone units to the $CH_2$ and aromatic protons of the benzyl alcohol (Fig. S1A). The thus calculated number average molecular weights (Table S1) were in good agreement with the aimed values, based on the monomer to initiator ratio.

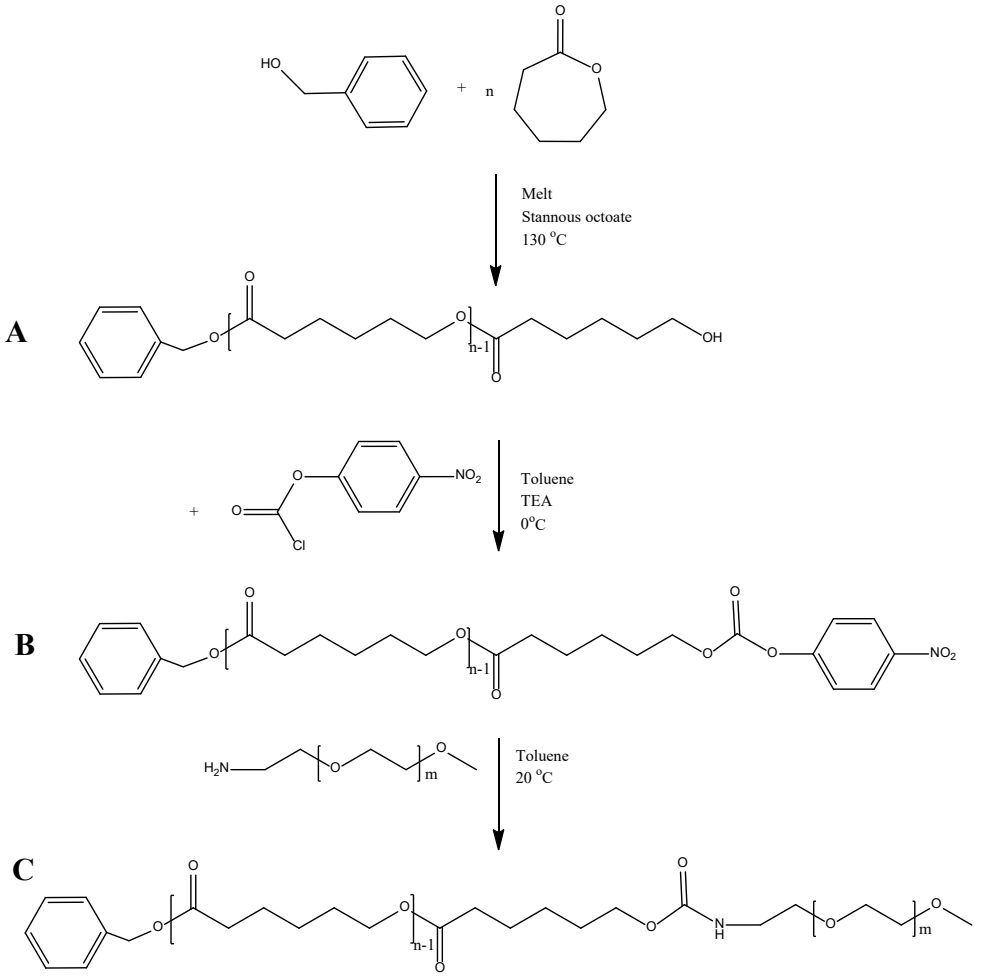


**Scheme S1.** Synthesis route for Ben-PCL-mPEG. A) Ring opening polymerization of ε-caprolactone with benzyl alcohol affords Ben-PCL-OH. B) Activation of the hydroxyl end group with p-nitrophenyl chloroformate. C) Coupling of mPEG-$NH_2$ to the activated Ben-PCL affords amphiphilic Ben-PCL-mPEG.

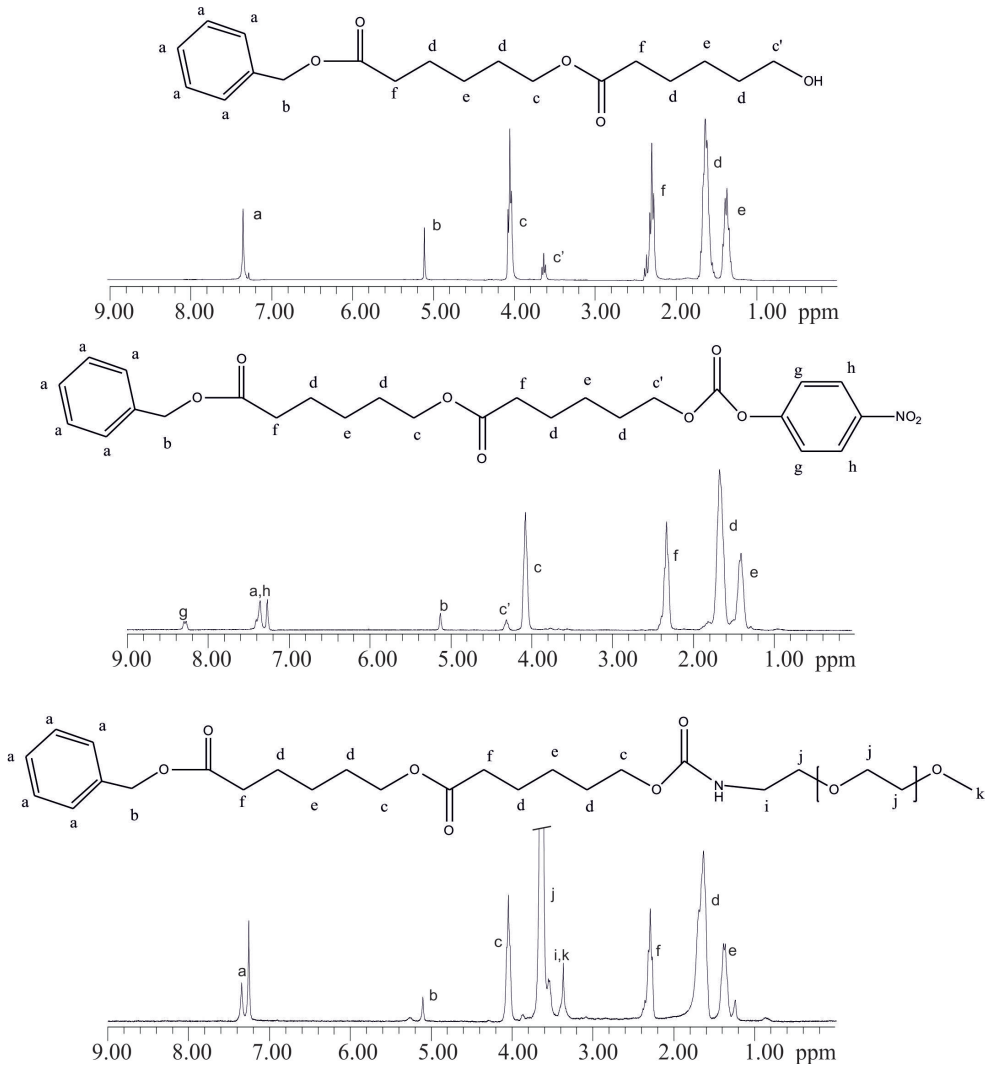


**Figure S1.** $^{1}$H NMR-spectra of A) Ben-PCL$_7$-OH, B) Ben-PCL$_7$-PNC and C) Ben-PCL$_7$-mPEG$_{45}$ measured in $CDCl_3$.

**Table S1.** Properties of synthesized intermediate PCLs and Ben-$PCL_n$-$mPEG_{45}$ block copolymers.

| Polymer | Aimed molecular weight (g/mol) | $M_n$ (g/mol) by $^1$H NMR | $M_n$ (g/mol) by GPC* | $M_w/M_n$ |
|---|---|---|---|---|
| mPEG-$NH_2$ | 2000 | 2100 | 1500 | 1.17 |
| Benzyl-$PCL_7$-OH | 906 | 750 | 440 | 1.08 |
| Benzyl-$PCL_7$-$mPEG_{45}$ | 2906 | 3000 | 2100 | 1.18 |
| Benzyl-$PCL_{11}$-OH | 1362 | 1100 | 600 | 1.10 |
| Benzyl-$PCL_{11}$-$mPEG_{45}$ | 3362 | 3300 | 2250 | 1.15 |
| Benzyl-$PCL_{14}$-OH | 1704 | 1600 | 900 | 1.07 |
| Benzyl-$PCL_{14}$-$mPEG_{45}$ | 3704 | 3650 | 2500 | 1.18 |
| Benzyl-$PCL_{19}$-OH | 2374 | 2200 | 1250 | 1.10 |
| Benzyl-$PCL_{19}$-$mPEG_{45}$ | 4274 | 4200 | 2700 | 1.19 |

* Relative $M_n$ using PEG for calibration.

The hydroxyl end groups of the different Ben-$PCL_n$-OH polymers were subsequently reacted with *p*-nitrophenyl chloroformate to yield *p*-nitrophenyl carbonate substituted polymers (PNC) (Scheme S1B). The $^1$H-NMR spectra showed the appearance of a new signal originating from the nitrophenyl protons at 7.4 and 8.3 ppm (Fig. S1B). Furthermore, the protons at position c' shifted from 3.6 to 4.3 ppm due to the substitution of the OH end group with PNC. The $^1$H-NMR spectra revealed that high conversions (>97%) were obtained based on the integral ratios of the signals.
Ben-$PCL_n$-$mPEG_{45}$ copolymers were subsequently obtained by reacting Ben-$PCL_n$-PNC and $mPEG_{45}$-$NH_2$ at a 1:1 ratio in toluene at room temperature (Scheme S1C). The $^1$H-NMR spectra (Fig. S1C) showed that peaks originating from the PNC disappeared and c' shifted to 4.05 ppm. The NH protons of the formed carbamate bonds were found at 5.3 ppm indicating successful coupling of the $mPEG_{45}$-$NH_2$ and Ben-$PCL_n$-PNC.
Molecular weights of Ben-$PCL_7$-$mPEG_{45}$, Ben-$PCL_{11}$-$mPEG_{45}$, Ben-$PCL_{14}$-$mPEG_{45}$ and Ben-$PCL_{19}$-$mPEG_{45}$ obtained by gel permeation chromatography (GPC) and by NMR in table S1.

## S2. Micelle characterization

### *S2.1. Critical micelle concentration (cmc)*

The cmc was determined with the pendant drop method using a home build setup consisting of a syringe with a needle (ø 1.5 mm) mounted in a syringe pump in front of a light source. A droplet with a volume of 15 µL was formed at a velocity of 2 µL/s and a picture was taken with an OCA 15EC camera. The surface tension was calculated according to the Young-Laplace equation using the SCA 20 software. To determine the critical micelle concentration, solutions/dispersions of Ben–PCL-mPEG

block copolymer with concentration ranging from 0.0001 to 10 mg/mL were prepared. By plotting the surface tension against the logarithm of the polymer concentration, the inflection point in the graph and thus the critical micelle concentration was determined. Measurements were performed at room temperature.

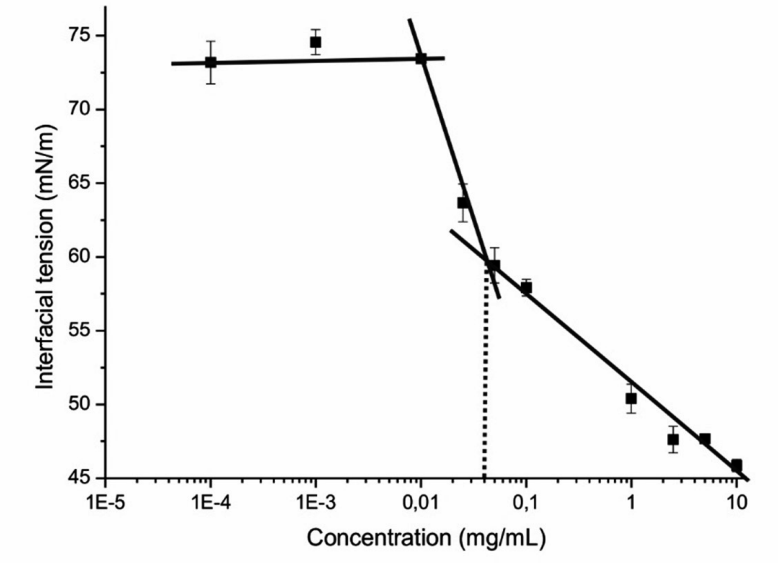


**Figure S2.** Critical micelle concentration of Ben-$PCL_7$-$mPEG_{45}$, determined by the pendant drop method. Interfacial tension was plotted against the logarithm of the polymer concentration, the inflection point in the graph and thus the critical micelle concentration was determined at 0.04 mg/mL for Ben-$PCL_7$-$mPEG_{45}$.

*S2.2. Dynamic light scattering*

The size and the size distribution of empty particles were measured by dynamic light scattering (DLS) using a Malvern CGS-3 multi-angle goniometer (Malvern ltd., Malvern), consisting of a HeNe laser source (λ=632.8nm, 22mW output power), temperature controller (Julabo water bath) and a digital correlator ALV-5000/EPP. Time correlation functions were analyzed using the ALV-60X0 Software V.3.X provided by Malvern, to obtain the Z-average hydrodynamic diameter of the particles ($Z_{ave}$) and the particle size distribution (polydispersity index, PDI). The samples in PBS were analyzed at 25 °C.

**Table S2.** Size and size distribution of empty Ben-$PCL_n$-$mPEG_{45}$ micelles and thermal properties of Ben-$PCL_n$-$mPEG_{45}$ copolymers.

| Polymer | Z-average diameter (nm)* | PDI[a] | PCL $T_m$ (°C) | PCL $\Delta H_m$ (J/g) | PEG $T_m$ (°C) | PEG $\Delta H_m$ (J/g) |
|---|---|---|---|---|---|---|
| Benzyl-$PCL_7$-$mPEG_{45}$ | 16±1 | 0.06±0.02 | 13.1 | 5.1 | 50.9 | 60.6 |
| Benzyl-$PCL_{11}$-$mPEG_{45}$ | 25±1 | 0.16±0.02 | 36.4 | 9.0 | 46.5 | 41.0 |
| Benzyl-$PCL_{14}$-$mPEG_{45}$ | 42±2 | 0.26±0.07 | 42.7 | 14.7 | 48.8 | 19.8 |
| Benzyl-$PCL_{19}$-$mPEG_{45}$ | 56±3 | 0.37±0.07 | 45.7† | 61.5† | † | † |

*N=3

†melting curves of PEG and PCL overlap in the DSC thermograms.

## S3. Other results

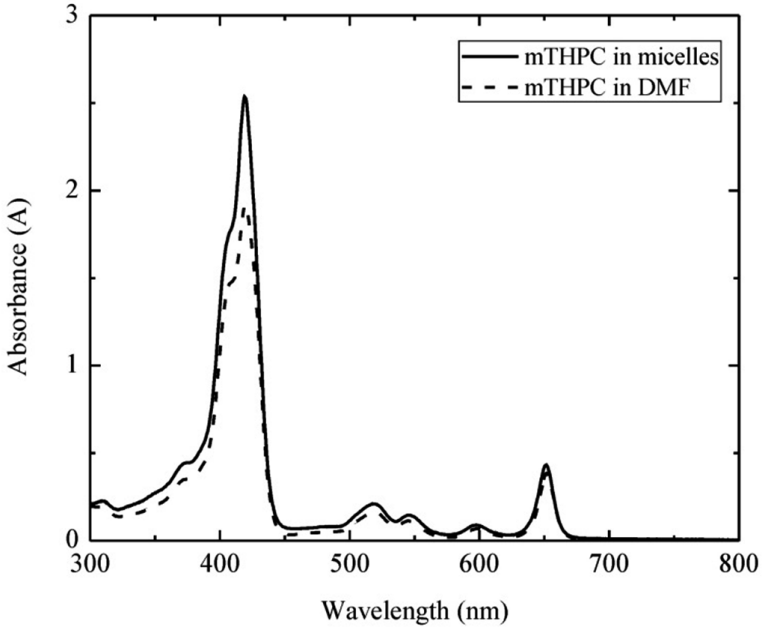


**Figure S3.** UV absorbance spectra of similar concentrations of mTHPC in DMF and mTHPC loaded in Ben-$PCL_7$-$mPEG_{45}$ micelles (at 20% loading).

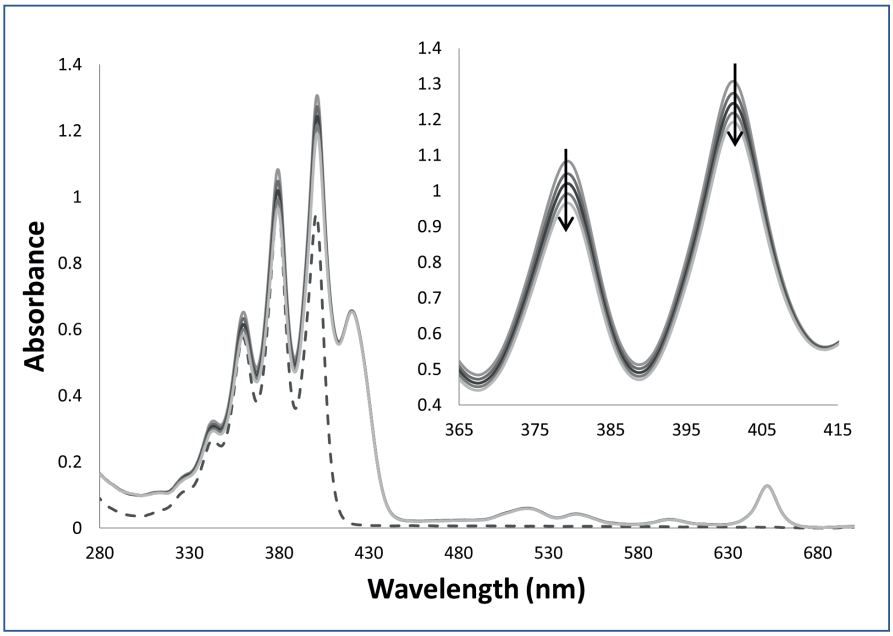


**Figure S4.** Time-dependent (t = 0 - 40 s) photobleaching of ADMA absorption in the presence of mTHPC-loaded micelles (2 mg/ml Ben-PCL-PEG, 0.05 mg/mL mTHPC, approx. 25× diluted) in $D_2O$, which is directly related to the photoinduced generation of singlet oxygen by the photosensitizer. Broken line is the spectrum of pure ADMA. Inset: detail of AMDA absorption decrease.

**Table S3**. Quantum yield and irradiation times (amounts are stock concentrations per mL; all samples have been diluted to a maximum Q-band absorption of 0.1 for mTHPC.

| | SAMPLE | $\phi_{\Delta\ (D2O)}$ | Irradiation time (s) * |
|---|---|---|---|
| | Eosin Y (reference) | 0,60 | 6 |
| **Varying polymer concentration (mTHPC: 0,4 mg)** | **10** mg BEN | 0,224 | 10 |
| | **8** mg BEN | 0,216 | 10 |
| | **6** mg BEN | 0,166 | 14 |
| | **4** mg BEN | 0,096 | 30 |
| | **2** mg BEN | 0,034 | 55 |
| **Varying mTHPC concentration (BEN-PCL7-PEG2000: 10 mg)** | **2** mg mTHPC | 0,076 | 20 |
| | **1** mg mTHPC | 0,164 | 15 |
| | **0,5** mg mTHPC | 0,224 | 10 |
| | **0,25** mg mTHPC | 0,319 | 10 |
| | **0,1** mg mTHPC | 0,425 | 8 |
| | **0,05** mg mTHPC | 0,461 | 7 |
| | **0,035** mg mTHPC | 0,409 | 8 |
| | **0,02** mg mTHPC | 0,267 | 12 |
| | **0,005** mg mTHPC | 0,280 | 20 |

* Time interval required to reach 3-4% decrease in ADMA absorption

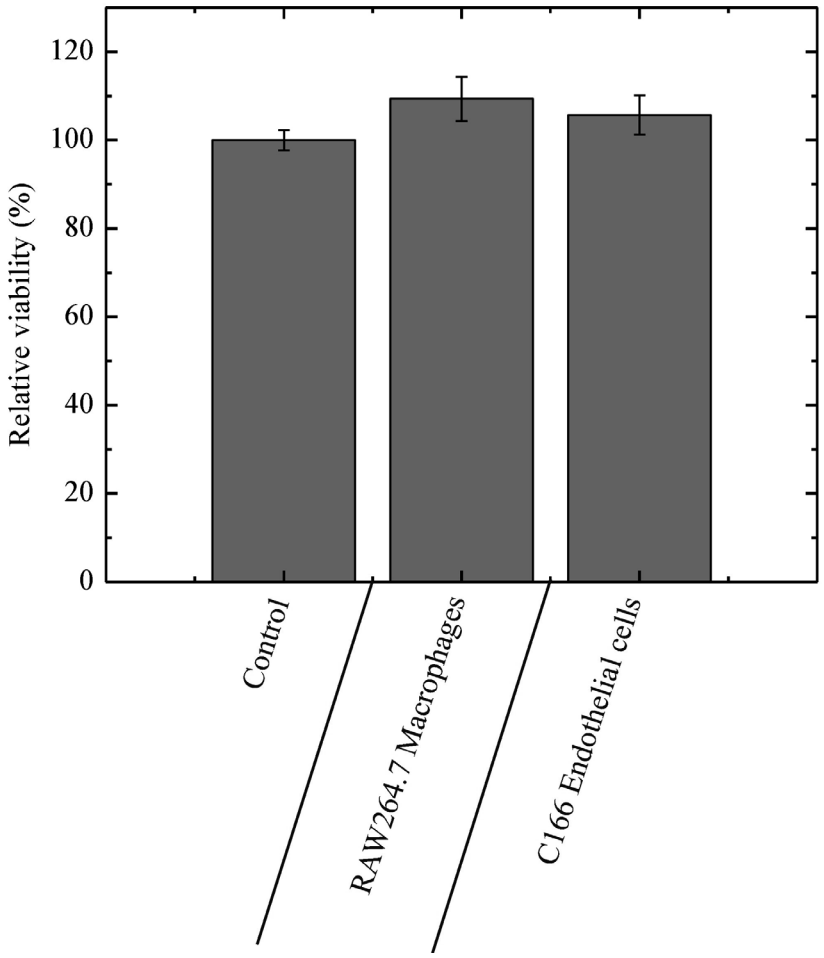


**Figure S5.** Dark-cytotoxicity by MTS assay of RAW264.7 macrophages and C166 endothelial cells incubated with 0.5 mg/mL Ben-$PCL_7$-$mPEG_{45}$ polymer and 100 μg/mL mTHPC; after 24 hours.

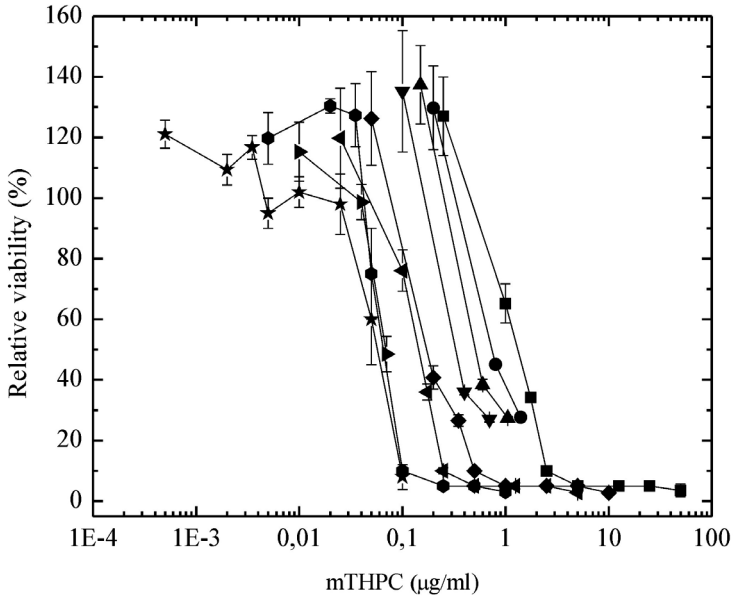


**Figure S6.** Photocytotoxicity by MTS assay of fixed polymer concentrations and varying mTHPC loadings on RAW264.7 macrophages after 24 hours of incubation. The cells were illuminated for 10 minutes, 3.04 mW/cm$^2$. Samples above the CMC are: 0.5 mg/mL Ben-PCL$_7$-mPEG$_{45}$, 0.4 mg/mL Ben-PCL$_7$-mPEG$_{45}$, 0.3 mg/mL Ben-PCL$_7$-mPEG$_{45}$, 0.2 mg/mL Ben-PCL$_7$-mPEG$_{45}$, 0.1 mg/mL Ben-PCL$_7$-mPEG$_{45}$, 0.05 mg/mL Ben-PCL$_7$-mPEG$_{45}$; Samples below the CMC are: 0.02 mg/mL Ben-PCL$_7$-mPEG$_{45}$, 0.01 mg/mL Ben-PCL$_7$-mPEG$_{45}$ and 0.001 mg/mL Ben-PCL$_7$-mPEG$_{45}$.

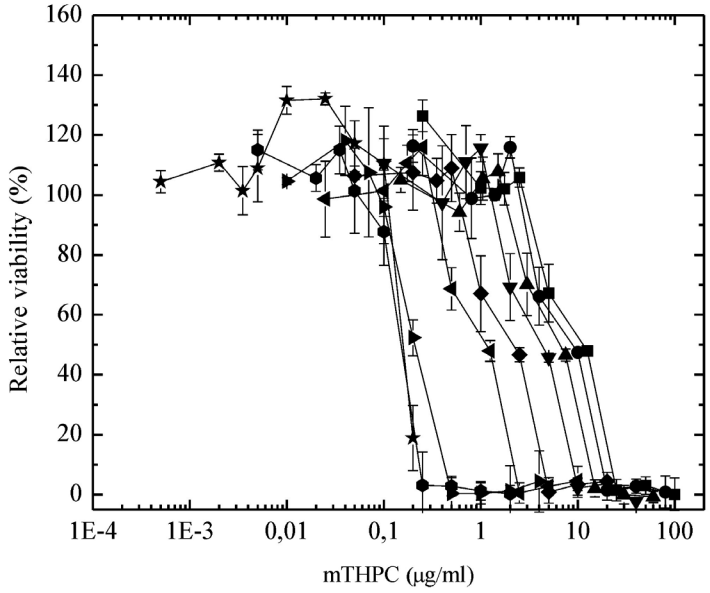


**Figure S7.** Photocytotoxicity by MTS assay of fixed polymer concentrations and varying mTHPC loadings on C166 endothelial cells after 24 hours of incubation. The cells were illuminated for 10 minutes, 3.04 mW/cm$^2$. Samples above the cmc are: 0.5 mg/mL Ben-PCL$_7$-mPEG$_{45}$, 0.4 mg/mL Ben-PCL$_7$-mPEG$_{45}$, 0.3 mg/mL Ben-PCL$_7$-mPEG$_{45}$, 0.2 mg/mL Ben-PCL$_7$-mPEG$_{45}$, 0.1 mg/mL Ben-PCL$_7$-mPEG$_{45}$, 0.05 mg/mL Ben-PCL$_7$-mPEG$_{45}$; Samples below the cmc are: 0.02 mg/mL Ben-PCL$_7$-mPEG$_{45}$, 0.01 mg/mL Ben-PCL$_7$-mPEG$_{45}$ and 0.001 mg/mL Ben-PCL$_7$-mPEG$_{45}$.

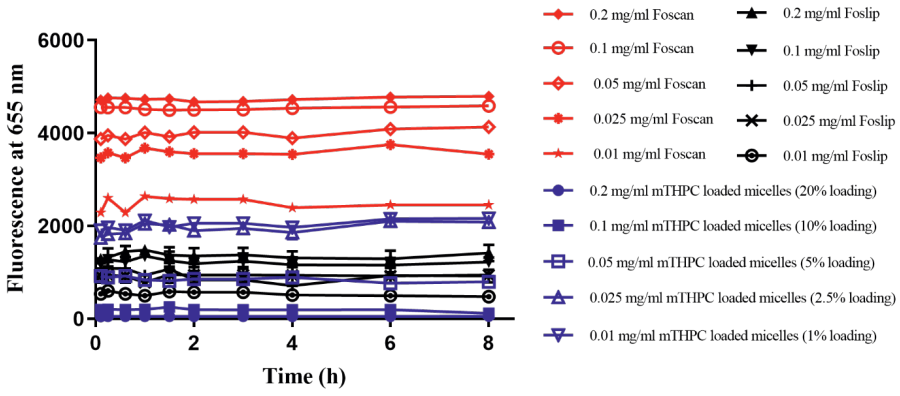


**Figure S8.** Fluorescence intensity ($\lambda_{ex}$ 420 nm, $\lambda_{em}$ 655 nm) as a function of time at 37 ℃; Foscan® and Foslip® stock solutions were diluted in ethanol : propylene glycol (40:60) and PBS (pH 7.4), respectively, while micelles of 10 mg/mL with different loading amounts (1% - 20% w/w) were individually prepared and diluted 10× in PBS, to obtain the indicated mTHPC concentrations.

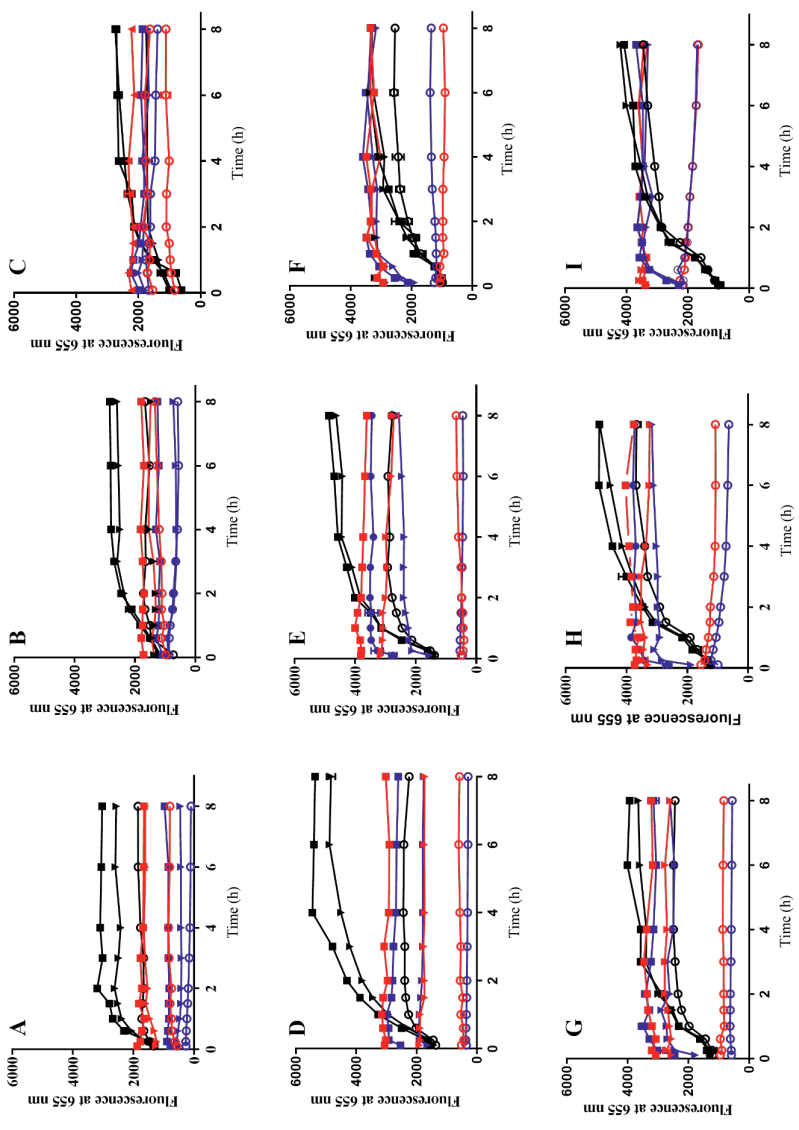


**Figure S9.** A)-I) Fluorescence intensity ($\lambda_{ex}$ 420 nm, $\lambda_{em}$ 655 nm) as a function of time at mTHPC concentration of 0.1 mg/mL (A, D, G), 0.05 mg/mL (B, E, H) and 0.025 mg/mL (C, F, I) in FBS, mouse plasma and human plasma, respectively. Foscan®, Foslip® and mTHPC loaded micelles were 10× diluted with FBS or plasma solutions and incubated while the mTHPC fluorescence was recorded at 37 °C over a period of 8 h (in duplicate). In A)-I) black lines, red lines and blue lines represent Foslip®, Foscan® and mTHPC loaded micelles ,respectively. Squares, triangles and open dots are for all samples in 90%, 50% and 10% FBS or plasma, respectively.

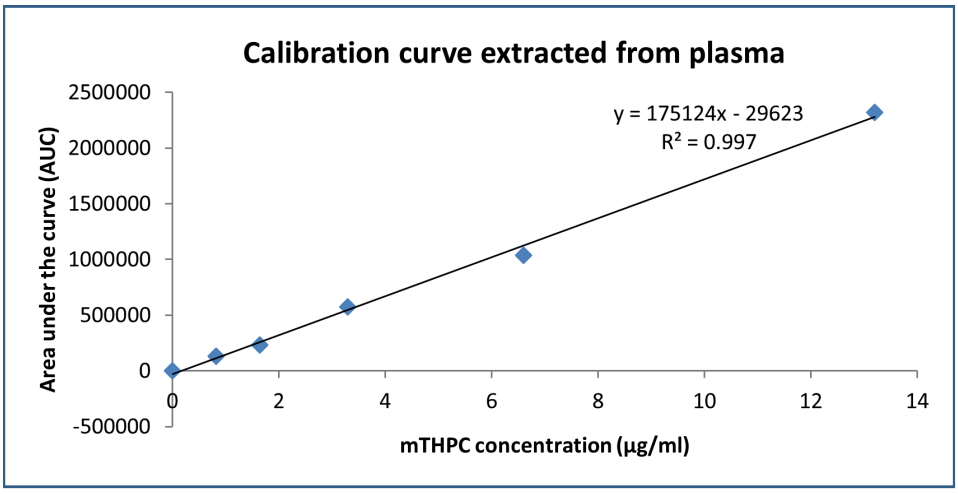


**Figure S10.** Calibration plot of the area under the peak versus mTHPC concentration from HPLC analysis after extraction from Balb/c mice plasma.

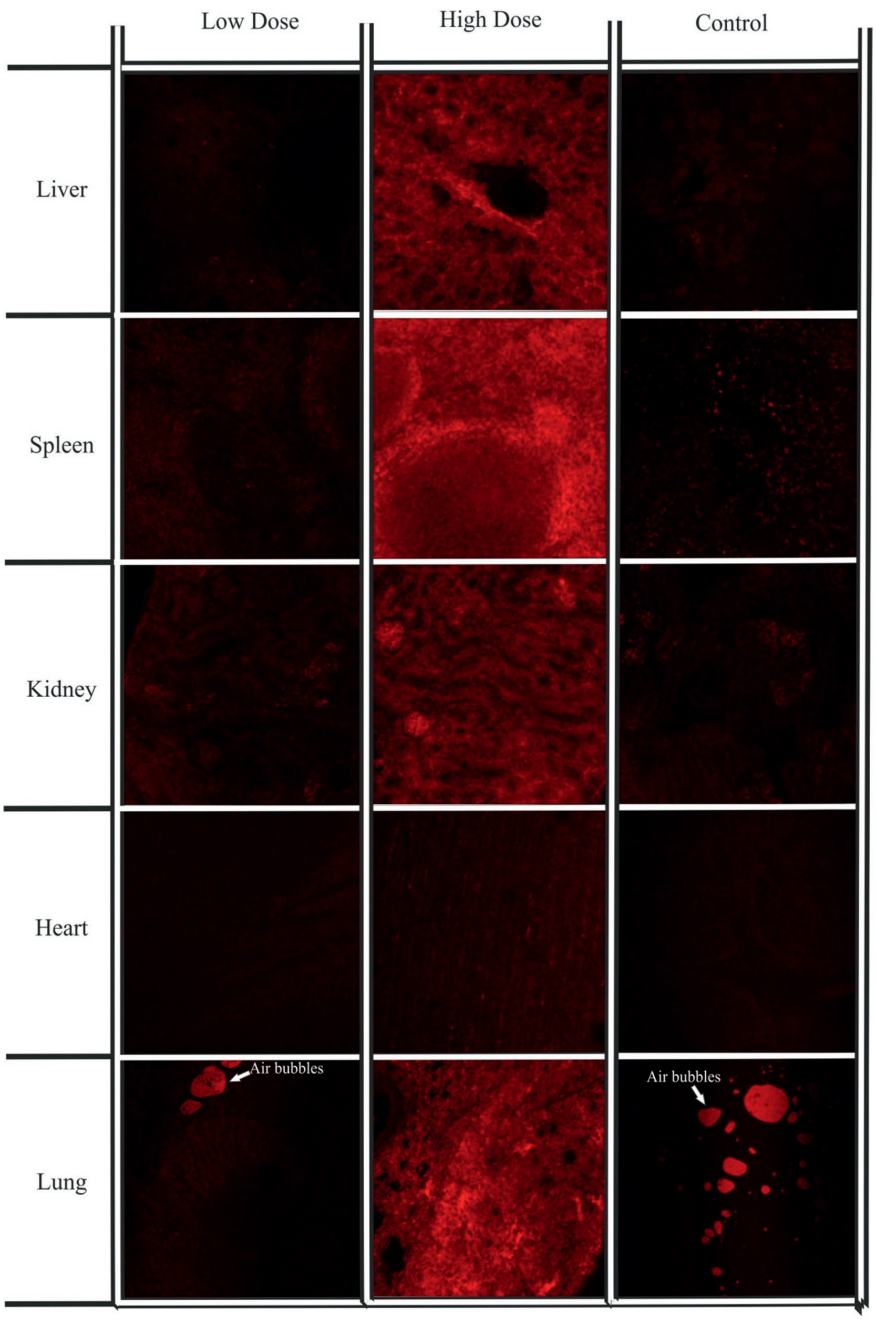


**Figure S11.** Confocal fluorescence images of organs in LDLR$^{-/-}$ApoB$^{100/100}$ mice.

# 3

# Chapter 3

## EGFR Targeted Nanobody Functionalized Polymeric Micelles Loaded with mTHPC for Selective Photodynamic Therapy

Yanna Liu [1], Luca Scrivano [1], Julia Denise Peterson [1], Marcel H.A.M. Fens [1], Irati Beltrán Hernández [1,2], Bárbara Mesquita [1], Javier Sastre Toraño [3], Wim E. Hennink [1], Cornelus F. van Nostrum [1], and Sabrina Oliveira [1,2*]

[1] Department of Pharmaceutics, Utrecht Institute for Pharmaceutical Sciences, Utrecht University, Utrecht, the Netherlands.
[2] Division of Cell Biology, Department of Biology, Utrecht University, Utrecht, the Netherlands.
[3] Department of Chemical Biology & Drug Discovery, Utrecht Institute for Pharmaceutical Sciences, Utrecht University, Utrecht, the Netherlands.

*Molecular Pharmaceutics 2020, 17, 1276−1292*

**Abstract**

Meta-tetra(hydroxyphenyl)chlorin (mTHPC) is one of the most potent second generation photosensitizers, clinically used for photodynamic therapy (PDT) of head and neck squamous cell carcinomas. However, improvements are still required concerning its present formulation (*i.e.* Foscan®, a solution of mTHPC in ethanol/propylene glycol (40:60 w/w)), as mTHPC has the tendency to aggregate in aqueous media, *e.g.* biological fluids, and it has limited tumor specificity. In the present study, polymeric micelles with three different diameters (17, 24 and 45 nm) based on benzyl-poly(ε-caprolactone)-*b*-poly(ethylene glycol) ($PCL_n$-PEG; n=9, 15 or 23) were prepared with mTHPC loadings ranging from 0.5 to 10 wt% using a film hydration method as advanced nano-formulations for this photosensitizer. To favor the uptake of the micelles by cancer cells that over-express the epidermal growth factor receptor (EGFR), the micelles were decorated with an EGFR targeted nanobody (named EGa1) through maleimide-thiol chemistry. The enhanced binding of the EGFR targeted micelles at 4 °C to EGFR over-expressing A431 cells, compared to low EGFR expressing HeLa cells, confirmed the specificity of the micelles. In addition, an enhanced uptake of mTHPC loaded micelles by A431 cells was observed when these were decorated with EGa1 nanobody, compared to non-targeted micelles. Both binding and uptake of targeted micelles were blocked by an excess of free EGa1 nanobody, demonstrating that these processes occur through EGFR. In line with this, mTHPC-loaded in EGa1-conjugated $PCL_{23}$-PEG (EGa1-$P_{23}$) micelles demonstrated 4 times higher photocytotoxicity on A431 cells, compared to micelles lacking the nanobody. Importantly, EGa1-$P_{23}$ micelles also showed selective PDT against A431 cells compared to the low EGFR-expressing HeLa cells. Finally, an *in vivo* pharmacokinetic study shows that after iv injection, mTHPC incorporated in the $P_{23}$ micelles displayed prolonged blood circulation kinetics, compared to free mTHPC, independently of the presence of EGa1. Thus, these results make these micelles a promising nanomedicine formulation for selective therapy.

**Keyword:** nanobody, targeting, polymeric micelles, selectivity, photodynamic therapy, EGFR

## 1. Introduction

Head and neck squamous cell carcinomas (HNSCC) are the 6th most prevalent malignancy globally, involving carcinomas in the mouth, throat, larynx, sinuses and lymph nodes of the neck and responsible for more than 650,000 new cases and about 330,000 deaths annually.[1,2] Photodynamic therapy (PDT) has attracted much attention in recent years as a treatment modality for HNSCC. This topical and minimally invasive treatment has decreased the likelihood of adverse side effects, such as late organ dysfunction, xerostomia and dysphagia, which are associated with conventional modalities, such as surgery and radiotherapy.[3-5] PDT involves illumination of oxygenated tissue after the systemic administration of a photosensitizer (PS).[6-8] The PS is activated by light of the absorbed wavelength, locally applied in the abnormal tissue by surface illumination or optical fibers.[6] The activated PS subsequently transfers its energy to nearby molecular oxygen, producing oxygen radicals and other reactive oxygen species (ROS). These ROS in turn cause oxidation of cellular components such as nucleic acids, proteins and lipids, inducing cellular apoptosis and/or necrosis, which subsequently leads to break-down of tumor associated vasculature and immune stimulation for tumor destruction.[6,9]
The highly potent, second-generation PS, meta-tetra(hydroxyphenyl)chlorin (mTHPC), also known by its generic name Temoporfin, has many advantages over first-generation photosensitizers (*e.g.* stronger phototoxicity and a longer absorption wavelength which is beneficial for light penetration in tumor tissue).[10,11] Its commercial formulation, Foscan® (solution in ethanol: propylene glycol 40:60 w/w), has been approved for PDT of HNSCC.[1,10] However, like most of the photosensitizers, mTHPC's hydrophobic characteristic (logP: ~9) promotes non-specific binding to cells, resulting in disposition of PS also in normal healthy tissues (*i.e.* no selective accumulation of the PS in tumorous tissues), which is responsible for damage to surrounding healthy tissues and the frequently observed and unwanted cutaneous photosensitivity in patients.[9,11-13] Additionally, upon administration, mTHPC is prone to aggregation in biological fluids, leading to lower ROS production and decreased therapeutic efficacy.[14,15]
To address these drawbacks, two liposomal mTHPC formulations are currently on the market: Foslip® and its PEGylated form FosPEG®, in which a polyethylene glycol (PEG) coating on the surface of the liposomes provides stealth characteristics, avoiding its recognition and rapid uptake by the reticuloendothelial system (RES) and resulting in longer circulation in blood.[13,16-18] Both liposomal mTHPCs have the ability to package large quantities of mTHPC into their lipid bilayers, and several publications describe some improvements regarding the selective accumulation of mTHPC in tumors due to the enhanced permeability and retention (EPR) effect,[19-21] even though both formulations showed a rapid release of the payload in the first 3 h after injection.[13,18,22] However, the relatively large hydrodynamic diameters of those liposomes (~110 nm) can cause heterogeneous distribution in the tumor tissues and inability

to penetrate the tumor interstitial matrix to reach the interior tumor cells, which can compromise their therapeutic efficacy.[23-27]

Polymeric micelles, consisting of a hydrophilic stealth corona (most commonly based on PEG), and a hydrophobic core that is suitable for accommodating hydrophobic compounds, are attractive and alternative drug delivery systems for hydrophobic drugs, particularly cytostatic agents.[28-31] Most importantly, polymeric micelles have small hydrodynamic diameters that can be tailored by the composition and molecular weight of the micelles forming block copolymers, as well as by the processing conditions.[32-34] Their small size, generally below 60 nm, makes them more suitable to extravasate the bloodstream, retain at the tumor through the EPR effect (passive targeting), and subsequently penetrate into the interior of the tumor with uniform distribution, being crucial factors for anti-tumoral efficacy of nanomedicines.[23,25,35]

After passive accumulation in tumors, furnishing a specific ligand on the surface of micelles was proposed to compensate for the potentially diminished uptake by the target cells due to the hydrophilic PEG layer and also to favor the intracellular internalization of the active payload by the target cancer cells.[36-39] Many cancer cells overexpress receptors that can be recognized by and interact with specific ligands, such as growth factors, antibodies, antibody fragments, or peptides, leading to enhanced target cell internalization of nanoparticles that have their surface decorated with these ligands.[40] A well-explored receptor in the context of HNSCC is the epidermal growth factor receptor (EGFR).[41] Nanobodies are small antibody fragments originated from heavy chain-only antibodies present in the blood of Camelidae. Also known as single domain antibodies, they are characterized by their small size, high stability, low immunogenic potential and high binding affinities to their antigens.[42-44] The EGFR targeted nanobody EGa1 has demonstrated its ability to bind to EGFR and be internalized by EGFR over-expressing cells, when conjugated to the surface of liposomes and polymeric micelles, without triggering EGFR's cascade of events for growth promotion.[38,43] It is worth noting that studies have suggested that small micelles especially in the hydrodynamic diameter range of 60 nm or less would be favorable for effectively binding the receptor and inducing receptor-mediated endocytic processes.[26,45-48]

In the present study, we synthesized poly(ε-caprolactone)-*b*-methoxypoly(ethylene glycol) ($PCL_n$-PEG) based copolymers with varying chain lengths of $PCL_n$ (n=9, 15, 23) and a fixed molecular weight of PEG (2 kDa), and used film hydration of these polymers to prepare mTHPC-loaded micelles with diameters less than 50 nm. Previously we showed that PCL-PEG micelles (around 28 nm in size) decorated with an EGFR targeted nanobody were selectively taken up by high EGFR over-expressing A431 cells, compared to EGFR negative E98 cells.[49] To further elaborate on this observation, in the present work we decorated the micelles having three different diameters (17, 24 and 45 nm) with EGFR targeted nanobody EGa1, using maleimide-thiol click chemistry.[50] The cellular binding and uptake of these micelles loaded with mTHPC

were evaluated by confocal fluorescence microscopy, using the EGFR over-expressing A431 cell line and the low EGFR expressing HeLa cell line. Photocytotoxicity of the micellar PS formulations was evaluated on both cell lines to reveal the potential of these formulations to improve the selectivity of PDT to EGFR over-expressing tumor cells. Finally, the *in vitro* stability and the *in vivo* pharmacokinetics of these micellar mTHPC formulations were studied in human plasma and A431 tumor-bearing mice, respectively.



## 2. Meterials and methods

### *2.1 Materials*

Poly(ethylene glycol) methyl ether amine (PEG-$NH_2$, 2000 g/mol) was synthesized as previously reported.[51] *N*-succinimidyl-*S*-acetylthioacetate (SATA, Pierce™) was purchased from Thermo Fisher Scientific (Massachusetts, USA). Maleimide-poly(ethylene glycol)-amine trifluoroacetic acid (Mal-PEG-$NH_2$·TFA, 2000 g/mol) was purchased from JenKem Technology (Dallas, USA). *m*-Tetra(hydroxyphenyl) chlorin (mTHPC) was obtained from Molekula (Munich, Germany). Optimem phenol red free (OptiMEM) was purchased from Invitrogen (Bleiswijk, the Netherlands). Hoechst 33342 solution (20 mM) was purchased from Thermo Fisher (Bleiswijk, the Netherlands). CellTiter 96® AQueous One Solution was obtained from Promega (Leiden, the Netherlands). All other reagents and deuterated chloroform ($CDCl_3$), dichloromethane (DCM) and toluene were obtained from Sigma-Aldrich (Zwijndrecht, the Netherlands). Phosphate-buffered saline (PBS, pH 7.4, containing 11.9 mM phosphates, 137 mM sodium chloride and 2.7 mM potassium chloride) was obtained from Fisher Bioreagents (Bleiswijk, the Netherlands). 7,9-dioxa-2,3-dithiaspiro[4.5] decan-8-one (*i.e.* 1,2-dithiolane-substituted trimethylene carbonate, DTC) was kindly provided by prof. Zhiyuan Zhong (Soochow University, SuZhou, China). Cyanine7 maleimide (Cy7-maleimide) was ordered from Lumiprobe Corporation (Hannover, Germany). All other solvents were obtained from Biosolve (Valkenswaard, the Netherlands). DCM, ε-caprolactone (ε-CL) and toluene were dried over 4Å molecular sieves (Sigma-Aldrich, Zwijndrecht, the Netherlands) prior to use. PEG-$NH_2$ and Mal-PEG-$NH_2$·TFA were dried overnight under vacuum at room temperature prior to use. All other reagents were used as received.

### *2.2 Synthesis of copolymers*

#### *2.2.1 Synthesis of benzyl-poly(ε-caprolactone)*

Benzyl-poly(ε-caprolactone)$_n$ ($PCL_n$-OH) with different degrees of polymerization were synthesized as previously described with a slight modification.[51] Benzyl alcohol (1.03 mL, 10 mmol) and ε-CL (6.09 mL (55 mmol), 15.74 mL (142 mmol) or 25.49 mL (230 mmol)) were introduced into a round flask and stirred at 130 °C under vacuum for

5 h to remove traces of water. Subsequently, $Sn(Oct)_2$ (0.02 mL, 0.5 mmol) was added and the reaction was allowed to occur under a nitrogen atmosphere for 4 to 6 h (until the complete conversion of ε-CL, as monitored by $^1$H-NMR). After cooling down to room temperature (RT), the formed PCL oligomers were dissolved in 10 mL of DCM and purified by precipitation in a 20-fold excess of cold diethyl ether (-20 °C). The precipitated products were recovered by filtration and the final products were obtained as a whitish powder after drying under vacuum overnight. $^1$H-NMR ($CDCl_3$): δ = 7.35 (b, aromatic protons, benzyl alcohol), 5.11 (s, $CCH_2O$), 4.05 (m, $CH_2CH_2O$), 3.65 (t, $CH_2CH_2OH$), 2.30 (m, $OC(O)CH_2$), 1.65 (m, $CH_2CH_2CH_2CH_2CH_2$), 1.38 (m, $CH_2CH_2CH_2CH_2CH_2$).

### *2.2.2 Synthesis of benzyl-poly(ε-caprolactone)-p-nitrophenyl formate*

The terminal hydroxyl group of $PCL_n$-OH was activated by nitrophenyl chloroformate (PNC) to obtain benzyl-poly(ε-caprolactone)-*p*-nitrophenyl formate ($PCL_n$-PNFs) according to a previous procedure with slight modification.[51] In short, the above obtained $PCL_n$ oligomers (4 g, corresponding to 3.5 mmol (n = 9), 2.2 mmol (n = 15), 1.5 mmol (n = 23)) were separately dissolved in 20 mL of dried toluene, followed by addition of triethylamine (TEA) (1.8 mL (13 mmol) for n = 9, 1.1 mL (7.7 mmol) for n = 15 or 0.7 mL (5.1 mmol) for n = 23) and PNC (2.64 g (13 mmol) for n = 9, 1.6 g (7.7 mmol) for n = 15, 0.5 g (5.1 mmol) for n = 23) with agitation. The reaction proceeded overnight with magnetic stirring at RT under a nitrogen atmosphere. The formed TEA·HCl precipitate was removed by centrifugation (5000 rpm, RT). The remaining supernatant was dropped into cold diethyl ether (-20 °C), and the precipitated solids were collected after filtration and drying under vacuum overnight. This procedure was repeated one time more and the final products were obtained as white powders. $^1$H-NMR ($CDCl_3$): δ = 8.27 (d, aromatic protons, PNF), 7.38 (m, aromatic protons, benzyl alcohol and PNF), 5.11 (s, $CCH_2O$), 4.29 (m, $CH_2CH_2OC(O)O$), 4.05 (m, $CH_2CH_2O$), 2.30 (m, $OC(O)CH_2$), 1.65 (m, $CH_2CH_2CH_2CH_2CH_2$), 1.38 (m, $CH_2CH_2CH_2CH_2CH_2$).

### *2.2.3 Synthesis of benzyl-poly(ε-caprolactone)-b-methoxy-poly(ethylene glycol)*

Benzyl-poly(ε-caprolactone)$_n$-*b*-methoxy-poly(ethylene glycol) ($PCL_n$-PEG) copolymers were synthesized as follows.[51] In brief, to a solution of PEG-$NH_2$ (0.6 g, 0.3 mmol) in 10 mL of dry toluene, the above obtained $PCL_n$-PNFs (0.3 mmol) were separately added. The reaction mixtures were stirred over night at RT under a nitrogen atmosphere. Next, the obtained solutions (yellowish due to released *p*-nitrophenol) were dropped in diethyl ether at RT and the yellowish polymer precipitates were collected after filtration. After evaporating remaining organic solvent under a nitrogen stream, the collected products were then suspended in deionized water and dialyzed (tubing with MWCO of 10 kDa) against water for 12 h to remove traces of the *p*-nitrophenol and unreacted PEG-

$NH_2$. After freeze-drying, the final products were obtained as white powders. $^1$H-NMR ($CDCl_3$): δ = 7.35 (b, aromatic protons, benzyl alcohol), 5.11 (s, CC$H_2$O), 4.05 (m, $CH_2CH_2O$), 3.64 (m, PEG protons), 3.38 (s, OC$H_3$), 2.30 (m, OC(O)C$H_2$), 1.65 (m, $CH_2CH_2CH_2CH_2CH_2$), 1.38 (m, $CH_2CH_2CH_2CH_2CH_2$).

*2.2.4 Synthesis of benzyl-poly(ε-caprolactone)-b-poly(ethylene glycol)-maleimide*

Benzyl-poly(ε-caprolactone)$_n$-*b*-poly(ethylene glycol)-maleimide ($PCL_n$-PEG-Mal) copolymers were synthesized as follows. Mal-PEG-$NH_2$·TFA (0.4 mg, 0.2 mmol) and dry TEA (0.3 mg, 0.24 mmol) were dissolved in 7 mL of dry toluene and the above obtained $PCL_n$-PNFs (0.2 mmol) were added under stirring. The molar ratio of Mal-PEG-$NH_2$·TFA:TEA:$PCL_n$-PNF was 1:1.2:1. The reaction proceeded overnight at RT under a nitrogen atmosphere. The formed TFA·TEA salts were removed by centrifugation and the remaining supernatants were dropped into diethyl ether at RT to precipitate the polymers, which was repeated twice. The products were obtained as light brown solids after filtration and drying under vacuum. $^1$H-NMR ($CDCl_3$): δ = 7.35 (m, aromatic protons, benzyl alcohol), 6.70 (s, maleimide protons), 5.11 (s, CC$H_2$O), 4.05 (m, $CH_2CH_2O$), 3.64 (m, PEG protons), 2.30 (m, OC(O)C$H_2$), 1.65 (m, $CH_2CH_2CH_2CH_2CH_2$), 1.38 (m, $CH_2CH_2CH_2CH_2CH_2$).

Quantification of the maleimide functional group of $PCL_n$-PEG-Mal was done by $^1$H-NMR analysis, by calculating the integral ratio between peaks from maleimide protons at 6.70 ppm and $CH_2$ from the terminal benzyl group at 5.11 ppm. UV-spectra of $PCL_n$-PEG-Mal copolymers in DCM (5 mg/mL) were recorded in the range 240-350 nm using quartz cuvette (1 cm) using a UV-2450 Shimadzu spectrophotometer, and the number of the maleimide groups per copolymer chain was also quantified by the absorption at 293 nm (maximum absorbance of maleimide group) and calibration by a series of Mal-PEG-$NH_2$ solutions in DCM.

*2.2.5 Synthesis and characterizations of Cy7 labeled DTC containing copolymer based on benzyl-poly(ε-caprolactone)-b-poly(ethylene glycol)*

Cy7 labeled polymer was synthesized in two steps. First, PCL-PDTC-PEG was synthesized using methanesulfonic acid (MSA) as the catalyst as previously described with slight modifications.[52,53] In short, CL (434 mg, 3.80 mmol), DTC (330 mg, 1.72 mmol) and mPEG-OH (421 mg, 0.21 mmol) were dissolved in 6 mL dry DCM, followed by addition of MSA (25 mg, 0.26 mmol) with agitation to initiate polymerization. The polymerization was conducted at 37 °C for 10 h under $N_2$ atmosphere and then TEA (equimolar to MSA) was added to terminate the reaction. The reaction solution was dropped into a 20-fold excess of cold diethyl ether (-20 °C) and the precipitate collected by filtration was dried under vacuum to give the final product as slightly yellow solid (809 mg, yield: 68%). $^1$H-NMR (600 MHz, $CDCl_3$): δ 4.29–4.00 (m, COO$CH_2CCH_2$OCO, $CH_2$OH), 3.63 (m, PEG protons), 3.37 (s, $CH_3$O), 2.97 (m,

C$CH_2$SS$CH_2$C), 2.32 (m, $CH_2CH_2CH_2COO$), 1.65 (m, $CH_2CH_2CH_2CH_2CH_2$), 1.39 (m, $CH_2CH_2CH_2CH_2CH_2$).

In the second step, 1.5 mL of a solution of the mixture of PCL/PDTC-PEG copolymer and Cy7-maleimide in DMF (46.8 mg/mL of PCL/PDTC-PEG and 3.7 mg/mL of Cy7-maleimide) was added dropwise to 16.5 mL of water. The homogenous dispersion was formed after gentle shaking by hands. 550 μL of tris(2-carboxyethyl)phosphine hydrochloride (TCEP, 40 mg/mL in water), was added to the dispersion. The dispersion was stirred for 4 h at RT, followed by addition of 100 μL of maleimide solution in DMF (150 mg/mL) to cap the unreacted free thiols and subsequent agitation for another 4 h. Finally, the dispersion was dialyzed with a dialysis tubing (MWCO =1 kDa) against THF/water (1/1, v/v), refreshing the dialysate after 24 h for in total 3 times, to remove the uncoupled Cy7-maleimide and maleimide. The final product was collected as a lightly green solid after lyophilization. To confirm the conjugation of Cy7 to the polymer, the resulting polymer was analyzed by GPC coupled with UV/Vis detector (detection wavelength of 700 nm) as described in section 2.3. The amount of Cy7 coupled to the polymer was analyzed by recording the absorbance of Cy7 coupled polymer at 755.5 nm using a UV-2450 Shimadzu spectrophotometer and calculated using the calibration curve of a series of standard solutions of Cy7-maleimde in DMF with concentrations ranging from 0 to 2.5 μg/mL.

### *2.3 Polymer characterization*

$^1$H nuclear magnetic resonance ($^1$H-NMR) spectra were recorded using a Bruker NMR spectrometer (600 MHz, Bruker), with chemical shifts reported in parts per million downfield from tetramethylsilane. Polymers were dissolved in $CDCl_3$ at a concentration of around 10 mg/mL. The central line of residual solvents ($CHCl_3$: δ 7.26 ppm) was used as the reference line. Peak multiplicity was designated as s (singlet), d (doublet), dd (double doublet), t (triplet), q (quartet), m (multiplet), and b (broad signal).

Calculation of DP and $M_n$: The average degree of polymerization (DP) of the synthesized caprolactone oligomers was determined from the ratio of the integral of the $CH_2$ protons of the ε-CL units (4.05 ppm, $CH_2CH_2O$) to the $CH_2$ protons of the benzyl alcohol (5.10 ppm, C$CH_2$O). The number of ethylene oxide units in the polymers was calculated by the integral ratio of the $CH_2$ protons of the benzyl alcohol (5.10 ppm, C$CH_2$O) to $CH_2$ protons of the PEG units (3.64 ppm, PEG proton). DP of PCL and PDTC in the obtained PCL-PDTC-PEG copolymer was determined from the ratio of the integral of the $CH_2$ protons of the CL units (1.39 ppm, $CH_2CH_2CH_2CH_2CH_2$), the protons of the DTC units (2.97 ppm, C$CH_2$SS$CH_2$C).The number average molecular weight ($M_n$) of the copolymers was determined by $^1$H-NMR and calculated from the resulting number of caprolactone units and ethylene oxide units. The number average molecular weight $M_n$, weight average molecular weight $M_w$ and polydispersity ($M_w/M_n$) of the synthesized polymers were determined by gel permeation chromatography (GPC,

Waters Alliance 2695 System), equipped with two PLgel Mesopore columns (300x7.5 mm, including a guard column, 50x7.5 mm). Dimethylformamide (DMF) containing 10 mM LiCl was used as the eluent at a flow rate of 1.0 mL/min at 65 °C. A differential refractive-index (RI) detector was used to record the chromatograms. Fifty µL of a 3-5 mg/mL polymer samples dissolved in DMF containing 10 mM LiCl were injected onto the column. Calibration was done using narrow poly(ethylene glycol) standards ranging from 430 to 26,100 g/mol and molecular weight of the PCL-PEG block copolymers were calculated using Empower 32 software.



### *2.4 Preparation and characterization of empty and mTHPC loaded polymeric micelles*

Empty micelles based on $PCL_n$-PEG (n=9, 15 or 23) were prepared by a film-hydration method, as described previously.[51] In detail, 10 mg of $PCL_n$-PEG or a mixture of 9 mg $PCL_n$-PEG and 1 mg $PCL_n$-PEG-Mal were dissolved in 1 mL of DCM. Next, DCM was evaporated under a nitrogen stream overnight and a thin solid film was obtained. Subsequently, 1 mL of PBS (pH 7.4) was added to hydrate the copolymer film. The mixture was heated up to 65 °C in a water bath for 15 min and then sonicated for 2 min at 40 °C to obtain a homogenous micellar dispersion. Next, the dispersion was equilibrated at RT for 15 min, followed by extrusion through 0.2 µm regenerated cellulose syringe filter (Phenex). The Z-average hydrodynamic diameter ($Z_{ave}$) and the size distribution (polydispersity index, PDI) of the formed micelles were determined at a fixed scattering angle of 173 °C at 25 °C using a ZetaSizer Nano S (Malvern). The zeta potential was measured at 25 °C using a Malvern Zetasizer NanoZ (Malvern Instruments, Malvern, UK) after the formed dispersion was 10 times diluted with 10 mM HEPES buffer (pH 7.4). Critical micelle concentration (CMC) of the different micelles consisting of a mixture of 90%$PCL_n$-PEG and 10%$PCL_n$-PEG-Mal was determined with the pendant drop method as reported previously.[51] The CMCs of micelles composed of 100%$PCL_n$-PEG were not measured because these micelles were not used for any of the studies described.

mTHPC loaded micelles (different loadings) were prepared by addition of mTHPC solution in THF (5 mg/mL, volume depending on the aimed wt% loading), to the above mentioned polymer solution in DCM and then the remaining procedures were the same as mentioned above. The absorbance of diluted micelles in DMF at 651.5 nm was recorded using a UV-2450 Shimadzu spectrophotometer and calibration was done using a series of standard solutions of mTHPC in DMF to calculate the drug loading capacity (LC) and drug loading efficiency (LE) according to the following equations.

$$LC\ (\%) = \frac{W_{ld}}{W_{ld} + W_p} \times 100\%$$

$$LE\ (\%) = \frac{W_{ld}}{W_{fd}} \times 100\%$$

in which $W_{ld}$, $W_{fd}$ and $W_p$ represent the mass of loaded mTHPC in the micelles, the feeding amount of mTHPC and the polymer mass, respectively.

*2.5 EGa1 conjugation to polymeric micelles*

The EGFR-targeted nanobody EGa1 as described by Hofman *et al.*[54] was produced and purified as described in [55], except that a slightly shorter tag for purification and detection was used, leading to protein with a theoretical molecular weight of 17097 Da (including the purification Tag, determined using ExPASy ProtParam tool). EGa1 was modified with *N*-succinimidyl-*S*-acetylthioacetate (SATA) at 1:5 EGa1:SATA molar ratio, followed by deacetylation to yield free thiol groups, as previously described.[55] SATA modified lysine units in EGa1 was assessed using liquid chromatography electrospray ionization time of flight mass spectroscopy (LC-ESI-TOF-MS) (1290 Infinity, Agilent technologies; 6560 Ion Mobility Q-TOF LC/MS, Agilent Technologies). Ellman's assay was performed according to the manufacturer's protocol, to quantify the average number of sulfhydryl (-SH) groups per EGa1 molecule after modification with SATA, *i.e.* by the reaction between Ellman's reagent (5,5'-dithiobis-(2-nitrobenzoic acid)) and free sulfhydryl groups to obtain the measurable yellow-colored product (2-nitro-5-thiobenzoic acid). Briefly, 50 µL of SATA-modified EGa1 solution and 10 µL of deprotection solution (1 M hydroxylamine hydrochloride in PBS containing 50 mM EDTA, pH 7.2) were mixed and added to 170 µL of reaction buffer (1 mM EDTA in PBS, pH 8) to which 50 µL of Ellman's reagent was added. As controls, 50 µL of native (*i.e.* non-modified) EGa1 or reduced native EGa1 (obtained by incubating native EGa1 with TCEP at 1:1 molar ratio) was added to the mixture of 50 µL of Ellman's reagent and 180 µL of reaction buffer. The solutions (280 µL) were transferred into a transparent 96-well plate and incubated at RT for 15 min. Next, absorbance at 412 nm was measured using UV-Vis spectroscopy (SPECTROstarNano, BMG LabTech) and average number of –SH groups per EGa1 nanobody was calculated using the calibration curve of a series of cysteine (Cys) solutions in reaction buffer with concentrations ranging from 4.62 to 116 nM.

For conjugation to the micelles, the deprotected EGa1:SATA was incubated with empty or mTHPC-loaded micelles (mTHPC loadings ranging from 0.5 to 10 wt%) composed of a mixture of 90wt% $PCL_n$-PEG and 10wt% $PCL_n$-PEG-Mal (10 mg/mL polymer concentration, prepared as described in section 2.4) at a maleimide:EGa1 molar ratio of 100:4.5 at RT for 1 h and at 4 °C for another 12 h, allowing reaction of the introduced thiol groups in the nanobodies with maleimide groups present on the

surface of micelles (the resulting micelles are abbreviated as EGa1-$P_n$ micelles, n=9, 15 or 23). This selected reaction condition was estimated to result in approximately 4.5 EGa1 molecules per micelles (assuming an aggregation number of 1000 $PCL_n$-PEG/ $PCL_n$-PEG-Mal polymer chain per micelle [56,57]). After conjugation, the unreacted maleimide groups in micelles were blocked by an excess of Cys (0.33 M in PBS, 100 µL added to 2 mL micellar dispersion). Non-targeted control micelles ($P_n$ micelles) were obtained by Cys-blocking the maleimide groups present in micelles that were not reacted with EGa1. After 1 h reaction at RT, unconjugated EGa1 (for the targeted formulations) and Cys (for the control formulations) were removed by 10 times washing with PBS using centrifugation with Vivaspin 6 tubes (MWCO: 50 kDa for n=9 and n=15; 100 kDa for n=23).



To confirm the conjugation of nanobody to micelles, sodium dodecyl sulphate-polyacrylamide gel electrophoresis (SDS-PAGE) of diluted micelles was performed. Briefly, samples were incubated with lithium dodecyl sulfate (LDS) running buffer (Bolt™, Novex, Life technologies) under reducing conditions at 80 °C for 10 min and then loaded into SDS-PAGE gel (Bolt™, 4-12% Bis-Tris Plus 1.0 mm x 10 well, Invitrogen Thermo Fisher Scientific). SDS-PAGE was performed at 80 V for about 1 h, using 2-(*N*-morpholino)ethanesulfonic acid (MES) buffer as the electrophoretic running solution. Next, the gel was stained using the Pierce Silver Stain Kit (Thermo Fisher Scientific) following the instruction provided by Thermo Fisher Scientific. The size and zeta-potential of the nanobody decorated micelles were determined as described in Section 2.4.

### *2.6 Cell culture*

Human epidermoid carcinoma A431 cells and human cervical carcinoma HeLa cells were obtained from the American Type Culture Collection (ATCC, Manassas, Virginia, USA). A431 and HeLa cells were cultured in Dulbecco modified eagle medium (DMEM) supplemented with glucose (1 g/L for A431 and 4.5 g/L for HeLa) and 10% (v/v) FBS. The cells were maintained at 37 °C in a humidified 5% $CO_2$ atmosphere. These conditions were used in all cell incubation steps described below. Both cells were grown in 75 $cm^2$ sterile T-flasks and passaged twice a week.

### *2.7 EGFR expression by A431 and HeLa cells*

Briefly, 100,000 A431 or HeLa cells/well dispersed in DMEM containing 10% (v/v) FBS were pipetted into 96-well plates (U-bottom). After being washed with PBS containing 1% bovine serum albumin (BSA), 50 µL/well of primary antibody (mouse anti-EGFR Ab-10, 0.2 mg/mL) was added to the cells and incubated for 45 min at 4 °C. Next, the cells were washed two times with PBS containing 1% BSA, followed by addition of secondary antibody (goat anti-mouse IgG-A488, 50 µL per well, 1 mg/mL). Subsequently, the 96-well plate was incubated for 30 min at 4 °C and then washed twice

with 1% BSA in PBS. The mean fluorescence intensity (MFI) was measured using a flow cytometer (Canto II, BD). At least 10,000 events per sample were required. EGFR expression in A431 cells was taken as 100%.

*2.8 Cell binding and uptake studies*

A431 and HeLa cells were used to investigate the binding and cellular uptake of EGa1-$P_n$ micelles loaded with mTHPC (prepared as described in Section 2.5). As controls, non-targeted $P_n$ micelles (devoid of nanobody) and EGa1 conjugated micelles co-incubated with a 9-fold excess of free EGa1 (competition group) were employed.

The binding of EGa1-micelles to A431 and HeLa cells was carried out at 4 °C. In detail, A431 and HeLa cells dispersed in 100 µL of DMEM containing 10% (v/v) FBS and glucose (1 g/L for A431 and 4.5 g/L for HeLa) were seeded into 96-well plates at a density of 12,000 cells/well and allowed to adhere overnight at 37 °C, 5% $CO_2$. To stain nuclei, Hoechst 33342 (1:1000 dilution in PBS) was added and incubated with the cells for 30 min at 37 °C. Next, EGa1 decorated micelles or non-targeted micelles were added to the wells containing fresh medium. For the competition group, medium in wells was replaced by fresh medium, followed by addition of an excess of free nanobody (final concentration was 0.05 mg/mL) and then immediately followed by addition of the EGa1 micelles. Cells were incubated with the micelles (or co-incubated with free EGa1) in the dark for 1 h at 4 °C. Thereafter, the cells were washed three times with PBS to remove non-bound micelles and subsequently fixed by incubating with 4% paraformaldehyde for 10 min. After removal of the paraformaldehyde solution and addition of 100 µL of PBS, confocal images were acquired on a fully automated Yokogawa High Content Imaging Platform (Model CV7000S, Yokogawa, Tokyo, Japan) equipped with a 60× water immersion objective using two channels: one channel ($\lambda_{ex}$ 405 nm, $\lambda_{em}$ 445 nm) for Hoechst 33342 (nuclei) and another ($\lambda_{ex}$ 405 nm, $\lambda_{em}$ 676 nm) for mTHPC.

The uptake of EGa1-$P_n$ micelles by A431 and HeLa cells was studied as follows: the different formulations (EGa1-micelles, non-targeted micelles and EGa1-micelles with free EGa1) were incubated with cells for 0.5, 1, 2, 3.5 and 7 h at 37 °C, with 5% $CO_2$. Hoechst 33342 (1:1000 dilution in PBS) was added 30 min before the end of the predetermined incubation period to stain the nuclei of cells. Next, DMEM medium containing formulations was removed from the wells and replaced by OptiMEM medium after washing the cells three times with OptiMEM medium. Thereafter, the plates were transferred into the above mentioned Yokogawa apparatus equipped with an incubation chamber set at 37 °C and 5% $CO_2$ and imaged using the same channels as mentioned for the cellular binding study.

For both experiments, Images were analysed with Columbus software and the fluorescence intensity of mTHPC was quantified by ImageJ software.

*2.9 Dark- and photo-cytotoxicity of mTHPC loaded micelles*

Targeted EGa1-$P_{23}$ micelles loaded with different mTHPC loadings (0.5 to 10% w/w) at a fixed polymer concentration (10 mg/mL in PBS) were prepared as described in Sections 2.4 and 2.5 and used to evaluate their dark toxicity and photo-cytotoxicity on both A431 and HeLa cells. As references, the corresponding mTHPC loaded $P_n$ micelles (non-targeted) and 'competition group' consisting of mTHPC loaded EGa1-$P_{23}$ micelles and a 9-fold excess of free EGa1 were employed. As an additional comparison, free mTHPC with concentrations ranging from 0.003 to 3.8 mg/mL were prepared by diluting a 5 mg/mL of mTHPC stock solution in the Foscan solvent consisting of ethanol and propylene glycol (40/60 w/w) (*i.e.* the solvent for its commercial formulation: Foscan®). These mTHPC solutions in Foscan solvent were fifty times diluted with DMEM containing 10% v/v FBS prior to incubation with the cells.

A representative procedure to evaluate the photocytotoxicity of micellar mTHPC formulations on cells at a final polymer concentration of 1 mg/mL was the following: 6000 A431 cells/well or 5000 Hela cells/well were seeded into 96-well plates and after overnight culture at 37 °C and 5% $CO_2$, the medium in the wells was replaced by the above mentioned mTHPC micellar dispersions (diluted 10 times in DMEM medium prior to use) with different wt% mTHPC loadings (EGa1 or non-targeted micelles) or mTHPC prepared by diluting the mTHPC solution in Foscan solvent with medium. For the competition group, medium containing free EGa1 (0.05 mg/mL) was used. The cells were subsequently incubated for 7 h in the dark, while the 2% mTHPC loaded EGa1 micelles and corresponding controls were also incubated for 2 and 4 h. After the indicated incubation period, medium with the formulations was removed and the cells were washed three times with DMEM medium. Next, the cells were then illuminated for 10 min with a light intensity of 3.5 mW/cm$^2$ (corresponding with 2.1 J/cm$^2$), using a homemade device consisting of 96 LED lamps (650 ± 20 nm, 1 LED per well), and then incubated with DMEM medium containing 10% (v/v) FBS overnight at 37 °C and 5% $CO_2$. Finally, cell viability was measured by MTS (see below).

Dark toxicity of micellar formulations on cells was determined after 7 and 24 h according to the same procedure for photocytotoxicity, except that cell viability was measured directly (without irradiation) by the MTS assay after washing off the formulations.

The MTS assay was performed according to the manufacturer's instruction. In short, to each well to which cells adhered also containing 100 µL medium including 10% (v/v) FBS, 20 µL of MTS reagent was added. Subsequently, the well plate was incubated at 37 °C and 5% $CO_2$ and the absorbances of the different wells at 490 nm were measured with a 96 well plate reader (Biochrom EZ Read 400 Microplate reader, Biochrom, U.K.) after approx. 1 h. The viability of the cells exposed to the different micellar formulations is reported as a percentage of the viability of the untreated cells. The half maximal effective concentrations ($EC_{50}$) of mTHPC formulations were obtained by analysis of the cell viability data with the GraphPad Prism 7.04 software

(nonlinear regression, log[inhibitor] vs. normalized response).

*2.10 Generation of singlet oxygen*

Singlet Oxygen Sensor Green (SOSG, Molecular Probes) was used to evaluate the generation of singlet oxygen induced by free mTHPC and $P_{23}$ micelles containing mTHPC. Solutions of free mTHPC and mTHPC loaded micelles were prepared at 25 μM in Foscan solvent and PBS pH 7.4, respectively. SOSG was added to these solutions from the stock (1 mM in methanol) to obtain a final concentration of 10 μM. Control samples without mTHPC and containing 10 μM of SOSG were also prepared. Samples were transferred to a quartz cuvette and illuminated with a filtered white light source at 645-665 nm at a fluence rate of 5 mW/cm$^2$. During illumination samples were stirred by placing a magnet inside the cuvette. At different time points, the cuvette was removed from the magnetic stirrer and fluorescence emission spectrum ($\lambda_{ex}$ = 488 nm) acquired with a Perkin Elmer Spectrometer LS50B ($\lambda_{em}$ = 500-750 nm).

*2.11 In vitro release of mTHPC loaded micelles in human plasma*

The *in vitro* release of mTHPC-loaded micelles with 5wt% mTHPC loading (prepared in PBS as described in section 2.4) was studied in human plasma at 37 °C, by monitoring the change of fluorescence intensity of mTHPC, as previously reported [51]. Foscan® (*i.e.* free mTHPC solution in ethanol/propylene glycol (40/60, w/w)) was used as reference. In short, different formulations were added to human plasma at a volume ratio of 1:9. As controls, samples were mixed with PBS or DMSO (1/9, v/v). After incubation at 37 °C, samples were taken at different time points (5 min, and 0.5, 1, 1.5, 2, 3, 5, 8 h) and placed in a 384-well plate to record the fluorescence intensity using a Jasco FP8300 spectrofluorometer (Japan) at 655 nm after excitation at 420 nm.
In addition, samples of Foscan® and micellar mTHPC formulation after being incubated with human plasma (1:9, v/v) at 37 °C for 5 h were taken and 1.5, 2, 4 and 30 times diluted with either human plasma or PBS. After incubation at 37 °C, samples were taken at 0.5, 1 and 2 h and placed in a 384-well plate to record the fluorescence intensity.

*2.12 In vivo pharmacokinetics*

For the *in vivo* pharmacokinetic study, non-targeted $P_{23}$ and targeted EGa1-$P_{23}$ micelles loaded with mTHPC (0.6wt % loading) were used and prepared as described in sections 2.4 and 2.5, except that micelles consisted of Cy7 labeled $PCL_{18}$-$PDTC_{7.5}$-PEG blended with non-labeled $PCL_{23}$-PEG and $PCL_{23}$-PEG-Mal (1.5/88.5/10, w/w/w) while free mTHPC was prepared by 2 times dilution of a stock solution of 120 μg/mL mTHPC in Foscan® solvent (*i.e.,* ethanol/propylene glycol, 40/60 w/w) with PBS (final mTHPC concentration is 60 μg/mL, corresponding to 0.6% mTHPC loading into micelles) prior to injection.
All animal experiments were approved by local and national regulatory authorities and

by the local Utrecht ethics welfare committee. Female Balb/c nude mice, weighing 20-28 g were purchased from Envigo (Horst, the Netherlands). Mice were housed in ventilated cages at 25 °C and 55% humidity under natural light/dark conditions and allowed free access to standard food and water. Mice were inoculated with $1x10^6$ A431 cells suspended in 100 µL PBS (pH 7.4) subcutaneously into the right flank. The experiments were performed 8-15 days later, when A431 tumor xenograft was developed with an approximate size of 100-300 $mm^3$. Tumors were measured using a digital caliper. The tumor volume V (in $mm^3$) was calculated using the equation $V = (\pi/6)LS^2$ where L is the largest and S is the smallest superficial diameter.



Three groups of mice (n = 4-5 per group) were intravenously (iv) injected via the tail vein with free mTHPC and (EGa1)-$P_{23}$ micelles in PBS at 0.6% mTHPC (w/w) loading, respectively (injection dose was 0.3 mg of mTHPC per kg bodyweight of the mouse). Blood samples (~60 µL) were collected in tubes with EDTA-anticoagulant via submandibular puncture from mice at 1 min, 1 h and 2 h, and vis cardiac puncture after 4 and 24 h, post injection. Collected blood samples were centrifuged at 1000 ×g for 15 min at 4 °C. To quantify the amount of Cy7 labeled micelles, 1 volume of collected supernatant of plasma was vortex-mixed with 1 volume of PBS. The intensity of the Cy7 fluorescence of the samples (20 µL) was detected at 800 nm using a LI-COR Odyssey imaging system and a calibration curve was prepared by a series of Cy7-maleimide solutions in the mixture of Balb/c mice plasma and PBS (1/1, v/v). To quantify the amount of mTHPC, 1 volume of collected plasma was vortex-mixed with 2 volume of acetonitrile: DMSO (4:1 v/v) for 1 minute. The mixture was centrifuged at 15,000 ×g for 10 minutes and the clear supernatant was collected and analyzed by high performance liquid chromatography (HPLC). The HPLC system consisted of a Waters X Select CSH C18 3.5 µm 4.6 x 150 mm column with 0.1 % trifluoroacetic acid in acetonitrile/water (60/40, v/v) as a mobile phase, using a flow rate of 1 mL/min. The injection volume was 20 µL and mTHPC was detected by a fluorescence detector set at $\lambda_{ex}$ 420 nm, $\lambda_{em}$ 650 nm with a retention time of about 3 min. The measuring range was from 0.005 µg/mL to 4 µg/mL and the detection limit was about 5 ng/mL. A calibration curve was obtained from a series of standard solutions of mTHPC in DMSO to which 45 µL of Balb/c mouse plasma was added, followed by mTHPC extraction using acetonitrile: DMSO (4/1, v/v) and HPLC analysis as described above.

### *2.13 Statistical analysis*

Statistical analysis was done by GraphPad Prism 7.04 software. Two way analysis of variance (ANOVA) was used to determine significance of cellular uptake between mTHPC loaded in targeted EGa1-$P_n$ micelles and relevant controls. Student t-test was performed to determine significance of EGFR expression between A431 and HeLa cells. A value of $p < 0.05$ was considered significant. Statistical significance is depicted as * $p < 0.05$, ** $p < 0.01$, *** $p < 0.001$.

## 3. Results and Discussion

### *3.1 Synthesis and characterization of copolymers*

A series of $PCL_n$-PEG and $PCL_n$-PEG-Mal copolymers was synthesized by a three-step process as described previously (**Scheme 1**).[51] First, ring opening polymerization of ε-CL in the melt initiated by benzyl alcohol and catalyzed by $Sn(Oct)_2$, at ε-CL/initiator molar ratios of 5.5/1, 14/1 and 23/1, respectively, was conducted to obtain the $PCL_n$-OH precursors with different PCL chain lengths, namely n= 9, 15 or 23 (*i.e.* average numbers as calculated from $^1$H-NMR data). It is noted that the introduction of terminal aromatic rings was used to stabilize the prepared micelles by π-π stacking.[58-60] Subsequently, the hydroxyl terminal groups of the different $PCL_n$-OH oligomers were activated by PNC and then conjugated with either PEG-$NH_2$ or Mal-PEG-$NH_2$ to yield $PCL_n$-PEG or $PCL_n$-PEG-Mal block copolymers with a carbamate linkage between the two blocks. The successful synthesis of the intermediate products and final $PCL_n$-PEG/$PCL_n$-PEG-Mal block copolymers was confirmed by $^1$H-NMR spectroscopy as described previously.[51] The characteristics of PCL oligomers and final copolymers are summarized in **Table 1**. This table shows that the calculated $M_n$ of the synthesized $PCL_n$ oligomers and $PCL_n$-PEG/$PCL_n$-PEG-Mal block copolymers as derived by $^1$H-NMR spectroscopic analysis were very well in line with the aimed values, based on the feed ratio of monomer to initiator, except for that with the shortest CL chain length which showed a higher $M_n$ relative to aimed value (actual n=9 while the feed ratio of ε-CL to benzyl alcohol was 5.5 to 1). Taking the relatively low yield (58%) of $PCL_9$-OH into account as compared to the larger $PCL_n$-OH (yields > 81%), this is most likely attributed to the loss of oligomers with the shortest PCL chains during the purification process. $^1$H-NMR spectra of $PCL_n$-PEG/$PCL_n$-PEG-Mal block copolymers (shown in **Figure S1**) show that the integral ratio of the $CH_2$ from benzyl alcohol at 5.11 ppm to ethylene oxide units from PEG at 3.64 ppm was about 1:110, which is close to the theoretical ratio (1: 95), demonstrating that almost all PCL oligomers were equiped with a PEG chain. It is noted that $^1$H-NMR spectra of $PCL_n$-PEG-Mal copolymers displayed a peak at 6.70 ppm that can be ascribed to maleimide protons with the integral ratio of 1:1 compared to $CH_2$ from benzyl alcohol at 5.11 ppm for the three different oligomers (**Figure S1**), which demonstrates that all polymer chains have one terminal maleimide group. The presence of maleimide groups on $PCL_n$-PEG-Mal was also confirmed by the appearance of an absorbance at 293 nm in the UV-Vis spectra of the polymers, which is also present in the Mal-PEG-$NH_2$, but absent in the UV-Vis spectra of PEG-$NH_2$ and $PCL_n$-PEG (see **Figure S2A**). Using calibration with Mal-PEG-$NH_2$ (see **Figure S2B**), it is calculated that all polymer chains carry a maleimide group which is in agreement with $^1$H-NMR analysis. Moreover, GPC analysis shows low polydispersity of the synthesized polymers ($M_w/M_n$ < 1.4) with a shift of $M_n$ with approximately 2 kDa as compared to the corresponding PCL oligomers, *e.g,* 2.5 kDa

of $PCL_9$-PEG *vs* 0.6 kDa of $PCL_9$-OH (representative GPC graphs shown in **Figure S3**; all the GPC data is summarized in **Table 1**). The peak shift indicates that indeed $PCL_n$-PEG/$PCL_n$-PEG-Mal block copolymers rather than a physical mixture of PCL oligomers and PEG were formed.

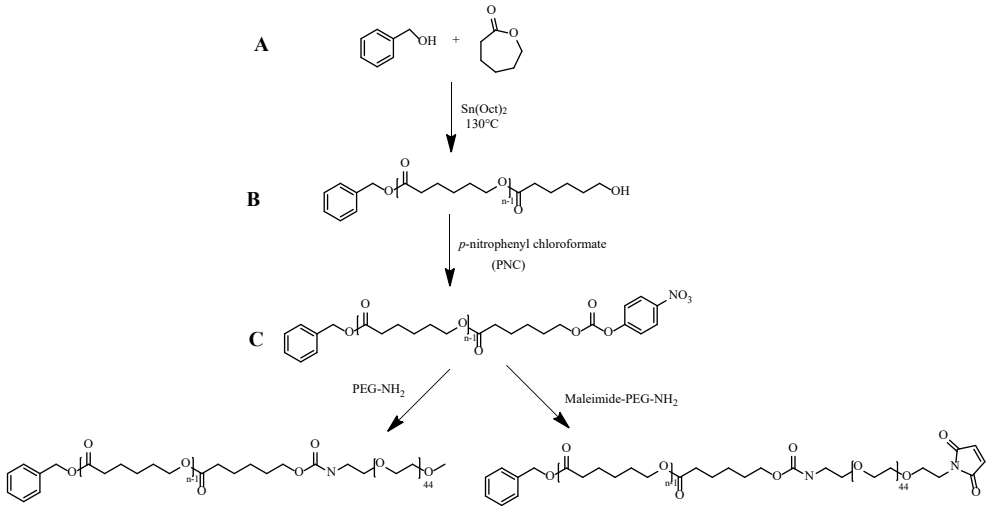


**Scheme 1.** Synthesis of $PCL_n$-PEG and $PCL_n$-PEG-Mal block copolymers: (A) Synthesis of $PCL_n$-OH by ring opening polymerization of ε-CL with benzyl alcohol; (B) Activation of the terminal hydroxyl with *p*-nitrophenyl chloroformate; (C) $PCL_n$-PEG/$PCL_n$-PEG-Mal copolymers synthesized by coupling of PEG-$NH_2$/Mal-PEG-$NH_2$ to the activated PCL oligomers.

In addition, to label $PCL_{23}$-PEG based polymer with the near-infrared (NIR) fluorophore Cy7 for *in vivo* pharmacokinetic study, DTC units containing disulfide bonds were introduced to PCL-PEG by ROP of CL and DTC (**Scheme S1**). Subsequently, the disulfide bonds in the resulting $PCL_{18}$-$PDTC_{7.5}$-PEG were reduced to free thiols by reducing agent (*i.e.* TCEP), which reacted with Cy7-maleimide via the thiol-maleimide reaction (**Scheme S1**). After the coupling reactions with the coupling efficiency of 17% (calculated based on the calibration curve of **Figure S4A**), on average, one polymer chain carried 0.17 Cy7 label. GPC chromatograms (**Figure S4B**) of the Cy7-labeled polymer showed the successful coupling of Cy7 with the polymer with negligible free Cy7 present in the resulting Cy7 labeled polymer.

**Table 1.** Characteristics of synthesized intermediates and $PCL_n$-PEG block copolymers.

| Polymer | Aimed molecular weight (kDa) | $^1$H-NMR | GPC | | | Yield (%) |
|---|---|---|---|---|---|---|
| | | $M_n$ (kDa) | $M_w$ (kDa) | $M_n$ (kDa) | $M_w/M_n$ | |
| **$PCL_9$-OH** | 0.8 | 1.1 | 0.7 | 0.6 | 1.12 | 58 |
| **$PCL_9$-PNF** | 1.0 | 1.3 | 0.7 | 0.6 | 1.12 | 58 |
| **$PCL_9$-PEG** | 3.0 | 3.1 | 2.7 | 2.5 | 1.06 | 82 |
| **$PCL_9$-PEG-Mal** | 3.1 | 3.5 | 3.0 | 3.0 | 1.03 | 78 |
| **$PCL_{15}$-OH** | 1.7 | 1.8 | 1.4 | 1.2 | 1.15 | 81 |
| **$PCL_{15}$-PNF** | 1.9 | 2.0 | 1.3 | 1.2 | 1.15 | 73 |
| **$PCL_{15}$-PEG** | 3.7 | 3.8 | 3.3 | 3.0 | 1.09 | 56 |
| **$PCL_{15}$-PEG-Mal** | 3.8 | 4.1 | 5.4 | 4.6 | 1.18 | 24 |
| **$PCL_{23}$-OH** | 2.7 | 2.7 | 2.1 | 1.8 | 1.12 | 82 |
| **$PCL_{23}$-PNF** | 2.9 | 2.9 | 2.0 | 1.9 | 1.10 | 76 |
| **$PCL_{23}$-PEG** | 4.7 | 4.7 | 3.7 | 3.2 | 1.16 | 57 |
| **$PCL_{23}$-PEG-Mal** | 4.8 | 5.1 | 5.8 | 4.1 | 1.40 | 74 |
| **PEG-$NH_2$** | n.a.[a] | 2.0 | 1.7 | 1.6 | 1.02 | n.a.[a] |
| **Mal-PEG-$NH_2$** | n.a.[a] | 2.6 | 2.0 | 2.0 | 1.02 | n.a.[a] |

[a] n.a. = Not applicable

### *3.2 Preparation of polymeric micelles*

Micelles composed of $PCL_n$-PEG and 9:1 mixtures of $PCL_n$-PEG and $PCL_n$-PEG-Mal (n=9, 15 and 23) at a polymer concentration of 10 mg/mL were prepared by a film hydration method (**Scheme 2**). **Table 2** shows that micelles with or without $PCL_n$-PEG-Mal had small hydrodynamic diameters (ranging from of 17-45 nm, with increasing PCL chain length) and zeta potential (near neutral), suggesting that the addition of $PCL_n$-PEG-Mal had no effect on the characteristics of the micelles. The critical micelle concentrations (CMC) of the micelles composed of 90% $PCL_n$-PEG and 10% $PCL_n$-PEG-Mal were in the range of previously published data on PCL-PEG.[51]

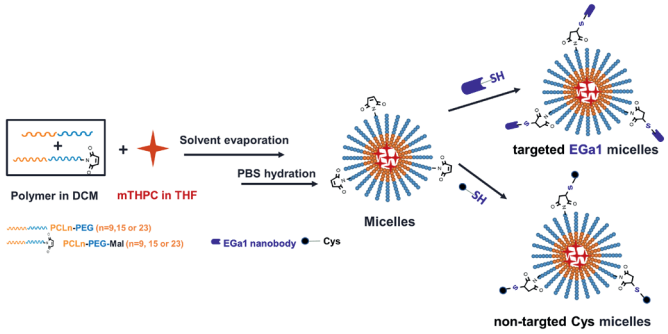


**Scheme 2**. Preparation of polymeric micelles conjugated with EGa1 (targeted) or Cys (non-targeted).



**Table 2.** Characteristics of micelles composed of $PCL_n$-PEG, and 9:1 (w/w) mixtures of $PCL_n$-PEG and $PCL_n$-PEG-Mal.

| Polymer(s) | $Z_{Ave}$ diameter (nm)[a] | PDI[a] | ζ-potential (mV)[a] | CMC (mg/mL) |
|---|---|---|---|---|
| $PCL_9$-PEG | 17±1 | 0.07±0.02 | -2.3±0.0 | 0.04 [51] |
| $PCL_9$-PEG/ $PCL_9$-PEG-Mal | 17±1 | 0.09±0.01 | -2.3±0.0 | 0.06 |
| $PCL_{15}$-PEG | 25±2 | 0.20±0.01 | -1.9±0.1 | n.d.[b] |
| $PCL_{15}$-PEG/ $PCL_{15}$-PEG-Mal | 26±3 | 0.20±0.02 | -2.0±0.3 | 0.05 |
| $PCL_{23}$-PEG | 43±2 | 0.20±0.01 | -1.9±0.4 | n.d.[b] |
| $PCL_{23}$-PEG/ $PCL_{23}$-PEG-Mal | 45±4 | 0.15±0.03 | -2.2±0.2 | 0.02 |

[a] Data were obtained from three independently prepared batches. [b]n.d. = Not determined

### *3.3 EGa1 modification and its conjugation to polymeric micelles*

EGa1 was produced and purified as described in [55] and characterized by LC-ESI-TOF-MS (**Figure S5A)**. A major peak with an m/z value at 17,096 Da was detected, in agreement with the theoretical mass of this protein. The EGa1 nanobody was modified using 5 equivalents of SATA reagent that can react with the six primary amines of the EGa1 protein (5 lysine amino acids and one at the N-terminal). The successful modification was demonstrated using LC-ESI-TOF-MS analysis (**Figure S5B)**, which clearly showed two peaks with m/z values corresponding to modification with 1 and 2 SATA units (mass: 116 Da) in the deconvoluted mass spectrum. Ellman's assay was carried out to quantify the average number of thiol groups present on EGa1 nanobody after deprotection of the SATA. The results show (**Figure S5C**) that reaction of EGa1 with SATA at a molar ratio of 1:5 led to approximately two sulfhydryl groups introduced per protein molecule. As controls, Ellman's assay on native (non-modified) EGa1 and reduced EGa1 (*i.e.* with one split disulphide bond) showed on average 0.19 and 1.93

thiols, respectively, as expected.

Micelles consisting of 9:1 mixtures of $PCL_n$-PEG and $PCL_n$-PEG-Mal (n=9, 15 and 23) were reacted with either Cys or deprotected EGa1-SATA to obtain non-targeted $P_n$ and targeted EGa1-$P_n$ micelles, respectively (**Scheme 2**). DLS shows that the sizes of $P_n$ and EGa1-$P_n$ micelles (**Table 3**) were comparable to those of the native micelles (**Table 2**), but the former had a slightly more negative surface charge at pH 7.4 (-4 to -6 mV for $P_n$ micelles decorated with Cys or EGa1 *vs* around -2 mV for native micelles) which can be explained by the presence of the negatively charged nanobody at pH 7.4 (theoretical pI ~6.6, according to ExPASy ProtParam tool) at the surface of the micelles. UV/Vis detection shows that mTHPC was quite efficiently (50-70%) encapsulated inside particles' core at different feeds (see **Table 3**).

**Table 3.** Characteristics of EGa1 and Cys decorated micelles (targeted EGa1-$P_n$ and non-targeted $P_n$ micelles) composed of 9:1 mixtures of $PCL_n$-PEG and $PCL_n$-PEG-Mal.

| | | | | 5 wt% feed | | 0.5 wt% feed | |
|---|---|---|---|---|---|---|---|
| **Polymer** | **Conjugated agent** | **$Z_{Ave}$ diameter (nm)** | **ζ-potential (mV)** | **LE%[a]** | **LC%[a]** | **LE%[a]** | **LC%[a]** |
| $PCL_9$-PEG/ $PCL_9$-PEG-Mal | Cys | 17±1 | -5.0±0.7 | 64 | 3.2 | 65 | 0.3 |
| | EGa1 | 18±1 | -6.2±1.5 | 64 | 3.2 | 65 | 0.3 |
| $PCL_{15}$-PEG/ $PCL_{15}$-PEG-Mal | Cys | 25±3 | -4.1±0.7 | 53 | 2.8 | 65 | 0.3 |
| | EGa1 | 27±2 | -5.5±1.1 | 53 | 2.8 | 65 | 0.3 |
| $PCL_{23}$-PEG/ $PCL_{23}$-PEG-Mal | Cys | 43±3 | -4.8±0.2 | 54 | 2.8 | 70 | 0.3 |
| | EGa1 | 45±5 | -5.2±0.7 | 54 | 2.8 | 70 | 0.3 |

[a] SD ≤ 1%.

To establish whether EGa1 was indeed covalently linked to the polymeric micelles and not physically adsorbed, an SDS-PAGE assay of the samples was performed (**Figure 1**). For all the three conjugated micelles, one band located at a slightly higher molecular weight than the EGa1 band appeared, as a result of the conjugation of EGa1 with one $PCL_n$-PEG-Mal polymer chain. A second band near 30 kDa appeared as well, most likely representing two $PCL_n$-PEG-Mal polymer chains conjugated to EGa1 molecule due to the presence of more than one SATA modifications on the nanobody. These two bands were not observed in the samples of micelles alone and micelles incubated with non-reactive (*i.e.* not deprotected) EGa1-SATA, further convincingly demonstrating successful conjugation of EGa1 to the micelles (see **Figure S6**). The band of the unconjugated EGa1 was not detected in the micellar samples, confirming its full removal through Vivaspin washes (**Figure 1**).

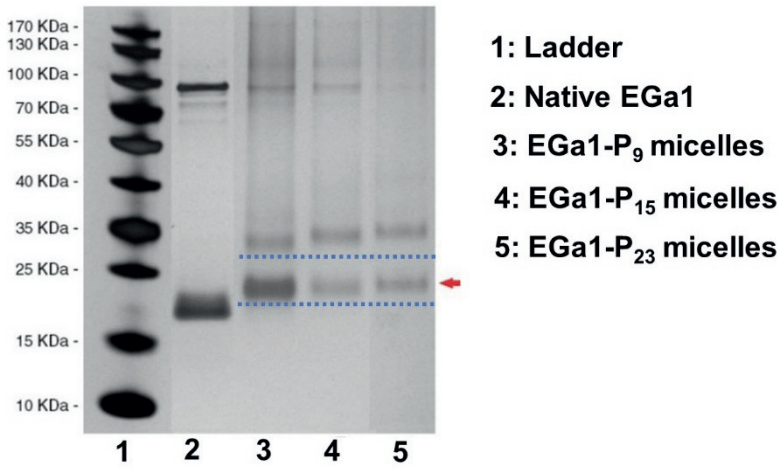




**Figure 1.** SDS-PAGE silver staining of mTHPC-loaded EGa1-conjugated micelles (EGa1-$P_n$ micelles) obtained after 10 washes with PBS following the overnight conjugation of micelles with deprotected EGa1-SATA. Native EGa1 was used as a control. Red arrow indicates band of EGa1 with one polymer chain conjugated.

### *3.4 Cell binding and uptake studies*

The cell binding capacity of EGa1 decorated micelles was studied with binding assays at 4 °C, at which cell transport processes (*e.g.* internalization) are markedly reduced, using two cell lines differing in EGFR expression level: A431 cells express 90% more EGFR compared to HeLa cells, as indicated by flow cytometry (**Figure S7**). For this, the intrinsic fluorescence of mTHPC was detected using confocal microscopy. **Figure 2A** shows the fluorescence intensity associated with A431 and HeLa cells after 1 h incubation of mTHPC loaded EGa1-$P_n$ micelles (n=9, 15 or 23) and relevant controls at 4 °C. EGa1-$P_{15}$ and EGa1-$P_{23}$ micelles clearly had extensive interaction with the membrane of A431 cells. However, cell association was less visible for the EGa1-$P_9$ micelles. This might be due to destabilization of these micelles as previously observed,[51] or particles' size (around 15 nm) that is too small to promote multivalent binding with the receptor.[26,45,48] For all the non-targeted controls ($P_n$ micelles), association with A431 cells was not observed. In addition, the binding observed for EGa1-$P_{15}$ and EGa1-$P_{23}$ micelles was absent in groups containing an excess of free EGa1, suggesting that the free EGa1 blocked the interaction of EGa1 conjugated micelles with EGFR on the surface of A431 cells. Also, fluorescence of mTHPC was not detected for low EGFR expressing HeLa cells for any of the formulations. These results indeed confirm that the EGa1 decorated micelles bind to the EGFR receptor on A431 cells, which also implies that conjugation of EGa1 to the micelles did not adversely affect the binding capability of the nanobody for its target.

To investigate the cellular internalization of the different formulations, mTHPC-loaded EGa1-$P_n$ micelles, their controls (non-targeted $P_n$ micelles and competition group), as well as free mTHPC were incubated with A431 and HeLa cells for different time points between 0.5 and 7 h at 37 °C. The representative microscopic images show that regarding the low EGFR expressing HeLa cells, only low fluorescence was visible after longer excitation times, as compared to the excitation times employed to image A431 cells (100 *vs* 50 msec, respectively), and no selectivity was observed between the different micelles (**Figure 2B**). In strong contrast, a substantial increase in fluorescence intensity of mTHPC for A431 cells after 7 h incubation with mTHPC-loaded targeted EGa1-$P_{15}$ and EGa1-$P_{23}$ micelles was observed, as compared to their non-targeted controls. Furthermore, uptake of these micelles was blocked by an excess of free EGa1 (**Figure 2B**), which implies that mTHPC is indeed taken up in the micellar form through these EGa1-$P_{15}$ and EGa1-$P_{23}$ micelles. Concerning the EGa1-$P_9$ micelles incubated with A431 cells, no difference in fluorescence intensity was observed compared to relevant controls, which is consistent with the binding study. This suggests that the small size (around 15 nm) of these micelles may cause uptake through other mechanisms rather than receptor binding followed by endocytosis,[26,45,48] or that this non-specific uptake is caused by released mTHPC from these (less stable) micelles.[51] Indeed, free mTHPC showed efficient uptake by A431 cells (**Figure S8**). The fluorescence signal of mTHPC, regardless of the used formulations, was predominantly located in the perinuclear regions rather than on the cell surface, which is in good agreement with previous studies of a liposomal (Foslip®) and a micellar formulation.[51,61,62] mTHPC in its free form was taken up efficiently by both A431 and HeLa cell lines at a similar level, as can be noticed from **Figure S8**, where stronger fluorescence was observed with even shorter excitation times than that used for imaging the micellar formulations. This confirms the known non-selective uptake of free mTHPC, which when compared to the uptake observed for the micellar formulations (**Figure S8** *vs* **Figure 2B**), demonstrates the possibility to enable selective uptake using EGa1 targeted micelles, as described in the present study.

Although differences in fluorescence intensity are observed between uptake of free mTHPC and micellar formulations containing the same dose of mTHPC (for instance, **Figure 2B** *vs* **Figure S8A**), comparison between these are difficult as lower uptake of micellar formulations could occur due to its PEG corona [63,64] and the mTHPC fluorescence is likely quenched in the micelles at such high PS loading (≥ 5wt%).[51] In respect of the micellar formulations, even if the fluorescence of mTHPC is (differently) quenched inside the micelles, each group ($P_n$, n=9, 15 and 23) has the same mTHPC loaded, thus comparisons of the fluorescence intensity are possible within the targeted, non-targeted, and the competition groups (**Figure 2B** and **2C**).

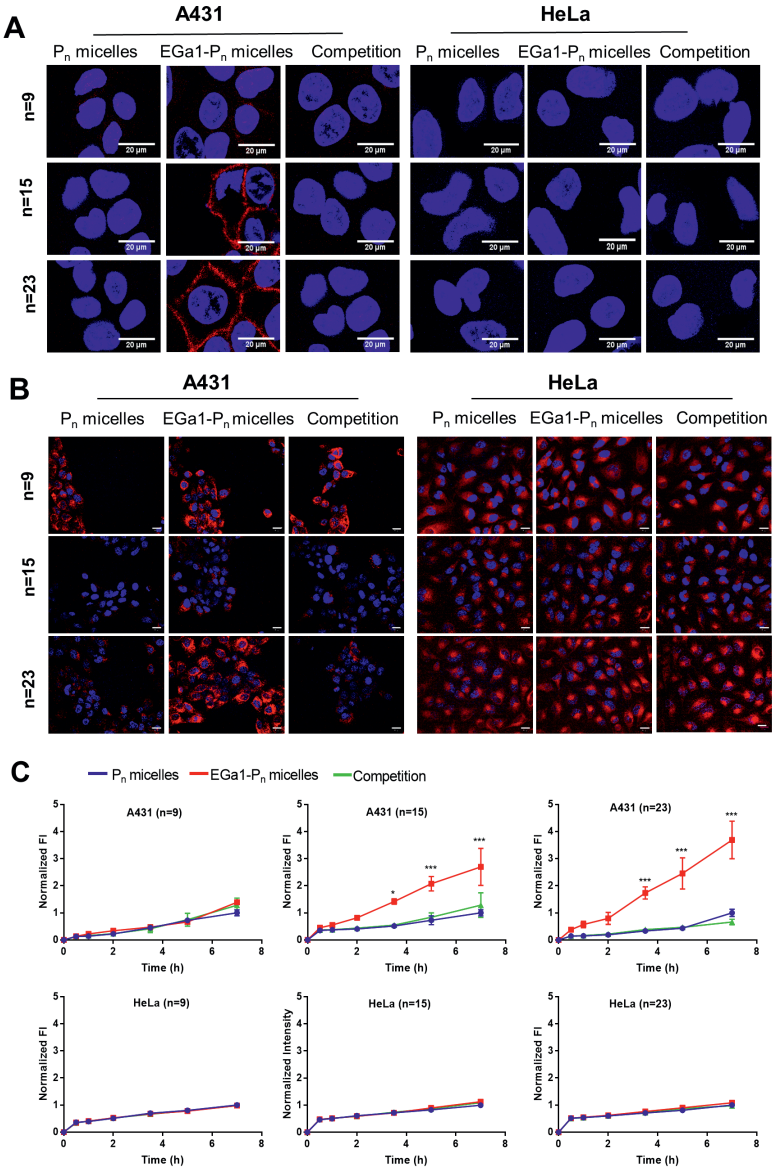


**Figure 2**. (A-B) Representative confocal fluorescence microscopic images of A431 and HeLa cells incubated with mTHPC-loaded micelles of three tested groups: $P_n$ micelles (non-targeted), EGa1-$P_n$ micelles (targeted) and competition group composed of EGa1-$P_n$ micelles co-incubated with a 9-fold excess of free EGa1, respectively (n=9, 15, 23; 5 wt% mTHPC loading used for micelles with n=9 and 15, and 10 wt% mTHPC loading used for micelles with n=23). Cells were incubated for 1 h at 4 °C (A) and for 7 h at 37 °C (B). Cell nuclei were stained in blue with Hoechst, while the fluorescence of mTHPC is presented in red. Scale bars indicate 20 μm. Excitation times applied for obtaining these confocal images were 50 msec for A431 cells and 100 msec for HeLa cells. (C) Quantification of fluorescence intensity of mTHPC ($\lambda_{ex}$ 405 nm, $\lambda_{em}$ 676 nm) of A431 and HeLa cells incubated with micellar formulations. The quantified fluorescence intensity was normalized by the intensity of $P_n$ micelles after 7 h incubation in each group and by the number of cells.

The quantified fluorescence intensity from the images (**Figure 2C**) indicates that the micelles showed a time-dependent increasing cellular uptake of fluorescent mTHPC by both A431 and HeLa cells. Most importantly, cellular uptake of mTHPC loaded targeted EGa1-$P_{15}$ and EGa1-$P_{23}$ micelles by A431 cells showed a statistically significant difference (*i.e.* 3-4 times higher after 7 h) as compared to non-targeted $P_{15}$ and $P_{23}$ micelles (red *vs* blue lines in **Figure 2C**). Most significant enhancement of cellular uptake as observed for EGa1-$P_{23}$ micelles relative to EGa1-$P_{15}$ micelles might be due to its excellent size (~45 nm) since it has been shown in previous studies that 40-50 nm nanoparticles are optimal for receptor mediated internalization.[45,48] Notably, the uptake by A431 cells can be blocked or prevented, by the co-incubation of EGa1 decorated micelles with an excess of free nanobody (**Figure 2C**, green curves). Whereas no difference was observed in cellular uptake by HeLa cells for the different formulations (**Figure 2C**), confirming that the uptake of the micelles by A431 cells is EGFR-mediated. Cellular uptake of mTHPC loaded $P_9$ based micelles was similar for all three groups and no beneficial effects of EGa1 decoration were observed, as was also concluded from earlier images (**Figure 2B**) and is in agreement with the non-detected cell association of mTHPC in the binding assay performed at 4 °C (**Figure 2A**). As mentioned before, this could be caused by the premature release of mTHPC from the micelles due to their instability [51] or other uptake mechanisms.[26,45,48] Altogether, these results confirm that the EGa1-$P_{15}$ and EGa1-$P_{23}$ micelles can selectively deliver mTHPC inside EGFR-overexpressed cells due to receptor-mediated cellular uptake.

### *3.5 Dark and photocytotoxicity of mTHPC loaded micelles*

Cytotoxicity assessment of empty micelles (**Figure S9**) shows that, regardless of EGa1 conjugation, they all have an excellent cytocompatibility, since no toxic effects were observed at 2 and 4 mg/mL. The *in vitro* dark and photocytotoxicity experiments were only carried out with mTHPC-loaded $P_{23}$ and EGa1-$P_{23}$ micelles because these micelles showed the highest cellular uptake by A431 cells (**Figure 2C**) as compared to $P_{15}$ micelles. Therefore, EGa1-$P_{23}$ and $P_{23}$ micelles with different mTHPC loadings were prepared (the actual LE% are shown in **Table 3** and **Table S1** and confirmation of successful EGa1 conjugation is shown in **Figure S10**). The toxicity of the micellar formulations was compared with that of free PS at the same concentrations.

As shown in **Figure 3** (green, red and blue lines), the different micellar PS formulations, including the one with the highest mTHPC loading of 76 μg/mL (corresponding to 10 wt% feed loading in micelles) showed no cytotoxicity on A431 and HeLa cells after incubation with cells in the dark for 7 and 24 h, irrespective of EGa1 presence. On the other hand, cells incubated with free mTHPC (medium also containing 2% ethanol/propylene glycol (40/60 w/w) solvent) displayed a dose- and time-dependent decrease of cell viability, suggesting toxicity of free mTHPC occurred even without illumination at mTHPC concentrations higher than 50 μg/mL after 7 h, and 20 μg/mL after 24

h (**Figure 3**, black and gray lines), respectively. It is worth mentioning that ethanol/propylene glycol solvent present in the cultural medium was not toxic for A431 and HeLa cells in the concentration range tested, suggesting that the observed toxicity of mTHPC is not ascribed to the used solubilization vehicle. Depending on the cell type used and incubation time, dark-toxicity of free mTHPC at concentrations between 2.5 and 100 μg/mL was also found in other studies.[62,65] Interestingly, these results imply that cytotoxicity of mTHPC in the absence of light could markedly be reduced by formulation in micelles, especially for the long incubation period, as shown previously also for its liposomal formulation (*i.e.* Foslip®).[65]



The photocytotoxicity of mTHPC loaded in $P_{23}$ micelles with or without EGa1 decoration towards A431 and HeLa cells was studied with various mTHPC concentrations at a fixed polymer concentration (1 mg/mL; far above the CMC of 0.02 mg/mL (see **Table 2**)), by illuminating the cells with 3.5 mW/cm$^2$ for 10 min after 7 h pre-incubation with the different PS formulations. **Figure 4A** shows that for A431 cells, mTHPC loaded micelles decorated with EGa1 nanobody (red line) had a significantly lower $EC_{50}$ value (10 mg/mL) than the non-targeted micelles and competition group (EGa1 micelles plus free EGa1) (38 and 48 mg/mL, respectively, see **Table S2**), demonstrating increased photocytotoxicity for the targeted micelles, which is most likely attributed to the higher extent of internalization resulting from EGa1 targeting (as shown in **Figure 2C**). No selective photocytotoxicity was seen in HeLa cells, neither with EGa1-$P_{23}$ micelles nor with their controls (non-target and competition groups). As expected, no selective killing capacity of A431 and HeLa cells was shown by free mTHPC, whether co-incubated with free EGa1 or not (**Figure 4B**). It is worth noting that $EC_{50}$ value of free mTHPC on A431 (~1.6 μg/mL) (calculated from **Figure 4B**, shown in **Table S2**) was lower than the best performing EGa1 decorated micellar formulation (10 mg/mL mTHPC), probably related to the higher internalization rate of free mTHPC, or a different intracellular distribution, which may affect singlet oxygen production or its efficacy.[51] In that respect, although difficult to predict what happens inside cells, we could confirm that mTHPC can still lead to generation of singlet oxygen when loaded inside micelles (**Figure S11**).

Importantly, at a polymer concentration of 1 mg/mL, photocytotoxicity of mTHPC loaded in EGa1-$P_{23}$ micelles was three times higher for A431 cells than for HeLa cells ($EC_{50}$ of approximate 10 μg/mL mTHPC for A431 *vs* about 30 μg/mL mTHPC for HeLa, see **Table S2**), suggesting effective selectivity in terms of photocytotoxicity between A431 and HeLa cells. This selectivity in photo-induced cell killing is most interesting for achieving the targeted PDT to EGFR over-expressing cancers.

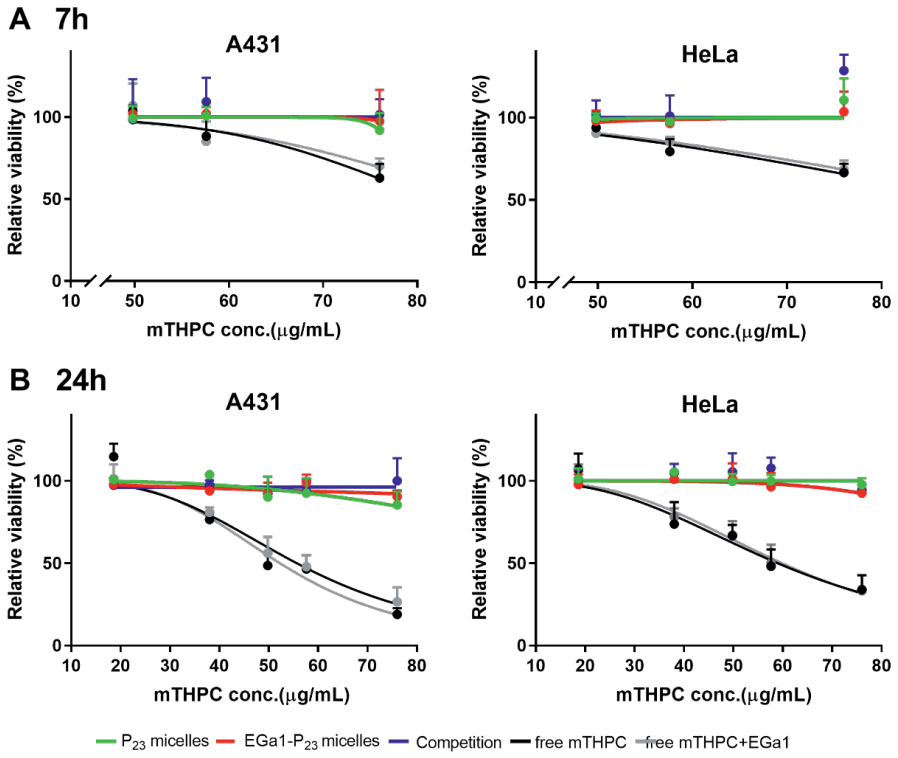


**Figure 3.** Dark-toxicity established using MTS assay of free mTHPC and mTHPC loaded in $P_{23}$ or EGa1-$P_{23}$ micelles (at 1 mg/mL polymer) at varying mTHPC loadings on A431 and Hela cells after 7 (A) and 24 h (B). In the legend, "competition" represents mTHPC loaded in EGa1-$P_{23}$ micelles co-incubated with free EGa1, while "free mTHPC+EGa1" indicates free mTHPC co-incubated with free EGa1.

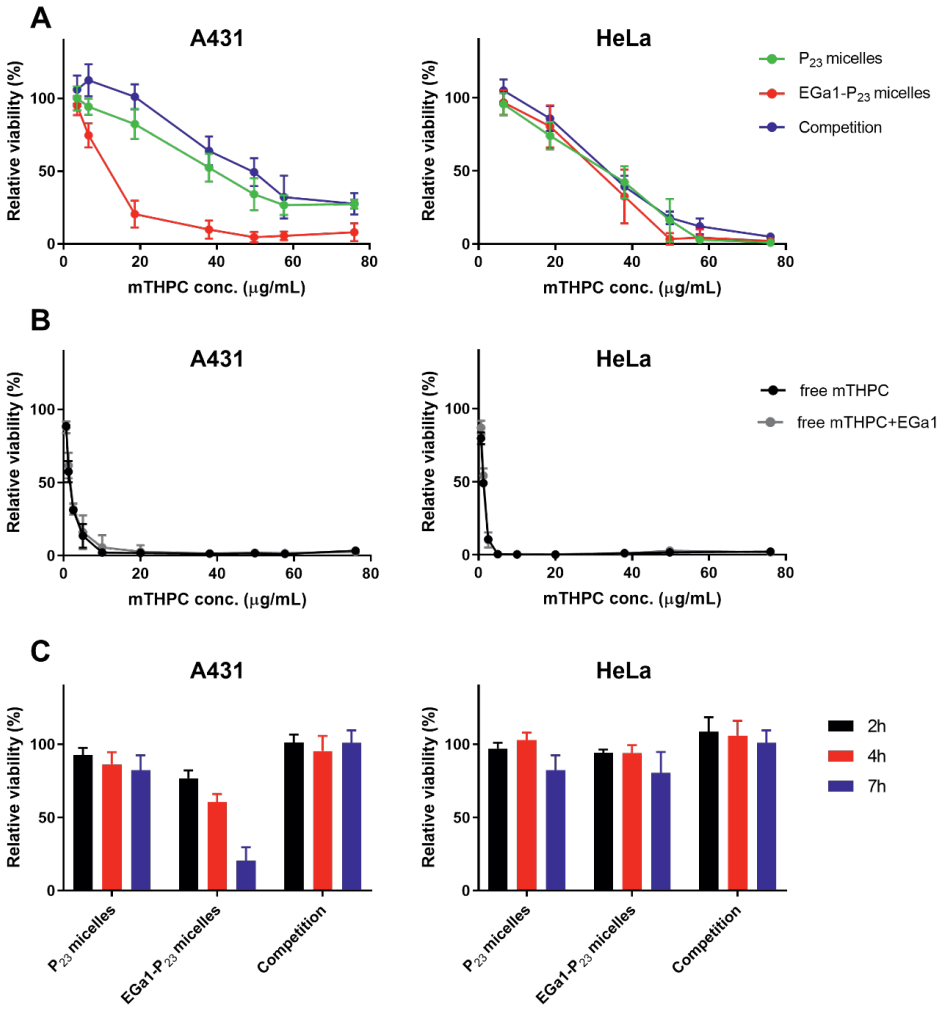


**Figure 4.** (A-B) Dose-dependent photocytotoxicity (MTS assay) on A431 and HeLa cells after 7 h of pre-incubation with: mTHPC loaded in $P_{23}$ micelles (non-targeted) or EGa1-$P_{23}$ micelles (targeted) composed of 1 mg/mL polymer and varying mTHPC loadings (A) or free mTHPC (B). (C) Time-dependent photocytotoxicity (MTS assay) on A431 and HeLa cells pre-incubated with mTHPC loaded in $P_{23}$ and EGa1-$P_{23}$ micelles (1 mg/mL polymer and 18.6 μg/mL mTHPC (corresponding to ~2 wt% mTHPC loading)). After the reported pre-incubation periods and washings, the cells were illuminated for 10 min, 3.5 mW/cm$^2$. In the legend, "competition" in (A) and (C) represents mTHPC loaded in EGa1-$P_{23}$ micelles and co-incubated with a 9-fold excess of free EGa1, while "Free mTHPC+EGa1" in (B) indicates free mTHPC co-incubated with a 9-fold excess of free EGa1.

To investigate the effect of the incubation time on photocytotoxicity, the cells were illuminated after incubation for 2, 4 and 7 h with mTHPC loaded EGa1-$P_{23}$ micellar formulations comprised of 1 mg/mL polymer and 18.6 μg/mL mTHPC (corresponding to ~2 wt% loading). **Figure 4C** shows that only A431 cells incubated with mTHPC

loaded in targeted EGa1-$P_{23}$ micelles showed a decrease of cell viability over time (*i.e.* time-dependent cell death). Whereas hardly any (time dependent) photocytotoxicity was observed at this concentration of mTHPC loaded in non-targeted micellar PS formulations, its competitive control on A431 cells, and for all formulations on HeLa cells (see also in **Figure 4A**). These results are in good agreement with cellular uptake observations in which we showed that EGa1 conjugated micelles were taken up to a higher extent than its controls by A431 cells (see **Figure 2C**). This indicates that the selective internalization of the PS-loaded micelles has a major contribution to cell killing (*i.e.* photocytotoxicity).

It is worth mentioning that other types of targeting ligands, such as folate and RGD peptide, have also been investigated for the targeted intracellular delivery of mTHPC in various cancer cells.[66-69] For example, Moret *et al* showed that mTHPC encapsulated in folate-targeted PEGylated liposomes (*i.e.* folate targeted FosPEG®) exhibited enhancement of internalization and photo-induced cytotoxicity of mTHPC, by maximum 2-fold and 1.5-fold, respectively, as compared to non-targeted liposomes, in folate receptor-positive KB cells.[67] However, a previous study on transferrin receptor targeted FosPEG® displayed that as compared to unmodified liposomes, transferrin-conjugated FosPEG® did not improve the intracellular accumulation and the photocytotoxicity of mTHPC in transferrin receptor-abundant OE21 cancer cells.[69] In contrast, $P_{23}$ micelles decorated with EGa1 nanobody used in our work exhibited significant improvement of internalization and photocytotoxicity of mTHPC on EGFR overexpressing A431 cells, by 4 times after 7 h incubation (**Figure 2C** and **4A**), as compared to the non-targeted micelles, indicating that our system has improved selectivity over the aforementioned liposomes. Our study indeed exemplifies that furnishing a targeting ligand, namely a nanobody, on nanoparticles is an attractive strategy for improving selectivity and efficacy of PDT *in vivo.*

### *3.6 In vitro release of mTHPC from micelles in human plasma*

Before investigating these micelles *in vivo*, we first investigated the *in vitro* release of mTHPC loaded in the best $P_{23}$ micelles in human plasma over time at 37 °C (**Figure 5**), and compared this with Foscan® (free mTHPC in solvent). Human plasma was selected, because it is biologically more relevant than a saline solution would be; however, this renders quantification of the released mTHPC difficult due to the small dimensions of the micelles that are difficult to separate from plasma proteins or lipoproteins that may contain released mTHPC. Therefore, for this stability study, we made use of the quenched state of the fluorescence resulting from the high mTHPC local concentration inside the micellar core.[51] Release of mTHPC from the micelles should decrease mTHPC local concentration inside the micelles, thus decreasing quenching and increase the fluorescence intensity. Similarly as observed in our previous study,[51] the fluorescence of mTHPC loaded micelles upon 10× dilution in PBS was low due to

fluorescence quenching, though stable in time over 8 h at 37 °C (**Figure S12A**). In contrast, upon 10x dilution in DMSO, the fluorescence of mTHPC loaded micelles was restored to the same level as free mTHPC, suggesting the dequenching of mTHPC due to the destruction of micelles by DMSO (**Figure S12B**). Upon 10× dilution in plasma, Foscan® gave stable fluorescence at a value of ~2,800 a.u. after 30 min incubation (**Figure 5**, black line). For micellar mTHPC formulation, fluorescence of mTHPC increased slightly within the first 3 h incubation, and then levelled off at ~1,000 a.u (**Figure 5A**, red line), which was significantly lower than that of free mTHPC (2800 a.u.). This result suggests that despite slightly initial release of mTHPC in the first 3 h, the majority of mTHPC was sufficiently retained in micelles in the presence of plasma for at least 8 h.

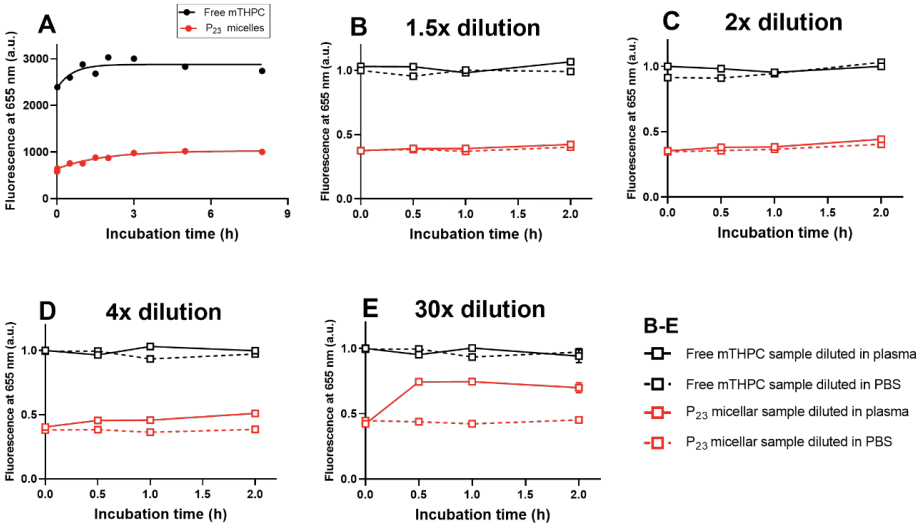


**Figure 5.** (A) Fluorescence intensity of free mTHPC (*i.e.*, Foscan®) and mTHPC loaded in $P_{23}$ micelles at a final mTHPC concentration of 40 mg/mL (corresponding to 5wt% mTHPC loading in micelles) in human plasma as a function of time; Foscan® and mTHPC loaded micelles were 10× diluted with full plasma and incubated while the mTHPC fluorescence was recorded at 37 °C over a period of 8 h. The fluorescence intensities of the corresponding mTHPC loaded micelles diluted with PBS were used as 0 h time-point. (B-E) Fluorescence intensity of free mTHPC and mTHPC loaded $P_{23}$ micelles in human plasma as a function of time after dilution, normalized by the intensity of the corresponding free mTHPC samples upon dilution with human plasma at 0 h; free mTHPC and mTHPC loaded micelles were pre-incubated with human plasma (1/9, v/v) at 37 °C for 5 h, and then further diluted 1.5, 2, 4 or 30× with human plasma or PBS, and further incubated, while the mTHPC fluorescence was recorded at 37 °C over a period of 2 h. The fluorescence intensities of mTHPC in different formulations recorded right after dilution were used as 0 h time-point.

To reveal whether the release of mTHPC from micelles is dependent of the ratio between micelles and plasma, mTHPC loaded $P_{23}$ micelles after incubation with human plasma

for 5 h, were further diluted with human plasma or PBS in different proportions. As a comparison, free mTHPC samples were treated under the same conditions. When the micelles preincubated with plasma were diluted with PBS, the fluorescence of mTHPC that was released from the micelles kept constant in time (**Figure 5B-E**, broken purple lines) and remained lower than diluted free mTHPC. Upon 1.5× and 2x diluting the plasma containing micelles with plasma instead of PBS, fluorescence of mTHPC remained stable and comparable as that observed when it was diluted in PBS (**Figure 5B** and **C**, solid red lines). With further increasing the dilution factor in plasma to 4 times, fluorescence of mTHPC in micelles only slightly increased during the first 1 h incubation and then levelled off (**Figure 5D**, solid red line). Surprisingly, the plateau fluorescence levels upon 1.5 to 4x dilution in plasma were much lower than that observed from the corresponding free mTHPC samples (**Figure 5B-D**, black lines), suggesting sufficient mTHPC retention in micelles in the presence of up to 40 times plasma (v/v). Even upon large dilution in plasma up to 30x (final polymer concentration: 0.03 mg/mL, close to CMC of 0.02 mg/mL, **Table 2**), lower fluorescence level of micellar mTHPC formulation was observed than of free mTHPC samples (**Figure 5E**). These results suggest that some extent of mTHPC can be retained in $P_{23}$ micelles in the presence of the large amount of plasma (300 times, v/v).

### *3.7 In vivo pharmacokinetics of mTHPC and micelles*

For successfully translating the *in vitro* selectivity of PDT into the *in vivo* situation, the prerequisite is prolonged circulation of nanocarriers. Therefore, the pharmacokinetic profiles of free mTHPC, Cy7 labeled $P_{23}$ and EGa1-$P_{23}$ micelles loaded with mTHPC were studied in mice bearing human A431 tumor xenografts. **Figure 6** shows that the incorporated mTHPC in micellar formulations and the corresponding micelles, regardless of being decorated with EGa1 or not, displayed similar clearance profiles (red and green line), suggesting that conjugated nanobody had a minor influence on the clearance of these micelles. More importantly, mTHPC in these micelles clearly showed slower elimination kinetics from the blood circulation than free mTHPC (**Figure 6A**, red and green lines *vs* black line) and also than when mTHPC was loaded into previously reported $P_9$ micelles,[51] particularly 4 h post injection (~45% for mTHPC in (EGa1)-$P_{23}$ micelles *vs* ~17% for mTHPC in its free form and $P_9$ micelles of the injected dose (ID) detected in blood). According to the semi-logarithmic plot (**Figure S13**), these data can be fitted by a two-phase decay model, which was also previously applied for liposomal mTHPC formulations and Foscan®.[15,70,71] The thus calculated pharmacokinetic parameters (**Table 4**) show two elimination half-lives and the area under the curve (AUC) values that characterize the pharmacokinetics of mTHPC and micelles. The half-lives of the alpha phase for mTHPC in micellar formulations, ranging from 0.7 to 1 h, were similar to that observed for the corresponding micelles (0.5 h). In line with this, AUC values, reflecting drug concentrations in plasma, of the incorporated

mTHPC and its corresponding micelles in this phase were also comparable (**Table 4**). The half-life and AUC values of the beta phase for both the incorporated mTHPC and the corresponding micelles were considerably larger than the alpha phase. However, although both showed similar AUC values, the half-lives of mTHPC in micelles in the beta phase were obviously shorter than that of the corresponding micelles (~14 *vs* ~18 h, **Table 4**), indicating that mTHPC is released at least partly from the micelles prior to being removed from the blood. This premature cargo release was also observed previously in various liposomal mTHPC formulations and other drug loaded nanocarriers.[71,72] Surprisingly, although the incorporated mTHPC in our micelles showed slightly shorter half-lives of the beta phase than when encapsulated in the liposome (14 *vs* 18 h), $P_{23}$ micelles with or without EGa1 appear to be superior to the best reported liposomal carrier consisting of $PEG_{2000}$-DSPE/EPC/EPG (similar $t_{1/2}$ α: 0.5 vs 0.7 h while $t_{1/2}$ β: 18 *vs* 14 h).[71] This indeed indicates an excellent stability of these micelles in circulation. Most importantly, mTHPC loaded in $P_{23}$ micelles, no matter with or without EGa1, showed a significant increase in half-lives in each corresponding phase, when compared to that of free mTHPC (~1 vs 0.04 h in the alpha phase and 14 *vs* 2 h in the beta phase, **Table 4**). Combined with the significantly enhanced AUC values of micellar mTHPC formulations in each phase (**Table 4**), this demonstrates the prolonged retention of mTHPC in the circulation resulting from the excellent stability of the $P_{23}$ micelles.

It is worth noting that free mTHPC (*i.e.* mTHPC dissolved in propylene glycol/PBS 20/30/50 v/v/v) was really difficult for iv injection due to acute mouse responses to relatively high organic solvent present in formulation. The administration of free mTHPC clearly led to discomfort in mice, manifested by tachypnea and being passive within 1 min post injection (in fact, two mice died upon iv injection). Such side effects were also observed in cats with spontaneous squamous cell carcinoma treated with Foscan®.[73] In addition, the mice treated with free mTHPC showed the loss of bodyweight (~1 g on average) 24 h post injection. In contrast, micellar mTHPC formulations were well tolerated and none of the micellar mTHPC treated mice showed any side effects during or after their administration. This suggests that the micellar formulations at injected polymer dose (~1 mg) were safe for *in vivo* applications.

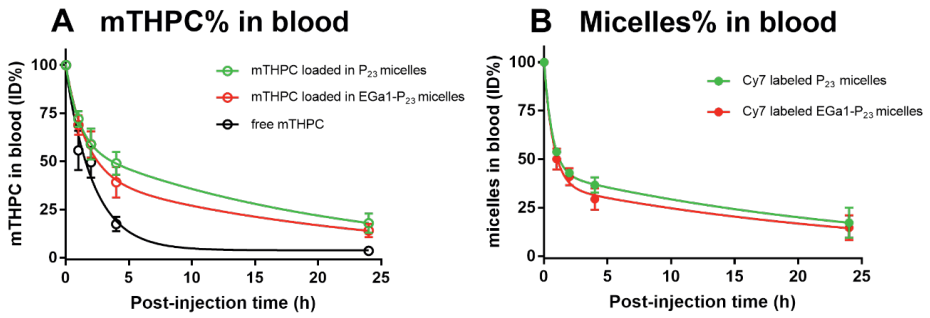


**Figure 6**. *In vivo* pharmacokinetics of free mTHPC (A) and Cy7 labeled (EGa1)-$P_{23}$ micelles (B) loaded with mTHPC (A) upon tail vein administration in A431 tumor-bearing Balb/c mice (0.3 mg mTHPC per kg bodyweight of the mouse, *i.e.* ~6 μg mTHPC). Blood samples taken at different time points were used to quantify the percentage of mTHPC and the corresponding Cy7 labeled micelles of the injected dose (%ID) present in systemic circulation. Data are presented as mean ± SD, N= 4.

**Table 4.** The half-life and the area under the curve (AUC) values of free mTHPC, mTHPC loaded in micelles and the corresponding (Cy7 labeled) micelles.

| Detection | Formulations | Half-life (h) | | AUC (h*%) | |
|---|---|---|---|---|---|
| | | Phase α | Phase β | Phase α | Phase β |
| **mTHPC** | Free mTHPC | 0.04 | 2.1 | 77 | 278 |
| | mTHPC in EGa1-$P_{23}$ micelles | 1.1 | 14.8 | 147 | 631 |
| | mTHPC in $P_{23}$ micelles | 0.7 | 14.1 | 150 | 778 |
| **Cy7** | EGa1-$P_{23}$ micelles | 0.5 | 18.3 | 124 | 513 |
| | $P_{23}$ micelles | 0.5 | 18.1 | 119 | 620 |

## 4. Conclusions

In the present study, PCL-PEG based micelles were decorated with the EGFR targeted nanobody EGa1 to render this formulation specific for EGFR overexpressing tumor cells. It is shown that EGa1 conjugated micelles are internalized upon specific binding of the nanobody with the EGFR receptor over-expressed on the surface of A431 cells, resulting in enhanced cellular uptake and photocytotoxicity on A431 cells, as compared to EGFR low expressing HeLa cells. The *in vivo* pharmacokinetic study shows prolonged circulation of mTHPC incorporated in $P_{23}$ micelles, compared to free mTHPC. In conclusion, the conjugation of EGa1 nanobody to the surface of these $P_{23}$ micelles has potential to significantly improve the selectivity and efficacy of PDT to EGFR over-expressing tumors.

**Acknowledgement**
Y. Liu is supported by a PhD scholarship from China Scholarship Council (CSC). Authors thank Dr. H. S. de Bruijn and Dr. D. J. Robinson for their assistance with determination of singlet oxygen generation.

## References


1. Biel, M. A. M. D. Photodynamic therapy of head and neck cancer-what's old and what's new. In handbook of photodynamic therapy: updates on recent applications of porphyrin-based compounds. *World Scientific.* **2016**, pp 439-458.
2. Bray, F.; Ferlay, J.; Soerjomataram, I.; Siegel, R. L.; Torre, L. A.; Jemal, A. Global cancer statistics 2018: GLOBOCAN estimates of incidence and mortality worldwide for 36 cancers in 185 countries. *CA Cancer J Clin* **2018,** *68*, 394-424.
3. Dirix, P.; Nuyts, S. Evidence-based organ-sparing radiotherapy in head and neck cancer. *The Lancet. Oncology* **2010,** *11*, 85-91.
4. Fung, C.; Grandis, J. R. Emerging drugs to treat squamous cell carcinomas of the head and neck. *Expert Opin Emerg Drugs* **2010,** *15*, 355-373.
5. Marur, S.; Forastiere, A. A. Head and neck squamous cell carcinoma: update on epidemiology, diagnosis, and treatment. *Mayo Clin. Proc.* **2016,** *91*, 386-396.
6. Meulemans, J.; Delaere, P.; Vander Poorten, V. Photodynamic therapy in head and neck cancer: Indications, outcomes, and future prospects. *Curr Opin Otolaryngol Head Neck Surg* **2019,** *27*, 136-141.
7. Dos Santos, A. F.; De Almeida, D. R. Q.; Terra, L. F.; Baptista, M. S.; Labriola, L. Photodynamic therapy in cancer treatment - an update review. *Journal of Cancer Metastasis and Treatment* **2019,** *5*, 1-20.
8. Kwiatkowski, S.; Knap, B.; Przystupski, D.; Saczko, J.; Kedzierska, E.; Knap-Czop, K.; Kotlinska, J.; Michel, O.; Kotowski, K.; Kulbacka, J. Photodynamic therapy - mechanisms, photosensitizers and combinations. *Biomed Pharmacother* **2018,** *106*, 1098-1107.
9. van Driel, P.; Boonstra, M. C.; Slooter, M. D.; Heukers, R.; Stammes, M. A.; Snoeks, T. J. A.; de Bruijn, H. S.; van Diest, P. J.; Vahrmeijer, A. L.; van Bergen En Henegouwen, P. M. P.; van de Velde, C. J. H.; Lowik, C.; Robinson, D. J.; Oliveira, S. EGFR targeted nanobody-photosensitizer conjugates for photodynamic therapy in a pre-clinical model of head and neck cancer. *J. Control. Release* **2016,** *229*, 93-105.
10. Baskaran, R.; Lee, J.; Yang, S. G. Clinical development of photodynamic agents and therapeutic applications. *Biomater. Res.* **2018,** *22*, 1-8.
11. Hopper, C. Photodynamic therapy: a clinical reality in the treatment of cancer. *The Lancet. Oncology* **2000,** *1*, 212-219.
12. de Visscher, S. A.; Kascakova, S.; de Bruijn, H. S.; van den Heuvel, A.; Amelink, A.; Sterenborg, H. J.; Robinson, D. J.; Roodenburg, J. L.; Witjes, M. J. Fluorescence localization and kinetics of mTHPC and liposomal formulations of mTHPC in the window-chamber tumor model. *Lasers Surg Med* **2011,** *43*, 528-536.
13. Bovis, M. J.; Woodhams, J. H.; Loizidou, M.; Scheglmann, D.; Bown, S. G.; Macrobert, A. J. Improved *in vivo* delivery of m-THPC via pegylated liposomes for use in photodynamic therapy. *J. Control. Release* **2012,** *157*, 196-205.
14. Redmond, R. W.; Land, E. J.; Truscott, T. G. Aggregation effects on the photophysical properties of porphyrins in relation to mechanisms involved in photodynamic therapy. *Advances in experimental medicine and biology* **1985,** *193*, 293-302.

15. Triesscheijn, M.; Ruevekamp, M.; Out, R.; Van Berkel, T. J.; Schellens, J.; Baas, P.; Stewart, F. A. The pharmacokinetic behavior of the photosensitizer meso-tetra-hydroxyphenyl-chlorin in mice and men. *Cancer chemotherapy and pharmacology* **2007,** *60*, 113-122.
16. Dos Santos, N.; Allen, C.; Doppen, A. M.; Anantha, M.; Cox, K. A.; Gallagher, R. C.; Karlsson, G.; Edwards, K.; Kenner, G.; Samuels, L.; Webb, M. S.; Bally, M. B. Influence of poly(ethylene glycol) grafting density and polymer length on liposomes: relating plasma circulation lifetimes to protein binding. *Biochim Biophys Acta* **2007,** *1768*, 1367-1377.
17. Klibanov, A. L.; Maruyama, K.; Torchilin, V. P.; Huang, L. Amphipathic polyethyleneglycols effectively prolong the circulation time of liposomes. *FEBS letters* **1990,** *268*, 235-237.
18. Torchilin, V. P. Recent advances with liposomes as pharmaceutical carriers. *Nat. Rev. Drug Discov.* **2005,** *4*, 145-160.
19. Maeda, H.; Wu, J.; Sawa, T.; Matsumura, Y.; Hori, K. Tumor vascular permeability and the EPR effect in macromolecular therapeutics: a review. *J. Control. Release* **2000,** *65*, 271-284.
20. Fang, J.; Nakamura, H.; Maeda, H. The EPR effect: Unique features of tumor blood vessels for drug delivery, factors involved, and limitations and augmentation of the effect. *Adv. Drug Deliv. Rev.* **2011,** *63*, 136-151.
21. Maeda, H. Toward a full understanding of the EPR effect in primary and metastatic tumors as well as issues related to its heterogeneity. *Adv. Drug Deliv. Rev.* **2015,** *91*, 3-6.
22. Reshetov, V.; Lassalle, H. P.; Francois, A.; Dumas, D.; Hupont, S.; Grafe, S.; Filipe, V.; Jiskoot, W.; Guillemin, F.; Zorin, V.; Bezdetnaya, L. Photodynamic therapy with conventional and PEGylated liposomal formulations of mTHPC (temoporfin): Comparison of treatment efficacy and distribution characteristics in vivo. *Int. J. Nanomedicine* **2013,** *8*, 3817-3831.
23. Cabral, H.; Matsumoto, Y.; Mizuno, K.; Chen, Q.; Murakami, M.; Kimura, M.; Terada, Y.; Kano, M. R.; Miyazono, K.; Uesaka, M.; Nishiyama, N.; Kataoka, K. Accumulation of sub-100 nm polymeric micelles in poorly permeable tumours depends on size. *Nat. Nanotechnol.* **2011,** *6*, 815-823.
24. Danhier, F. To exploit the tumor microenvironment: Since the EPR effect fails in the clinic, what is the future of nanomedicine? *J. Control. Release* **2016,** *244*, 108-121.
25. Jain, R. K.; Stylianopoulos, T. Delivering nanomedicine to solid tumors. *Nat. Rev. Clin. Oncol.* **2010,** *7*, 653-664.
26. Jiang, W.; Kim, B. Y.; Rutka, J. T.; Chan, W. C. Nanoparticle-mediated cellular response is size-dependent. *Nat. Nanotechnol.* **2008,** *3*, 145-150.
27. Yuan, F.; Leunig, M.; Huang, S. K.; Berk, D. A.; Papahadjopoulos, D.; Jain, R. K. Microvascular permeability and interstitial penetration of sterically stabilized (stealth) liposomes in a human tumor xenograft. *Cancer research* **1994,** *54*, 3352-3356.
28. Deng, C.; Jiang, Y.; Cheng, R.; Meng, F.; Zhong, Z. Biodegradable polymeric micelles for targeted and controlled anticancer drug delivery: Promises, progress and prospects. *Nano Today* **2012,** *7*, 467-480.
29. Varela-Moreira, A.; Shi, Y.; Fens, M. H. A. M.; Lammers, T.; Hennink, W. E.; Schiffelers, R. M. Clinical application of polymeric micelles for the treatment of cancer. *Materials Chemistry Frontiers* **2017,** *1*, 1485-1501.

30. Cabral, H.; Kataoka, K. Progress of drug-loaded polymeric micelles into clinical studies. *J. Control. Release* **2014,** *190*, 465-476.
31. Houdaihed, L.; Evans, J. C.; Allen, C. Overcoming the road blocks: advancement of block copolymer micelles for cancer therapy in the clinic. *Mol. Pharmaceutics* **2017,** *14*, 2503-2517.
32. Gaucher, G.; Dufresne, M. H.; Sant, V. P.; Kang, N.; Maysinger, D.; Leroux, J. C. Block copolymer micelles: Preparation, characterization and application in drug delivery. *J. Control. Release* **2005,** *109*, 169-188.
33. Park, J. H.; Lee, S.; Kim, J.-H.; Park, K.; Kim, K.; Kwon, I. C. Polymeric nanomedicine for cancer therapy. *Progress in Polymer Science* **2008,** *33*, 113-137.
34. Bagheri, M.; Bresseleers, J.; Varela-Moreira, A.; Sandre, O.; Meeuwissen, S. A.; Schiffelers, R. M.; Metselaar, J. M.; van Nostrum, C. F.; van Hest, J. C. M.; Hennink, W. E. Effect of formulation and processing parameters on the size of mPEG- b-p(HPMA-Bz) polymeric micelles. *Langmuir* **2018,** *34*, 15495-15506.
35. Danhier, F.; Feron, O.; Preat, V. To exploit the tumor microenvironment: Passive and active tumor targeting of nanocarriers for anti-cancer drug delivery. *J. Control. Release* **2010,** *148*, 135-146.
36. Chang, E.; Yu, W. W.; Colvin, V. L.; Drezek, R. Quantifying the influence of surface coatings on quantum dot uptake in cells. *Journal of Biomedical Nanotechnology* **2005,** *1*, 397-401.
37. Pirollo, K. F.; Chang, E. H. Does a targeting ligand influence nanoparticle tumor localization or uptake? *Trends Biotechnol* **2008,** *26*, 552-558.
38. Talelli, M.; Rijcken, C. J.; Oliveira, S.; van der Meel, R.; van Bergen En Henegouwen, P. M.; Lammers, T.; van Nostrum, C. F.; Storm, G.; Hennink, W. E. Nanobody-shell functionalized thermosensitive core-crosslinked polymeric micelles for active drug targeting. *J. Control. Release* **2011,** *151*, 183-192.
39. Martinez-Jothar, L.; Beztsinna, N.; van Nostrum, C. F.; Hennink, W. E.; Oliveira, S. Selective cytotoxicity to HER2 positive breast cancer cells by saporin-loaded nanobody-targeted polymeric nanoparticles in combination with photochemical internalization. *Mol. Pharmaceutics* **2019,** *16*, 1633-1647.
40. Ruoslahti, E.; Bhatia, S. N.; Sailor, M. J. Targeting of drugs and nanoparticles to tumors. *J. Cell Biol.* **2010,** *188*, 759-768.
41. Zimmermann, M.; Zouhair, A.; Azria, D.; Ozsahin, M. The epidermal growth factor receptor (EGFR) in head and neck cancer: its role and treatment implications. *Radiat. Oncol.* **2006,** *1*, 1-6.
42. Dolk, E.; van Vliet, C.; Perez, J. M.; Vriend, G.; Darbon, H.; Ferrat, G.; Cambillau, C.; Frenken, L. G.; Verrips, T. Induced refolding of a temperature denatured llama heavy-chain antibody fragment by its antigen. *Proteins* **2005,** *59*, 555-564.
43. Oliveira, S.; Schiffelers, R. M.; van der Veeken, J.; van der Meel, R.; Vongpromek, R.; van Bergen En Henegouwen, P. M.; Storm, G.; Roovers, R. C. Downregulation of EGFR by a novel multivalent nanobody-liposome platform. *J. Control. Release* **2010,** *145*, 165-175.
44. Oliveira, S.; Heukers, R.; Sornkom, J.; Kok, R. J.; van Bergen en Henegouwen, P. M. P. Targeting tumors with nanobodies for cancer imaging and therapy. *J. Control. Release* **2013,** *172*, 607-617.
45. Gao, H.; Shi, W.; Freund, L. B. Mechanics of receptor-mediated endocytosis. *Proceedings of the National Academy of Sciences of the United States of America* **2005,** *102*, 9469-9474.

46. Prabha, S.; Zhou, W. Z.; Panyam, J.; Labhasetwar, V. Size-dependency of nanoparticle-mediated gene transfection: Studies with fractionated nanoparticles. *Int. J. Pharm.* **2002,** *244*, 105-115.
47. Zhang, S.; Li, J.; Lykotrafitis, G.; Bao, G.; Suresh, S. Size-dependent endocytosis of nanoparticles. *Adv. Mater.* **2009,** *21*, 419-424.
48. Sykes, E. A.; Chen, J.; Zheng, G.; Chan, W. C. W. Investigating the impact of nanoparticle size on active and passive tumor targeting efficiency. *ACS Nano* **2014,** *8*, 5696-5706.
49. van Lith, S. A.; van Duijnhoven, S. M.; Navis, A. C.; Leenders, W. P.; Dolk, E.; Wennink, J. W.; van Nostrum, C. F.; van Hest, J. C. Legomedicine-a versatile chemo-enzymatic approach for the preparation of targeted dual-labeled llama antibody-nanoparticle conjugates. *Bioconjug. Chem.* **2017,** *28*, 539-548.
50. Ravasco, J.; Faustino, H.; Trindade, A.; Gois, P. M. P. Bioconjugation with maleimides: A useful tool for chemical biology. *Chemistry* **2019,** *25*, 43-59.
51. Wennink, J. W. H.; Liu, Y.; Makinen, P. I.; Setaro, F.; de la Escosura, A.; Bourajjaj, M.; Lappalainen, J. P.; Holappa, L. P.; van den Dikkenberg, J. B.; Al Fartousi, M.; Trohopoulos, P. N.; Yla-Herttuala, S.; Torres, T.; Hennink, W. E.; van Nostrum, C. F. Macrophage selective photodynamic therapy by meta-tetra(hydroxyphenyl)chlorin loaded polymeric micelles: A possible treatment for cardiovascular diseases. *Eur. J. Pharm. Sci.* **2017,** *107*, 112-125.
52. Couffin, A.; Delcroix, D.; Martín-Vaca, B.; Bourissou, D.; Navarro, C. Mild and efficient preparation of block and gradient copolymers by methanesulfonic acid catalyzed ring-opening polymerization of caprolactone and trimethylene carbonate. *Macromolecules* **2013,** *46*, 4354-4360.
53. Delcroix, D.; Martín-Vaca, B.; Bourissou, D.; Navarro, C. Ring-opening polymerization of trimethylene carbonate catalyzed by methanesulfonic acid: Activated monomer versus active chain end mechanisms. *Macromolecules* **2010,** *43*, 8828-8835.
54. Hofman, E. G.; Ruonala, M. O.; Bader, A. N.; van den Heuvel, D.; Voortman, J.; Roovers, R. C.; Verkleij, A. J.; Gerritsen, H. C.; van Bergen En Henegouwen, P. M. EGF induces coalescence of different lipid rafts. *J. Cell. Sci.* **2008,** *121*, 2519-2528.
55. van der Meel, R.; Oliveira, S.; Altintas, I.; Haselberg, R.; van der Veeken, J.; Roovers, R. C.; van Bergen en Henegouwen, P. M.; Storm, G.; Hennink, W. E.; Schiffelers, R. M.; Kok, R. J. Tumor-targeted nanobullets: Anti-EGFR nanobody-liposomes loaded with anti-IGF-1R kinase inhibitor for cancer treatment. *J. Control. Release* **2012,** *159*, 281-289.
56. Yin, H.; Lee, E. S.; Kim, D.; Lee, K. H.; Oh, K. T.; Bae, Y. H. Physicochemical characteristics of pH-sensitive poly(L-histidine)-*b*-poly(ethylene glycol)/poly(L-lactide)-*b*-poly(ethylene glycol) mixed micelles. *J Control. Release* **2008,** *126*, 130-138.
57. Ehrhart, J.; Mingotaud, A. F.; Violleau, F. Asymmetrical flow field-flow fractionation with multi-angle light scattering and quasi elastic light scattering for characterization of poly(ethyleneglycol-b-varepsilon-caprolactone) block copolymer self-assemblies used as drug carriers for photodynamic therapy. *J. Chromatogr. A* **2011,** *1218*, 4249-4256.
58. Shi, Y.; van Steenbergen, M. J.; Teunissen, E. A.; Novo, L.; Gradmann, S.; Baldus, M.; van Nostrum, C. F.; Hennink, W. E. $\pi$-$\pi$ stacking increases the stability and loading capacity of thermosensitive polymeric micelles for chemotherapeutic drugs. *Biomacromolecules* **2013,** *14*, 1826-1837.

59. Carstens, M. G.; Bevernage, J. J. L.; van Nostrum, C. F.; van Steenbergen, M. J.; Flesch, F. M.; Verrijk, R.; de Leede, L. G. J.; Crommelin, D. J. A.; Hennink, W. E. Small oligomeric micelles based on end group modified mPEG–oligocaprolactone with monodisperse hydrophobic blocks. *Macromolecules* **2007,** *40*, 116-122.

60. Carstens, M. G.; van Nostrum, C. F.; Verrijk, R.; de Leede, L. G.; Crommelin, D. J.; Hennink, W. E. A mechanistic study on the chemical and enzymatic degradation of PEG-Oligo(epsilon-caprolactone) micelles. *J. Pharm. Sci.* **2008,** *97*, 506-518.

61. Lassalle, H. P.; Wagner, M.; Bezdetnaya, L.; Guillemin, F.; Schneckenburger, H. Fluorescence imaging of Foscan and Foslip in the plasma membrane and in whole cells. *J Photochem Photobiol B* **2008,** *92*, 47-53.

62. Reidy, K.; Campanile, C.; Muff, R.; Born, W.; Fuchs, B. mTHPC-mediated photodynamic therapy is effective in the metastatic human 143B osteosarcoma cells. *Photochem Photobiol* **2012,** *88*, 721-727.

63. Chen, Y.; Tezcan, O.; Li, D.; Beztsinna, N.; Lou, B.; Etrych, T.; Ulbrich, K.; Metselaar, J. M.; Lammers, T.; Hennink, W. E. Overcoming multidrug resistance using folate receptor-targeted and pH-responsive polymeric nanogels containing covalently entrapped doxorubicin. *Nanoscale* **2017,** *9*, 10404-10419.

64. Xie, J.; Xu, C.; Kohler, N.; Hou, Y.; Sun, S. Controlled PEGylation of monodisperse $Fe_3O_4$ nanoparticles for reduced non-specific uptake by macrophage cells. *Advanced Materials* **2007,** *19*, 3163-3166.

65. Kiesslich, T.; Berlanda, J.; Plaetzer, K.; Krammer, B.; Berr, F. Comparative characterization of the efficiency and cellular pharmacokinetics of Foscan- and Foslip-based photodynamic treatment in human biliary tract cancer cell lines. *Photochem. Photobiol. Sci.* **2007,** *6*, 619-627.

66. Syu, W. J.; Yu, H. P.; Hsu, C. Y.; Rajan, Y. C.; Hsu, Y. H.; Chang, Y. C.; Hsieh, W. Y.; Wang, C. H.; Lai, P. S. Improved photodynamic cancer treatment by folate-conjugated polymeric micelles in a KB xenografted animal model. *Small* **2012,** *8*, 2060-2069.

67. Moret, F.; Scheglmann, D.; Reddi, E. Folate-targeted PEGylated liposomes improve the selectivity of PDT with meta-tetra(hydroxyphenyl)chlorin (m-THPC). *Photochem Photobiol Sci.* **2013,** *12*, 823-834.

68. Wu, J.; Feng, S.; Liu, W.; Gao, F.; Chen, Y. Targeting integrin-rich tumors with temoporfin-loaded vitamin-E-succinate-grafted chitosan oligosaccharide/d-alpha-tocopheryl polyethylene glycol 1000 succinate nanoparticles to enhance photodynamic therapy efficiency. *Int. J. Pharm.* **2017,** *528*, 287-298.

69. Paszko, E.; Vaz, G. M.; Ehrhardt, C.; Senge, M. O. Transferrin conjugation does not increase the efficiency of liposomal Foscan during in vitro photodynamic therapy of oesophageal cancer. *Eur. J. Pharm. Sci.* **2013,** *48*, 202-210.

70. Cramers, P.; Ruevekamp, M.; Oppelaar, H.; Dalesio, O.; Baas, P.; Stewart, F. A. Foscan uptake and tissue distribution in relation to photodynamic efficacy. *Br J Cancer* **2003,** *88*, 283-290.

71. Decker, C.; Schubert, H.; May, S.; Fahr, A. Pharmacokinetics of temoporfin-loaded liposome formulations: correlation of liposome and temoporfin blood concentration. *J. Control. Release* **2013,** *166*, 277-285.

72. Shi, Y.; van der Meel, R.; Theek, B.; Oude Blenke, E.; Pieters, E. H.; Fens, M. H.; Ehling, J.; Schiffelers, R. M.; Storm, G.; van Nostrum, C. F.; Lammers, T.; Hennink, W. E. Complete regression of xenograft tumors upon targeted delivery of paclitaxel via Pi-Pi stacking stabilized polymeric micelles. *ACS Nano* **2015,** *9*, 3740-3752.

73. Buchholz, J.; Kaser-Hotz, B.; Khan, T.; Rohrer Bley, C.; Melzer, K.; Schwendener, R. A.; Roos, M.; Walt, H. Optimizing photodynamic therapy: in vivo pharmacokinetics of liposomal meta-(tetrahydroxyphenyl)chlorin in feline squamous cell carcinoma. *Clin. Cancer Res.* **2005,** *11*, 7538-7544.

## Supporting information

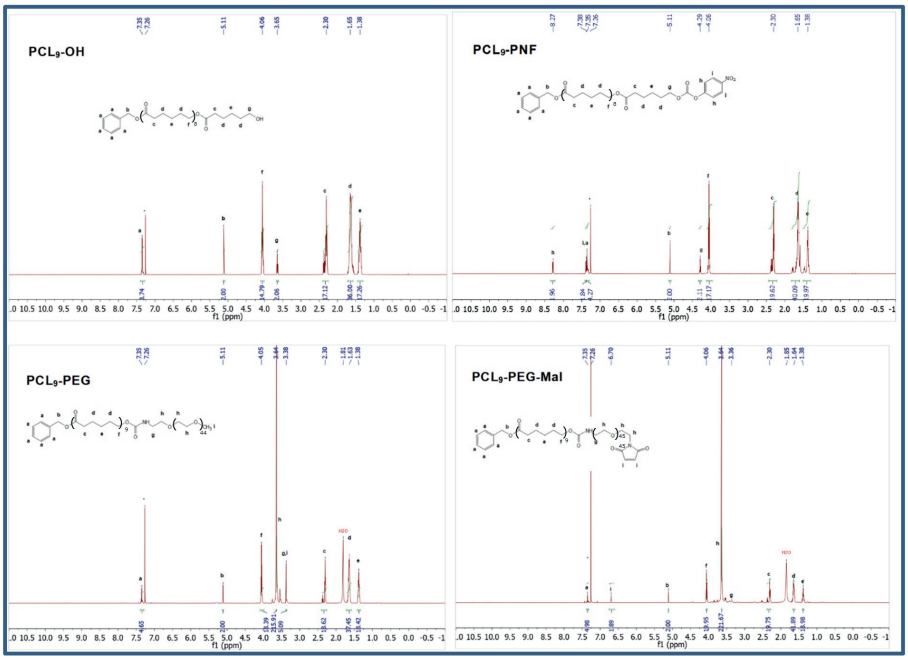


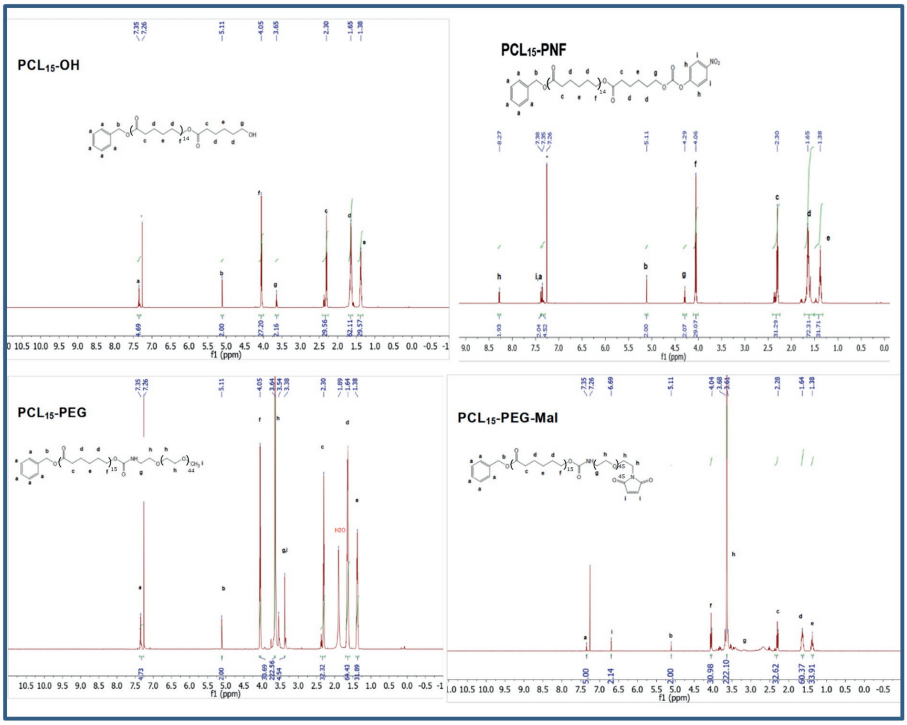

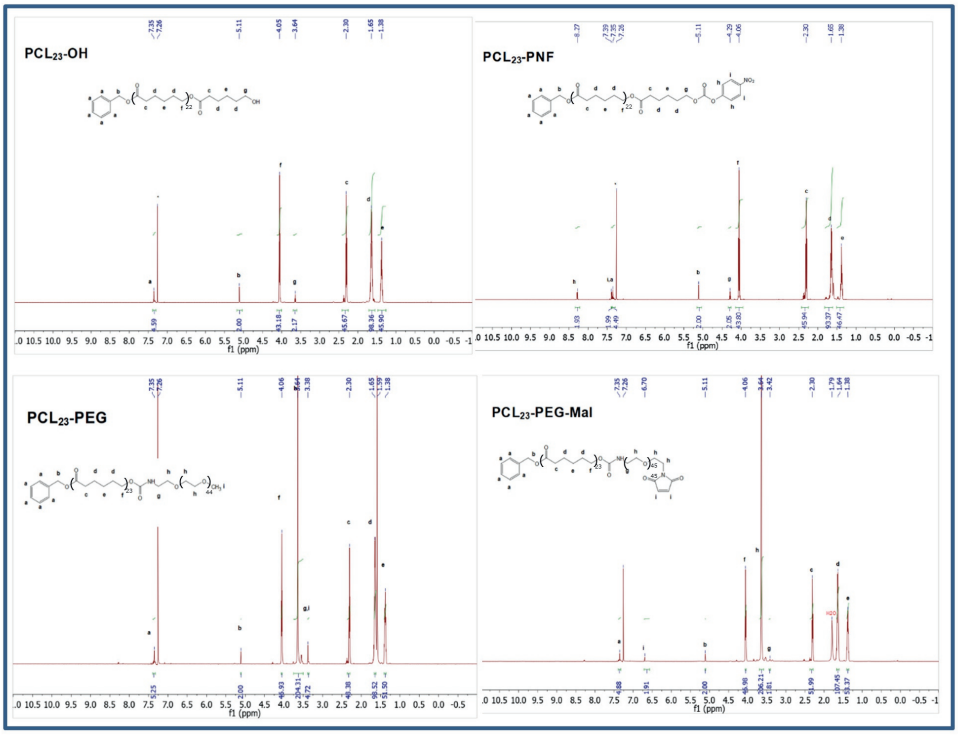


**Figure S1.** $^{1}$H NMR spectra of the $PCL_n$ oligomers, intermediate products and final $PCL_n$-PEG/$PCL_n$-PEG-Mal block copolymers (n=9, 15 and 23).

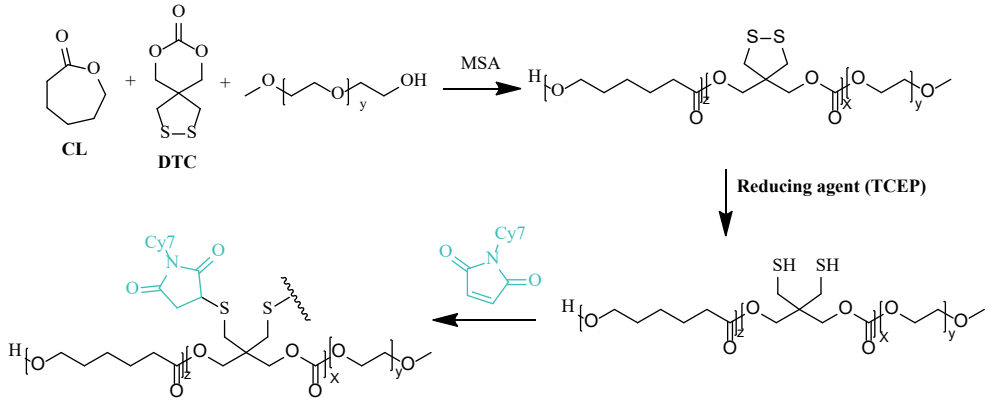


**Scheme S1**. Synthesis and Cy7 labeling of PCL-PDTC-PEG.

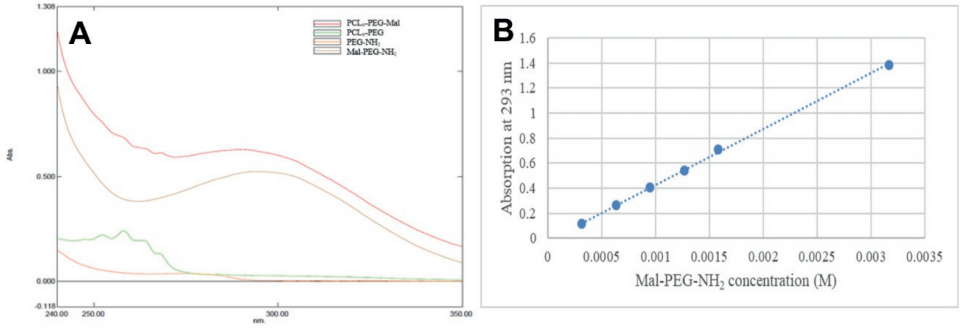


**Figure S2.** (A) UV-Vis spectra of $PCL_9$-PEG-Mal, Mal-PEG-$NH_2$, $PCL_9$-PEG, PEG-$NH_2$ in DCM at a polymer concentration of 5 mg/mL and (B) calibration curve of Mal-PEG-$NH_2$ in DCM.

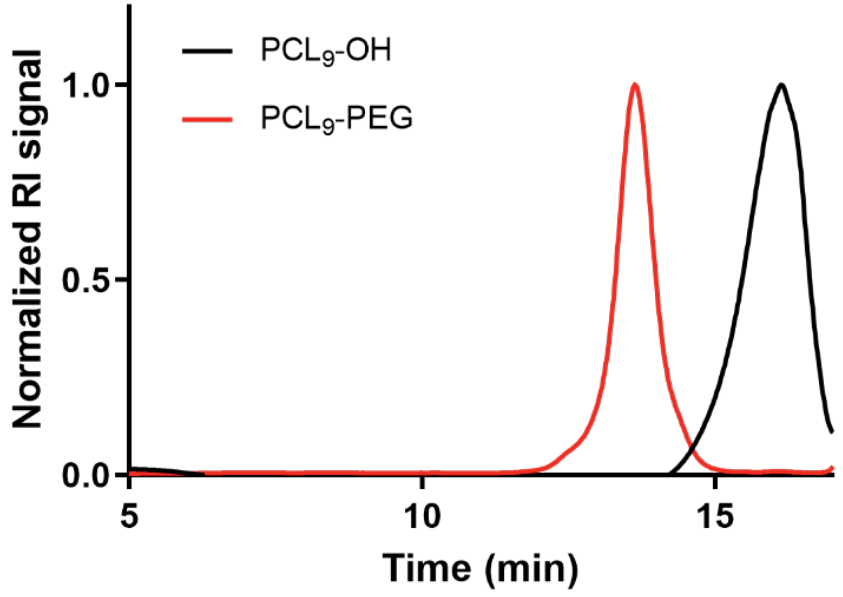


**Figure S3.** GPC chromatograms of $PCL_9$-OH and $PCL_9$-PEG recorded by refractive index (RI) detector.

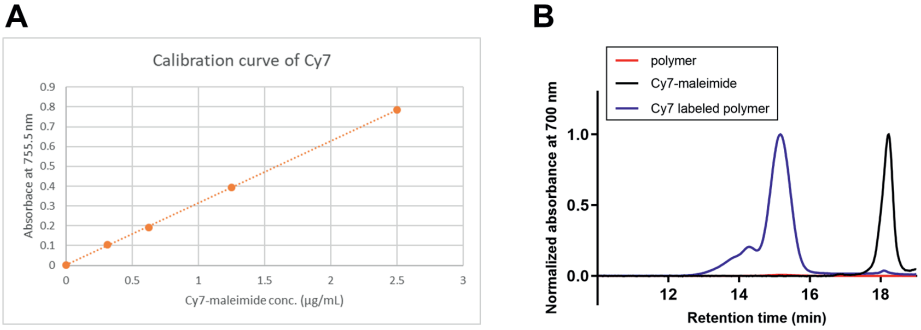


**Figure S4.** (A) Calibration curve of Cy7-maleimide in DCM, recorded at 755.5 nm and (B) GPC curves of Cy7-maleimide, $PCL_{18}$-$PDTC_{7.5}$-PEG polymer and Cy7-labeled $PCL_{18}$-$PDTC_{7.5}$-PEG polymer, recorded at 700 nm by UV/Vis detector.

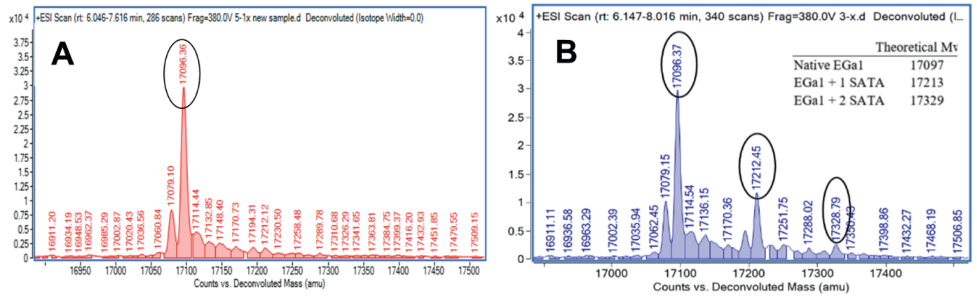


C

| | Native EGa1 | Reduced EGa1 | EGa1-SATA |
|---|---|---|---|
| **Average number of sulfhydryls** | 0.19±0.01 | 1.93±0.13 | 1.84±0.06 |

**Figure S5.** (A-B) LC-ESI-TOF-MS spectra of native EGa1 (A) and SATA modified EGa1 (B) at a 1:5 molar ratio of EGa1 to SATA, respectively. The inset of theoretical mass in (B) correlated with the molecular weight of 0 to 2 SATA molecules conjugated to one EGa1 molecule. (C) the number of sulfhydryls (-SH) per native EGa1, reduced EGa1 and SATA modified EGa1 after 1:5 molar incubation ratio of EGa1 to SATA based on Ellman's assay.


**Figure S6.** SDS-PAGE silver staining of SATA-EGa1 and micelles composed of 9:1 mixtures of $PCL_n$-PEG and $PCL_n$-PEG-Mal incubated with/without (protected) SATA-EGa1. A is the protein ladder; lane B represents SATA-modified EGa1; lanes C-E are $P_n$ micelles incubated with protected EGa1-SATA (n=9 (C), n=15 (D), n=23 (E)); lanes F-H display $P_n$ micelles alone (n=9 (F), n=15 (G), n=23 (H)).

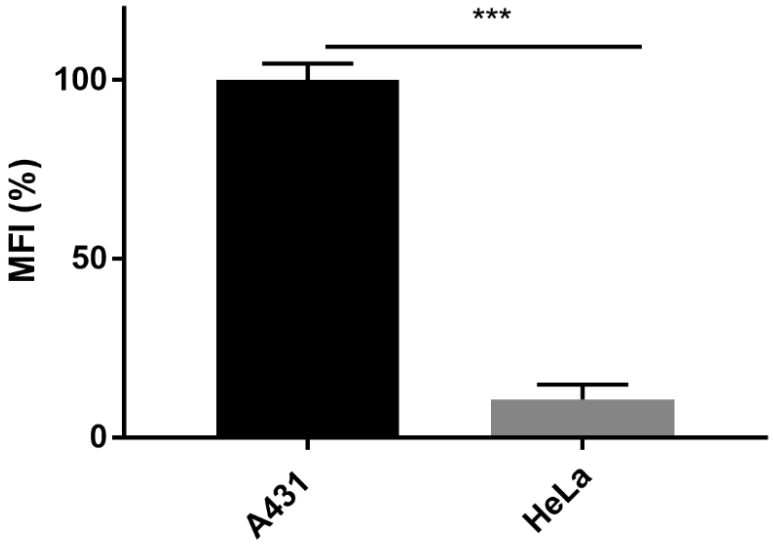


**Figure S7.** EGFR expression in A431 and HeLa cells as determined by flow cytometry, using cells that were incubated with an antibody against the EGFR receptor. *** represents $p < 0.001$.

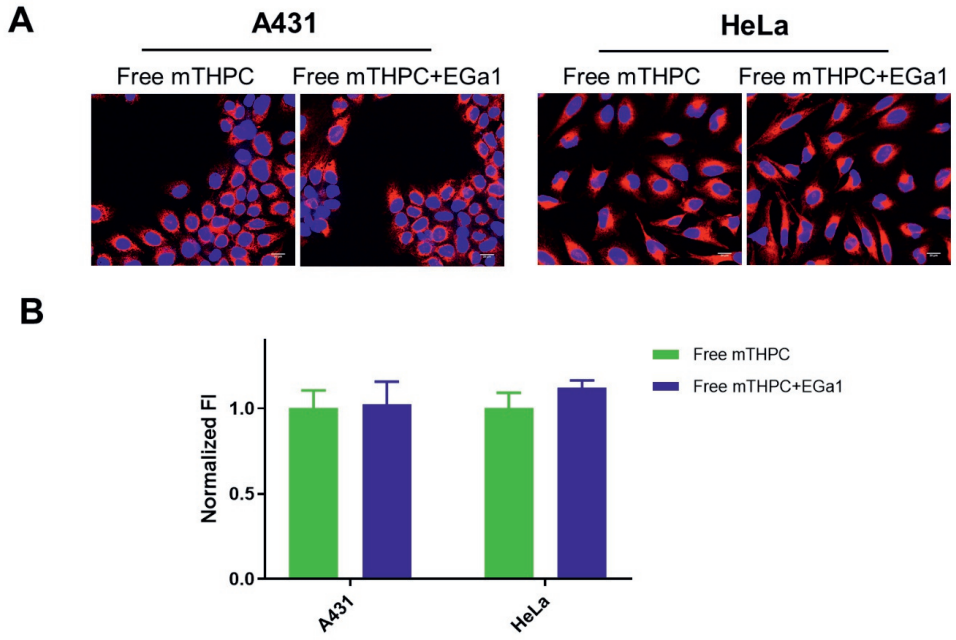


**Figure S8.** (A) Representative confocal fluorescence microscopic images of A431 and HeLa cells incubated with free mTHPC and mTHPC containing a 9 fold excess of free EGa1 (named free mTHPC+EGa1) for 7 h at 37 °C. mTHPC concentration was 38 μg/mL, corresponding to a concentration using 5wt% mTHPC-loaded micelles as used in Figure 2. Cell nuclei are stained in blue with Hoechst, while fluorescence of mTHPC is represented in red. Scale bars indicate 20 μm. The images were taken using the same parameters in both cells (excitation times requied for images were 25 msec). (B) Quantification of fluorescence intensity of mTHPC ($\lambda_{ex}$ 405 nm, $\lambda_{em}$ 676 nm) in A431 and HeLa cells by ImageJ. The quantified fluorescence intensity was normalized by the intensity of mTHPC in A431 cells and by the number of cells.

### *S1 Cytotoxicity of empty micelles*

EGa1-$P_n$ micelles without mTHPC loading and their corresponding non-targeted micelles at a fixed polymer concentration of 10 mg/mL in PBS (prepared as described in Section 2.4 and 2.5) were employed to assess the cytotoxicity of the empty micelles on A431 and HeLa cells, following the similar protocol in photo-cytotoxicity study (described in section 2.9) with a slight adjustment of the volume ratio between the medium and the micellar dispersions, depending on the predetermined polymer concentration. For instance, to get a final polymer concentration of 4 mg/mL, 80 μL of micellar dispersions was added to 120 μL medium and the cells were cultured for 24 h at 37 °C. Cell viability was determined by MTS assay.

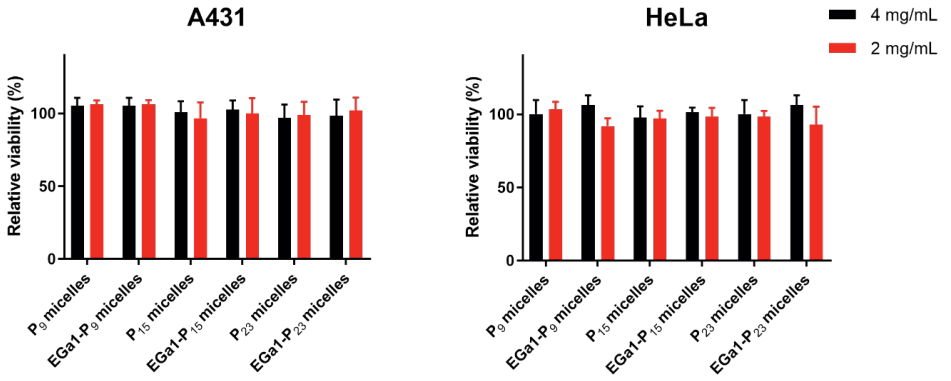


**Figure S9.** Cytotoxicity assessed by MTS assay of empty targeted EGa1-$P_n$ and non-targeted $P_n$ micelles composed of 2 and 4 mg/mL $PCL_n$-PEG/$PCL_n$-PEG-Mal (9:1) polymer on A431 and HeLa cells after 24 h incubation at 37 ℃ (n = 9, 15 and 23, respectively). N=3.

**Table S1.** Loading efficiency (LE) and loading capacity (LC) of mTHPC loaded in $P_{23}$ micelles decorated with EGa1 nanobody (targeted) or cysteines only (non-targeted).

| Feed ratio of mTHPC to polymer(wt%) | $P_{23}$ micelles (non-targeted) | | EGa1-$P_{23}$ micelles (targeted) | |
|---|---|---|---|---|
| | LE% | LC% | LE% | LC% |
| **1%** | 65 | 0.3 | 65 | 0.3 |
| **2%** | 94 | 1.8 | 93 | 1.8 |
| **4%** | 94 | 3.6 | 95 | 3.6 |
| **6%** | 83 | 4.7 | 83 | 4.7 |
| **8%** | 72 | 5.4 | 72 | 5.4 |
| **10%** | 76 | 7.1 | 76 | 7.1 |

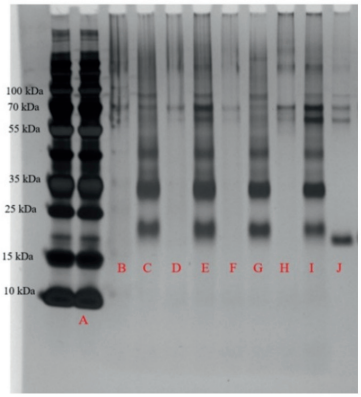


**Figure S10.** SDS-PAGE silver staining of mTHPC-loaded EGa1-conjugated and unconjugated micelles (*i.e.* EGa1-$P_{23}$ micelles (lanes I, G, E, C) and $P_{23}$ micelles (lanes H, F, D, B), respectively) with 2, 4, 6, 8 wt% mTHPC, respectively, after 10 washings with PBS using centrifugation with Vivaspin-6 tubes along with native EGa1 control (J). Lane A represents a protein ladder.

**Table S2.** $EC_{50}$ of free mTHPC and mTHPC loaded in micelles (1 mg/mL polymer) on A431 and HeLa cells after 7 h incubation.

| | $EC_{50}$ (μg/mL) | |
|---|---|---|
| | **A431** | **HeLa** |
| **$P_{23}$ micelles** | 38.3±1.9 | 29.2±2.6 |
| **EGa1-$P_{23}$ micelles** | 10.4±0.7 | 28.5±1.8 |
| **Competition** | 48.3±3.1 | 32.7±1.0 |
| **Free mTHPC** | 1.6 ±0.1 | 1.2[a] |
| **Free mTHPC+EGa1** | 1.7±0.1 | 1.3[a] |

[a] SD < 0.1.



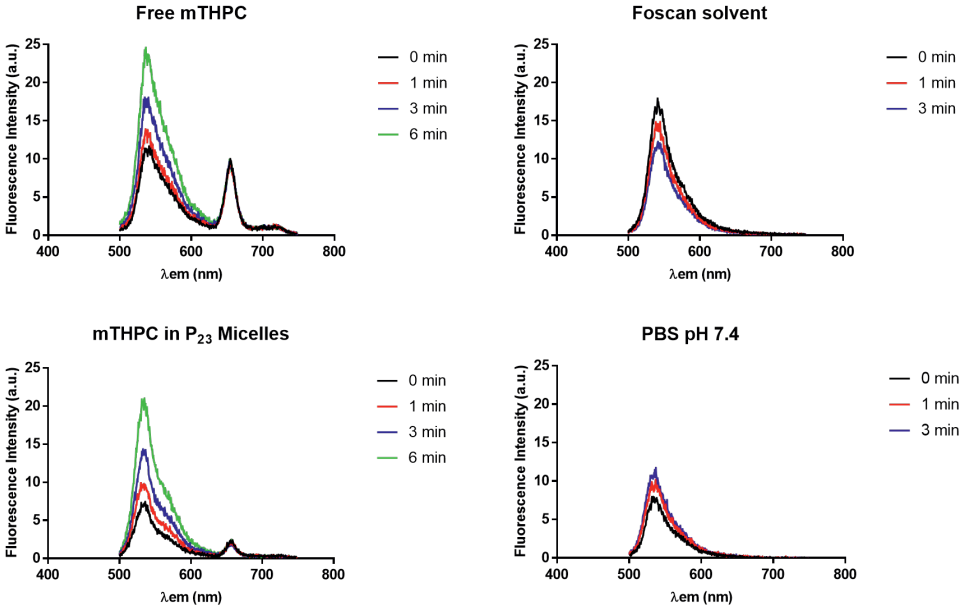


**Figure S11.** Fluorescence emission spectrum of singlet oxygen sensor green reagent in free mTHPC solution or its solvent only; in mTHPC in $P_{23}$ micelles, or in PBS pH 7.4. Measurements performed after 0, 1, 3 or 6 min of illumination with a filtered white light source at 645-665 nm at a fluence rate of 5 mW/cm$^2$.

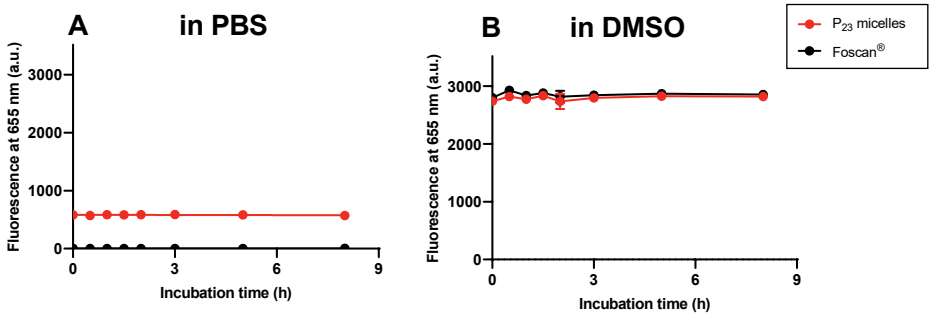


**Figure S12.** Fluorescence intensity ($\lambda_{ex}$ 420 nm, $\lambda_{em}$ 655 nm) as a function of time at 37 °C in PBS (A) and DMSO (B); Foscan® and micelles of 10 mg/mL with 5wt% loading amounts were prepared and diluted 10× in PBS or DMSO, to obtain the final mTHPC concentration of 40 mg/mL.

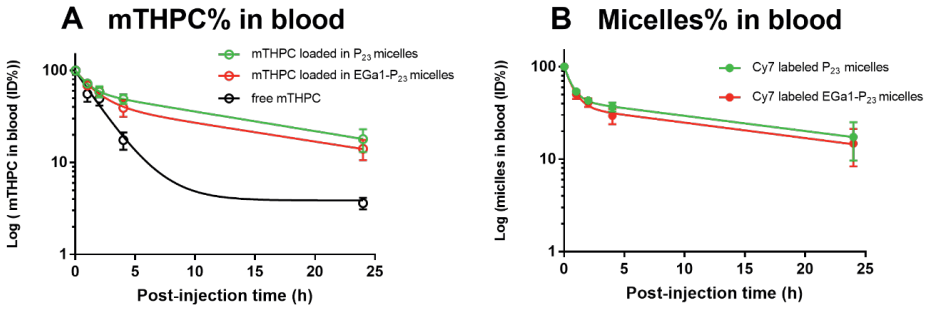


**Figure S13.** (A-B) The log-concentration of free mTHPC (A) and Cy7 labeled (EGa1)-$P_{23}$ micelles (B) loaded with mTHPC (A) in blood overtime upon tail vein administration in A431 tumor-bearing Balb/c mice (0.3 mg mTHPC per kg bodyweight of the mouse, *i.e.,* ~6 µg mTHPC). Blood samples taken at different time points were used to quantify the percentage of mTHPC and the corresponding Cy7 labeled micelles of the injected dose (%ID) present in systemic circulation. Data are presented as mean ± SD, N= 4.

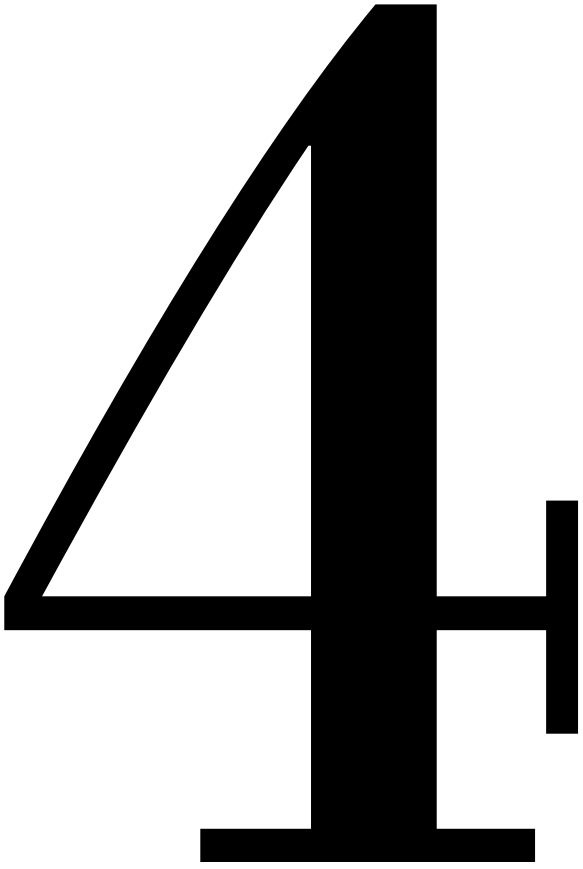

# Chapter 4

## π-π-Stacked Poly(ε-caprolactone)-*b*-poly(ethylene glycol) Micelles Loaded with a Photosensitizer for Photodynamic Therapy

Yanna Liu [1], Marcel H.A.M. Fens [1], Bo Lou [1], Nicky C.H. van Kronenburg [1], Roel F.M. Maas-Bakker [1], Robbert J. Kok [1], Sabrina Oliveira [1,2], Wim E. Hennink [1] and Cornelus F. van Nostrum [1,*]

[1] Department of Pharmaceutics, Utrecht Institute for Pharmaceutical Sciences, Utrecht University, Universiteitsweg 99, 3508 TB Utrecht, the Netherlands
[2] Division of Cell Biology, Neurobiology and Biophysics, Department of Biology, Utrecht University, Padualaan 8, 3584 CH Utrecht, the Netherlands.

*Pharmaceutics 2020, 12(4), 338*

**Abstract**

To improve the in vivo stability of poly(ε-caprolactone)-*b*-poly(ethylene glycol) (PCL-PEG)-based micelles and cargo retention by π-π stacking interactions, pendant aromatic rings were introduced by copolymerization of ε-caprolactone with benzyl 5-methyl-2-oxo-1,3-dioxane-5-carboxylate (TMC-Bz). It was shown that the incorporation of aromatic rings yielded smaller micelles (18–30 nm) with better colloidal stability in PBS than micelles without aromatic groups. The circulation time of i.v. injected micelles containing multiple pendant aromatic groups was longer ($t_{1/2}$-α: ~0.7 h; $t_{1/2}$-β: 2.9 h) than that of micelles with a single terminal aromatic group ($t_{1/2}$ < 0.3 h). In addition, the in vitro partitioning of the encapsulated photosensitizer (meta-tetra(hydroxyphenyl)chlorin, mTHPC) between micelles and human plasma was favored towards micelles for those that contained the pendant aromatic groups. However, this was not sufficient to fully retain mTHPC in the micelles in vivo, as indicated by similar biodistribution patterns of micellar mTHPC compared to free mTHPC, and unequal biodistribution patterns of mTHPC and the host micelles. Our study points out that more detailed in vitro methods are necessary to more reliably predict in vivo outcomes. Furthermore, additional measures beyond π-π stacking are needed to stably incorporate mTHPC in micelles in order to benefit from the use of micelles as targeted delivery systems.

**Keywords:** polymer micelles; photodynamic therapy; in vitro release; circulation kinetics; biodistribution

## 1. Introduction

Photodynamic therapy (PDT) is a minimally invasive form of therapy that has been approved for treatment of various types of cancers, including head and neck tumors, basal cell carcinoma, cervical, endobronchial, esophageal, bladder, and gastric cancers [1,2]. Compared to conventional treatments, such as surgery, radiation and chemotherapy, PDT has important advantages, including reduced toxicity for healthy tissues, lack of drug resistance mechanisms, and favorable cosmetic outcomes. Furthermore, evidence of immune activation has been described after PDT, capable of leading to antitumor immunity [3,4]. PDT is based on a photochemical reaction between a light activatable molecule (i.e., photosensitizers (PS)), light, and molecular oxygen, which are harmless individually [1]. In combination, PS can be excited by light of the wavelength matching its absorption maximum and can subsequently transfer its energy to molecular oxygen to yield singlet oxygen species (ROS), which are highly reactive with biomolecules present in cytoplasma or cell membranes, leading to cell death [5,6]. Effective cancer PDT is, however, hindered by some undesired properties in PS. Most PS molecules—including the clinically approved second generation PS, meta-tetra(hydroxyphenyl)chlorin (mTHPC)—are highly hydrophobic due to the extended delocalized aromatic π electron system. This promotes non-specific binding to cells, resulting in unspecific distribution of PS in healthy tissues (i.e., no selective accumulation of the PS in tumorous tissues), which can cause skin toxicity [7–9]. Moreover, the poor water solubility caused by the high hydrophobicity makes PS prone to aggregation in aqueous solutions, leading to lower ROS generation and decreased therapeutic efficacy [9–11].

Loading of PS in polymeric micelles is a promising approach to address these challenges [12]. Polymeric micelles are self-assembled nanostructures based on amphiphilic block copolymers formed in an aqueous solution and have been extensively investigated as drug delivery systems, particularly for the targeted delivery of hydrophobic drugs [13–16]. Polymeric micelles are characterized by a well-defined structure, containing a hydrophobic core and a hydrophilic shell. The micellar core has a high capacity to accommodate hydrophobic compounds, including photosensitizers, while the hydrophilic shell, which is mostly composed of poly(ethylene glycol) (PEG), can result in prolonged retention of polymeric micelles in the blood circulation by delaying their recognition and rapid uptake by the reticuloendothelial system (RES) [17–20]. In addition, micelles have customizable sizes ranging from 10 to 100 nm, which is favorable for the passively targeted delivery of loaded hydrophobic drugs to the aimed sites via the enhanced permeability retention (EPR) effect [21,22]. Previous research by our group showed that micelles based on poly(ε-caprolactone)-*b*-methoxy poly(ethylene glycol) (PCL-PEG) block copolymers can be loaded with the photosensitizer mTHPC with very high loading capacity [23]. However, in a recent study, we showed a rapid release of this PS in the circulation after i.v. administration of the mTHPC-loaded PCL-

PEG-based micelles [24]. The poor stability in the circulation is currently considered a limitation for micelles for successful clinical applications [24–27]. This instability is most likely due to a combination of extraction of the cargo from the micelles and micellar destabilization resulting from a large dilution volume upon injection or binding of drug–polymer chains to blood components (e.g., albumin, lipoproteins) [28].

To overcome their inherent instability, physical interactions through π-π stacking have been investigated to enhance the stability of polymeric micelles. For example, Kataoka et al. previously reported that micelles consisting of poly(ethylene glycol)-poly(aspartate) block copolymers derived with multiple pendant 4-phenyl-1-butanol showed high paclitaxel retention in vivo [29]. Shi et al. demonstrated that paclitaxel-loaded micelles based on methoxy-poly(ethylene glycol)-*b*-poly(*N*-(2-benzoyloxypropyl) methacrylamide) (mPEG-*b*-p(HPMAm-Bz) had a significantly prolonged circulation time, good drug retention, and enhanced tumor accumulation, which resulted in substantially improved antitumor efficacy that was attributed to noncovalent stacking interactions between Bz groups and aromatic groups present in the drug [30–32]. In another study, thermosensitive HPMAm-lactate-based micelles that contained HPMAm-Bz (~30 mol%) units as comonomers were used to encapsulate a hydrophobic PS (i.e., $Si(sol)_2Pc$, an axially solketal-substituted silicon phthalocyanine), showing enhanced loading capacity and significantly improved retention of PS during 9 days of storage in phosphate-buffered saline (PBS) at 37 °C as compared to $Si(sol)_2Pc$ loaded in HPMAm-lactate-based micelles lacking the aromatic comonomers [33].

The abovementioned studies prompted us to stabilize PCL-PEG micelles in the current study by π-π stacking interactions through introduction of multiple pendant aromatic moieties in the hydrophobic core. To this end, aromatic rings were incorporated in the hydrophobic polymer chains by ring-opening copolymerization of ε-caprolactone (CL) with a benzyl-functionalized trimethylene carbonate, namely benzyl 5-methyl-2-oxo-1,3-dioxane-5-carboxylate (TMC-Bz). For comparison, PCL-PEG diblock copolymers without and with one aromatic unit at the terminal PCL chain end were synthesized. Then, mTHPC was selected as a model PS with high aromaticity and hydrophobicity, and was encapsulated in polymeric micelles that were prepared from the resulting block copolymers. The effect of aromatic π-π stacking interaction on the loading capacity, possible PS aggregation in the micellar core, and stability of mTHPC-loaded micelles were studied. The photocytotoxicity of the micellar PS formulations was evaluated on both A431 and HeLa tumor cell lines by a 3-(4,5-dimethylthiazol-2-yl)-5-(3-carboxymethoxyphenyl)-2-(4-sulfophenyl)-2*H*-tetrazolium (MTS) assay. Importantly, blood circulation kinetics and biodistribution of the micelles and the incorporated mTHPC were studied and compared with free mTHPC in A431 tumor-bearing mice using fluorescence intensity measurements and high performance liquid chromatography analysis, respectively, while the biodistribution of micelles was also visualized by 2D fluorescence reflectance imaging to reveal the correlation behavior between the cargo and its host micelles.

## 2. Materials and Methods

### *2.1. General*

The ε-caprolactone (CL), methoxy-poly(ethylene glycol) (mPEG-OH, 2000 g/mol), methanesulfonic acid (MSA, ≥99.0%), pyridine (99.8%), benzyl bromide (98%), and triethylamine (TEA) were obtained from Sigma-Aldrich (Zwijndrecht, the Netherlands). Phosphate-buffered saline (PBS, pH 7.4, containing 11.9 mM phosphates, 137 mM sodium chloride and 2.7 mM potassium chloride) was obtained from Fischer Bioreagents (Bleiswijk, the Netherlands). Standard regenerated cellulose dialysis tubing (Spectra/Por®6) with a molecular weight cutoff (MWCO) of 1 kDa was purchased from Spectrumlabs (Rancho Dominguez, CA, USA). Radioimmunoprecipitation assay (RIPA) lysis buffer (10×, 0.5 M Tris-HCl, pH 7.4, 1.5 M NaCl, 2.5% deoxycholic acid, 10% NP-40, 10 mM EDTA) was purchased from Merck KGaA (Darmstadt, Germany). The 2,2-*Bis*-thiomethyl-trimethylene carbonate (TTC) was kindly provided by Professor Zhiyuan Zhong (Soochow University, Suzhou, China). Human epidermoid carcinoma A431 and human cervical carcinoma HeLa cells were obtained from the American Type Culture Collection (ATCC, Manassas, Virginia, USA). All other solvents and reagents were obtained from Biosolve (Valkenswaard, the Netherlands). The mPEG-OH was azeotropically dried from toluene prior to use. Dichloromethane (DCM, peptide synthesis grade), toluene, and dimethylformamide (DMF) were dried over 4Å molecular sieves (Sigma-Aldrich, Zwijndrecht, the Netherlands) prior to use. All other reagents were used as received.

The $^{1}H/^{13}C$-NMR spectra of the synthesized monomer and polymers were recorded using a Bruker NMR spectrometer (600 MHz, Bruker, Billerica, MA, USA). The different samples were dissolved in $CDCl_3$ at concentrations of approximately 15 mg/mL. Chemical shifts of residual solvent ($CHCl_3$: δ 7.26 and 77 for proton and carbon spectrum, respectively) were used as the reference lines. Peak multiplicity is designated as s (singlet), d (doublet), t (triplet), and m (multiplet).

### *2.2. Synthesis of Monomer and Polymers*

#### *2.2.1. Synthesis of Monomer*

##### *2.2.1.1. Synthesis of Benzyl 2,2-bis(hydroxymethyl)propionate*

Benzyl 2,2-bis(hydroxymethyl)propionate was synthesized as previously described (Scheme 1A) [34] and obtained as white needle crystals (47.8 g, yield: 67%) with a melting point of 73 °C (Figure S1A, Supplementary Materials). $^{1}H$-NMR (600 MHz, $CDCl_3$): δ 7.38 (m, $OCOCH_2\underline{\boldsymbol{C_6H_5}}$), 5.21 (s, $OCO\underline{\boldsymbol{CH_2}}C_6H_5$), 3.95-3.72 (m, $HO\underline{\boldsymbol{CH_2}}C\underline{\boldsymbol{CH_2}}OH$), 1.09 (s, $C\underline{\boldsymbol{CH_3}}$). $^{13}C$-NMR (150 MHz, $CDCl_3$): δ 175.2,135.6, 128.6, 128.3, 127.8, 68.3, 66.7, 49.2, 17.1.

##### *2.2.1.2. Synthesis of Benzyl 5-methyl-2-oxo-1,3-dioxane-5-carboxylate*

Benzyl 5-methyl-2-oxo-1,3-dioxane-5-carboxylate (i.e., trimethylene carbonate

functionalized by benzyl group (TMC-Bz)) was synthesized as previously described (Scheme 1A) [34]. The product was obtained as a white solid (40.6 g, yield: 97%) and further purified by recrystallization from ethyl acetate prior to being used for polymerization. The product after recrystallization was composed of white needle crystals and its melting point shifted from 73 (before recrystallization) to 75 °C (Figure S1B, Supplementary Materials). $^{1}$H-NMR (600 MHz, $CDCl_3$): δ 7.38 (m, $OCOCH_2\underline{\boldsymbol{C_6H_5}}$), 5.22 (s, $OCO\underline{\boldsymbol{CH_2}}C_6H_5$), 4.71(m, $COO\underline{\boldsymbol{CH_2}}C\underline{\boldsymbol{CH_2}}OCO$,), 4.21 (m, $COO\underline{\boldsymbol{CH_2}}C\underline{\boldsymbol{CH_2}}OCO$), 1.33 (s, $OCH_2C\underline{\boldsymbol{CH_3}}$). $^{13}$C-NMR (150 MHz, $CDCl_3$): δ 170.9, 147.4, 134.7, 128.7, 128.2, 72.9, 67.9, 40.2, 17.6.

### *2.2.2. Synthesis of Polymers*

#### *2.2.2.1. Synthesis of P(CL/TMC-Bz)-PEG*

A representative procedure for the synthesis of poly(ε-caprolactone)-*co*-poly(benzyl 5-methyl-2-oxo-1,3-dioxane-5-carboxylate)-*b*-poly(ethylene glycol) (P(CL/TMC-Bz)-PEG, Scheme 1B) was carried out as previously described [35,36]. Briefly, CL (342 mg, 3.0 mmol), TMC-Bz (750 mg, 3.0 mmol), and mPEG-OH (660 mg, 0.33 mmol) were dissolved in 7 mL dry DCM, followed by addition of MSA (37 mg, 0.39 mmol) with agitation. The reaction was allowed to proceed at 37 °C under $N_2$ atmosphere. At predetermined time points, samples were withdrawn from the reaction mixture and analyzed using $^{1}$H-NMR spectroscopy to monitor monomer conversion in time, and thus the polymerization kinetics of CL and TMC-Bz. After 10 h, TEA (54 μL, 0.39 mmol; equimolar to MSA) was added to terminate the reaction. The cooled reaction solution was dropped into a 20-fold excess of cold diethyl ether (–20 °C) and the precipitate was collected by filtration and dried under vacuum to give the final product (entry 7 in Table 1).

PCL-PEG (Entries 1 and 5, Table 1) and P(TMC-Bz)-PEG (entry 3, Table 1) block copolymers were synthesized using MSA as the catalyst under the same conditions by polymerization of only CL or TMC-Bz, respectively.

The polymerization kinetics were determined by monitoring the decrease of peak integrals of methylene of CL at 2.66 ppm and methylene of benzyl group in TMC-Bz at 4.69 ppm. The peak originating from the three methoxy protons of mPEG-OH at 3.37 ppm was used as the reference peak to normalize the integrals.

#### *2.2.2.2. Synthesis of Bz-PCL-PEG*

To obtain benzylated PCL-PEG (Bz-PCL-PEG), the hydroxyl end groups of PCL-PEG were reacted with benzoyl chloride (Scheme 1C), as reported before [37]. In short, 1.2 g of PCL-PEG was dissolved in 6 mL dry DCM, which also contained a 5-fold molar excess of TEA compared to PCL-PEG. This solution was subsequently added dropwise to a solution of 5 equivalents of benzoyl chloride in 3 mL of dry DCM and stirred overnight under a nitrogen atmosphere. Finally, the solvent was removed under reduced

pressure and the obtained residue was dissolved in DCM and purified by precipitation in an excess of diethyl ether (−20 °C). The collected precipitate of Bz-PCL-PEG was dried under vacuum and obtained as a white solid.

### *2.3. Polymer Characterization*

The average degree of polymerization (DP) of CL or TMC-Bz in the obtained copolymers was determined by $^1$H-NMR; that is, from the ratio of the integral of the $CH_2$ protons of the CL units (1.39 ppm, 2H, $CH_2CH_2\underline{\boldsymbol{CH_2}}CH_2CH_2$) or the $CH_2$ protons of benzyl groups in the poly(TMC-Bz) block (5.15 ppm, 2H, $O\underline{\boldsymbol{CH_2}}C_6H_5$) to the methyl protons of mPEG-OH (3.37 ppm, 3H, $\underline{\boldsymbol{CH_3}}O$), respectively. The number average molecular weight ($M_n$) of the block copolymers was calculated from the resulting DP of CL and TMC-Bz units and the molecular weight of the PEG block.

Gel permeation chromatography (GPC) analysis of the synthesized polymers was conducted to determine the number average molecular weight ($M_n$), weight average molecular weight ($M_w$), and polydispersity (PDI, equal to $M_w/M_n$) of the obtained block copolymers, using two PLgel Mesopore columns (300 × 7.5 mm, including a guard column, 50 × 7.5 mm) coupled with a differential refractive index (RI) detector. Poly(ethylene glycol)s of narrow molecular weights ranging from 430 to 26,100 g/mol were used as calibration standards. The eluent was DMF containing 10 mM LiCl, the elution rate was 1.0 mL/min, and the temperature was set at 65 °C [24].

Differential scanning calorimetry (DSC) was carried out using a Discovery DSC (TA Instruments, New Castle, Delaware, USA) calibrated with indium. Samples (~5 mg) were heated with a ramp of 3 °C/min up to 150 °C (modulated), annealed for 5 min, cooled down at 3 °C/min to −80 °C (modulated), again annealed for 5 min, and subsequently heated at 3 °C/min up to 150 °C (modulated). Melting temperatures ($T_m$) were obtained from the onset of the peaks of the total heat flow and the melting enthalpies ($\Delta H_m$) were recorded from the total heat flow. Glass transition temperatures ($T_g$) are defined as the point of inflection of the step change observed in the reversing heat flow curve. Data for the second heating cycle were recorded.

### *2.4. Synthesis and Characterization of Cy7-Labeled P(CL/TTC)-PEG*

For in vivo studies, Cy7-labeled polymers were obtained by first synthesizing a block copolymer containing pendant thiol groups (i.e., poly(ε-caprolactone-*co*-2,2-*bis*-thiomethyl-trimethylene carbonate)-*b*-poly(ethylene glycol) (P($CL_{18}$-$TTC_{7.5}$)-PEG)), and allowing this polymer to react with maleimide-functionalized near-infrared (NIR) fluorophore Cyanine7 (Cy7) (Lumiprobe Corporation, Hannover, Germany), as described previously (Scheme S1, Supplementary Materials) [38]. In short, CL was copolymerized with TTC using mPEG-OH as an initiator and MSA as a catalyst (molar ratio of CL/TTC/mPEG-OH was 18/8/1), following the same procedure as described in Section 2.2.2.1 for the synthesis of P(CL/TMC-Bz)-PEG. Subsequently,

the disulfide bonds in the resulting P($CL_{18}$-$TTC_{7.5}$)-PEG were reduced using tris(2-chloroethyl) phosphate (TCEP) to yield free thiol groups, which in turn were used for reaction with Cy7-maleimide (0.64 equivalent per polymer chain) via the thiol-maleimide reaction (Scheme S1, Supplementary Materials). After the reaction (4 h at room temperature), the unreacted free thiols were blocked by reaction with maleimide (4 h at room temperature), and subsequently, the unreacted maleimide and unreacted Cy7 were removed by dialysis against THF/water (50:50 volume ratio) for 3 days. The successful coupling of Cy7 with the polymer and complete removal of free Cy7 was demonstrated by GPC analysis, with which the amount of Cy7 in the copolymer was quantified using UV-Vis detection at 755.5 nm, showing 17% coupling efficiency, as reported previously [38]. On average, one polymer chain carried 0.17 Cy7 label.

### *2.5. Preparation and Characterization of Empty and mTHPC-Loaded Micelles*

Empty micelles were prepared by a nanoprecipitation method, as previously described and with a slight modification [39]. In short, 10 mg of block copolymer was dissolved in dimethylsulfoxide (DMSO, 100 µL). After vortexing for 1 min, the mixture was heated up to 70 °C for 5 min to obtain a homogenous solution. This warm solution was cooled down to room temperature and then added dropwise to PBS at 1:9 volume ratio. A homogenous micellar dispersion was formed after gentle shaking, followed by dialysis using tubing (MWCO = 1 kDa) against PBS at room temperature for 12 h. The micellar dispersion obtained after dialysis was filtered through a 0.2 µm syringe filter. The Z-average hydrodynamic diameter ($Z_{ave}$) and polydispersity index (PDI) of the formed micelles after dialysis were determined by dynamic light scattering (DLS) at a fixed scattering angle of 173° and at 25 °C using a ZetaSizer Nano S (Malvern, Surrey, United Kingdom).

The mTHPC-loaded micelles (different loading percentages) were prepared as follows. A certain volume of mTHPC solution in DMSO (10 mg/mL added volume depending on the aimed wt% loading) was added to the weighted polymer, followed by addition of a certain volume of DMSO to obtain a final polymer concentration of 100 mg/mL. Subsequently, the procedures were the same as mentioned above (i.e., the mixture was heated and then added to PBS, followed by dialysis against PBS). The absorbance of the micellar dispersion diluted in DMSO was recorded at 651.5 nm using a UV-2450 Shimadzu spectrophotometer (Kyoto, Japan) and calibration was done using a series of standard solutions of mTHPC in DMSO to determine the mTHPC loading [24]. The loading efficiency (LE) and loading capacity (LC) of mTHPC were calculated using the following equations (1) and (2), respectively:

$$LE\ (\%) = \frac{mTHPC\ loaded\ (mg)}{mTHPC\ in\ the\ feed\ (mg)} x100\% \qquad (1)$$

$$LC\ (\%) = \frac{mTHPC\ loaded\ (mg)}{polymer\ \ used\ (mg) + mTHPC\ loaded\ (mg)} x100\% \qquad (2)$$

### *2.6. Aggregation State of mTHPC*

The mTHPC-loaded micelles with different loadings of mTHPC were prepared in PBS, as described in Section 2.5. The micellar dispersions were diluted 10 times in PBS (the final polymer concentration was 1 mg/mL). The fluorescence intensity of mTHPC was recorded using a Jasco FP8300 spectrofluorometer (Tokyo, Japan) at 655 nm (excitation at 420 nm) and plotted against the concentration of mTHPC loaded in the micelles.

### *2.7. In Vitro Release of mTHPC-Loaded Micelles in Human Plasma*

The in vitro release of mTHPC-loaded micelles with 5 wt% mTHPC loading (prepared in PBS as described in Section 2.5) was studied in human plasma at 37 °C by monitoring the change of fluorescence intensity of mTHPC, as previously reported [24]. Foscan® (i.e., free mTHPC solution in ethanol/propylene glycol (40:60, *w/w*)) was used as a reference. In short, different formulations were added to human plasma at a volume ratio of 1:9. As controls, samples were diluted with PBS (1:9, *v/v*). After incubation at 37 °C, samples were taken at different time points (5 min, and 0.5, 1, 1.5, 2, 3, 5, 8 h) and pipetted into the wells of a 384-well plate to record the fluorescence intensity, as described in Section 2.6.

In addition, samples of Foscan® and micellar mTHPC formulation were taken after incubation with human plasma (1:9, *v/v*) at 37 °C for 5 h, and then 1.5, 2, 4, and 30 times diluted with either human plasma or PBS. After incubation at 37 °C, samples were taken at 0.5, 1, and 2 h and transferred into a 384-well plate to record the fluorescence intensity.

### *2.8. Dark Cytotoxicity and Photo-Cytotoxicity of Empty and mTHPC-Loaded Micelles*

A431 and HeLa cells were cultured in Dulbecco's modified Eagle's medium (DMEM) containing glucose (1 g/L for A431 and 4.5 g/L for HeLa) and supplemented with 10% (*v/v*) fetal bovine serum (FBS). The cells were kept in culture at 37 °C in a humidified 5% $CO_2$ atmosphere.

Dispersions of empty and mTHPC-loaded micelles (with various loadings) were prepared in PBS (10 mg/mL polymer), as described in Section 2.5. The stock dispersions were diluted in DMEM medium (2.5 and 5 times dilution for empty micelles and 10 times dilution for the mTHPC-loaded micelles) prior to cell exposure for evaluation of their cytotoxicity (empty micelles), dark cytotoxicity, and photo-cytotoxicity (mTHPC-loaded micelles) on A431 and HeLa cells.

The cells were seeded into 96-well plates at a density of 6000 A431 cells/well or 5000 Hela cells/well and incubated overnight at 37 °C and 5% $CO_2$. Subsequently, the

medium (100 μL) in the wells was replaced by 100 μL of the above-described empty or mTHPC-loaded micellar dispersions. To evaluate the photocytotoxicity of the different micellar mTHPC formulations, the cells were incubated first in the dark for 7 h at 37 °C and 5% $CO_2$ with the different formulations. Next, the medium with the formulations was removed and cells were washed three times with DMEM medium. Subsequently, the cells in 100 μL of fresh DMEM were illuminated for 10 min with a light intensity of 3.5 mW/cm$^2$ (corresponding to 2.1 J/cm$^2$), using a homemade device consisting of 96 LED lamps (650 ± 20 nm, 1 LED per well), and then incubated overnight at 37 °C and 5% $CO_2$. Finally, cell viability was measured as described before [24], by recording the absorbances of the different wells at 490 nm after the cells were exposed for approximately 1 h to a CellTiter 96® $AQ_{ueous}$ One Solution (Promega, Leiden, the Netherlands) containing 3-(4,5-dimethylthiazol-2-yl)-5-(3-carboxymethoxyphenyl)-2-(4-sulfophenyl)-2*H*-tetrazolium (i.e., MTS assay).

For determination of the cytotoxicity of empty polymeric micelles (without mTHPC loading) and dark toxicity of the above described mTHPC-loaded micelles, the cells were incubated with the different formulations in the dark for 24 h at 37 °C and 5% $CO_2$, and subsequently the cell viability was determined directly (without irradiation) by the MTS assay after washing off the formulations [24].

### *2.9. In Vivo Studies of mTHPC and Micelles in A431 Tumor-Bearing Mice*

For the in vivo studies, P($CL_{9.1}$-TMC-$Bz_{7.7}$)-PEG and Bz-$PCL_{17.6}$-PEG micelles loaded with mTHPC (0.6 wt% loading) were used and prepared as described in Section 2.5, except that micelles were labeled by mixing the block copolymer with Cy7-labeled P($CL_{18}$-$TTC_{7.5}$)-PEG (at a ratio of 98.5% to 1.5% *w/w*). A formulation of free mTHPC was prepared by 1:1 dilution of a 120 μg/mL mTHPC stock solution in Foscan® solvent (i.e., ethanol/propylene glycol, 40/60 *w/w*) with PBS (final mTHPC concentration was 60 μg/mL, corresponding to an equal dose of injected mTHPC as micellar formulation. The animal experiments were approved by the Central Animal Experiments Committee (approval number #AVD108002016544) and the Animal Welfare Body Utrecht (approval number WP# 544-2-04). Female Balb/c nude mice, weighing 20–28 g, were purchased from Envigo (Horst, the Netherlands). Mice were housed in ventilated cages at 25 °C and 55% humidity under natural light/dark conditions. Food and water were provided ad libitum during the entire study. Mice were inoculated with 1 × 10$^6$ A431 cells suspended in 100 μL PBS subcutaneously into the right flank. When the tumors reached an approximate size of 100–300 mm$^3$ (between 7 and 14 days after injection of the tumor cells), mice were included in the studies. Tumors were measured using a digital caliper. The tumor volume V (in mm$^3$) was calculated using the equation $V = (\pi/6)LS^2$, in which L is the largest and S is the smallest superficial diameter [30].

*2.9.1. Circulation Kinetics*

Three groups of tumor-bearing mice (*n* = 4-6 per group) were intravenously (i.v.) injected via the tail vein with free mTHPC formulation (i.e., mTHPC dissolved in diluted Foscan solvent (ethanol/propylene glycol/PBS 20:30:50 *v/v/v*)) or Cy7-labeled mTHPC micelles, respectively, at injection doses of 300 μg mTHPC/kg, corresponding to ~6 μg mTHPC in ~120 μL per individual mouse with average body weight of ~25 g. Blood samples were collected in tubes with EDTA anticoagulant via submandibular puncture (~60 μL) from mice at 1 min (100% injection control), then at 1 and 2 h, and via cardiac puncture (~200 μL) at 4 or 24 h post-injection. For the latter, mice were killed through cervical dislocation while under deep isoflurane anesthesia. The collected blood samples were centrifuged at 1000× *g* for 15 min at 4 °C. The plasma supernatant was collected, extracted using acetonitrile/DMSO (4:1, *v/v*), and analyzed by high-performance liquid chromatography (HPLC) and a LI-COR Odyssey imaging system to quantify the amount of mTHPC and Cy7-labeled micelles, respectively, as previously described [38]. Plasma concentration curves were analyzed by non-compartmental analysis with the PKSolver add-in for Microsoft Excel [40].



*2.9.2. Biodistribution*

The mice were sacrificed 4 (3–6 animals per group) or 24 h (3–6 animals per group) after i.v. administration of the formulations. Tumors and a panel of organs (spleen, liver, lung, heart, kidney, skin, femur, and brain) were excised and imaged ex vivo by 2D fluorescence reflectance imaging (FRI) using a Pearl Trilogy imager from LI-COR and then stored at −80 °C until further processing for quantification. Organs and tumors from three untreated animals were used as controls.

To quantify the content of mTHPC and micelles in the tumors and the different organs, the excised tissue samples were treated as follows. First, 100 μL of RIPA lysis buffer was added to 100 mg of sliced tissues or organs. The mixture was homogenized by a tissue grinder (Percellys 24) at a speed of 6000/s for 60 s (for femur samples, 6000/s for 180 s) and the homogenate was subsequently aliquoted. To determine the mTHPC concentration in the samples, 1 volume of an aliquot of the homogenate (30 μL) was mixed with 120 μL of acetonitrile/DMSO (4:1 *v/v*) and vortexed for 1 min. The mixture was then centrifuged at 15,000× *g* for 10 min. Next, 50 μL of the obtained supernatant was injected into the HPLC system consisting of a Waters X Select Charged Surface Hybrid (CSH) C18 3.5 μm 4.6 x 150 mm column coupled with a fluorescence detector set at $\lambda_{ex}$ 420 nm and $\lambda_{em}$ 650 nm to analyze mTHPC concentration [38]. The mobile phase was 0.1 % trifluoroacetic acid in acetonitrile/water (60:40, *v/v*) at a flow rate of 1 mL/min. The measuring range was from 0.005 to 4 μg/mL and the detection limit was 5 ng/mL. Calibration curves were obtained from a series of standard solutions of mTHPC in DMSO, to which 45 μL of the corresponding homogenized tissue samples obtained from control mice (i.e., not treated with any formulations) was added, followed by

mTHPC extraction using acetonitrile/DMSO (4:1, *v/v*) and HPLC analysis.
To determine the concentration of Cy7-labeled micelles in the tissue homogenates, 1 volume of another aliquot of the homogenate (30 μL) was vortex-mixed with 2 volumes of RIPA lysis buffer (60 μL) for 1 min. The fluorescence of Cy7 in the mixture (20 μL) was detected at the 800 nm channel (i.e., $\lambda_{ex}$ 785 nm and $\lambda_{em}$ 820 nm), using a LI-COR Odyssey scanner imaging system, and a calibration curve was obtained using samples with different concentrations of Cy7-labeled copolymer in a mixture of RIPA buffer (1 volume) and the corresponding homogenized tumor or organ samples (2 volumes) obtained from non-treated mice.
It is noted that skin accumulation of different formulations was not included, as grinding of the skin was more problematic in our preliminary test, which could lead to unreliable quantification. In addition, a study by Bovis et al. suggested that mTHPC accumulation in the skin was limited [8].

### *2.10. Statistical Analysis*

Statistical analysis was done by GraphPad Prism 8.3.0 software. Two-way analysis of variance (ANOVA) was used to determine the statistical significance of biodistribution among different mTHPC formulations. A value of $p < 0.05$ was considered significant. Statistical significance is depicted as * $p < 0.05$, ** $p < 0.01$, *** $p < 0.001$.

## 3. Results and Discussion

### *3.1. Synthesis and Characterization of Monomer and Polymers*

To synthesize benzyl 5-methyl-2-oxo-1,3-dioxane-5-carboxylate (i.e., trimethylene carbonate functionalized by benzyl group, TMC-Bz), 2,2-bis(hydroxymethyl) propionate was first benzylated by reaction with benzyl bromide, followed by reaction with triphosgene (Scheme 1A). After purification, TMC-Bz was obtained in a high yield (97 %) as a white crystalline solid. The structures of the intermediate product and TMC-Bz were confirmed by $^{1}H/^{13}C$ NMR spectroscopy (Figure S2, Supplementary Materials).

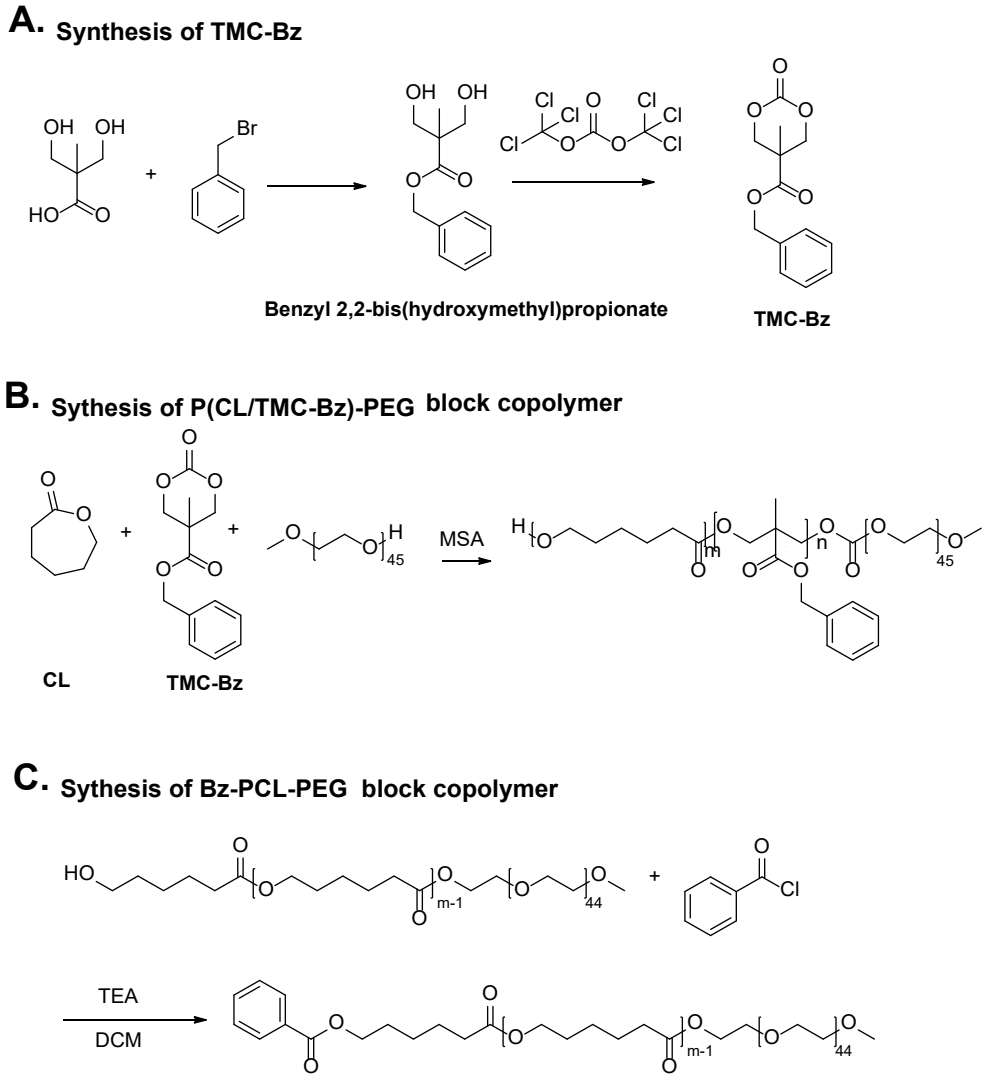


**Scheme 1.** Synthesis of benzyl 5-methyl-2-oxo-1,3-dioxane-5-carboxylate (TMC-Bz) (**A**), polymers of P(CL/TMC-Bz)-PEG (**B**), and Bz-PCL-PEG (**C**).

The block copolymers synthesized by the ring-opening polymerization of CL or TMC-Bz, initiated by mPEG-OH and catalyzed by MSA using different CL/TMC-Bz/initiator molar ratios (Scheme 1B), were obtained as white solids in a yield of ~65%, and their chemical structures were characterized by $^{1}$H NMR (Figure S3–S5, Supplementary Materials). The characteristics of the obtained block copolymers are shown in Table 1. The compositions of the resulting block copolymers as determined by $^{1}$H-NMR fit well with those expected from the ratios of the monomers in the feed. GPC analysis shows narrow molar mass distributions ($M_w/M_n \leq 1.1$), suggesting the absence of significant side

reactions, such as transesterification [35,41–43]. For the ring-opening copolymerization of CL and TMC-Bz, similar polymerization rates of the two monomers were observed, as shown in Figure 1A for a CL/TMC-Bz/mPEG-OH feed molar ratio of 9:9:1 (i.e., entry 7, Table 1). The $^1$H-NMR spectrum of the resulting block copolymer (Figure 1B) displayed three groups of peaks in the ester region at 3.90–4.40 ppm, corresponding to the three kinds of $CH_2O$-carbonyl linkages in the different diad structures that are present in the poly(ester-carbonate) block (i.e., TMC-Bz-TMC-Bz, CL-TMC-Bz, and CL-CL, respectively) [42,44]**.** This demonstrates a random distribution of CL and TMC-Bz in the resulting P(CL/TMC-Bz)-PEG copolymers (entires 2, 4, 6, and 7, Table 1) which is in good agreement with the equal reactivity of the two monomers.
It is noted that the same characteristics of $PCL_{17.6}$-PEG and its terminal benzyl derivative (i.e., Bz-$PCL_{17.6}$-PEG) (entries 4 and 8, Table 1) indicate that loss of materials and undesired side reactions did not occur during the process of post-modification of the end groups (Scheme 1C). The assignments of the corresponding NMR peaks of Bz-$PCL_{17.6}$-PEG (Figure S6, Supplementary Materials) were in line with those reported previously [37]. In addition, the $^1$H-NMR spectrum of Bz-$PCL_{17.6}$-PEG (Figure S6, Supplementary Materials) shows that the integral ratio of the protons of the terminal Bz group at 7-8 ppm to the terminal $OCH_3$ group of PEG at 3.37 ppm was 5:3 (corresponding with a molar ratio of Bz/$OCH_3$ of 1:1), demonstrating that all polymer chains carry a terminal benzyl end group.

**Table 1.** Characteristics of the synthesized (Bz-)PCL-PEG and PCL/TMC-Bz)-PEG block copolymers.

| Entry | Feed Ratio of CL/ TMC-Bz/PEG (mol/mol/mol) | Composition of the Obtained Block Copolymers [a] | $M_n$ [b] | $M_w$ (GPC) [c] | $M_n$ (GPC) [c] | $M_w/M_n$ (GPC) | $T_g$ (°C) | $T_m$ (°C) | $\Delta H_m$ (J/g) |
|---|---|---|---|---|---|---|---|---|---|
| **1** | 9/0/1 | $PCL_9$-PEG | 3.2 | 2.7 | 2.5 | 1.11 | - | 43 | 120 |
| **2** | 4.5/4.5/1 | P($CL_{5.3}$-TMC-$Bz_{4.5}$)-PEG | 3.9 | 2.7 | 2.5 | 1.06 | -29 | 39 | 72 |
| **3** | 0/9/1 | P(TMC-$Bz_{8.6}$)-PEG | 4.3 | 2.9 | 2.7 | 1.05 | -12 | 35 | 82 |
| **4** | 4.5/9/1 | P($CL_{4.8}$-TMC-$Bz_{9.2}$)-PEG | 5.0 | 3.1 | 3.0 | 1.05 | -11 | 32 | 64 |
| **5** | 18/0/1 | $PCL_{17.6}$-PEG | 4.2 | 2.9 | 2.7 | 1.09 | - | 42 | 107 |
| **6** | 14/4/1 | P($CL_{13.5}$-TMC-$Bz_{3.7}$)-PEG | 4.7 | 3.0 | 2.7 | 1.11 | -47 | 38 | 89 |
| **7** | 9/9/1 | P($CL_{9.1}$-TMC-$Bz_{7.7}$)-PEG | 5.2 | 3.5 | 3.3 | 1.08 | -19 | 39 | 67 |
| **8** | - | Bz-$PCL_{17.6}$-PEG | 4.3 | 2.9 | 2.7 | 1.09 | - | 40 | 110 |

[a] Given numbers are degrees of polymerization of CL and TMC-Bz as determined by $^1$H-NMR; [b] determined by NMR; [c] calibration with PEG.

The thermal properties of the obtained block copolymers were investigated by DSC (Table 1, representative thermograms are shown in Figure S7, Supplementary Materials). All block copolymers showed only one $T_m$ at around 40 °C, close to that of mPEG-OH (48 °C), which is in accordance with previous data [24,45]. For the copolymers, crystallinity (i.e., $\Delta H_m$) of PEG corrected for its weight fraction in the corresponding polymer chains was well in accordance with that of the mPEG-OH (measured $\Delta H_m$ was 182 J/g) (Figure S8A, Supplementary Materials), demonstrating that in the solid

state, PEG and the polyester/carbonate blocks were phase-separated in the crystalline PEG domain and amorphous P(CL-TMC-Bz) (entries 2, 4, 6 and 7, Table 1) with $T_g$'s, ranging from −47 to −11 °C. These $T_g$'s can be described by the Fox equation (Figure S8B, Supplementary Materials), suggesting a random distribution of CL and TMC-Bz in the polymer chains, which is in line with that observed from NMR analysis (Figure 1B). These amorphous domains are obviously not miscible with PEG. The PCL-PEG block copolymers (entries 1, 5, and 8, Table 1) were almost fully crystalline: both PCL and PEG have their $T_m$'s around 45 °C [45], while the P(TMC-Bz)-PEG (entry 3, Table 1) block copolymer had $T_g$ at −12 °C, which resulted from the P(TMC-Bz) block and is in reasonable agreement with the $T_g$ of $PTMC_{80}$ (−25 °C) [35].



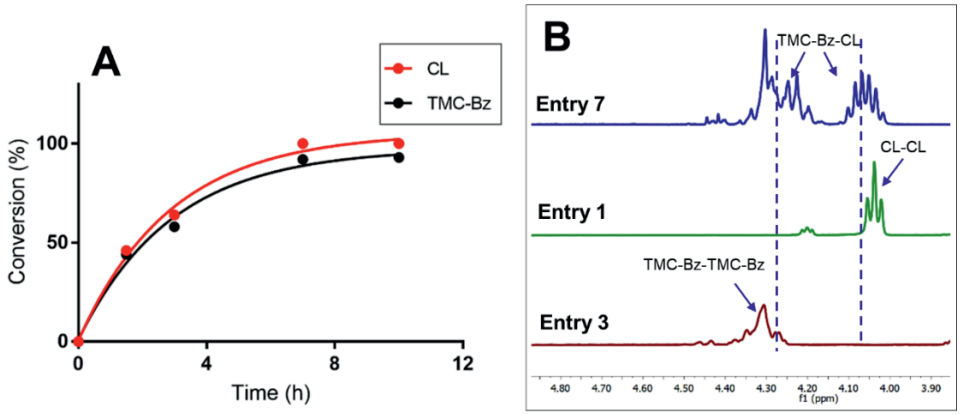


**Figure 1.** (**A**) Conversion of CL (red dots) and TMC-Bz (black dots) monitored by $^1$H-NMR analysis as a function of time (entry 7, Table 1). (**B**) $^1$H-NMR spectrum of the P($CL_{9.1}$-TMC-$Bz_{7.7}$)-PEG block copolymer (entry 7) in the region of methylene protons linked to oxy-carbonyl group (C***H*****$_2$**OCO), showing three different diad sequences in the copolymer. The spectra of $PCL_9$-PEG and P(TMC-$Bz_{8.6}$)-PEG copolymers presented as entry 1 and 3 were used as references for assignments of the CL-CL and TMC-Bz-TMC-Bz diads, respectively. The entries presented in the legend correspond to the same entries in Table 1.

### *3.2. Preparation and Characterization of Polymeric Micelles*

Empty polymeric micelles were prepared at a polymer concentration of 10 mg/mL using a nanoprecipitation method by dropping a polymer solution in DMSO into an excess of PBS followed by dialysis. DLS measurements (Figure 2A) demonstrate that $PCL_9$-PEG (entry 1, Table 1) without aromatic rings formed directly after dialysis micelles with a size of 27 nm and a PDI of ~0.3, which was in the range observed previously for low molecular weight oligolactates-*b*-PEG and oligocaprolactones-*b*-PEG ($M_n$ < 1.8 kDa) with unmodified hydroxyl end groups [37,45]. Importantly, the size and PDI of the $PCL_9$-PEG micelles (Figure S9A and B, Supplementary Materials) further increased to ~80 nm (PDI ~0.4) during 24 h storage at room temperature, in combination with an increased derived count rate from 2000 to 6000 (Figure S9C, Supplementary Materials),

demonstrating formation of aggregates, pointing to a low colloidal stability. Similarly, the larger $PCL_{17.6}$-PEG micelles (entry 5, Table 1) showed a size of ~600 nm with PDI of ~0.7 even directly after dialysis. On the other hand, micelles from the corresponding benzyl-terminated polymer (entry 8, Table 1) showed substantially decreased size and size distribution (23 nm with PDI of 0.3, Figure 2A). This result is in accordance with our previous studies, in which it was demonstrated that micelles based on $PCL_9$-PEG with a benzyl end group showed smaller size (17 nm), lower PDI (<0.1), and better stability than the non-benzylated polymer micelles [24,38].

Figure 2A shows that the different micelles based on P(CL/TMC-Bz)-PEG or P(TMC-Bz)-PEG block copolymers with different amounts of pendant benzyl groups (Entries 2–4, 6 and 7, Table 1) had small hydrodynamic diameters that slightly increased with the increasing chain length of the hydrophobic blocks (from 17-23 nm) with PDIs < 0.1 (Figure 2A). It is noted that the different aromatic substituted micelles, including Bz-$PCL_{17.6}$-PEG micelles, retained their small sizes and low PDIs for at least 7 days in PBS at room temperature (Figure 2A, green columns). Overall, these results demonstrate that aromatic groups, regardless of their positions and the amounts in the polymer chains, stabilized the cores of micelles based on PCL-PEG. In addition, from the perspective of in vivo application, the relatively small sizes of these stable micelles are expected to favor both their accumulation in tumors through the EPR effect [21,22] and subsequent penetration into the tumor with uniform distribution, being crucial factors for anti-tumoral efficacy of nanomedicines [46–48].

The P(CL/TMC-Bz)-PEG and (Bz-)PCL-PEG-based micelles were loaded with mTHPC with loading efficiencies of ≥80%, as determined by UV-Vis analysis (Figure 2B, solid lines), independent of the composition of copolymers used, which led to a linear increase of loading capacity up to ~8 wt % with increasing mTHPC feed (Figure 2B, dash lines).

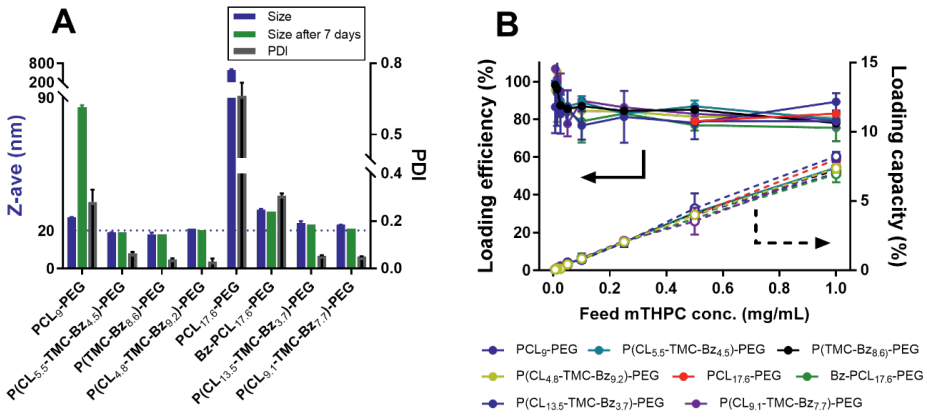


**Figure 2.** (**A**) Z-average hydrodynamic diameter ($Z_{ave}$, blue and green columns) and polydispersity index (PDI, black columns) of different empty polymeric micelles (10 mg/mL). (**B**) Loading efficiency and loading capacity of different micelles (10 mg/mL polymer) for mTHPC at various mTHPC feed concentrations.

### *3.3. Aggregation State of mTHPC in Polymeric Micelles*

The influence of the number of aromatic rings in the copolymers on the aggregation state of mTHPC in the different micelles was determined by measuring the quenching of its fluorescence [24,33,49]. For example, Shi et al. showed that the quenching concentration of a phthalocyanine (i.e., $Si(sol)_2Pc$) in aromatic-substituted thermosensitive micelles (0.45 mg/mL polymer) increased around 300 times to 16 µg/mL compared to that in corresponding non-aromatic micelles (~0.05 µg/mL) [33]. As discussed in Section 3.2, polymeric micelles prepared from non-modified PCL-PEG copolymers showed low stability. Therefore, only the aromatic micelles with either benzyl-modified end groups or differing contents of benzyl pendant groups in the polymer chains were loaded with increasing amounts of mTHPC and the fluorescence intensity of mTHPC was measured. Figure 3A shows that the different mTHPC-loaded micelles exhibited similar fluorescence profiles. The fluorescence of mTHPC-loaded micelles increased almost linearly with increasing mTHPC loading from 0.06 to 0.5% *w/w* (i.e., ~0.6 to ~5 µg/mL mTHPC; the final polymer concentration was 1 mg/mL). However, at higher loading percentages, mTHPC showed a rapid decrease in fluorescence intensity with increasing mTHPC loading, suggesting that fluorescence quenching resulting from mTHPC in the micelles occurred at ~10 µg/mL (corresponding to 1 wt% mTHPC loading), in agreement with our previous work on mTHPC-loaded Bz-PCL-PEG micelles [24]. A higher maximum fluorescence was observed when mTHPC was loaded in P(CL/TMC-Bz)-PEG micelles with a high content of aromatic rings (i.e., molar ratio of PTMC-Bz/PCL in polymer chains >0.3; Figure 3A, cyan, pink, yellow, and purple lines), because of the observed slightly later onset of quenching.

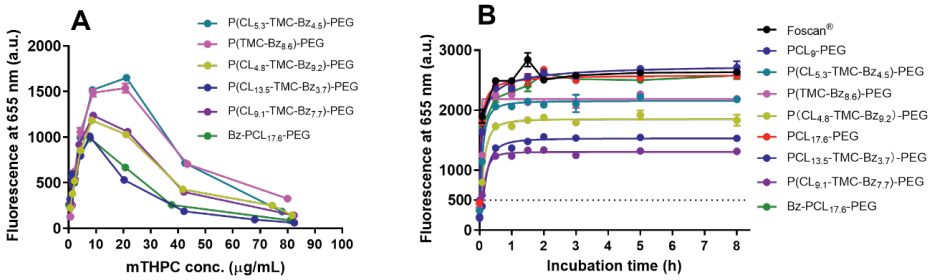


**Figure 3.** (**A**) Fluorescence intensity ($\lambda_{ex}$ 420 nm, $\lambda_{em}$ 655 nm) of various amounts of mTHPC loaded in different micelles; micelles of 10 mg/mL with different loading amounts (0.06–10% *w/w*) were individually prepared and each diluted 10× in PBS to obtain varying mTHPC concentrations. (**B**) Fluorescence intensity of Foscan® and mTHPC loaded in different micelles at a final mTHPC concentration of 40 µg/mL (corresponding to 5wt% mTHPC feed loading in micelles) in human plasma as a function of time; Foscan® and mTHPC-loaded micelles were 10× diluted with full plasma and incubated, while the mTHPC fluorescence was recorded at 37 °C over a period of 8 h. The fluorescence intensities of the corresponding mTHPC-loaded micelles diluted with PBS were used as the 0 h timepoint.

### *3.4. In Vitro Release of mTHPC from Micelles in Human Plasma*

The quenched state of the fluorescence when mTHPC is present in the micelles above 0.5% *w/w* loading (see Figure 3A) was used to investigate the in vitro stability of the mTHPC micellar formulations in human plasma [24]. When mTHPC is released from the micelles, this should lead to less quenching (i.e., increase in fluorescence intensity) as the local concentration inside the micelles is decreased, which is reinforced due to fluorescence of the free mTHPC likely bound to plasma proteins. For this purpose, the fluorescence of different micellar dispersion with 5wt% mTHPC feed loading, as well as mTHPC in its free form (Foscan®), was assessed in human plasma over time at 37 °C (Figure 3B). As expected, the fluorescence of mTHPC-loaded micelles upon 10× dilution in PBS did not change in time over 8 h at 37 °C (Supplementary Figure S10). Upon 10× dilution in plasma, Foscan® gave the highest immediate fluorescence, which increased slightly further during the first 30 min incubation and then remained stable at a value of ~2600 arbitrary units (a.u.; Figure 3B, black line). For all micellar mTHPC formulations (Figure 3B), substantial increase of fluorescence was observed to different levels within the first 1 h of incubation, and then the fluorescence intensities leveled off, reflecting different degrees of release of mTHPC from the micelles [24]. Interestingly, the plateau fluorescence intensities of mTHPC loaded in non-aromatic $PCL_9$-PEG or $PCL_{17.6}$-PEG micelles and Bz-$PCL_{17.6}$-PEG micelles (Figure 3B, blue, red, and green lines) were identical to that of Foscan® (at ~2600 a.u.), suggesting that the release was almost complete. This suggests that incorporating a single terminal aromatic group did not improve the retention of mTHPC in micelles in plasma, despite the enhanced colloidal stability of those micelles in PBS (see Figure 2A). In contrast, when mTHPC was loaded in micelles based on P(CL/TMC-Bz)-PEG or P(TMC-Bz)-PEG (i.e., with pendant aromatic rings), fluorescence intensities increased to lower levels than those loaded in the micelles from non-aromatic and chain-end modified polymers with a similar total length of hydrophobic blocks (Figure 3B, pink and cyan lines vs. blue line, or purple and dark blue lines vs. red and green lines). When the total length of hydrophobic blocks was kept more or less constant, the fluorescence intensity of mTHPC leveled off from 2600 a.u. (red line) to 1500 a.u.(dark blue line) and 1300 a.u. (purple line) as the content of TMC-Bz units increased from 0 to 4 and 8 units per polymer chain, respectively. On the other hand, when the degree of polymerization of TMC-Bz was ~8, the plateau fluorescence intensities of mTHPC were 2200 a.u. (pink line), 1800 a.u. (yellow line), and 1300 a.u. (purple line), with increasing total degree of polymerization (and thus molecular weight) of hydrophobic blocks from 8 to 14 and 17 units, respectively. Taken together, in plasma, mTHPC was most efficiently retained in micelles consisting of P($CL_{9.1}$-TMC-$Bz_{7.7}$)-PEG, which have the most TMC-Bz units and the longest hydrophobic blocks (Figure 3B, purple line). These results convincingly show that the retention of mTHPC in micelles was improved by pendant aromatic rings on the polymer backbone, while the extent of improvement depended on both the

hydrophobic chain length and the number of aromatic moieties. The reported findings can be explained by the increased hydrophobic interactions and π-π stacking between the hydrophobic blocks of P($CL_{9.1}$-TMC-$Bz_{7.7}$)-PEG and mTHPC, which can to some extent prevent the extraction of the cargo from the micelles or the micellar destabilization resulting from the binding of mTHPC or amphiphilic polymer molecules with proteins such as albumin and lipoproteins present in human plasma.

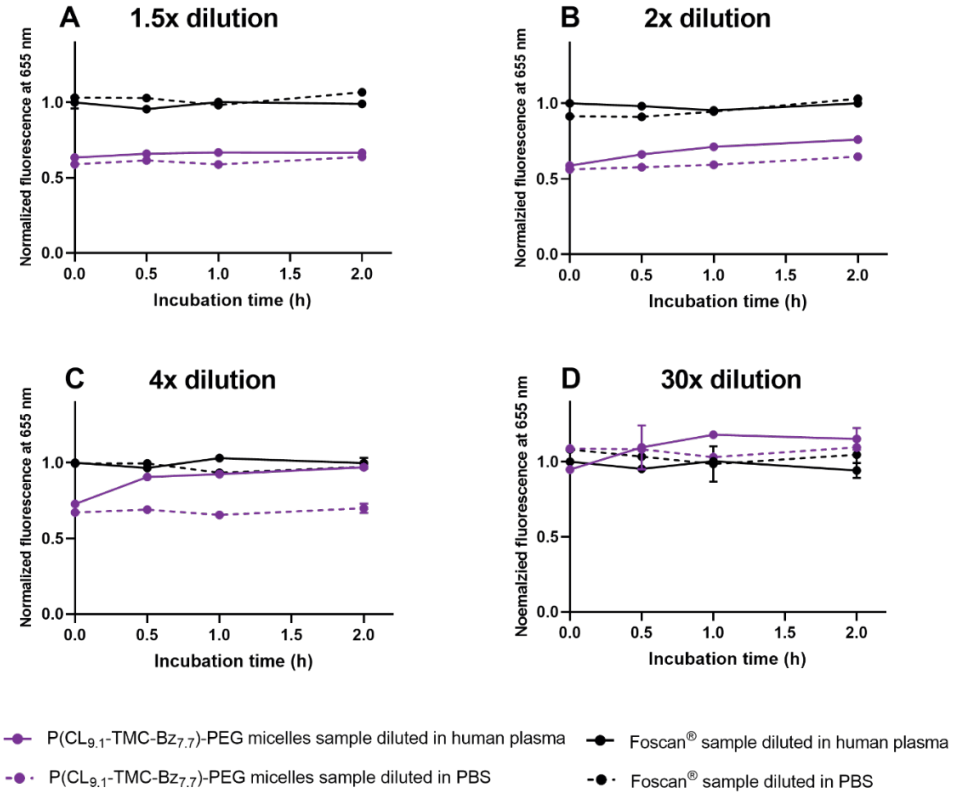


**Figure 4.** Fluorescence intensity of Foscan® and mTHPC-loaded P($CL_{9.1}$-TMC-$Bz_{7.7}$)-PEG micelles in human plasma and PBS as a function of time after dilution, normalized by the intensity of the corresponding Foscan® samples upon dilution with human plasma at 0 h; Foscan® and mTHPC-loaded micelles were pre-incubated with human plasma (1:9, *v/v*) at 37 °C for 5 h, then further diluted 1.5× (A), 2× (B), 4× (C), or 30× (D) with human plasma or PBS, and further incubated while the mTHPC fluorescence was recorded at 37 °C over a period of 2 h. The fluorescence intensities of mTHPC in different formulations recorded directly after dilution were used as the 0 h timepoint. The normalized fluorescence intensities were used because of a slight fluctuation of fluorescence intensity for different batches of samples, which showed an identical trend in a different independent experiment.

To establish whether the observation of different plateau fluorescence levels of mTHPC-loaded micelles containing TMC-Bz is the result of simple equilibrium partitioning of

mTHPC between micelles and plasma proteins, mTHPC-loaded P($CL_{9.1}$-TMC-$Bz_{7.7}$)-PEG micelles, after incubation with human plasma for 5 h, were further diluted with human plasma or PBS in different proportions and compared with Foscan® samples treated the same way. The solid black lines in Figure 4 show that upon further dilutions in human plasma, regardless of the dilution factors, the fluorescence of Foscan® samples was constant for 2 h and comparable to that observed upon dilution in PBS (broken black lines). The latter observation suggests that the amount of proteins present before further dilution was already sufficient to solubilize the amount of mTHPC that was present. When micelles were first incubated with plasma and subsequently diluted with PBS, the fluorescence intensity of mTHPC that was released from the micelles did not change in time (Figure 4, broken purple lines) and remained lower than diluted Foscan®, except for the highest dilution factor, which may point to further extraction of the PS from the micelles. Upon 1.5× dilution of the micelles with plasma instead of with PBS, the fluorescence intensity of mTHPC remained constant over time, which was again lower than the fluorescence intensity of the Foscan® sample (compare the solid purple line with the solid black line in Figure 4A). However, with further increase of the dilution factor of micelles in plasma to 2 and 4 times, the fluorescence of mTHPC in micelles showed an increase during the first 1 h incubation and then leveled off at different values (Figure 4B,C, solid purple lines). Upon 2x dilution in plasma, the plateau fluorescence was still lower than that observed from the corresponding Foscan® sample, while in the case of 4x dilution, the plateau fluorescence intensity of micellar mTHPC reached an identical level as observed in the Foscan® sample in plasma. Also, upon extensive dilution in plasma (30×), Foscan® and micellar mTHPC exhibited similar fluorescence levels (Figure 4D, purple lines). These results indicate that complete release of mTHPC from P($CL_{9.1}$-TMC-$Bz_{7.7}$)-PEG micelles was achieved when more plasma (≥4 times) was added. In other words, the equilibrium partitioning of mTHPC between micelles and plasma depends not only on the strength of the interaction with the polymer, but also on the ratio between micelles and plasma.

### *3.5. Dark Cytotoxicity and Photo-Cytotoxicity of Empty and mTHPC-Loaded Polymeric Micelles*

Cell viability assays were performed on A431 and HeLa tumor cell lines to assess the cytocompatibility of the empty micellar formulations and to determine the dark toxicity and photo-toxicity of mTHPC-loaded micelles. These experiments were carried out with micelles based on Bz-$PCL_{17.6}$-PEG and three micelles based on polymers with pendant aromatic groups (i.e., P(CL/TMC-Bz)-PEG) with different PCL/PTMC-Bz ratios. Although all used micelles showed required colloidal stability in PBS (Figure 2A), the latter displayed better stability in human plasma (Figure 3B), as shown in Sections 3.2 and 3.4. Figure S11 (Supplementary Materials) shows that both A431 and HeLa cells incubated with empty micelles retained their viability at polymer concentrations up

to 4 mg/mL, demonstrating that the different micelles have excellent cytocompatibility. As shown in Figure 5A,B, mTHPC-loaded in these different micelles, even with the highest mTHPC concentration up to 81 μg/mL, showed no cytotoxicity on A431 and HeLa cells after incubation with cells in the dark for 24 h. However, we showed before that free mTHPC (i.e., Foscan®) was toxic to cells without illumination at mTHPC concentrations higher than 50 μg/mL after 7 h and 20 μg/mL after 24 h [38]. This markedly decreased dark cytotoxicity of mTHPC by loading in the micelles is in line with previous observations using other micellar and liposomal formulations of mTHPC [50–52].

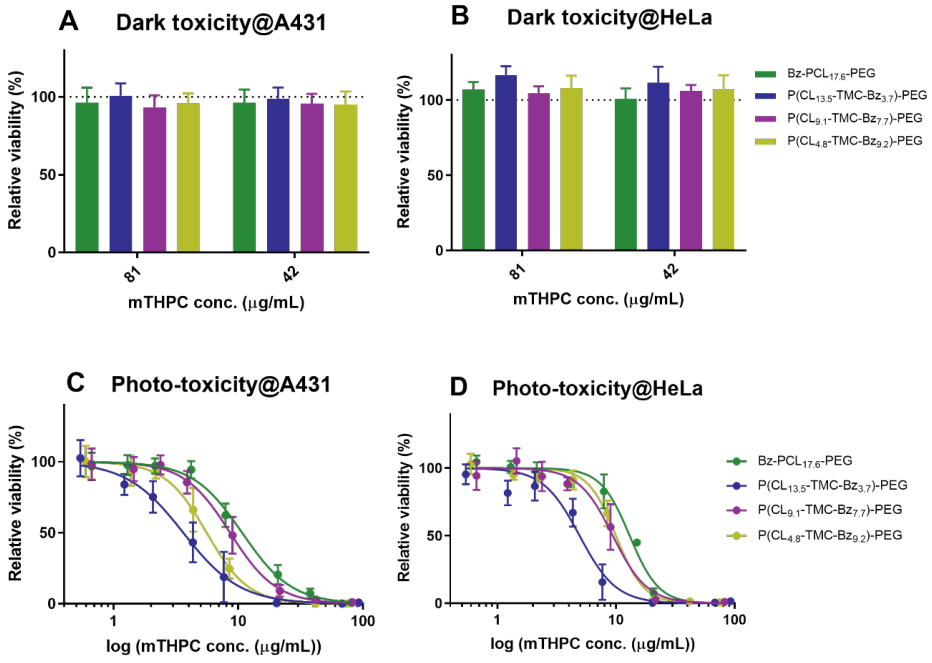


**Figure 5.** (**A**,**B**) Dark-toxicity established using cytotoxicity MTS assay of mTHPC loaded in micelles consisting of Bz-PCL-PEG and P(CL-TMC-Bz)-PEG (i.e., entries 4 and 6–8 from Table 1) at 1 mg/mL polymer and two different mTHPC loadings (10 wt% and 5wt% feeding, respectively) on A431 and HeLa cells after 24 h. (**C**,**D**) Dose-dependent photocytotoxicity (MTS assay) on A431 and HeLa cells after 7 h of pre-incubation with a series of mTHPC-loaded micelles; micelles of 10 mg/mL with different loading amounts were individually prepared and each was diluted 10× in DMEM to obtain the corresponding mTHPC concentrations. After the pre-incubation period and washing, the cells were illuminated for 10 min at 3.5 mW/cm$^2$.

The observed lack of dark toxicity could have been the result of no uptake of the micelles. However, our previous studies showed that PCL-PEG-based micellar mTHPC formulations and free mTHPC can both be effectively taken up by cells [38]. Indeed, photocytotoxicity studies (Figure 5C,D) show that the different micellar mTHPC

formulations were able to induce cell killing upon irradiation and exhibited comparable cytotoxic effects on A431 and HeLa cells (half-maximal effective concentration ($EC_{50}$) values were approximate 4–11 μg/mL for A431 cells and 5–13 μg/mL for HeLa cells, respectively; see Table 2). The $EC_{50}$ value of Bz-$PCL_{17.6}$-PEG on A431 cells was lower than previously observed when mTHPC was loaded in micelles from slightly bigger benzyl-terminated Bz-$PCL_{23}$-PEG polymers (~35 μg/mL) under the same conditions [38]. A similar trend (i.e., increasing photocytotoxicity with decreasing polymer molecular weight) was observed before and attributed to faster intracellular degradation of smaller PCL-PEG block copolymers, and thus faster release of mTHPC after internalization by the cells [24]. It is worth noting that the observed $EC_{50}$ values of these micellar mTHPC formulations on A431 and HeLa cells were slightly higher than free mTHPC (~1.5 μg/mL, Table 2), probably related to the less efficient cellular internalization of PEGylated micelles [53–55] or the relatively time-consuming degradation of polymers for release and activation of the PS [24].

**Table 2.** $EC_{50}$ of free mTHPC and mTHPC-loaded in micelles (1 mg/mL polymer) on A431 and HeLa cells, obtained from the curves of Figure 5.

| | $EC_{50}$ (μg/mL) | |
|---|---|---|
| | **A431** | **HeLa** |
| Free mTHPC | 1.6 ± 0.1 [38] | 1.2 [38] |
| Bz-$PCL_{17.6}$-PEG | 10.7 ± 0.5 | 13.0 ± 0.8 |
| P($CL_{13.5}$-TMC-$Bz_{3.7}$)-PEG | 3.6 ± 0.2 | 4.9 ± 0.4 |
| P($CL_{9.1}$-TMC-$Bz_{7.7}$)-PEG | 8.6 ± 0.3 | 9.4 ± 0.6 |
| P($CL_{4.8}$-TMC-$Bz_{9.2}$)-PEG | 5.6 ± 0.1 | 10.0 ± 0.6 |

### *3.6. Pharmacokinetics and Biodistribution of mTHPC in its Free Form and Loaded in Cy7-Labeled Bz-$PCL_{17.6}$-PEG and P($CL_{9.1}$-TMC-$Bz_{7.7}$)-PEG Micelles in A431 Tumor-Bearing Mice*

The circulation time and biodistribution of mTHPC-loaded micelles were studied using mice bearing human A431 tumor xenografts of 100–300 $mm^3$. NIR fluorescence of Cy7-labeled micelles and mTHPC concentrations as measured in plasma and organ and tumor homogenates, thus addressing both polymer and photosensitizer contents of the samples. Micelles consisting of Bz-$PCL_{17.6}$-PEG and P($CL_{9.1}$-TMC-$Bz_{7.7}$)-PEG were chosen because both copolymers have comparable chain lengths of hydrophobic blocks (~18 units of either CL with the final unit capped with a benzyl group, or CL plus TMC-Bz) but different contents of aromatic units. Importantly, both micellar PS formulations showed similar phototoxicity on cells (Figure 5C,D) but markedly different release behaviors in vitro (Figure 3B).

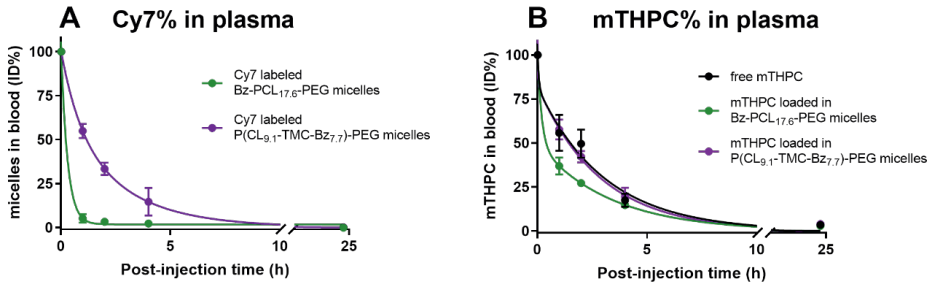


**Figure 6.** Plasma disappearance of free mTHPC (i.e., Foscan® formulation) and 0.6 wt% mTHPC-loaded Cy7-labeled micelles, showing Cy7 levels (**A**) and mTHPC levels (**B**) as % of injected doses (ID) upon tail vein administration in A431 tumor-bearing Balb/c mice (300 μg mTHPC per kg bodyweight of the mouse, i.e., ~6 μg mTHPC and ~1 mg polymer per mouse with injection volume of ~120 μL). Data are presented as mean ± SD, *n* = 3-5.



The plasma concentrations were determined after intravenous administration of free mTHPC or Cy7-labeled micelles loaded with mTHPC into mice via the tail vein. As reported in our previous study [38], administration of free mTHPC (i.e., mTHPC dissolved in diluted Foscan solvent (ethanol/propylene glycol/PBS 20:30:50 *v/v/v*) inflicted side effects such as tachypnea, passiveness immediately post-injection, and loss of body weight (~1 g on average) within 24 h. However, none of the micellar mTHPC treated mice showed any (short term) side effects during or after their administration, suggesting micellar formulations at the injected polymer dose (~1 mg) are well tolerated for in vivo applications**.**

**Table 3.** The half-life and the area under the curve (AUC) values of mTHPC in different formulations and the corresponding (Cy7-labeled) micelles.

| Detection | Formulation | Half-life (h) | | AUC (h*%) | Volume of Distribution (mL/kg) | Clearance (mL/kg/h) |
|---|---|---|---|---|---|---|
| | | Phase α [a] | Phase β | | | |
| **Cy7** | Bz-PCL$_{17.6}$-PEG micelles | <0.3 | - | 72 | 306 | 81.4 |
| | P(CL$_{9.1}$-TMC-Bz$_{7.7}$)-PEG micelles | ~0.7 | 2.9 | 319 | 77 | 18.4 |
| **mTHPC** | Free mTHPC | ≤0.5 | 2.1 | 442 | 120 | 13.2 |
| | mTHPC in Bz-PCL$_{17.6}$-PEG micelles | ≤0.5 | 2.5 | 350 | 180 | 16.7 |
| | mTHPC in P(CL$_{9.1}$-TMC-Bz$_{7.7}$)-PEG micelles | ≤0.5 | 2.0 | 464 | 120 | 12.6 |

[a] Initial phase half-lives (t½-α) were estimated from plasma disappearance rates during the first hour after administration, while half-lives of the terminal phase (t½-β) were calculated from non-compartmental analysis. Distribution volumes and clearances were calculated assuming a standard blood volume of 58.5 mL/kg [24].

The analysis of Cy7 levels in plasma (Figure 6A) showed that the elimination rate of P($CL_{9.1}$-TMC-$Bz_{7.7}$)-PEG micelles was significantly slower as compared to that of Bz-$PCL_{17.6}$-PEG micelles (e.g., 55% vs 5% of the injected dose (ID) remaining in plasma after 1 h). Non-compartment analysis was used to determine the pharmacokinetic parameters of both micelles, including terminal half-life, area under the curve (AUC), and clearance. As shown in Table 3, Bz-$PCL_{17.6}$-PEG and P($CL_{9.1}$-TMC-$Bz_{7.7}$)-PEG micelles significantly differed in AUC values, and consequentially had large differences in distribution and clearance volumes. The differences in pharmacokinetic parameters primarily relate to the initial phase of the plasma curves (i.e., before 1 h); most likely they relate to differences in stability of the micelles, indicating more rapid dissociation of Bz-$PCL_{17.6}$-PEG micelles into unimers as compared to P($CL_{9.1}$-TMC-$Bz_{7.7}$)-PEG micelles. This is most likely attributed to relatively stronger π-π stacking between the polymer chains in the latter micelles [30,56].

Figure 6B shows the plasma concentrations of mTHPC after administration of either free mTHPC or the micellar formulations. It is clear that free mTHPC and mTHPC loaded in micelles displayed comparable mTHPC levels and showed similar decay profiles in the circulation (Figure 6B). A rapid initial elimination was observed, for which half-lives ($t_{½}$-α) of ~0.5 h or less were estimated. Non-compartmental analysis of the mTHPC curves provided terminal half-lives ($t_{½}$-β), AUCs, and derived pharmacokinetic parameters, such as distribution volumes and clearance. It can be concluded from the results presented in Table 3 (bottom part) that those pharmacokinetic parameters were comparable between both free mTHPC and micellar mTHPC formulations. In addition, significant differences of pharmacokinetic parameters were observed between both Bz-$PCL_{17.6}$-PEG micelles and the loaded mTHPC, indicating that PS and polymer dissociated rapidly upon their injection into the circulation. On the other hand, for P($CL_{9.1}$-TMC-$Bz_{7.7}$)-PEG micellar formulation, pharmacokinetic parameters of mTHPC (Table 3, bottom part) were tightly associated with those derived from Cy7 analysis (Table 3, top part). However, due to coincidently similar data observed for free mTHPC and Cy7, it is difficult to conclude based on these parameters whether mTHPC was released from P($CL_{9.1}$-TMC-$Bz_{7.7}$)-PEG micelles or retained in the micelles. However, the in vitro release study in human plasma (Figure 3B, purple line and Figure 4) suggests that premature release of mTHPC from micelles most likely also occurred in the circulation for these micelles. Similarly, it was reported that paclitaxel loaded in thermosensitive micelles containing aromatic HPMAm-Bz units in the hydrophobic blocks exhibited a similar pharmacokinetic profile as when loaded in micelles without aromatic groups and as compared to free paclitaxel, despite the significantly improved in vitro stability and drug retention by π-π stacking [30,56]. Additionally, paclitaxel loaded in thermosensitive HPMAm-lactate-based micelles also showed the same pharmacokinetic data as the drug in its free form [57]. In addition, premature cargo release was also observed previously in various liposomal mTHPC formulations and other mTHPC-loaded micelles [24,58]. This release can be attributed to the high binding affinity of mTHPC with plasma (lipo)proteins,

leading to mTHPC redistribution from intact micelles to these plasma components [59–61]. It is noted that the relatively long circulation time of (released) mTHPC in the β phase is probably due to released mTHPC that subsequently binds to lipoproteins, which can act as endogenous carriers for mTHPC [62,63].

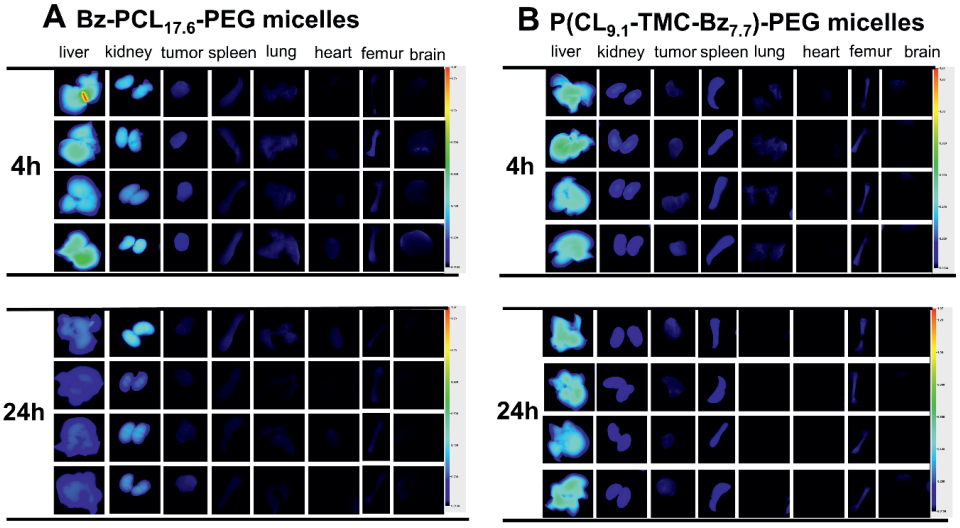


**Figure 7.** Ex vivo fluorescence reflectance imaging (FRI) analysis of the accumulation of the Cy7-labeled Bz-$PCL_{17.6}$-PEG (**A**) and P($CL_{9.1}$-TMC-$Bz_{7.7}$)-PEG (**B**) micelles in tumors and healthy organs after 4 and 24 h administration. Images, obtained at $\lambda_{em}$ 820 nm with $\lambda_{ex}$ 785 nm are from 4 different mice at each timepoint ($n$ = 4).

Tumors and organs were excised from mice that were sacrificed at 4 and 24 h after i.v. injection and Cy7-labeled micelles deposited in these tissues were visualized using 2D fluorescence reflectance imaging (FRI) and subsequently quantified by fluorescence intensity. It is noted that before taking out the organs, cervical dislocation followed by a cardiac puncture was performed for all mice, through which a substantial volume of blood was drawn from the animal in order to minimize the background signal from residual blood in the tissues. As shown in Figure 7, ex vivo images indicate that both Bz-$PCL_{17.6}$-PEG and P($CL_{9.1}$-TMC-$Bz_{7.7}$)-PEG micelles were found to primarily accumulate in liver, followed by kidneys and spleen. Different organ distribution profiles were observed for the two micellar formulations. As an explanation, Bz-$PCL_{17.6}$-PEG micelles accumulated in liver and kidneys at 4 h and while the accumulation in liver decayed, kidney accumulation persisted upon 24 h after administration. Accumulation of P($CL_{9.1}$-TMC-$Bz_{7.7}$)-PEG micelles in the kidneys was less pronounced and these micelles showed prolonged residence up to 24 h in the liver, and to a lesser extent in the spleen. In line with the imaging results, the quantified fluorescence intensities (Figure 8) show that the prominent liver accumulation of both micelles (Figure

8A) was observed to be ~15% ID/g at 4 h, in line with previous reports [30,64], most likely due to their clearance by the mononuclear phagocytic system (MPS) [65–67]. However, 24 h post-injection, Bz-PCL$_{17.6}$-PEG micelles decreased significantly to approximately 5% ID/g liver, while P(CL$_{9.1}$-TMC-Bz$_{7.7}$)-PEG micelles remained at similar levels in the liver as observed at 4 h. Additionally, the residence of the P(CL$_{9.1}$-TMC-Bz$_{7.7}$)-PEG micelles in the spleen was significantly longer than Bz-PCL$_{17.6}$-PEG micelles (4.6% vs 1.4% ID/g after 24 h, Figure 8D). These results suggest better stability of the P(CL$_{9.1}$-TMC-Bz$_{7.7}$)-PEG micelles than the micelles from Bz-terminated polymers, most likely due to strong π-π stacking resulting from the multiple Bz groups per polymer chain in the micelles of the former. Cy7 levels from Bz-PCL$_{17.6}$-PEG and P(CL$_{9.1}$-TMC-Bz$_{7.7}$)-PEG micelles could be detected in kidneys with ~6% and ~4% ID/g (Figure 8B) at 4 h, respectively, which decreased slightly at 24 h. The observed kidney accumulation was most likely due to dissociation of Cy7-labeled unimers from the micelles, which have a molecular size below the threshold of glomerular filtration [65].

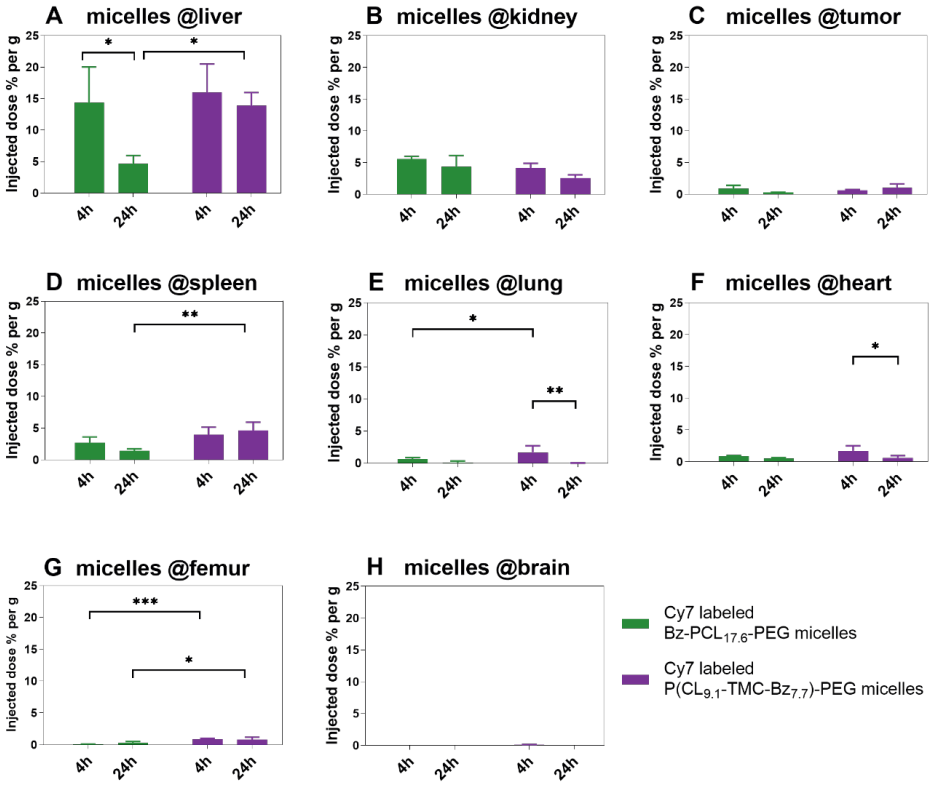


**Figure 8.** Biodistribution of Cy7-labeled micelles in tumor and main organs of mice after 4 and 24 h administration. Data are indicated as the percentage of the injected Cy7 dose (%ID) present per gram of tumor or organ ($n$ = 3-5). * $p < 0.05$, ** $p < 0.01$, *** $p < 0.001$.

Interestingly, although no micelles were detected in the circulation after 24 h (Figure 6), accumulation of P($CL_{9.1}$-TMC-$Bz_{7.7}$)-PEG micelles in tumors increased from 0.6 % ID/g at 4 h to approximate 1% ID/g at 24 h (Figure 8C). In contrast, no tumor accumulation of Bz-$PCL_{17.6}$-PEG micelles was found at 24 h. This suggests that after 4 h, the remaining P($CL_{9.1}$-TMC-$Bz_{7.7}$)-PEG micelles in the circulation (15 % ID, Figure 6) were (at least partly) intact and progressively accumulated in tumors via overtime EPR effect. In addition, P($CL_{9.1}$-TMC-$Bz_{7.7}$)-PEG micelles accumulated in significantly higher amounts in the femur at 4 and 24 h than Bz-$PCL_{17.6}$-PEG micelles (Figure 8G). This also indicates the higher amount of intact micelles present in the circulation, since it was previously reported that relatively small nanoparticles (generally below 60 nm) tend to accumulate in MPS-enriched bone marrow [68,69].

To study a possible correlation of biodistribution between mTHPC and micelles, Figure 9 displays the biodistribution in tumors and a panel of organs of mTHPC that was injected in free form and using Bz-$PCL_{17.6}$-PEG or P($CL_{9.1}$-TMC-$Bz_{7.7}$)-PEG formulations. The first conclusion is that the biodistribution of micellar mTHPC was similar to that of free mTHPC. The highest mTHPC levels were seen in liver and spleen, followed by lungs (Figure 9A,D,E). These are all tissues containing reticuloendothelial cells with a rich MPS, which are known to preferentially accumulate photosensitizers [8,70–72]. The accumulation of mTHPC in the liver at 4 h was similar to the accumulation of polymers in the liver (i.e., ~15% ID per gram), which then decreased significantly to about 5% ID/g at 24 h (Figure 9A). Higher accumulation of mTHPC in lungs was observed after 4 h than after 24 h (Figure 9E), most likely due to the blood fraction (containing mTHPC) after 4 h present in the excised lungs of non-perfused mice. However, in spleen and lungs, higher accumulation of mTHPC (~8-15% ID/g, Figure 9D,E, green and purple columns) was detected than that of the corresponding host micelles (≤5% ID/g, Figure 8D,E). The values of mTHPC accumulation were consistent with those reported for mTHPC when dosed using different liposomal formulations [58,72–73]. It is noted that although similar mTHPC content was detected per gram for the three organs, the total mTHPC accumulation in liver was significantly higher than that in spleen and lungs (e.g., ~15% ID per liver vs. ~1% ID per spleen or lung at 4 h; Figure S12A,D,E of Supplementary Materials) due to the high weights of liver samples (~1 g on average). Apart from liver, spleen, and lungs, regardless of the timepoints, similar amounts of mTHPC (~2–3% ID/g) were accumulated in tumor, kidney, heart, and femur (Figure 9B,C,F,G), suggesting unspecific biodistribution of mTHPC. Accumulated mTHPC levels resulting from being loaded in Bz-$PCL_{17.6}$-PEG and P($CL_{9.1}$-TMC-$Bz_{7.7}$)-PEG micelles in these organs and tissues (Figure 9C,F,G, green and purple columns) were higher as compared to the corresponding host micelles (<1%) (Figure 8C,F,G), except those in the kidney (Figure 8B and 9B). This loose association of the distribution pattern between mTHPC and the host micelles confirmed the fast release of mTHPC from both micelles. It is noted that neither the PS nor the micelles showed disposition in the

brain (Figure 8H and 9H), which is a well-perfused organ; thus, the background signal from residual blood in the tissues appears minimal.

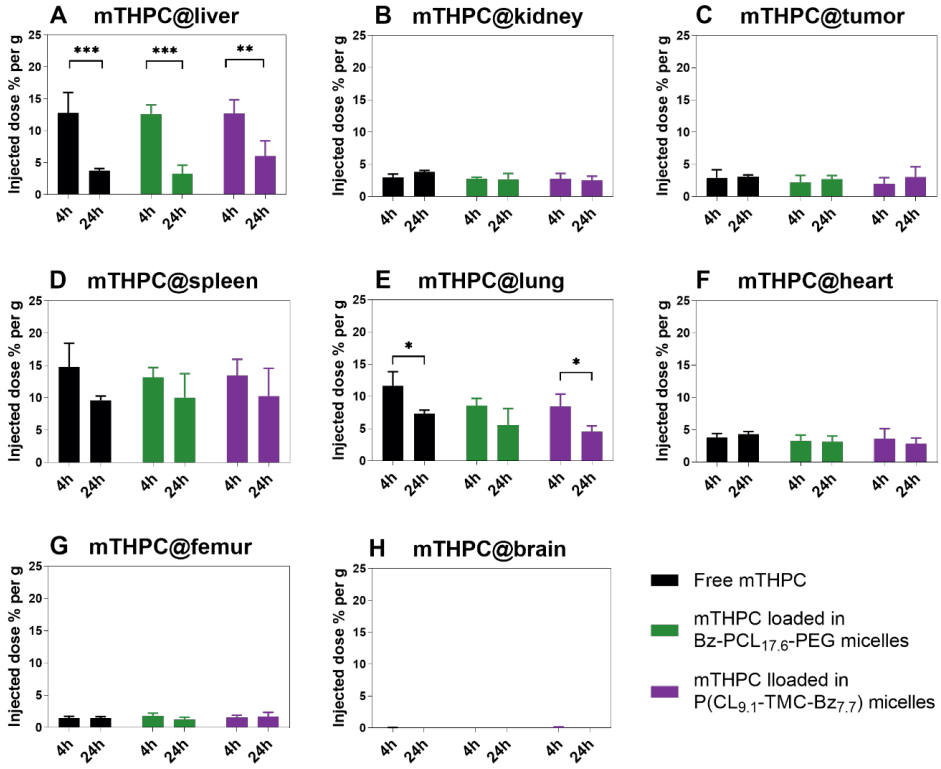


**Figure 9.** Biodistribution of free mTHPC and mTHPC loaded in micelles in tumors and main organs of mice after 4 and 24 h administration at mTHPC dose of 0.3 mg/kg. Data are indicated as the percentage of the injected mTHPC dose (%ID) present per gram of tumor or organ ($n$ = 3-5). * $p < 0.05$, ** $p < 0.01$, *** $p < 0.001$.

## 4. Conclusions

In the present study, we showed that i.v. injected micelles containing multiple pendant aromatic groups (i.e., TMC-Bz monomers) in the hydrophobic blocks of the PCL-PEG-based block copolymers displayed longer circulation times in mice than micelles with a single terminal aromatic group, and that incorporating the pendant aromatic groups improved retention of the photosensitizer mTHPC in human plasma in vitro. Despite those promising features, similar biodistribution of micellar mTHPC as compared to free mTHPC—and importantly, unequal biodistribution patterns of mTHPC and the host micelles—indicated premature release of mTHPC from these micelles in vivo.

Our study emphasizes the necessity to investigate the in vivo behavior, particularly biodistribution, of both the micellar carrier and the incorporated cargo, as such data can provide important information about the fate of PS-loaded nanocarriers. Our study shows that additional measures beyond π-π stacking are needed to stably incorporate mTHPC in the micelles in order to benefit from them as carriers that are able to deliver the payload in pathological tissue by passive or active targeting.

**Author Contributions:** Conceptualization, C.F.v.N.; funding acquisition, Y.L. and C.F.v.N.; investigation, Y.L., M.H.A.M.F., B.L., N.C.H.v.K., and R.F.M.M.-B.; methodology, R.J.K.; supervision, S.O., W.E.H., and C.F.v.N.

**Funding:** Y. Liu is supported by a PhD scholarship from China Scholarship Council (CSC).

**Conflicts of Interest:** The authors declare no conflict of interest.

## References


1. van Straten, D.; Mashayekhi, V.; de Bruijn, H.S.; Oliveira, S.; Robinson, D.J. Oncologic photodynamic therapy: Basic principles, current clinical status and future directions. *Cancers* **2017**, *9*, 1–54.
2. Yakavets, I.; Millard, M.; Zorin, V.; Lassalle, H.P.; Bezdetnaya, L. Current state of the nanoscale delivery systems for temoporfin-based photodynamic therapy: Advanced delivery strategies. *J. Control. Release* **2019**, *304*, 268–287.
3. Agostinis, P.; Berg, K.; Cengel, K.A.; Foster, T.H.; Girotti, A.W.; Gollnick, S.O.; Hahn, S.M.; Hamblin, M.R.; Juzeniene, A.; Kessel, D.; et al. Photodynamic therapy of cancer: An update. *CA Cancer J. Clin.* **2011**, *61*, 250–281.
4. Hernández, I.; Yu, Y.; Ossendorp, F.; Korbelik, M.; Oliveira, S. Preclinical and clinical evidence of immune responses triggered in oncologic photodynamic therapy: Clinical recommendations. *J. Clin. Med.* **2020**, *9*, 1–25.
5. Meulemans, J.; Delaere, P.; Vander Poorten, V. Photodynamic therapy in head and neck cancer: Indications, outcomes, and future prospects. *Curr. Opin. Otolaryngol. Head Neck Surg.* **2019**, *27*, 136–141.
6. van Driel, P.; Boonstra, M.C.; Slooter, M.D.; Heukers, R.; Stammes, M.A.; Snoeks, T.J.A.; de Bruijn, H.S.; van Diest, P.J.; Vahrmeijer, A.L.; van Bergen En Henegouwen, P.M.P.; et al. EGFR targeted nanobody-photosensitizer conjugates for photodynamic therapy in a pre-clinical model of head and neck cancer. *J. Control. Release* **2016**, *229*, 93–105.
7. Hopper, C. Photodynamic therapy: A clinical reality in the treatment of cancer. *Lancet. Oncol.* **2000**, *1*, 212–219.
8. Bovis, M.J.; Woodhams, J.H.; Loizidou, M.; Scheglmann, D.; Bown, S.G.; Macrobert, A.J. Improved in vivo delivery of m-THPC via pegylated liposomes for use in photodynamic therapy. *J. Control. Release* **2012**, *157*, 196–205.
9. Kwiatkowski, S.; Knap, B.; Przystupski, D.; Saczko, J.; Kedzierska, E.; Knap-Czop, K.; Kotlinska, J.; Michel, O.; Kotowski, K.; Kulbacka, J. Photodynamic therapy—Mechanisms, photosensitizers and combinations. *Biomed. Pharmacother.* **2018**, *106*, 1098–1107.
10. Redmond, R.W.; Land, E.J.; Truscott, T.G. Aggregation effects on the photophysical properties of porphyrins in relation to mechanisms involved in photodynamic therapy. *Adv. Exp. Med. Biol.* **1985**, *193*, 293–302.
11. Triesscheijn, M.; Ruevekamp, M.; Out, R.; Van Berkel, T.J.; Schellens, J.; Baas, P.; Stewart, F.A. The pharmacokinetic behavior of the photosensitizer meso-tetra-hydroxyphenyl-chlorin in mice and men. *Cancer Chemother. Pharmacol.* **2007**, *60*, 113–122.
12. van Nostrum, C.F. Polymeric micelles to deliver photosensitizers for photodynamic therapy. *Adv. Drug Deliv. Rev.* **2004**, *56*, 9–16.
13. Deng, C.; Jiang, Y.; Cheng, R.; Meng, F.; Zhong, Z. Biodegradable polymeric micelles for targeted and controlled anticancer drug delivery: Promises, progress and prospects. *Nano Today* **2012**, *7*, 467–480.
14. Varela-Moreira, A.; Shi, Y.; Fens, M.H.A.M.; Lammers, T.; Hennink, W.E.; Schiffelers, R.M. Clinical application of polymeric micelles for the treatment of cancer. *Mater. Chem. Front.* **2017**, *1*, 1485–1501.

15. Cabral, H.; Kataoka, K. Progress of drug-loaded polymeric micelles into clinical studies. *J. Control. Release* **2014**, *190*, 465–476.
16. Houdaihed, L.; Evans, J.C.; Allen, C. Overcoming the road blocks: Advancement of block copolymer micelles for cancer therapy in the clinic. *Mol. Pharm.* **2017**, *14*, 2503–2517.
17. Dos Santos, N.; Allen, C.; Doppen, A.M.; Anantha, M.; Cox, K.A.; Gallagher, R.C.; Karlsson, G.; Edwards, K.; Kenner, G.; Samuels, L.; et al. Influence of poly(ethylene glycol) grafting density and polymer length on liposomes: Relating plasma circulation lifetimes to protein binding. *Biochim. Biophys. Acta* **2007**, *1768*, 1367–1377.
18. Klibanov, A.L.; Maruyama, K.; Torchilin, V.P.; Huang, L. Amphipathic polyethyleneglycols effectively prolong the circulation time of liposomes. *FEBS Lett.* **1990**, *268*, 235–237.
19. Torchilin, V.P. Recent advances with liposomes as pharmaceutical carriers. *Nat. Rev. Drug Discov.* **2005**, *4*, 145–160.
20. Tan, C.; Wang, Y.; Fan, W. Exploring polymeric micelles for improved delivery of anticancer agents: Recent developments in preclinical studies. *Pharmaceutics* **2013**, *5*, 201–219.
21. Maeda, H. Toward a full understanding of the EPR effect in primary and metastatic tumors as well as issues related to its heterogeneity. *Adv. Drug Deliv. Rev.* **2015**, *91*, 3–6.
22. Maeda, H.; Wu, J.; Sawa, T.; Matsumura, Y.; Hori, K. Tumor vascular permeability and the EPR effect in macromolecular therapeutics: A review. *J. Control. Release* **2000**, *65*, 271–284.
23. Hofman, J.W.; Carstens, M.G.; van Zeeland, F.; Helwig, C.; Flesch, F.M.; Hennink, W.E.; van Nostrum, C.F. Photocytotoxicity of mTHPC (temoporfin) loaded polymeric micelles mediated by lipase catalyzed degradation. *Pharm. Res.* **2008**, *25*, 2065–2073.
24. Wennink, J.W.H.; Liu, Y.; Makinen, P.I.; Setaro, F.; de la Escosura, A.; Bourajjaj, M.; Lappalainen, J.P.; Holappa, L.P.; van den Dikkenberg, J.B.; Al Fartousi, M.; et al. Macrophage selective photodynamic therapy by meta-tetra(hydroxyphenyl)chlorin loaded polymeric micelles: A possible treatment for cardiovascular diseases. *Eur. J. Pharm. Sci.* **2017**, *107*, 112–125.
25. Gong, J.; Chen, M.; Zheng, Y.; Wang, S.; Wang, Y. Polymeric micelles drug delivery system in oncology. *J. Control. Release* **2012**, *159*, 312–323.
26. Sheridan, C. Proof of concept for next-generation nanoparticle drugs in humans. *Nat. Biotechnol.* **2012**, *30*, 471–473.
27. Wang, A.Z.; Langer, R.; Farokhzad, O.C. Nanoparticle delivery of cancer drugs. *Annu. Rev. Med.* **2012**, *63*, 185–198.
28. Talelli, M.; Barz, M.; Rijcken, C.J.F.; Kiessling, F.; Hennink, W.E.; Lammers, T. Core-crosslinked polymeric micelles: Principles, preparation, biomedical applications and clinical translation. *Nano Today* **2015**, *10*, 93–117.
29. Hamaguchi, T.; Matsumura, Y.; Suzuki, M.; Shimizu, K.; Goda, R.; Nakamura, I.; Nakatomi, I.; Yokoyama, M.; Kataoka, K.; Kakizoe, T. NK105, a paclitaxel-incorporating micellar nanoparticle formulation, can extend in vivo antitumour activity and reduce the neurotoxicity of paclitaxel. *Br. J. Cancer* **2005**, *92*, 1240–1246.

30. Shi, Y.; van der Meel, R.; Theek, B.; Oude Blenke, E.; Pieters, E.H.; Fens, M.H.; Ehling, J.; Schiffelers, R.M.; Storm, G.; van Nostrum, C.F.; et al. Complete regression of xenograft tumors upon targeted delivery of paclitaxel via π-π stacking stabilized polymeric micelles. *ACS Nano* **2015**, *9*, 3740–3752.
31. Shi, Y.; Lammers, T.; Storm, G.; Hennink, W.E. Physico-chemical strategies to enhance stability and drug retention of polymeric micelles for tumor-targeted drug delivery. *Macromol. Biosci.* **2017**, *17*, 1–11.
32. Zhuang, W.; Wang, Y.; Cui, P.; Xing, L.; Lee, J.; Kim, D.; Jiang, H.; Oh, Y. Applications of π-π stacking interactions in the design of drug-delivery systems. *J. Control. Release* **2019**, *294*, 311–326.
33. Shi, Y.; Elkhabaz, A.; Yengej, F.A.; van den Dikkenberg, J.; Hennink, W.E.; van Nostrum, C.F. π-π stacking induced enhanced molecular solubilization, singlet oxygen production, and retention of a photosensitizer loaded in thermosensitive polymeric micelles. *Adv. Healthc. Mater.* **2014**, *3*, 2023–2031.
34. Pratt, R.C.; Nederberg, F.; Waymouth, R.M.; Hedrick, J.L. Tagging alcohols with cyclic carbonate: A versatile equivalent of (meth)acrylate for ring-opening polymerization. *Chem. Commun.* **2008**, 114–116,
35. Couffin, A.; Delcroix, D.; Martín-Vaca, B.; Bourissou, D.; Navarro, C. Mild and efficient preparation of block and gradient copolymers by methanesulfonic acid catalyzed ring-opening polymerization of caprolactone and trimethylene carbonate. *Macromolecules* **2013**, *46*, 4354–4360.
36. Delcroix, D.; Martín-Vaca, B.; Bourissou, D.; Navarro, C. Ring-opening polymerization of trimethylene carbonate catalyzed by methanesulfonic acid: Activated monomer versus active chain end mechanisms. *Macromolecules* **2010**, *43*, 8828–8835.
37. Carstens, M.G.; van Nostrum, C.F.; Ramzi, A.; Meeldijk, J.D.; Verrijk, R.; de Leede, L.L.; Crommelin, D.J.; Hennink, W.E. Poly(ethylene glycol)-oligolactates with monodisperse hydrophobic blocks: Preparation, characterization, and behavior in water. *Langmuir* 2005, *21*, 11446–11454.
38. Liu, Y.; Scrivano, L.; Peterson, J.D.; Fens, M.H.A.M.; Hernández, I.B.; Mesquita, B.; Toraño, J.S.; Hennink, W.E.; Nostrum, C.F.; Oliveira, S. EGFR targeted nanobody functionalized polymeric micelles loaded with mTHPC for selective photodynamic therapy. *Mol. Pharmaceutics* **2020**, *17*, 1276–1292.
39. Bagheri, M.; Bresseleers, J.; Varela-Moreira, A.; Sandre, O.; Meeuwissen, S.A.; Schiffelers, R.M.; Metselaar, J.M.; van Nostrum, C.F.; van Hest, J.C.M.; Hennink, W.E. Effect of formulation and processing parameters on the size of mPEG-*b*-p(HPMA-Bz) polymeric micelles. *Langmuir* **2018**, *34*, 15495–15506.
40. Zhang, Y.; Huo, M.; Zhou, J.; Xie, S. PKSolver: An add-in program for pharmacokinetic and pharmacodynamic data analysis in Microsoft Excel. *Comput. Methods Programs Biomed.* **2010**, *99*, 306–314.
41. Schindler, A.; Hibionada, Y.M.; Pitt, C.G. Aliphatic polyesters. III. Molecular weight and molecular weight distribution in alcohol-initiated polymerizations of ε-caprolactone. *J. Polym. Sci. Polym. Chem. Ed.* **1982**, *20*, 319–326.
42. Pêgo, A.P.; Zhong, Z.; Dijkstra, P.J.; Grijpma, D.W.; Feijen, J. Influence of catalyst and polymerization conditions on the properties of 1,3-trimethylene carbonate and ε-caprolactone copolymers. *Macromol. Chem. Phys.* **2003**, *204*, 747–754.

43. Loontjens, C.A.M.; Vermonden, T.; Leemhuis, M.; van Steenbergen, M.J.; van Nostrum, C.F.; Hennink, W.E. Synthesis and characterization of random and triblock copolymers of ε-caprolactone and (Benzylated)hydroxymethyl glycolide. *Macromolecules* **2007**, *40*, 7208–7216.
44. Ling, J.; Zhu, W.; Shen, Z. Controlling ring-opening copolymerization of ε-caprolactone with trimethylene carbonate by scandium Tris(2,6-di-tert-butyl-4-methylphenolate). *Macromolecules* **2004**, *37*, 758–763.
45. Carstens, M.G.; Bevernage, J.J.L.; van Nostrum, C.F.; van Steenbergen, M.J.; Flesch, F.M.; Verrijk, R.; de Leede, L.G.J.; Crommelin, D.J.A.; Hennink, W.E. Small oligomeric micelles based on end group modified mPEG–oligocaprolactone with monodisperse hydrophobic blocks. *Macromolecules* **2007**, *40*, 116–122.
46. Cabral, H.; Matsumoto, Y.; Mizuno, K.; Chen, Q.; Murakami, M.; Kimura, M.; Terada, Y.; Kano, M.R.; Miyazono, K.; Uesaka, M.; et al. Accumulation of sub-100 nm polymeric micelles in poorly permeable tumours depends on size. *Nat. Nanotechnol.* **2011**, *6*, 815–823.
47. Danhier, F.; Feron, O.; Preat, V. To exploit the tumor microenvironment: Passive and active tumor targeting of nanocarriers for anti-cancer drug delivery. *J. Control. Release* **2010**, *148*, 135–146.
48. Jain, R.K.; Stylianopoulos, T. Delivering nanomedicine to solid tumors. *Nat. Rev. Clin. Oncol.* **2010**, *7*, 653–664.
49. Rijcken, C.J.; Hofman, J.W.; van Zeeland, F.; Hennink, W.E.; van Nostrum, C.F. Photosensitiser-loaded biodegradable polymeric micelles: Preparation, characterisation and in vitro PDT efficacy. *J. Control. Release* **2007**, *124*, 144–153.
50. Gaio, E.; Scheglmann, D.; Reddi, E.; Moret, F. Uptake and photo-toxicity of Foscan®, Foslip® and Fospeg® in multicellular tumor spheroids. *J. Photochem. Photobiol. B* **2016**, *161*, 244–252.
51. Gyenge, E.B.; Hiestand, S.; Graefe, S.; Walt, H.; Maake, C. Cellular and molecular effects of the liposomal mTHPC derivative Foslipos in prostate carcinoma cells in vitro. *Photodiagno. Photodyn. Ther.* **2011**, *8*, 86–96.
52. Kiesslich, T.; Berlanda, J.; Plaetzer, K.; Krammer, B.; Berr, F. Comparative characterization of the efficiency and cellular pharmacokinetics of Foscan- and Foslip-based photodynamic treatment in human biliary tract cancer cell lines. *Photochem. Photobiol. Sci.* **2007**, *6*, 619–627.
53. Chen, Y.; Tezcan, O.; Li, D.; Beztsinna, N.; Lou, B.; Etrych, T.; Ulbrich, K.; Metselaar, J.M.; Lammers, T.; Hennink, W.E. Overcoming multidrug resistance using folate receptor-targeted and pH-responsive polymeric nanogels containing covalently entrapped doxorubicin. *Nanoscale* **2017**, *9*, 10404–10419.
54. Terashima, T.; Sugita, T.; Fukae, K.; Sawamoto, M. Synthesis and single-chain folding of amphiphilic random copolymers in water. *Macromolecules* **2014**, *47*, 589–600.
55. Xie, J.; Xu, C.; Kohler, N.; Hou, Y.; Sun, S. Controlled PEGylation of monodisperse $Fe_3O_4$ nanoparticles for reduced non-specific uptake by macrophage cells. *Adv. Mater.* **2007**, *19*, 3163–3166.
56. Shi, Y.; van Steenbergen, M.J.; Teunissen, E.A.; Novo, L.; Gradmann, S.; Baldus, M.; van Nostrum, C.F.; Hennink, W.E. π-π stacking increases the stability and loading capacity of thermosensitive polymeric micelles for chemotherapeutic drugs. *Biomacromolecules* **2013**, *14*, 1826–1837.

57. Soga, O. Biodegradable Thermosensitive Polymers: Synthesis, Characterization and Drug Delivery Applications. Ph.D. Thesis, Utrecht University, Utrecht, The Netherlands, 2006; pp. 87–102.
58. Decker, C.; Schubert, H.; May, S.; Fahr, A. Pharmacokinetics of temoporfin-loaded liposome formulations: Correlation of liposome and temoporfin blood concentration. *J. Control. Release* **2013**, *166*, 277–285.
59. Polo, L.; Valduga, G.; Jori, G.; Reddi, E. Low-density lipoprotein receptors in the uptake of tumour photosensitizers by human and rat transformed fibroblasts. *Int. J. Biochem. Cell Biol.* **2002**, *34*, 10–23.
60. Chowdhary, R.; Sharif, I.; Chansarkar, N.; Dolphin, D.; Delaney, S.; Meadows, H. Correlation of photosensitizer delivery to lipoproteins and efficacy in tumor and arthritis mouse models; comparison of lipid-based and Pluronic P123 formulations. *J. Pharm. Pharm. Sci.* **2003**, *6*, 198–204.
61. Sasnouski, S.; Zorin, V.; Khludeyev, I.; D'Hallewin, M.A.; Guillemin, F.; Bezdetnaya, L. Investigation of Foscan interactions with plasma proteins. *Biochim. Biophys. Acta* **2005**, *1725*, 394–402.
62. Michael-Titus, A.T.; Whelpton, R.; Yaqub, Z. Binding of temoporfin to the lipoprotein fractions of human serum. *Br. J. Clin. Pharmacol.* **1995**, *40*, 594–597.
63. Reshetov, V.; Zorin, V.; Siupa, A.; D'Hallewin, M.A.; Guillemin, F.; Bezdetnaya, L. Interaction of liposomal formulations of meta-tetra(hydroxyphenyl)chlorin (temoporfin) with serum proteins: Protein binding and liposome destruction. *Photochem. Photobiol.* **2012**, *88*, 1256–1264.
64. Shi, Y.; Kunjachan, S.; Wu, Z.; Gremse, F.; Moeckel, D.; van Zandvoort, M.; Kiessling, F.; Storm, G.; van Nostrum, C.F.; Hennink, W.E.; et al. Fluorophore labeling of core-crosslinked polymeric micelles for multimodal in vivo and ex vivo optical imaging. *Nanomedicine* **2015**, *10*, 1111–1125.
65. Noguchi, Y.; Wu, J.; Duncan, R.; Strohalm, J.; Ulbrich, K.; Akaike, T.; Maeda, H. Early phase tumor accumulation of macromolecules: A great difference in clearance rate between tumor and normal tissues. *Jpn. J. Cancer Res.* **1998**, *89*, 307–314.
66. Allmeroth, M.; Moderegger, D.; Biesalski, B.; Koynov, K.; Rösch, F.; Thews, O.; Zentel, R. Modifying the body distribution of HPMA-based copolymers by molecular weight and aggregate formation. *Biomacromolecules* **2011**, *12*, 2841–2849.
67. Allmeroth, M.; Moderegger, D.; Gundel, D.; Buchholz, H.G.; Mohr, N.; Koynov, K.; Rosch, F.; Thews, O.; Zentel, R. PEGylation of HPMA-based block copolymers enhances tumor accumulation in vivo: A quantitative study using radiolabeling and positron emission tomography. *J. Control. Release* **2013**, *172*, 77–85.
68. Deshantri, A.K.; Varela Moreira, A.; Ecker, V.; Mandhane, S.N.; Schiffelers, R.M.; Buchner, M.; Fens, M. Nanomedicines for the treatment of hematological malignancies. *J. Control. Release* **2018**, *287*, 194–215.
69. Sarin, H. Physiologic upper limits of pore size of different blood capillary types and another perspective on the dual pore theory of microvascular permeability. *J. Angiogenesis Res.* **2010**, *2*, 1–19.
70. Cramers, P.; Ruevekamp, M.; Oppelaar, H.; Dalesio, O.; Baas, P.; Stewart, F.A. Foscan uptake and tissue distribution in relation to photodynamic efficacy. *Br. J. Cancer* **2003**, *88*, 283–290.
71. Gomer, C.J.; Dougherty, T.J. Determination of [3H]- and [14C] hematoporphyrin derivative distribution in malignant and normal tissue. *Cancer Res.* **1979**, *39*, 146–151.

72. Reshetov, V.; Lassalle, H.P.; Francois, A.; Dumas, D.; Hupont, S.; Grafe, S.; Filipe, V.; Jiskoot, W.; Guillemin, F.; Zorin, V.; et al. Photodynamic therapy with conventional and PEGylated liposomal formulations of mTHPC (temoporfin): Comparison of treatment efficacy and distribution characteristics in vivo. *Int. J. Nanomed.* **2013**, *8*, 3817–3831.

73. Svensson, J.; Johansson, A.; Grafe, S.; Gitter, B.; Trebst, T.; Bendsoe, N.; Andersson-Engels, S.; Svanberg, K. Tumor selectivity at short times following systemic administration of a liposomal temoporfin formulation in a murine tumor model. *Photochem. Photobiol.* **2007**, *83*, 1211–1219.

74. Liu, Y.; Scrivano, L.; Peterson, J.D.; Fens, M.H.A.M.; Hernández, I.B.; Mesquita, B.; Toraño, J.S.; Hennink, W.E.; Nostrum, C.F.; Oliveira, S. EGFR targeted nanobody functionalized polymeric micelles loaded with mTHPC for selective photodynamic therapy. *Mol. Pharmaceutics* **2020**, *17*, 1276–1292.

75. Couffin, A.; Delcroix, D.; Martín-Vaca, B.; Bourissou, D.; Navarro, C. Mild and efficient preparation of block and gradient copolymers by methanesulfonic acid catalyzed ring-opening polymerization of caprolactone and trimethylene carbonate. Macromolecules **2013**, 46, 4354-4360.

## Supporting information

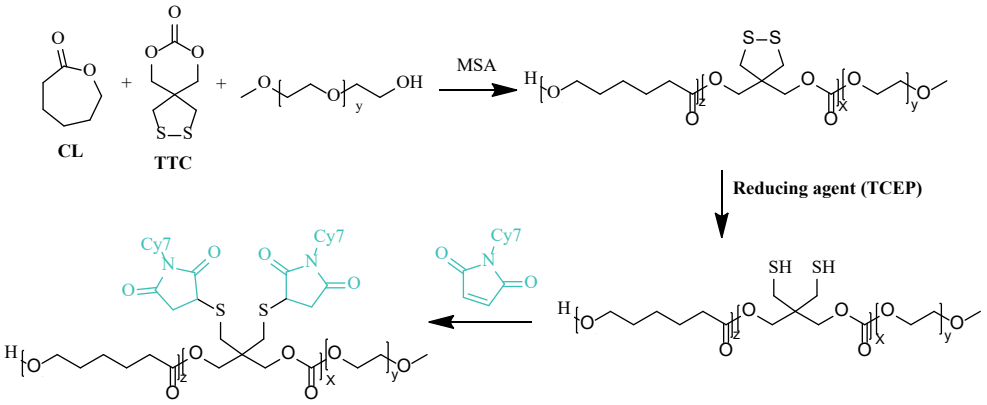


**Scheme S1**. Synthesis and Cy7 labeling of P($CL_{18}$-$TTC_{7.5}$)-PEG [1].

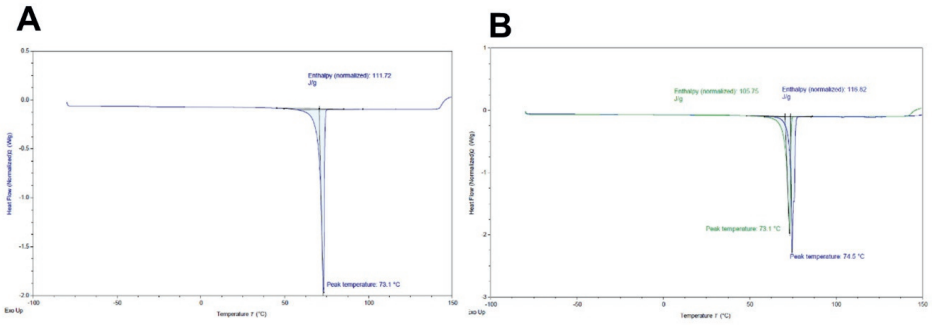


**Figure S1**. Thermograms of benzyl 2,2-bis(hydroxymethyl)propionate (A) and benzyl 5-methyl-2-oxo-1,3-dioxane-5-carboxylate (before (green line) and after (blue line) recrystallization) (B), recorded by DSC.

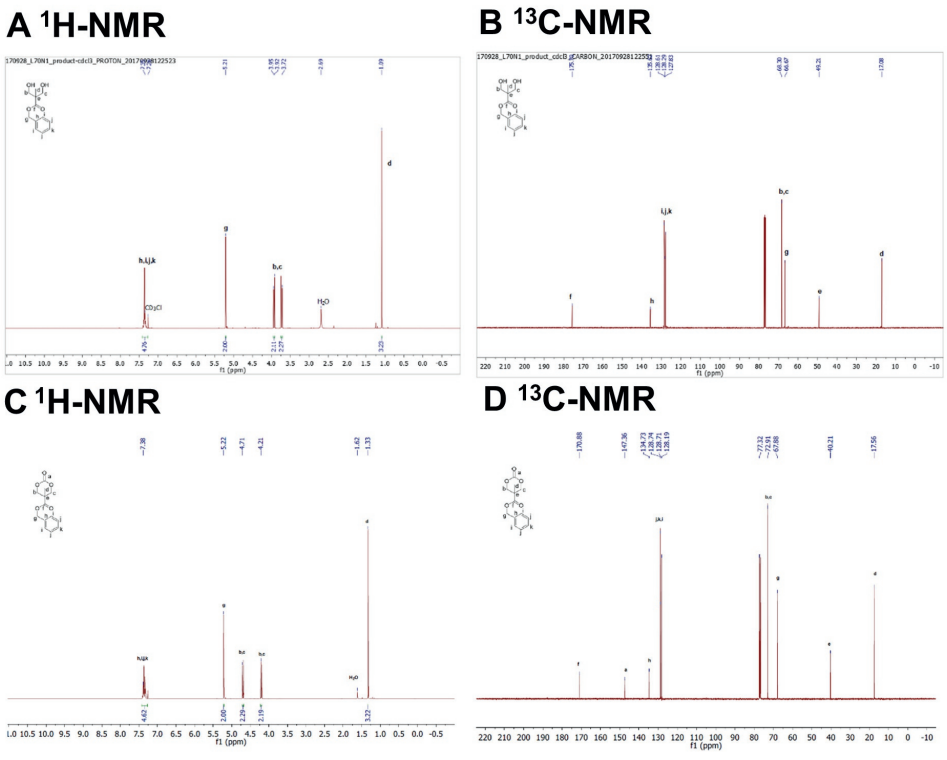


**Figure S2.** $^{1}H/^{13}C$ NMR spectra of the benzyl 2,2-bis(methylol)propionate intermediate (A, B) and benzyl 5-methyl-2-oxo-1,3-dioxane-5-carboxylate (*i.e.,* TMC-Bz) (C, D).

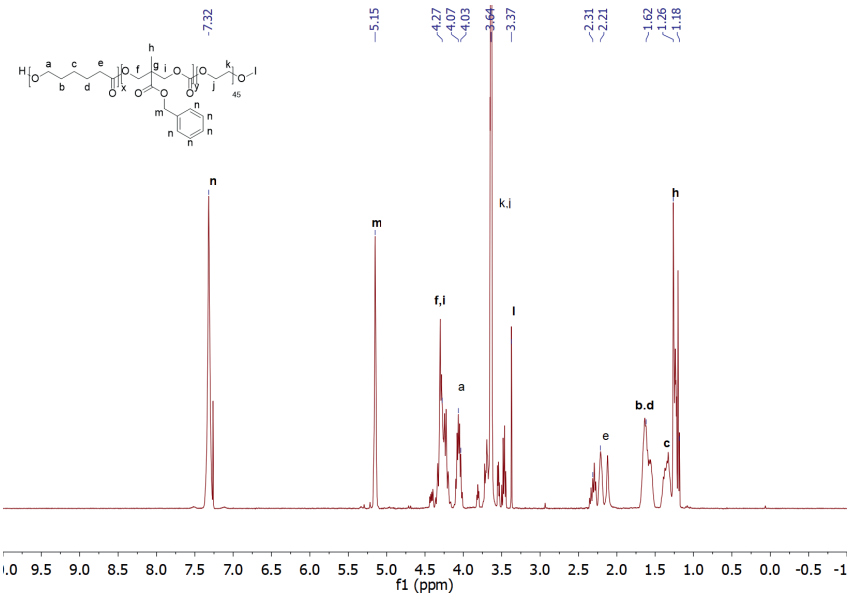


**Figure S3**. $^1$H NMR spectrum of P(CL-TMC-Bz)-PEG. $^1$H-NMR (600 MHz, $CDCl_3$): δ 7.34 (m, $CH_2\underline{\boldsymbol{C_6H_5}}$), 5.15 (s, $\underline{\boldsymbol{CH_2}}C_6H_5$), 4.30–4.05 (m, $COO\underline{\boldsymbol{CH_2}}C\underline{\boldsymbol{CH_2}}OCO$, $COCH_2CH_2CH_2CH_2\underline{\boldsymbol{CH_2}}O$), 3.64 (m, PEG protons), 3.38 (s, 3H, $\underline{\boldsymbol{CH_3}}O$), 2.30 (m, $CH_2CH_2\underline{\boldsymbol{CH_2}}COO$), 1.62 (m, $CH_2\underline{\boldsymbol{CH_2}}CH_2\underline{\boldsymbol{CH_2}}CH_2$), 1.34 (m, $CH_2CH_2\underline{\boldsymbol{CH_2}}CH_2CH_2$), 1.27-1.21 (m, $OCH_2C\underline{\boldsymbol{CH_3}}$).

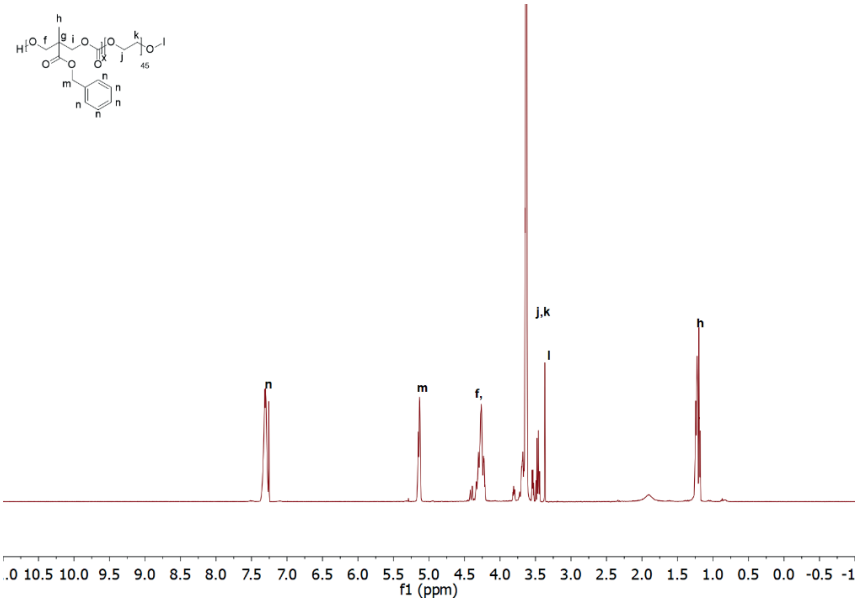


**Figure S4**. $^1$H NMR spectrum of P(TMC-Bz)-PEG. $^1$H-NMR (600 MHz, $CDCl_3$): δ 7.34 (m, $CH_2\underline{\boldsymbol{C_6H_5}}$), 5.15 (s, $\underline{\boldsymbol{CH_2}}C_6H_5$), 4.30–4.05 (m, $COO\underline{\boldsymbol{CH_2}}C\underline{\boldsymbol{CH_2}}OCO$, $COCH_2CH_2CH_2CH_2\underline{\boldsymbol{CH_2}}O$), 3.64 (m, PEG protons), 3.38 (s, 3H, $\underline{\boldsymbol{CH_3}}O$), 1.28 (m, $OCH_2C\underline{\boldsymbol{CH_3}}$).

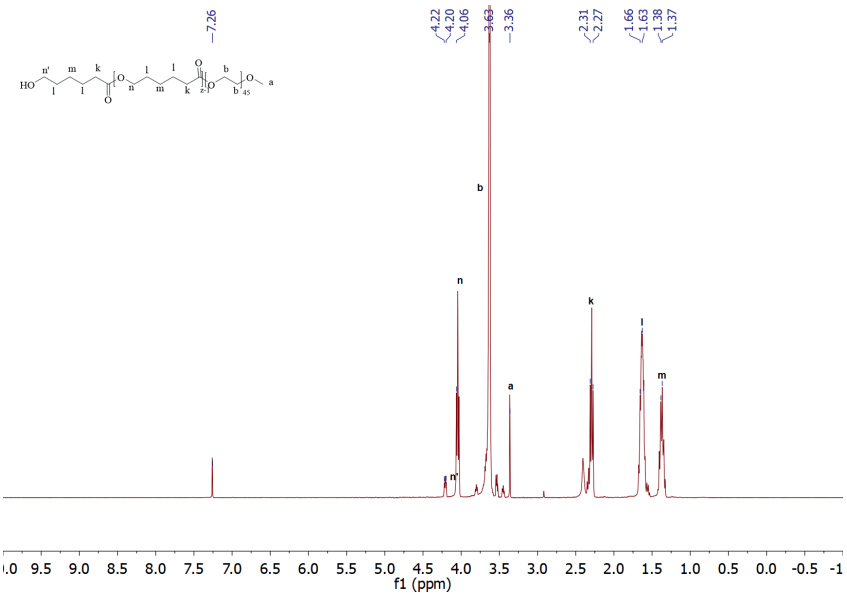


**Figure S5**. $^{1}$H NMR spectrum of PCL-PEG. $^{1}$H-NMR (600 MHz, $CDCl_3$): δ 4.29–4.00 (m, COO***CH*****$_2$**, $CH_2$***CH*****$_2$**OH), 3.64 (m, PEG protons), 3.37 (s, ***CH*****$_3$**O), 2.29 (m, $CH_2CH_2$***CH*****$_2$**COO), 1.66 (m, $CH_2$***CH*****$_2$**$CH_2$***CH*****$_2$**$CH_2$), 1.38 (m, $CH_2CH_2$***CH*****$_2$**$CH_2CH_2$).

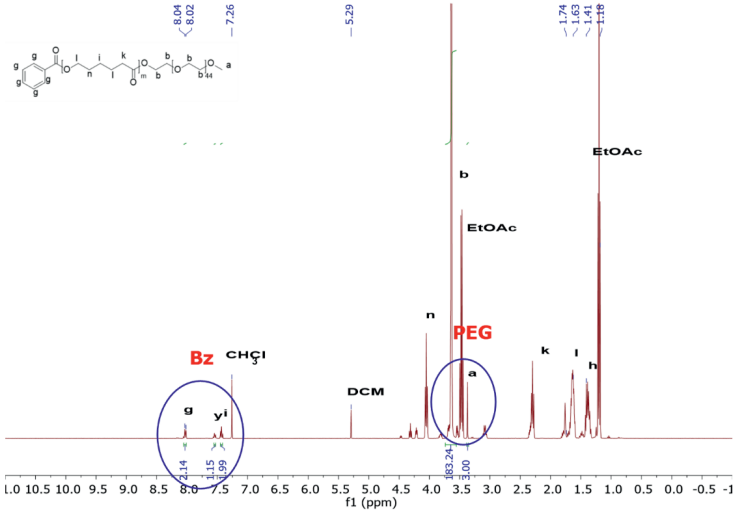


**Figure S6.** $^{1}$H NMR spectrum of Bz-PCL-PEG. $^{1}$H-NMR (600 MHz, $CDCl_3$): δ 8.0 (d, 2H, aromatic CH), 7.53 (t, 1H, aromatic CH), 7.41 (t, 2H, aromatic CH), 4.29 (t, 2H, $C_6H_5COO$***CH*****$_2$**), 4.20–4.00 (m, COO***CH*****$_2$**, $CH_2$***CH*****$_2$**OH), 3.64 (m, PEG protons), 3.37 (s, ***CH*****$_3$**O), 2.29 (m, $CH_2CH_2$***CH*****$_2$**COO), 1.66 (m, $CH_2$***CH*****$_2$**$CH_2$***CH*****$_2$**$CH_2$), 1.38 (m, $CH_2CH_2$***CH*****$_2$**$CH_2CH_2$).

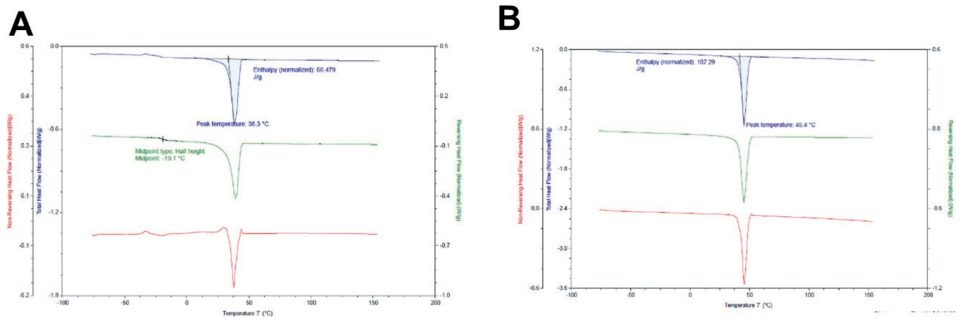


**Figure S7**. Thermograms of P($CL_{9.1}$-TMC-$Bz_{7.7}$)-PEG (Entry 7, table 1) and $PCL_{17.6}$-PEG (Entry 5, table 1), recorded by DSC.

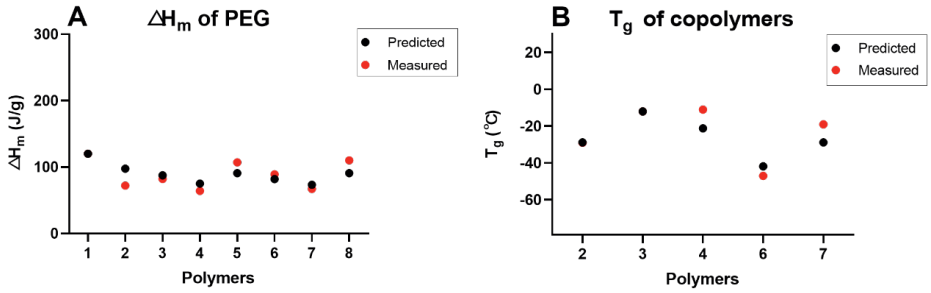


**Figure S8.** (A) Measured $\Delta H_m$'s of PEG in the synthesized block copolymers (red dots), corrected for the weight fraction of PEG of the block copolymer. The predicted $\Delta H_m$'s (black dots) were obtained by using mPEG-OH (measured $\Delta H_m$ of 182 J/g and the weight fraction of PEG in the block copolymers) as the reference. (B) Measured $T_g$'s of the synthesized P(CL-TMC-Bz)-PEG copolymers (red dots) with random CL and TMC-Bz sequence. Predicted $T_g$'s (black dots) were calculated based on FOX equation in which $T_g$ of –60 °C for high molecular weight $PCL_{80}$ [2] and $T_g$ of –12 °C for P(TMC-Bz) (obtained from P(TMC-$Bz_{8.6}$)-PEG, Entry 3, table 1) were used as the reference for the prediction. The numbers of the polymers on the x-axis correspond to the same entries in table 1.

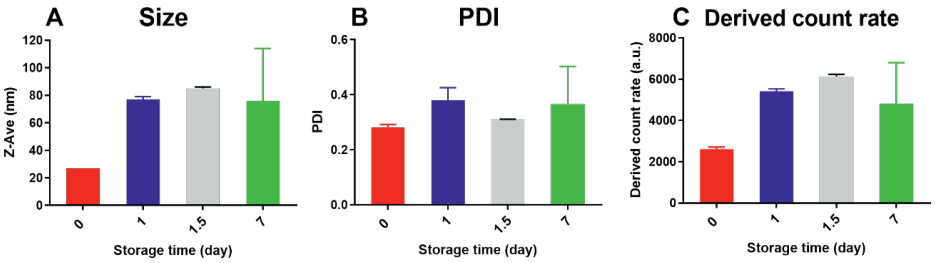


**Figure S9.** Size (A), PDI (B) and derived count rate (C) of $PCL_9$-PEG micelles in PBS after storage at room temperature over a period of 7 days.

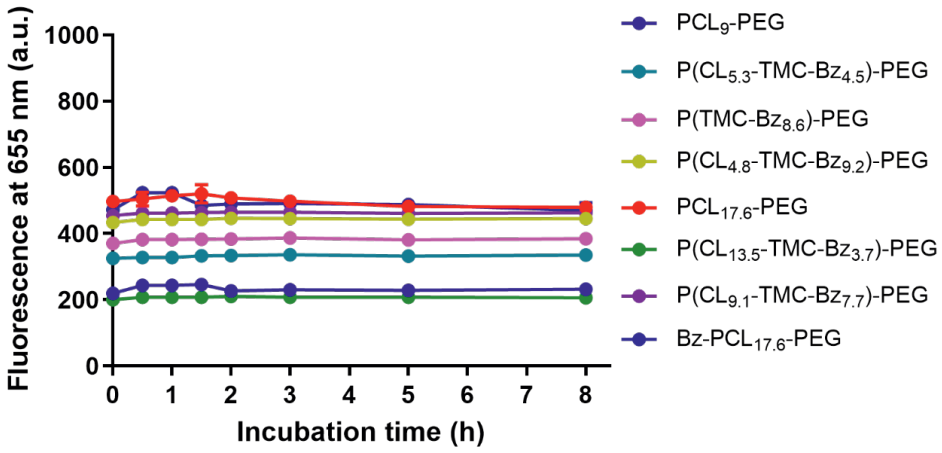


**Figure S10.** Fluorescence intensity ($\lambda_{ex}$ 420 nm, $\lambda_{em}$ 655 nm) as a function of time at 37 °C in PBS; micelles of 10 mg/mL with 5 wt% loading amounts were prepared and diluted 10× in PBS, to obtain the final mTHPC concentration of 40 mg/mL.

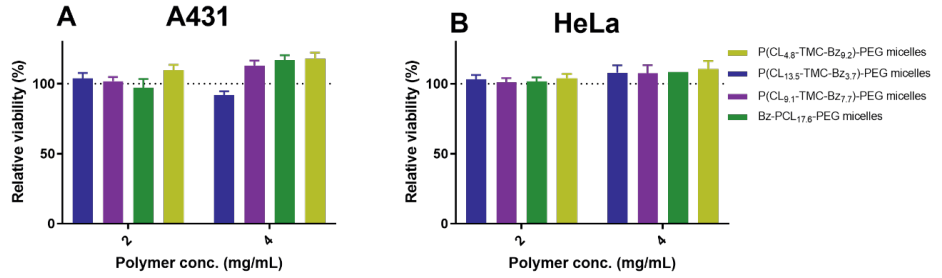


**Figure S11.** Cytotoxicity by MTS assay of different empty micelles composed of 2 and 4 mg/mL polymer on A431 and HeLa cells after 24 h incubation (n = 3).

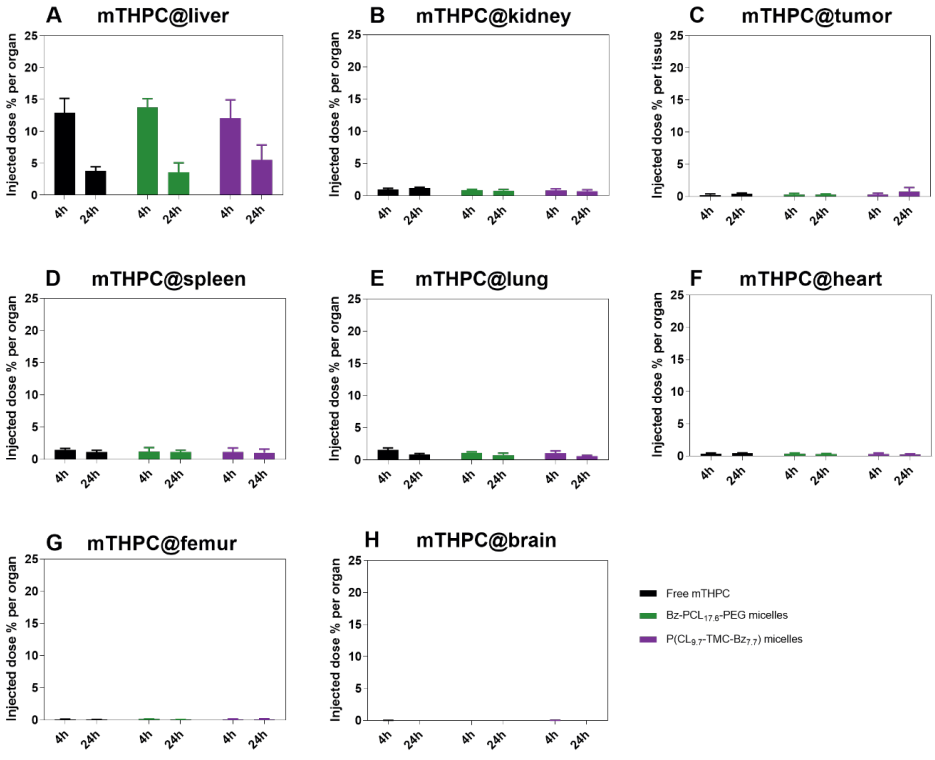


**Figure S12.** Biodistribution of free mTHPC and mTHPC loaded in micelles in tumor and main organs of mice after 4 and 24 h administration of the formulations at a mTHPC dose of 0.3 mg/kg. Data are indicated as the percentage of the injected mTHPC (%ID) present per organ/tumor (n = 3-5).

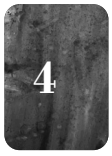
4

# 5

# Chapter 5

## Dithiolane Crosslinked Poly(ε-caprolactone)-based Micelles: Impact of Monomer Sequence, Nature of Monomer and Reducing Agent on the Dynamic Crosslinking Properties

Yanna Liu [1], Mies J. van Steenbergen [1], Sabrina Oliveira [1,2], Wim E. Hennink [1], and Cornelus F. van Nostrum [1]

[1] Department of Pharmaceutics, Utrecht Institute for Pharmaceutical Sciences, Utrecht University, Universiteitsweg 99, 3508 TB Utrecht, the Netherlands
[2] Division of Cell Biology, Neurobiology and Biophysics, Department of Biology, Utrecht University, Padualaan 8, 3584 CH Utrecht, the Netherlands.

*Macromolecules 2020, 53 (16), 7009–7024*

**Abstract**

Dithiolanes are interesting moieties to obtain dynamic and reversible crosslinks between polymer chains. To synthesize copolymers of two different dithiolane-containing cyclic carbonate monomers and ε-caprolactone (CL), ring-opening polymerization (ROP) was used by mPEG as initiator and acidic diphenyl-phosphate (DPP), methanesulfonic-acid (MSA), alkaline 1,5,7-triazabicyclo[4.4.0]dec-5-ene (TBD) or metallic $Sn(Oct)_2$ as catalysts. The ROP was conducted in dichloromethane at 37 °C with DPP and MSA as catalyst, at room temperature using TBD as catalyst, and in toluene at 110 °C using $Sn(Oct)_2$ as catalyst. The type of catalyst was shown to have a pronounced influence on the different monomer reactivities and occurrence of transesterification reactions, and therefore, the monomer sequence. Interestingly, it was demonstrated that self-crosslinkable copolymers were obtained with the dithiolane units connected closely to the polymer backbone, whereas the presence of a linker unit between the dithiolane and the backbone prevented self-crosslinking. The obtained amphiphilic PEGylated block copolymers formed micelles by nanoprecipitation in aqueous environment and crosslinked spontaneously by disulfide-exchange during subsequent dialysis, independent of the monomer sequence, comonomer ratio, or the presence of reducing agents. The dithiolane crosslinked micelles showed reduction-responsive dissociation in the presence of 10 mM glutathione, making them promising drug delivery systems for intracellularly triggered cargo release.

## 1. Introduction

Ring-opening polymerization (ROP) of cyclic esters and/or carbonates has attracted interest for many years, since the resulting polymers *i.e.,* polyesters, polycarbonates and poly(ester-*co*-carbonate)s are biodegradable and biocompatible and as such are particularly appealing for pharmaceutical and biomedical applications, *e.g.,* nanoparticulate drug carriers and tissue engineering.[1-5] ROP of cyclic esters and/or carbonates has been extensively studied using various types of catalysts, *e.g.,* basic organo-catalysts like 1,5,7-triazabicyclo[4.4.0]dec-5-ene (TBD), acid organo-catalysts like sulfonic acids, and metallic catalysts like $Sn(Oct)_2$. Catalysis mechanisms are greatly different, *e.g.,* bifunctional activation mechanism by TBD *vs* coordination–insertion by a metallic catalyst.[6-8] These different mechanisms might lead to different polymerization behavior of monomers, thus yielding copolymers with different structural parameters *e.g.,* composition, microstructure (*i.e.*, the monomer sequence) and polydispersity, which are important factors that determine the properties of polymers, and thus their applications.[9-13] For instance, it has been demonstrated that an acidic organocatalyst, diphenyl phosphate (DPP), and a basic organocatalyst, TBD, have different ring-opening copolymerization behaviors of cyclic carbonate based monomers, leading to copolymers with random and blocky microstructures, respectively.[13] In this regard, understanding the role of the catalyst in the kinetics of polymerization becomes important, since it offers an important opportunity to satisfy different applications by preparing polymers with different molecular features (monomer sequence, predictable molar masses, narrow molecular weight distribution, etc.) via catalytic tuning.

Polymeric micelles prepared from biodegradable (co)polymers have received extensive interest as delivery systems for *e.g.,* anti-cancer drugs, owing to advantageous features such as improved aqueous solubility of encapsulated hydrophobic drugs, selective accumulation at the tumor sites via enhanced permeability and retention (EPR) effects,[14-18] and decreased systemic side effects.[16,19,20] However, although polymeric micelles are promising nanocarriers, they are still challenged by their instability in the circulation, which often lead to premature drug release, diminished ability to selectively reach target sites, and suboptimal therapeutic efficacy.[16,21-23] To address these drawbacks, reversible crosslinking of polymeric micelles particularly using reduction-sensitive disulfide linkages is a highly attractive approach, enabling stability in the circulation and trigger drug release by decrosslinking at the target site, *i.e.,* the cytoplasm or the cell nucleus in tumor cells.[18,24-26] This was shown in the pioneering work by Regen *et al.*, who demonstrated the use of cyclic 1,2-dithiolanes to crosslink and thus stabilize liposomes.[27] Dithiolane crosslinked nanoparticles based on lipoic acid were later shown to display enhanced stability under physiological conditions and triggered intracellular drug release after being de-crosslinked in the cytoplasm of cancer cells.[28] Recently, a series of tumor-targeted core crosslinked micelles and

polymersomes based on pendant dithiolanes has shown efficient delivery of doxorubicin and siRNA to tumor xenografts in nude mice.[29-36] Similar chemistry has also been used to generate dynamically crosslinked hydrogels.[37] The necessary conditions and mechanism to generate dithiolanes-derived crosslinking in nanoparticles have been described in several publications. Some studies showed that crosslinking of dithiolanes in nanoparticles requires a reducing agent (RA) (*e.g.,* DTT; typically 10 to 50 mol% RA to disulfide bonds) that induces the disulfide-exchange ring opening polymerization of cyclic dithiolanes initiated by sulfhydryl (-SH) groups.[27,28,37-42] On the other hand, in other studies it has been described that dithiolane crosslinked nanoparticles are formed spontaneously when these dithiolane containing polymers are dispersed in water (*i.e.,* without the need of free thiol as the initiator).[29-32,43] However, no existing study provides a comprehensive and detailed exploration of the dithiolane crosslinked network in nanoparticles or potentially influential factors (*e.g.,* polymer structure, the presence of reducing agents and concentrations).

In the present paper, we introduce pendant dithiolane rings as crosslinkable moieties in poly(ε-caprolactone)-*b*-poly(ethylene glycol) (pCL-PEG) block copolymers by ring-opening copolymerization of ε-caprolactone (CL, a cyclic ester) with a dithiolane-substituted cyclic carbonate with or without a flexible diester linker between the dithiolane ring and the cyclic carbonate unit (*i.e.*, 1,2-dithiolane-substituted trimethylene carbonate (DTC) and 1,2-dithiolane-4-diester functionalized trimethylene carbonate (DdeTC), respectively) (**Figure 1**). Both monomers have been described before as crosslinkable units in polycarbonates and poly(ester carbonate)s.[29,31,32,37,42] Since, as explained above, different catalysts might yield copolymers with different monomer sequences, and thus likely different crosslinking behavior, the influence of the selected catalyst on (co)polymerization behavior of CL and carbonate monomers was evaluated. Therefore, three different types of catalysts, *i.e.,* acidic (DPP or methanesulfonic acid (MSA)), basic (TBD) or metallic ($Sn(Oct)_2$) were used as catalysts in the ROP of CL and DTC using PEG-OH (2 kDa) as initiator, and the polymerization kinetics and the monomer sequence of the obtained block copolymers were studied by $^{1}H$- and $^{13}C$-NMR analysis. Subsequently, micelles based on the obtained p(CL-*co*-DTC)-PEG and p(CL-*co*-DdeTC)-PEG were prepared using a nanoprecipitation method. The rate and extent of crosslinking of these micelles in the presence and absence of different reducing agents, namely (tris(2-carboxyethyl)phosphine hydrochloride (TCEP), dithiothreitol (DTT) and glutathione (GSH)), were investigated by *in-situ* monitoring of the UV absorbance over time of the dithiolane pendant rings. Moreover, the reversibility of the crosslinking and the reductive response of the dithiolane crosslinked p(CL-*co*-DTC)-PEG micelles in the presence of TCEP or GSH were evaluated to gain insight into the aimed behavior of the micelles in tumor cells, *i.e.,* intracellular drug release.

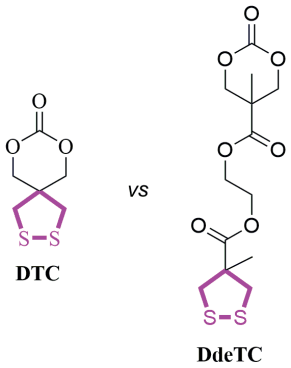


**Figure 1.** Structures of the 1,2-dithiolane- and 1,2-dithiolane-4-diester-substituted trimethylene carbonate (*i.e.,* DTC and DdeTC).

## 2. Experimental section

### *2.1 Materials*

2-((4-Methyl-1,2-dithiolane-4-carbonyl)oxy)ethyl-5-methyl-2-oxo-1,3-dioxane-5-carboxylate (*i.e.,* 1,2-dithiolane-4-diester functionalized trimethylene carbonate, DdeTC) was synthesized as previously described (Scheme S1; $^{1}H/^{13}C$-NMR spectra in Figure S17 and S18 in supporting information).[37,42,44] 7,9-Dioxa-2,3-dithiaspiro[4.5]decan-8-one (*i.e.,* 1,2-dithiolane-substituted trimethylene carbonate, DTC) was kindly provided by prof. Zhiyuan Zhong (Soochow University, Suzhou, China). ε-Caprolactone (CL), methoxy-poly(ethylene glycol) (mPEG-OH, 2000 g/mol), tin (II) 2-ethylhexanoate ($Sn(Oct)_2$), diphenyl phosphate (DPP, 99%), methanesulfonic acid (MSA, ≥99.0%), 1,5,7-triazabicyclo[4.4.0]dec-5-ene (TBD, 98%), tris(2-carboxyethyl)phosphine hydrochloride (TCEP), 1,4-dithiothreitol (DTT, ≥99%), L-glutathione (GSH, ≥98%), and triethylamine (TEA) were obtained from Sigma-Aldrich (Zwijndrecht, the Netherlands). Phosphate-buffered saline (PBS, pH 7.4, containing 11.9 mM phosphates, 137 mM sodium chloride and 2.7 mM potassium chloride) was obtained from Fischer Bioreagents (Bleiswijk, the Netherlands). Standard regenerated cellulose dialysis tubing (Spectra/Por®6) with molecular weight cutoff (MWCO) of 1 kDa was purchased from Spectrumlabs (Rancho Dominguez, Califonia, USA). Ellman's Reagent (5,5-dithio-bis-(2-nitrobenzoic acid) was purchased from Fisher Scientific (Loughborough, UK). All other solvents and reagents were obtained from Biosolve (Valkenswaard, the Netherlands). mPEG-OH was azeotropically dried from toluene prior to use. Dichloromethane (DCM, peptide synthesis grade) and toluene were dried over 4Â molecular sieves (Sigma-Aldrich, Zwijndrecht, the Netherlands) prior to use. All other reagents were used as received.

*2.2 Synthesis of (co)polymers*

*2.2.1 Simultaneous ring opening (co)polymerization*

*2.2.1.1 Copolymerization of CL and DTC catalyzed by DPP, MSA or TBD*

The copolymerization of CL and DTC was initiated by mPEG–OH (2000 g/mol) and catalyzed by different agents (DPP, MSA or TBD). A representative procedure for the synthesis of p(CL-*co*-DTC)-PEG (**Entry 2**, table 1) catalyzed by MSA was carried out as previously described with slight modifications. [9,45] CL (410 mg, 3.6 mmol), DTC (308 mg, 1.6 mmol) and mPEG-OH (800 mg, 0.4 mmol) were dissolved in 6 mL dry DCM, followed by addition of MSA (50 mg, 0.52 mmol) (CL/DTC/mPEG-OH/MSA molar ratio: 9/4/1/1.3) with agitation to initiate polymerization. The polymerization proceeded at 37 ℃ for 10 h under $N_2$ atmosphere and then TEA (0.52 mmol, equimolar to MSA) was added to neutralize the catalyst and terminate the reaction. The reaction solution was subsequently dropped into a 20-fold excess of cold diethyl ether (-20 °C) and the precipitate, collected by filtration, was dried under vacuum to give the final product (**Entry 2** in table 1) as slightly yellow solid (1100 mg, yield: 71%).

The copolymerization of CL and DTC using DPP or TBD as catalyst followed a similar procedure with slight modifications: molar ratios of CL/DTC/mPEG-OH/DPP and CL/DTC/mPEG-OH/TBD were adjusted to 9/4/1/10 [13] and 9/4/1/0.25 [46], respectively. The applied reaction times are shown in table 1 and when TBD was used as catalyst, the reaction was carried out at room temperature (RT) and the termination reagent was replaced by benzoic acid. The yields for the polymerizations catalyzed by DPP and TBD were 70 and 55%, respectively.

As references, pCL-PEG (**Entries 7** and **11**, table 1) and pDTC-PEG block copolymers (**Entries 8** and **12**, table 1) were synthesized using MSA or TBD as catalysts under the same conditions, by polymerization of only CL or DTC, respectively. The polymers were precipitated in cold diethyl ether (-20 °C) to obtain the pCL-PEG block copolymer as white powder (yield: ~60% in both cases) and the pDTC-PEG block copolymer as yellowish solid (yield: ~65% in both cases).

*2.2.1.2 Copolymerization of CL and DTC catalyzed by $Sn(Oct)_2$*

CL (205 mg, 1.8 mmol), DTC (154 mg, 0.8 mmol) and mPEG-OH (400 mg, 0.2 mmol) were dissolved in 3 mL dry toluene. Then, a catalytic amount of $Sn(Oct)_2$ (1 mg, 0.01 mmol) (CL/DTC/mPEG-OH/ $Sn(Oct)_2$ molar ratio: 9/4/1/0.05) was added and the reaction was allowed to proceed at 110 °C for 19 h under $N_2$ atmosphere. Subsequently, the cooled reaction solution was dropped into a 20-fold excess of cold diethyl ether (-20 °C). The precipitate was recovered by filtration and dried under vacuum to give the final product (**Entry 4** in table 1) as slightly yellow solid (500 mg, yield: 63%).

*2.2.1.3 (Co)polymerization of CL and DdeTC catalyzed by MSA*

DdeTC without or with CL was (co)polymerized using mPEG-OH as the initiator and MSA as the catalyst (the molar ratios of DdeTC/mPEG-OH/MSA and DdeTC/CL/mPEG-OH/MSA were 8/1/1.3 and 4/9/1/1.3, respectively), following a similar procedure as described in 2.2.1.1 except that DTC was substituted by DdeTC. The obtained polymer was precipitated in cold diethyl ether (-20 °C). After drying under vacuum, p(CL-*co*-DdeTC)-PEG (**Entry 15**, table 1) was obtained as slightly yellow solid (700 mg, yield: 55%) and pDdeTC-PEG block copolymer (**Entry 16**, table 1) as yellowish solid (500 mg, yield: 45%).

*2.2.2 Sequential ring opening (co)polymerization*

*2.2.2.1 Polymerization with sequential feeding of DTC first followed by CL*

Sequential copolymerization of DTC first and then CL using MSA as the catalyst (**Entry 5**, table 1) was carried out as follows: to the solution of DTC (154 mg, 8 mmol) and mPEG-OH (400 mg, 0.2 mmol) in 3 mL DCM, MSA (25 mg, 0.26 mmol) was added with agitation. After stirring for 18 h at 37 °C under $N_2$ atmosphere, CL (201 mg, 1.8 mmol) was introduced into the reaction mixture. The reaction continued at 37 °C under $N_2$ atmosphere for 2 h and was then terminated by addition of TEA (equal molar to MSA). The final molar ratio of CL/DTC/mPEG-OH/MSA was 9/4/1/1.3. Next, the reaction solution was dropped into a 20-fold excess of cold diethyl ether (-20 °C) and the precipitate was collected by filtration and dried under vacuum overnight to give the final product as yellowish solid (500 mg, yield: 66%).

The copolymerization with sequential feeding of DTC first followed by CL and catalyzed by TBD was conducted at RT following a procedure similar to the above mentioned, with a slight adjustment of reaction times as shown in table 1 (**Entry 9**) and the molar feed ratio of CL/DTC/mPEG-OH/TBD (9/4/1/0.25). The polymer was precipitated in cold diethyl ether (-20 °C) and the yield was ~65%.

*2.2.2.2 Polymerization with sequential feeding of CL first followed by DTC*

Sequential copolymerization of CL, followed by DTC using MSA or TBD as the catalyst was conducted following a similar procedure as mentioned in section 2.2.2.1, but with a slight modification of the polymerization times as shown in table 1 (**Entries 6** and **10**). The copolymers were precipitated in cold diethyl ether (-20 °C) and the final copolymers (**Entries 6** and **10**, table 1) were obtained as yellowish and slightly sticky solids (yield: ~60% for both cases).

*2.3 Polymerization kinetics*

Polymerization kinetics were determined as follows: 20 μL samples of the reaction solutions during polymer synthesis (as described in section 2.2.1) were withdrawn at different time points using a syringe and transferred into a NMR tube containing 0.8

mL $CDCl_3$ and an excess amount of the corresponding compound that was used to terminate the reaction (see section 2.2.1.1) and the $^1$H-NMR spectrum was subsequently recorded. The conversion of CL, DTC or DdeTC was determined by respectively comparing the integrals of the peaks at 2.66 ppm (two protons of methylene from CL), 3.07 ppm (four protons of dithiolane ring from DTC unit) or 4.70 ppm (two protons of trimethylene carbonate from DdeTC monomer) at each time point to its corresponding integral at the start of the experiment. The peak originating from the three methoxy protons of mPEG-OH at 3.37 ppm was used as the reference peak to normalize the integrals. Total polymerization times reported in table 1 were established by the time that the plateau conversions were reached based on $^1$H-NMR analysis.

*2.4 Polymer characterization*

$^1$H/$^{13}$C-NMR spectra were recorded using a Bruker NMR spectrometer (600 MHz, Bruker), with chemical shifts reported in parts per million downfield from tetramethylsilane. Polymers were dissolved in $CDCl_3$ at concentrations of approximately 15 mg/mL. Chemical shifts of residual solvent ($CHCl_3$: δ 7.26 and 77 for proton and carbon spectrum, respectively) were used as the reference lines. Peak multiplicity is denoted as s (singlet), d (doublet), dd (double doublet), t (triplet), q (quartet), m (multiplet), and b (broad signal). Based on $^1$H-NMR spectra, the average degree of polymerization (DP) of CL, DTC or DdeTC in the obtained copolymers was determined from the ratio of the integrals of the $CH_2$ protons of the CL units (1.39 ppm, $CH_2CH_2\underline{\boldsymbol{CH_2}}CH_2CH_2$), the protons of the DTC units (2.97 ppm, $C\underline{\boldsymbol{CH_2}}SS\underline{\boldsymbol{CH_2}}C$) or the DdeTC units (2.92 ppm, $C\underline{\boldsymbol{CH_2}}SS\underline{\boldsymbol{CH_2}}C$) to the methyl protons of mPEG-OH (3.37 ppm, $\underline{\boldsymbol{CH_3}}O$) (equations (1)-(3)), respectively. The number average molecular weight ($M_n$) of the polymers was thus calculated from the resulting DP of CL, DTC and DdeTC units.

$$\text{Equation (1): DP of CL} = \frac{\text{Integral (H at 1.39 ppm)}/2}{\text{Integral (H at 3.37 ppm)}/3}$$

$$\text{Equation (2): DP of DTC} = \frac{\text{Integral (H at 2.97 ppm)}/4}{\text{Integral (H at 3.37 ppm)}/3}$$

$$\text{Equation (3): DP of DdeTC} = \frac{\text{Integral (H at 2.92 ppm)}/2}{\text{Integral (H at 3.37 ppm)}/3}$$

Gel permeation chromatography (GPC, Waters Alliance 2695 System equipped with two PLgel Mesopore columns (300x7.5 mm, including a guard column, 50x7.5 mm)), was performed using dimethylformamide (DMF) containing 10 mM LiCl as solvent at a flow rate of 1.0 mL/min at 65 °C. A differential refractive-index (RI) detector was used to record the chromatograms. Fifty μL of 3-5 mg/mL samples dissolved in DMF containing 10 mM LiCl were injected onto the column. The number average molecular weight ($M_n$), weight average molecular weight ($M_w$) and the molecular weight

distribution ($M_w/M_n$) of the obtained copolymers were calculated by Empower 32 software using narrow poly(ethylene glycol) standards ranging from 430 to 26,100 g/mol (from PSS, Mainz, Germany) for calibration.
Differential scanning calorimetry (DSC) was carried out using a Discovery DSC, TA Instruments, calibrated with indium. Samples (~5 mg) were heated with a ramp of 3 °C/min up to 150 °C (modulated), annealed for 5 min, cooled down at 3 °C/min to –80 °C (modulated), again annealed for 5 min and subsequently heated with 3 °C/min up to 150 °C (modulated). Melting temperatures ($T_m$) were obtained from the onset of the peaks of the total heat flow and the melting enthalpies ($\Delta H_m$) were recorded from the total heat flow. Glass transition temperatures ($T_g$) are defined as the point of inflection of the step change observed in the reversing heat flow curve. Data of the second heating cycle were recorded.

*2.5 Influence of different reducing agents on dynamic crosslinking of micelles*
Micellar dispersions were prepared from the obtained block copolymers by a nanoprecipitation method.[47] In short, a solution of the copolymer in DMF (40 mg/mL of p(CL-*co*-DTC)-PEG or 100 mg/mL of p(CL-*co*-DdeTC)-PEG) was added dropwise to PBS at 1/9 volume ratio. A homogenous micellar dispersion was formed after gentle shaking by hands. Various reducing agents (RA, *i.e.,* DTT, TCEP or GSH, as solutions in PBS), at molar ratios of RA to the dithiolane rings present in the micellar dispersion ranging from 0 to 2, were added to the micellar dispersion, followed by adjusting to the same volume by the addition of a certain volume of PBS. After incubation with RA at 37 °C for 7 h, the different micellar dispersions were dialyzed with a dialysis tubing (MWCO =1 kDa) against PBS at RT for 12 h.[31] The absorbance of the dithiolane rings in DTC and DdeTC units at λ = 326 and 328 nm, respectively, was recorded from the micellar samples withdrawn at different time points before and after dialysis using a Shimadzu UV-2450 spectrophotometer (Shimadzu, Japan). In addition, samples collected from the above mentioned micellar dispersions were freeze-dried and subsequently re-dispersed in DMF at 5 mg/mL for GPC analysis as described in section 2.4. Ellman's assay was performed according to the manufacturer's protocol to quantify the concentration of sulfhydryl (-SH) groups present in the micellar dispersions before and after dialysis.

*2.6 Decrosslinking of micelles by reducing agents*
The response of the dithiolane core-crosslinked micelles towards various reducing agents was determined by DLS and GPC analysis. Briefly, spontaneously crosslinked micelles were prepared by the nanoprecipitation method (without exposure to RA), *i.e.,* by dropwise addition of the polymer solution in DMF to PBS (pH 7.4) at a volume ratio of 1:9 followed by dialysis against PBS for 12 h, as described in section 2.5. The micelles were subsequently incubated either with 2 equiv. of TCEP (a 30 mg/mL solution in

PBS) relative to dithiolanes or with PBS (the same volume as TCEP solution) for 2 h at 37 °C . Thereafter, DMF or PBS was added at a volume ratio of 1:4 at RT for 24 h. The Z-average hydrodynamic diameter ($Z_{ave}$) and polydispersity index (PDI) of the micelles before and after addition of DMF or PBS were determined by DLS at a fixed scattering angle of 173 ° at 25 °C using a ZetaSizer Nano S (Malvern).
Besides, the spontaneously crosslinked micellar dispersions were incubated respectively with TCEP, DTT or GSH dissolved in PBS (final concentration of 10 mM) for 7 h at 37 °C . Next, the micellar dispersions were freeze-dried and then dispersed in DMF at 5 mg/mL, followed by filtration (0.22 μm) for GPC analysis as described in section 2.4.

*2.7 Reversibility of the crosslinking in micelles*

To investigate the reversibility of the dithiolane crosslinking, the micelles crosslinked by TCEP and subsequently dialyzed as described in section 2.5 were aged for 96 h at RT (referred to as the 1st cycle). The resulting crosslinked micelles were incubated with TCEP, using molar ratios to the dithiolanes ranging from 0 to 2 for 7 h at 37 °C, dialyzed against PBS for 12 h and after dialysis in PBS aged for the indicated time points at RT (referred to as the 2nd cycle). In addition, samples collected from the micellar dispersions were freeze-dried and then dissolved in DMF at 5 mg/mL. The samples were filtered (0.22 μm) and then analyzed by GPC analysis as described in section 2.4.

## 3. Results and Discussion

*3.1 Effect of catalyst on the monomer sequence in the copolymers*

*3.1.1 Copolymers synthesized by simultaneous ring opening copolymerization of CL with DTC or DdeTC*

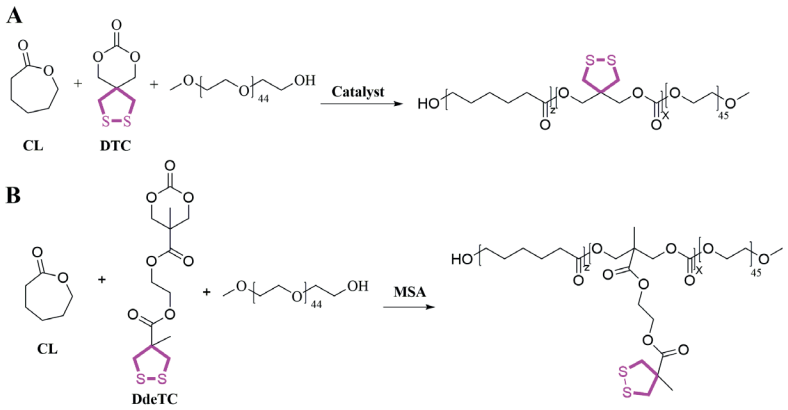


**Scheme 1.** Ring opening polymerization of CL with two different dithiolane based monomers initiated by mPEG-OH: simultaneous copolymerization with (A) DTC and (B) DdeTC.

Simultaneous ROP of CL and DTC initiated by the macroinitiator mPEG-OH at a CL/DTC/PEG molar ratio of 9/4/1 (**Scheme 1A**) was carried out using different catalysts, *i.e.,* acidic (DPP or MSA), basic (TBD) or metallic ($Sn(Oct)_2$) catalysts, to investigate the effect of the type of catalyst on the monomer sequence in the obtained copolymers (structures of these catalysts are shown in **Figure S1** of supporting information). To this end, the conversion of each monomer was measured by $^1$H-NMR analysis, and the relative reactivities of both monomers were determined by monitoring the decrease of peak integrals of methylene of CL at 2.66 ppm and the dithiolane ring in DTC at 3.07 ppm. **Figures 2A** and **B** clearly show that 1.3 equivalents of MSA relative to the initiator (PEG) displayed higher catalytic activity than 10 equivalents of DPP (almost complete conversions of both monomers in 7 h *vs* 28 h, despite the larger molar excess of the latter catalyst). As reported in the literature, acid (DPP or MSA) catalyzed ROP proceeds via a bifunctional activation mechanism, *i.e.,* these catalysts act simultaneously both as a hydrogen-bond donor to the carbonyl oxygen in the monomers and as a hydrogen-bond acceptor to the hydroxyl proton of the propagating alcohol, achieving activation of both the electrophile and the nucleophile (**Scheme S2A** and **S2B** in supporting information).[48,49] Therefore, the difference in reactivity of the two catalysts can be ascribed to the higher acidity of the hydrogen atom (H-bonding donor) in MSA (pKa = -0.6)[50] than that in DPP (pKa = 2),[48] resulting in a higher electrophilic activity and shortening of the polymerization time. Importantly, CL and DTC displayed similar polymerization rates for both acidic catalysts (**Figure 2A** and **B**), suggesting random incorporation of both monomers in the propagating chains. The kinetics of DPP-catalyzed copolymerization is in line with the findings reported by Wei *et al.*, who showed that similar polymerization rates of DTC and another carbonate based monomer (*i.e.,* trimethylene carbonate, TMC) indeed led to a random pDTC/pTMC copolymer.[13] It is noted that under MSA catalysis, polymerization kinetics of CL and DdeTC (**Figure S2**, supporting information) were also similar and comparable to that observed with CL and DTC (**Figure 2B**), suggesting DTC and DdeTC have comparable reactivity. However, using MSA as the catalyst, Couffin et al. reported higher reactivity of CL than that of TMC [9], which may indicate that the reactivity of the cyclic carbonate is influenced by the substituents. The comparable reactivity of cyclic ester CL and cyclic carbonates (DTC or DdeTC) under acidic catalysis is probably attributed to electrophilic activation of both monomers, thereby minimizing possible charge density differences on the carbonyl C-atom caused by their intrinsic structures.

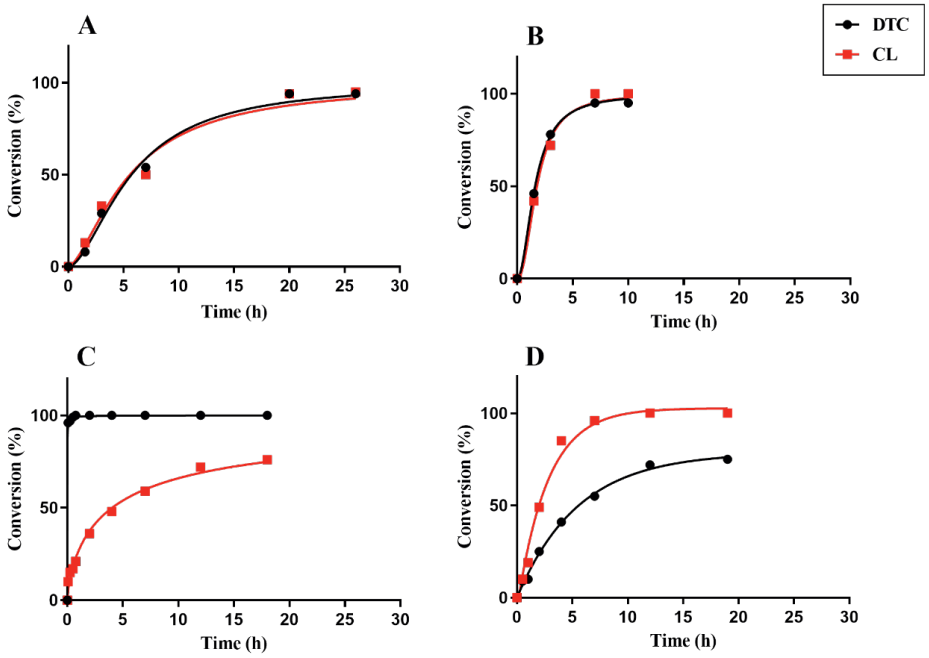


**Figure 2.** Conversion of CL (red squares) and DTC (black dots) monitored by $^{1}$H-NMR as a function of time using (A) DPP, (B) MSA, (C) TBD and (D) $Sn(Oct)_2$ as the catalyst, respectively, with CL/DTC/initiator molar ratio of 9/4/1 (**Entries 1-4**, table 1). The ROP reaction was conducted in DCM at 37 °C using DPP and MSA as the catalyst, in DCM at RT using TBD as the catalyst, and in toluene at 110 °C using $Sn(Oct)_2$ as the catalyst.

In contrast to the acid catalyzed ROP, CL had a significantly lower polymerization rate than DTC when basic TBD was used as the catalyst: CL needed 18 h to achieve 76% conversion, whereas DTC was quantitatively consumed within 30 min (**Figure 2C**). These large differences in reactivity lead to preferential DTC incorporation at the start of the polymerization reaction, which in turn results in a block copolymer structure of the hydrophobic polyester/carbonate segment if no transesterification and chain termination occurred. In a previous study, when DTC was copolymerized with TMC, DTC had also significantly higher reactivity than the comonomer using TBD as the catalyst, indeed yielding a blocky copolymer.[13] From a mechanistic point of view, TBD catalyzed ROP most likely also proceeds via a bifunctional activation mechanism as mentioned above for acidic catalysis (**Scheme S2A-C** in supporting information).[51] However, the obvious difference between acidic and basic catalysts is that in the latter case, the monomers are activated by the nucleophilic attack of the amine nitrogen in TBD to the carbonyl of the monomers along with transfer of the adjacent protonated nitrogen to the oxygen in monomers (*i.e.,* the incipient alkoxide) to generate the TBD amide (as shown in **Scheme S2C** of supporting information). Thus, the different

reactivities of DTC and CL can probably be explained by the more active intermediate TBD-amide formed from cyclic carbonate (DTC) than the one formed from the cyclic ester (CL), due to the presence of the extra oxygen atom as an electron withdrawing group on the β-position, facilitating esterification with the hydrogen-bond activated alcohol (final step in **Scheme S2C** of supporting information). On the contrary, in metallic $Sn(Oct)_2$ catalyzed ROP (**Figure 2D**), CL reacted slightly faster than DTC (96% *vs* 55% conversion for CL and DTC, respectively, after 7 h), which is consistent with a previous observation on the $Sn(Oct)_2$ catalyzed random copolymerization of CL and TMC at 120 ℃.[52] This suggests the possible formation of a gradient copolymer, whose monomer composition varies gradually along the growing polymer chain, *i.e.*, in this case, CL may be enriched in the polymer segment initially formed and then due to change of the relative monomers' concentration, incorporation of DTC gradually increases and prevails in the copolymer chain formed after longer reaction times, assuming that no termination and transesterification occur.[10,53] The ROP catalyzed by $Sn(Oct)_2$ operates by a "coordination-insertion" mechanism, consisting of initiating an alcohol by an "in-situ" formed stannous alkoxide with $Sn(Oct)_2$ and propagating the polymer chain by monomer insertion into the $-S_n-O-$ bond (**Scheme S2D** in supporting information).[54] With this "coordination-insertion" mechanism, the driving force for the polymerization of CL is most likely the favorable release of torsional strain in a 7-membered CL ring.[55]

As shown in **Table 1** (Entries 1-4), the compositions of the copolymers as determined by $^1$H-NMR correspond well with those expected from the ratios of the monomer feed. The apparent $M_n$ of the polymers obtained from GPC using PEG calibration, as reported in **Table 1**, was lower than $M_n$ calculated from $^1$H-NMR, which is most likely attributed to the more hydrophilic and molecularly swollen PEG-OH used for GPC calibration than the obtained copolymers. Copolymers obtained by DPP, MSA and $Sn(Oct)_2$ catalysis (**Entries 1**, **2** and **4**, table 1) displayed highly similar monomodal GPC curves with narrow molar mass distributions ($M_w/M_n < 1.2$) (**Figure 3**, purple, cyan and red lines), suggesting the cross-propagation of both monomers and the absence of side reactions such as transesterification.[9,12,56,57] However, for the copolymer synthesized using TBD as the catalyst (**Entry 3**, table 1), the GPC curve (**Figure 3**, green line) showed a broad and bimodal molecular weight distribution. Such a bimodal distribution was previously also observed by TBD catalyzed polymerization of a cyclic phosphoester monomer using benzyl alcohol as an initiator.[58] In our case, the broad distribution is most likely caused by transesterification while the bimodal distribution might be explained by the large difference in monomer reactivity, leading to inability of homogeneous cross-propagation of both monomers and thus resulting in a highly multi-disperse (heterogeneous) composition of the obtained polymer chains.

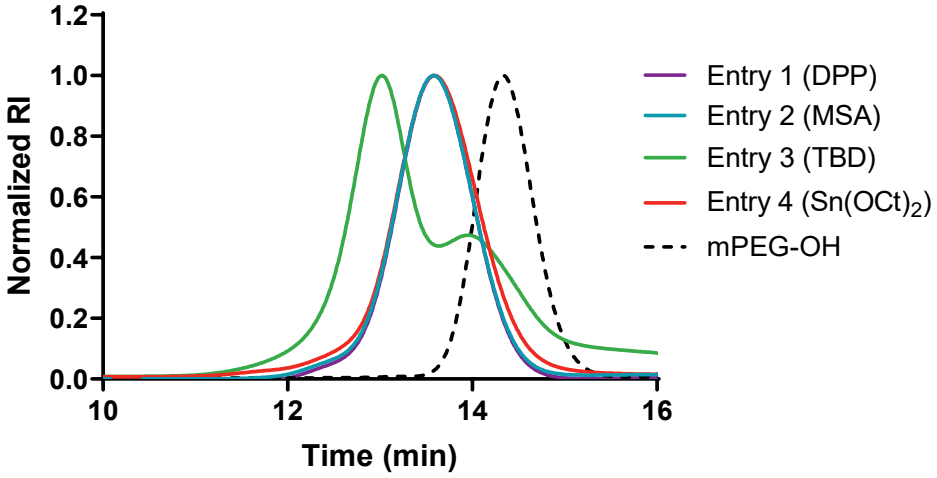


**Figure 3.** GPC curves of p(CL-*co*-DTC)-PEG block copolymers obtained by simultaneous copolymerization of CL and DTC at a CL/DTC/mPEG-OH feed molar ratio of 9/4/1 using different catalyst: DPP (Entry 1), MSA (Entry 2), TBD (Entry 3) and $Sn(Oct)_2$ (Entry 4), respectively. All the entries presented in the legend correspond to the ones of table 1. mPEG-OH (2 kDa) was used as a reference.

Considering the advantages of MSA-catalyzed ROP in terms of high reaction rate, the lack of residual metal contaminants, mild polymerization conditions and minimized transesterifications as compared to the other three catalysts, this catalyst was selected for synthesizing p(CL-*co*-DTC)-PEG block copolymers with different compositions (CL with DTC at molar ratios of 9/8 and 18/8). Besides, MSA was used for preparation of a p(CL-*co*-DdeTC)-PEG block copolymer, *i.e.,* by simultaneous copolymerization of CL with DdeTC at a molar ratio of 9/4 (**Scheme 1B)**. As shown in **Table 1 (Entries 13-15**), p(CL-*co*-DTC)-PEG and p(CL-*co*-DdeTC)-PEG block copolymers were successfully synthesized with high conversion of both monomers and $M_n$'s in close proximity with expected values (as indicated by $^1$H-NMR analysis in table 1). GPC analysis shows that these copolymers (**Entries 13-15**, table 1**)** had narrow molecular weight distributions ($M_w/M_n$ < 1.2), which is comparable to p($CL_9$-$DTC_{3.9}$)-PEG synthesized at CL/DTC molar ratio of 9/4 (**Entry 2**, table 1**)**, suggesting the absence of the transesterification and termination side reactions, regardless of feed ratios of the two monomers and the substituent structure of dithiolanes present in cyclic carbonate based monomer.

pCL-PEG, pDTC-PEG and pDdeTC-PEG block copolymers (**Entries 7**, **8** and **16**, table 1) synthesized by MSA-catalyzed homo-polymerization of CL, DTC or DdeTC initiated by mPEG-OH, displayed narrow molecular weight distributions based on GPC analysis as well ($M_w/M_n$ < 1.1). $M_n$ values according to $^1$H-NMR analysis were all as expected from the monomer/initiator feeds, except for pDdeTC-PEG whose lower $M_n$ relative to the aimed can be explained by the incomplete conversion of the monomer (75% conversion value led to an actual degree of polymerization of 5, while the feed ratio of DdeTC/

initiator was 8/1: entry 16 in table 1). Overall, the results of $^{1}$H-NMR and GPC analysis in **Table 1** (see **entries 2**, **5-8** and **13-16**) indicate that MSA is an excellent organocatalyst for controlled (co)polymerization of cyclic esters and/or cyclic carbonates.

The different monomer sequences (block, random or gradient) in the obtained copolymers were determined by $^{1}$H/$^{13}$C-NMR analysis, according to previously described methods. [9,12,13,59] $^{1}$H-NMR spectra of the different copolymers formed by the simultaneous copolymerization of CL and DTC (**Figure 4A** and **Figure S3A** in supporting information) displayed three groups of peaks in the ester region at 4.00-4.30 ppm, corresponding to the three kinds of $CH_2O$-carbonyl linkages in the different diad structures that are present in the poly(ester-carbonate) block (*i.e.,* DTC-DTC, CL-DTC and CL-CL, respectively). [12,59] In line with $^{1}$H-NMR analysis, the $^{13}$C-NMR spectra showed two signals in the caprolactone-carbonyl region at 173.5 and 172.9 ppm, which are assigned to CL-CL and CL-DTC diads, respectively (**Figure 4B** and **Figure S3B** in supporting information). [13,60,61] DTC-carbonyl peaks in the $^{13}$C-NMR are located at approximately 155 ppm (not shown), but the intensities of those peaks were relatively low and slightly above noise due to low amount of DTC used. The peaks are assigned based on the reference spectra of block copolymers synthesized by MSA catalysis that only contain CL or DTC blocks (presented as entry 7 and 8, respectively, in **Figure 4**).

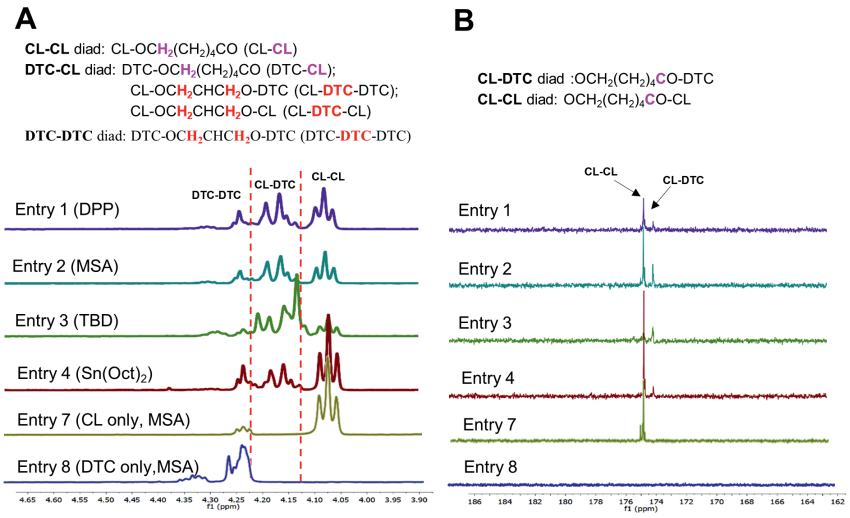


**Figure 4.** $^{1}$H (A) and $^{13}$C (B) -NMR spectra of p(CL-*co*-DTC)-PEG block copolymers obtained with DPP (Entry 1), MSA (Entry 2), TBD (Entry 3) and $Sn(Oct)_2$ (Entry 4) as catalysts, respectively, at a CL/DTC/initiator feed molar ratio of 9/4/1. $^{1}$H-NMR spectra (600 MHz, $CDCl_3$) show the region of methylene protons linked to oxy-carbonyl group ($C\underline{\boldsymbol{H}_2}OCO$) while $^{13}$C-NMR spectra (150 MHz, $CDCl_3$) display the region of the caprolactone-carbonyl carbons. The structures of different diads are displayed above the spectra. The reference spectra of block copolymers synthesized using MSA as catalyst that besides PEG, only contain CL or DTC blocks are presented as entry 7 and 8, respectively. All the entries presented in the legend correspond to the same entries in table 1.

**Table 1.** Characteristics of copolymers obtained by simultaneous and sequential polymerization of CL and/or DTC or DdeTC with different catalysts.

| Entry | Abbreviation of the obtained copolymers | Catalyst | Order of monomer addition | Aimed $M_n$ [a] | $^1$H-NMR[c] | | | | GPC | | | DSC | |
|---|---|---|---|---|---|---|---|---|---|---|---|---|---|
| | | | | | Reaction time (h) | CL/DTC or DdeTC conversion (%) | $M_n$ [a] | Microstructure of copolymers | $M_w$ [a] | $M_n$ [a] | $M_w/M_n$ | $T_g/T_m$ (C) | $\Delta H_m$ (J/g) |
| **1** | p($CL_9$-$DTC_{3.8}$)-PEG | DPP | simultaneous | 4.0 | 28 | 91/94 | 3.9 | Random | 2.9 | 2.7 | 1.07 | -36/42 | 81 |
| **2** | p($CL_9$-$DTC_{3.9}$)-PEG | MSA | simultaneous | 4.0 | 10 | 100/95 | 4.0 | Random | 2.9 | 2.7 | 1.07 | -36/42 | 82 |
| **3** | p($CL_{8.4}$-$DTC_{3.9}$)-PEG | TBD | simultaneous | 4.0 | 18 | 76/100 | 3.9 | Random | 3.5 | 2.9 | 1.21 | -40/43 | 85 |
| **4** | p($CL_{10.1}$-$DTC_{3.1}$)-PEG | $Sn(Oct)_2$ | simultaneous | 4.0 | 19 | 100/75 | 4.0 | Gradient | 2.9 | 2.7 | 1.10 | -37/42 | 94 |
| **5** | p($CL_{9.1}$-*b*-$DTC_{4.1}$)-PEG | MSA | DTC first, then CL | 4.0 | 18/2 | 100/100 | 4.0 | Blocky | 2.5 | 2.4 | 1.07 | -43/41 | 92 |
| **6** | p($DTC_{3.8}$-*b*-$CL_9$)-PEG | MSA | CL first, then DTC | 4.0 | 2/18 | 100/97 | 4.0 | Blocky | 2.7 | 2.6 | 1.05 | -42/40 | 92 |
| **7** | p$CL_{9.1}$-PEG | MSA | CL only | 3.2 | 2 | 100/- | 3.2 | - | 2.5 | 2.4 | 1.05 | -/45 | 125 |
| **8** | p$DTC_4$-PEG | MSA | DTC only | 3.0 | 18 | -/92 | 3.0 | - | 2.0 | 2.0 | 1.03 | -6.3/43 | 131 |
| **9** | p($CL_9$-$DTC_{3.9}$)-PEG | TBD | DTC first, then CL | 4.0 | 0.5/12 | 97/100 | 4.0 | Random | 4.7 | 3.6 | 1.31 | -40/43 | 80 |
| **10** | p($DTC_{4.3}$-*b*-$CL_{8.9}$)-PEG | TBD | CL first, then DTC | 4.0 | 12/12 | 79/94 | 4.0 | Blocky | 2.7 | 2.6 | 1.03 | -36/40 | 92 |
| **11** | p$CL_{8.8}$-PEG | TBD | CL only | 3.2 | 12 | 79/- | 3.2 | - | 2.4 | 2.3 | 1.04 | -/49 | 122 |
| **12** | p$DTC_{3.7}$-PEG | TBD | DTC only | 3.0 | 0.5 | -/100 | 3.0 | - | 3.5 | 2.0 | 1.75 | -/42 | 130 |
| **13** | p($CL_9$-$DTC_{6.6}$)-PEG | MSA | simultaneous | 4.8 | 10 | 97/90 | 4.5 | Random | 3.0 | 2.9 | 1.07 | -17/40 | 82 |
| **14** | p($CL_{18}$-$DTC_{7.5}$)-PEG | MSA | simultaneous | 5.8 | 10 | 95/98 | 5.7 | Random | 4.0 | 3.6 | 1.11 | -31/36 | 61 |
| **15**[b] | p($CL_9$-$DdeTC_{3.1}$)-PEG | MSA | simultaneous | 4.7 | 10 | 97/96 | 4.3 | Random | 3.3 | 2.8 | 1.16 | -40/40 | 95 |
| **16**[b] | p$DdeTC_5$-PEG | MSA | DdeTC only | 4.6 | 10 | -/75 | 3.9 | - | 3.0 | 2.9 | 1.08 | -17/43 | 67 |
| **17** | mPEG-OH | | - | - | - | - | - | - | 1.8 | 1.8 | 1.03 | -/48 | 182 |

[a] units are in kDa.

[b] these polymers were synthesized using DdeTC as the (co)monomer, while the other copolymers (entries 1-14) were synthesized using DTC as the co(monomer).

[c] $^1$H-NMR spectra of the polymers and the assignments of the corresponding NMR peaks are shown in **Figure S19-S34** of supporting information.

The observation that the copolymers synthesized using DPP and MSA as catalyst displayed all diads in the NMR spectra (**Figure 4A**, entries 1 and 2, and **Figure S3** in supporting information) demonstrates a random distribution of CL and DTC in the obtained p(CL-*co*-DTC)-PEG block copolymers, as can be expected because of the similar polymerization kinetics of both monomers (**Figure 2A** and **B**). For the p(CL-*co*-DTC)-PEG block copolymer synthesized by TBD-catalyzed ROP, the presence of relatively strong signals at 4.1-4.18 ppm in the $^{1}$H-NMR spectrum and at 172.9 ppm in the $^{13}$C-NMR spectrum (**Figure 4**, entry 3), being indicative of the link of CL and DTC units (*i.e.*, CL-DTC diads), suggests that the copolymer also had a highly randomized chain structure. This is however inconsistent with expectations based on the substantially different reactivities of the two monomers (**Figure 2C**), strongly indicating that significant transesterification occurred along with chain propagation (**Figure 3**, green line). For the copolymer obtained using $Sn(Oct)_2$ as catalyst (**Figure 4**, entry 4), the peak intensities in the $^{1}$H-NMR spectrum of the CL-CL and DTC-DTC diads were obviously higher and the corresponding CL-DTC diads were lower as compared to that of the corresponding copolymers obtained using DPP and MSA as catalysts. Also, an intense signal assigned to CL-CL diads at 173.5 ppm was displayed in the $^{13}$C-NMR spectrum (**Figure 4B**, entry 4). Combined with the different polymerization kinetics as observed for the monomers under $Sn(Oct)_2$ catalysis (**Figure 2D**), this indicates the existence of an enriched CL segment in the head of the formed chains and an enriched DTC segment in the tail of the chains and points to the expected gradient microstructure of this copolymer. Obviously no transesterification occurred that is in line with our previous publication, in which we showed that transesterification in ROP of CL and (benzylated) hydroxymethyl glycolide using $Sn(Oct)_2$ as catalyst was strongly temperature dependent and was minimized at 110 °C.[57]

Just like the p(CL-*co*-DTC)-PEG block copolymers discussed above, the p(CL-*co*-DdeTC)-PEG block copolymer (synthesized using MSA as the catalyst) showed the characteristic peaks at 4.00-4.45 ppm in the $^{1}$H-NMR spectrum, corresponding to CL-CL, CL-DdeTC and DdeTC-DdeTC linkages, and at 173.6 and 172.8 ppm in the $^{13}$C-NMR spectrum, corresponding to CL-CL and CL-DdeTC diads (**Figure S4** in supporting information). This random monomer sequence is in line with the observed random microstructure of p(CL-*co*-DTC)-PEG block copolymer obtained under the same reaction condition (**Figure 4**, entry 2) and also in agreement with the expectation from the comparable reactivities of CL and DdeTC, that was observed above.

### *3.1.2 Copolymers synthesized by sequential ring opening copolymerization of CL with DTC*

To investigate the potential of synthesizing p(CL-*co*-DTC)-PEG block copolymers with a blocky monomer order in the hydrophobic block and demonstrate the living nature of the polymerization, sequential copolymerization of CL and DTC initiated by mPEG-

OH was performed using MSA or TBD as the catalyst. These catalysts were chosen due to their markedly different catalytic properties in the simultaneous copolymerization process (as discussed in section 3.1.1). As can be seen from the results (**Entries 5**, **6**, **9** and **10**, table 1), in MSA-catalyzed ROP, regardless of the sequential feeding order of CL and DTC (**Entries 5** and **6**), the conversions of both monomers were quite high (≥97%) and the resulting copolymer compositions based on $^1$H-NMR agreed well with the feed composition and is comparable to what has been observed with simultaneous copolymerization of both monomers (*i.e.,* **Entry 2**, table 1). $^1$H-NMR analysis in table 1 clearly shows that the $M_n$ of the block copolymers obtained by sequential copolymerization increased upon feeding of the second monomer. For instance, $M_n$ increased from 2.0 kDa for PEG to 3.0 kDa upon the first polymerization of DTC (**Entry 17** *vs* **8**, table 1) and then to 4.0 kDa after subsequent copolymerization with CL (**Entry 8** *vs* **6**, table 1). This is also supported by GPC analysis (**Figure 5A**), which showed a continuous peak shift to shorter retention time upon feeding of the first and then the second monomer (*e.g.,* black dotted *vs* yellow *vs* blue line), respectively, while the molecular weight distributions remained monomodal and narrow ($M_w/M_n$ < 1.1, table 1). Overall, the results of $^1$H-NMR and GPC analysis suggest that chain extension occurred emphasizing the living character of the polymerization, resulting in a high level of control with no significant transesterification.

With TBD as the catalyst, and when the sequential polymerization of the comonomers was performed in the order of DTC first followed by CL (**Entry 9**, table 1), the composition of the obtained block copolymer based on $^1$H-NMR analysis agreed with the feed composition with almost complete conversions of both monomers. However, from GPC analysis (**Figure 5B**), it can be seen that the thus prepared block copolymer had a broad bimodal molecular-weight distribution (blue line) with a polydispersity index of 1.31 in line with that obtained by simultaneous copolymerization of the comonomers (purple line). This phenomenon has been previously reported for copolymers synthesized by sequential polymerization of TMC first, followed by CL at a 50/50 molar ratio using yttrium isopropoxide catalysis ($M_w/M_n$ = 3.7), which was attributed to a relatively slow ring-opening of CL by the living poly(TMC) chain end in comparison to the CL polymerization by living CL growing ends.[12] However, in our case, pDTC-PEG synthesized under the same condition also displayed a bimodal molecular weight distribution (**Figure 5B**, yellow line), indicating that the highly multi-dispersity in the copolymer composition occurred already in the initiation step. This suggests that not all of the potentially active groups (OH) of mPEG-OH in the reaction mixture acted as an initiator of the polymerization since one of GPC peaks partly overlapped with mPEG-OH. This may be attributed to the fast ring opening of DTC along with fast chain growth (*i.e.,* propagation rate ≥ initiation rate), which was also observed for TBD-catalyzed simultaneous copolymerization of CL and DTC (**Figure 3**, green line). However, in contrast, homo-polymerization of either CL or DTC

under mild acid MSA catalysis or of CL (which is less reactive relative to DTC) under TBD catalysis is likely characterized by a fast reaction of the PEG terminal OH with the monomers followed by relatively slow reaction of the formed PEG-monomer adduct with other monomers and thus leading to block copolymers with narrow molecular weight distribution ($M_w/M_n$ = 1.03-1.05), as indicated by GPC analysis of pCL-PEG (**Figure 5**, red lines, entries 7 and 11) and pDTC-PEG (**Figure 5A**, yellow line, entry 8). For the copolymer synthesized by TBD-catalyzed ROP of CL first, followed by DTC (**Entry 10**, table 1), the composition and $M_n$ calculated by $^1$H-NMR of the final block copolymer still well matched with the expected values based on the monomer/initiator ratios. $^1$H-NMR analysis shows that the $M_n$ of the block copolymer was comparable to the one prepared catalyzed by MSA, *i.e.,* increasing from 2.0 kDa for PEG to 3.2 kDa after first polymerization of CL (**Entry 17** *vs* **11**, table 1), and then to 4.0 kDa after polymerization of DTC in the second step (**Entry 11** *vs* **10**, table 1). In line with this, GPC analysis (**Figure 5B**) showed similar trend of increases of $M_n$ in the first and second step, respectively (**Figure 5B**, black dotted *vs* red *vs* green line), while a monomodal molecular-weight distribution of the final block copolymer remained as narrow as its control pCL-PEG ($M_w/M_n$ < 1.1) (green *vs* red line). This indicates that the formation of multi-disperse copolymers can be avoided by first polymerizing the slowly reacting CL (initiation rate > propagation rate) to produce living CL growing chain ends (**Figure 5B**, red line), followed by polymerization with DTC (**Figure 5B**, green line).



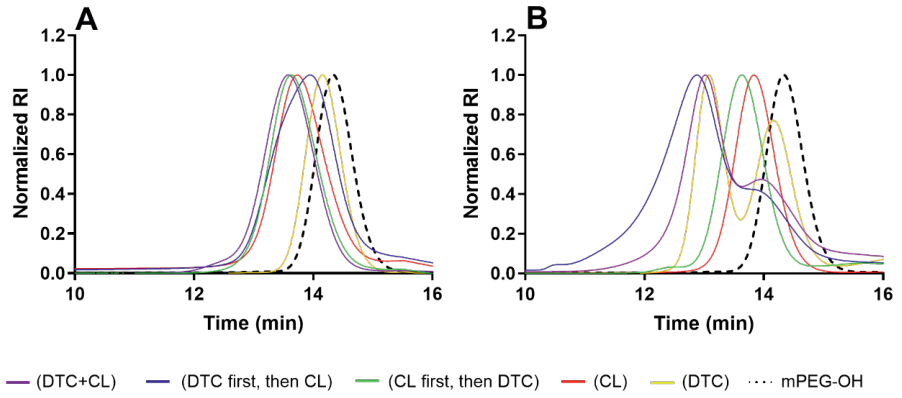


**Figure 5.** GPC traces of p(CL-*co*-DTC)-PEG block copolymers obtained by simultaneous and sequential copolymerization of CL with DTC at a CL/DTC/mPEG-OH feed molar ratio of 9/4/1, using MSA (A) and TBD (B) as the catalyst. Purple lines represent the block copolymers obtained by simultaneous copolymerization of CL and DTC, corresponding to entries 2 and 3 in table 1; blue lines represent the block copolymers obtained by sequential polymerization of DTC first, followed by CL, corresponding to entries 5 and 9 in table 1; green lines represent the block copolymers obtained by sequential polymerization of CL first and then DTC, corresponding to entries 6 and 10 in table 1; red and yellow lines represent pCL-PEG and pDTC-PEG obtained by homo-polymerization of either CL or DTC, corresponding to entries 7, 11 (the former) and 8, 12 (the latter) in table 1.

$^{1}H/^{13}C$-NMR analysis were used to determine the monomer sequence of the obtained block copolymers. Using MSA as catalyst (**Figure 6A** and **B**, entries 5 and 6), the block copolymers prepared by sequential copolymerization of CL and DTC, regardless of the feed order, had minor signals of the link between CL and DTC units (*i.e.*, CL–DTC diads) but displayed increased signals attributed to the presence of the CL-CL and DTC-DTC blocks as compared to the polymer obtained by simultaneous copolymerization (*i.e.,* **Figure 6A** and **B**, entry 2). These results strongly indicate highly blocky structures of the polyester/carbonate block of the formed p($CL_{9.1}$-*b*-$DTC_{4.1}$)-PEG and p($DTC_{3.8}$-*b*-$CL_{9}$)-PEG (Entries 5 and 6, table 1) block copolymers with no signs of transesterification that would randomize the monomer sequence. Surprisingly, in the case of TBD catalysis, for the block copolymer obtained by polymerization of DTC first followed by CL, the NMR spectra (**Figure 6C** and **D**, entry 9) indicate random CL and DTC sequences (*i.e.,* by the presences of CL-DTC diads in the δ 4.10–4.18 ppm region and at 172.9 ppm of the $^{1}H$ and $^{13}C$ spectra, respectively), with relative peak intensities as high as that observed in the NMR spectrum of the polymer obtained by simultaneous copolymerization of CL and DTC (*i.e.,* **Figure 6C** and **D**, entry 3). These results suggest that copolymerization of DTC first followed by CL yielded a random copolymer, most likely due to the occurrence of substantial transesterification. However, the NMR signals in the CL-DTC diad regions were hardly observed in the spectra when the copolymer was synthesized by reverse feeding of the monomers (*i.e.,* CL first, followed by DTC), while the increased signals assigned to CL-CL and DTC-DTC linkages do indicate a blocky structure (**Figure 6C** and **D**, entry 10).

Previously it was reported that sequential copolymerization of CL and a functionalized TMC (the feeding order of both monomers was not reported) using TBD as catalyst with a monomer to initiator ratio of 80/80/1 indeed produced a random copolymer due to transesterification.[9] Also such chain reshuffling reactions were observed with sequential copolymerization of L-lactide and TMC using 1,8-diazabicyclo[5.4.0]undec-7-ene (DBU) as catalyst.[11] An explanation for our observations could be CL that is present during polymerization, as in the cases of simultaneous copolymerization of CL and DTC and sequential copolymerization of DTC first and then CL, could lead to transesterification reactions, along with chain propagation. The incidence of these side reactions is most likely because the carbonate ester bonds in the DTC-DTC linkages formed when DTC was polymerized first, are not as stable as the ester bonds in DTC-CL or CL-CL diads, and could react intra- or inter-molecularly with propagating hydroxyl chain ends. When the stable ester bonds were formed first, which is the case of ROP of CL first, the subsequently added DTC was not able to break the formed ester bonds, thus resulting in prevailing chain propagation with negligible transesterification reactions.

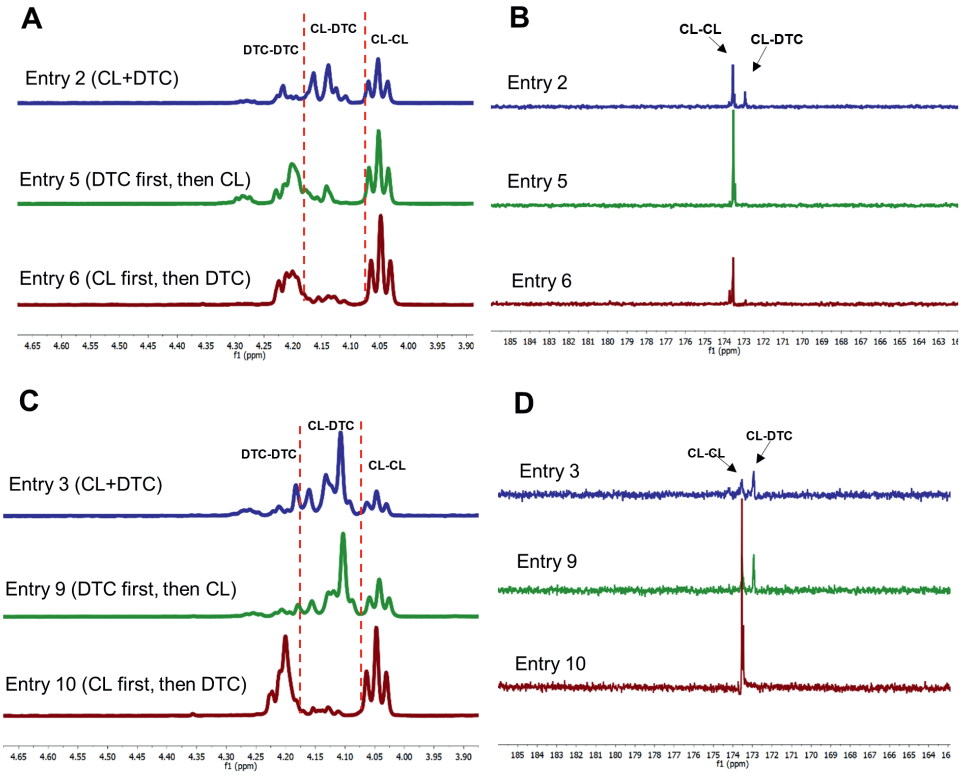


**Figure 6.** $^{1}$H (A, C) and $^{13}$C (B, D) -NMR spectra of p(CL-*co*-DTC)-PEG block copolymers obtained by simultaneous and sequential copolymerization of CL and DTC at a CL/DTC/mPEG-OH feed molar ratio of 9/4/1, using MSA (A, B) and TBD (C, D) as the catalyst, respectively. $^{1}$H-NMR spectra (600 MHz, $CDCl_3$) show the region of methylene protons linked to oxy-carbonyl group (C***H*****$_2$**OCO) while $^{13}$C-NMR spectra (150 MHz, $CDCl_3$) display the region of the caprolactone-carbonyl carbons. Entries 2 and 3 were obtained by simultaneous polymerization of CL and DTC. All the entries correspond to the same entries in table 1.

### *3.2 Thermal properties of the copolymers*

The thermal properties of the obtained block copolymers were investigated by DSC (**Table 1**). Only one $T_m$ at 40-45 °C close to that of mPEG-OH (48 °C) was detected, which is in accordance with previous data.[62,63] For the obtained p(CL-*co*-DTC)-PEG and p(CL-*co*-DdeTC)-PEG block copolymers (Entries 1-4, 5, 6, 9, 10 and 13-15, table 1), degrees of crystallinities (*i.e.,* $\Delta H_m$) of PEG corrected for its weight fraction in the corresponding block copolymers (**Figure S5A**, supporting information) were in good agreement with that of the mPEG-OH (182 J/g, **Entry 17**, table 1), demonstrating that these block copolymers were phase separated in the solid state in crystalline PEG domains and amorphous p(CL-*co*-DTC) or p(CL-*co*-DdeTC) domains with $T_g$'s, ranging from -47 to -11 °C. These amorphous domains are obviously not miscible with PEG. It is noted that $T_g$'s of p(CL-*co*-DTC)-PEG and p(CL-*co*-DdeTC)-PEG block copolymers (Entries 1-3, 9 and 13-15, table

1) with random distribution of CL and DTC or DdeTC as confirmed by NMR analysis (**Figure 4** and **6** and **Figure S3** and **S6** of supporting information) and discussed in section 3.1, can be indeed described by the FOX equation (**Figure S5B**, supporting information). The pCL-PEG block copolymers (Entries 7 and 11, table 1) were almost fully crystalline: both PEG and pCL have their $T_m$ around 45 °C [63] while the pDTC-PEG (Entry 8, table 1) and pDdeTC-PEG (Entry 16, table 1) block copolymers had crystallinity from PEG and amorphous pDTC and pDdeTC domains with $T_g$'s at -6.3 and -17 °C, respectively.

*3.3 Effect of reducing agents on the dynamic crosslinking properties of micelles*

The capability of dithiolanes in DTC units to crosslink nanoparticles has been reported in previous studies.[29,31,32] In the present work, DTC units were successfully introduced to PEG-poly(ε-caprolactone)-based block copolymers, as discussed in section 3.1, and therefore, the reduction of the dithiolanes present in these block copolymers by different reducing agents was investigated. For this purpose, micellar dispersions were prepared from p($CL_{18}$-$DTC_{7.5}$)-PEG block copolymer with a random monomer order in the hydrophobic block (**Entry 14**, table 1) at a final polymer concentration of 4 mg/mL using a nanoprecipitation method. The obtained micelles dispersed in PBS were subsequently incubated with reducing agents that had none, one or two thiol moieties (*i.e.,* TCEP, GSH or DTT, respectively) at molar ratios to dithiolanes varying from 0 to 2 at 37 °C. The state change of the dithiolanes towards the reducing agent (RA) (*i.e.,* the ring opening of the dithiolane groups by reduction of the disulfide bridge in the polymer structure) was monitored by recording changes in the absorbance of DTC at 326 nm.[38,42] **Figure 7A** shows that incubation of micelles with TCEP and DTT for 1 h caused a RA-concentration dependent linear decrease in the absorbance of the micellar dispersions at 326 nm, up to 1 equivalent of RA. It is noted that prolonged incubation (up to 40 h) did not result in a further decrease of the absorbance and thus the formed sulfhydryls were preserved in a reduced state for at least 40 h. In line with this, Ellman's assay demonstrated quantitative formation of free thiol groups in the micellar dispersions with series of molar ratios of TCEP to dithiolanes (**Figure S6**, black dots, supporting information). Although the same sulfhydryl quantification by Ellman's assay could not be performed using DTT as reducing agent due to interference of the thiol groups of this compound, **Figure 7A** clearly indicates that TCEP and DTT were able to cleave the disulfide bonds in the dithiolane rings of DTC units to free thiol groups. In contrast, no change in the absorbance at 326 nm was observed for the p($CL_{18}$-$DTC_{7.5}$)-PEG micellar dispersion even after addition of a two-fold equivalent of GSH and incubation for 58 h (**Figure 7A**, blue line). This indicates that the dithiolane rings remained intact in the presence of GSH, meaning that the reductive capacity of GSH was too low to break the disulfide bonds in dithiolanes. The fact that GSH is a less strong reducing agent than TCEP and DTT has been reported in other papers.[64,65]

In the second step, to crosslink the reduced micelles, the reducing agent was removed by dialysis, during or after which (intra- or inter-molecular) disulfides bonds can be formed

by oxidation. To follow this process, the absorbance of the reduced micelles at 326 nm was monitored over time after removing the reducing agents by dialysis. Interestingly, for p($CL_{18}$-$DTC_{7.5}$)-PEG micelles pre-incubated with TCEP or DTT, the absorbance of DTC units was slightly lower or similar directly after dialysis as compared to the corresponding values before dialysis (Abs ~0.75, **Figure 7B** and **C**, "AD+0h" *vs* "BD"). However, absorbance increased slowly when kept in PBS at RT ("AD+24h" to "AD+96h" in **Figure 7B** and **C**) to finally reach the same level as for the micelles that were not exposed to a RA (i.e. black dots). The final absorbance value of ~0.6 corresponds to ~20% change compared to the absorbance before dialysis (~0.75) in the absence of RA. In line with this, Ellman's assay of the TCEP-reduced micelles (**Figure S6**, supporting information) showed that the concentration of sulfhydryls in the micellar dispersion before and after dialysis were comparable (black *vs* red dots), but decreased to negligible concentration during 4 days' aging after dialysis (blue dots). Also, the appearance of a peak at 11 min retention time in GPC traces of these micelles shows that crosslinking of micelles occurred between 0 and 96 h after dialysis (solid lines in **Figure S7A** and **B**, respectively, supporting information). These results suggest that free thiols present in the micelles, obtained by the cleavage of the dithiolanes using a reducing agent, slowly oxidized in time after dialysis and preferably (~80%) returned to its original state of five-member dithiolanes, while a minority of them (max. ~20%) formed new and intermolecular disulfide bonds.

As indicated in **Figure 7B-D** (black dots), for the p($CL_{18}$-$DTC_{7.5}$)-PEG micelles without pre-treatment with RA, the absorbance dropped from approximately 0.75 to 0.60 during dialysis. After dialysis, the absorbance did not change during further incubation for 96 h. In the GPC chromatograms of the p($CL_{18}$-$DTC_{7.5}$)-PEG block copolymer after dialysis (red dotted line in **Figure S7A** of supporting information), the peak height of the original polymer at ~13 min reduced and a new peak appeared at a higher molecular weight (retention time of ~11 min), while the total area under the curve remained almost similar. The relative molecular weight of the new peak (*i.e.,* 13 kDa) suggests that approx. 4 polymer chains are connected, which is lower than expected for a fully crosslinked micelle. Although the absolute molecular weight (and thus number of connected polymers) may be higher, this is probably the result of the relatively low crosslink density (20%) and dynamic nature of the crosslinking, causing that some loosely connected polymer chains are decrosslinked when dissolved in DMF. Overall, these results suggest that approximately 20% of the dithiolane rings were spontaneously (*i.e.,* without being triggered by a RA) converted during dialysis into intermolecular bonds by disulfide exchange (probably a radical process) which in turn resulted in crosslinking of the core of the micelles. In line with this, it has been reported that p($TMC_{190}$-$DTC_{25}$)-PEG polymersomes [32,66] and cRGD/TAT conjugated p($CL_{17.5}$-$DTC_{5.2}$)-PEG micelles spontaneously crosslinked after dialysis due to the presence of dithiolanes.[31] These nanoparticles showed complete disappearance of dithiolanes after dialysis by the UV/vis, indicating that their crosslink densities were much higher than that of p($CL_{18}$-$DTC_{7.5}$)-PEG micelles (as evidenced by the UV/vis and GPC data). As expected,

p($CL_{18}$-$DTC_{7.5}$)-PEG micelles that were incubated with GSH (**Figure 7D**) gave the same results as for micelles that were not treated with any RA (**Figure 7A**), due to insufficient reduction power of GSH as mentioned above.[64,65] The driving force for spontaneous formation of the disulfide crosslinked network during the dialysis process is probably the removal of remaining organic solvent (10% DMF after the nanoprecipitation) resulting in condensation of the core of micelles, bringing the dithiolanes in the core in close vicinity to each other to allow disulfide-exchange reactions to proceed.[29]

The obtained results demonstrate that the disulfides in micelles derived from dithiolanes have dynamic properties. Its redox state (*e.g.,* the number of free thiols) can be influenced by addition of a RA, but the final equilibrium state in the absence of RA (*i.e.,* ratio between intramolecular and intermolecular disufide bonds) is not affected by pre-incubation with RA. Thus the RA in fact acts as a catalyst that accelerates the reduction of dithiolane but does not affect the final thermodynamic equilibrium.

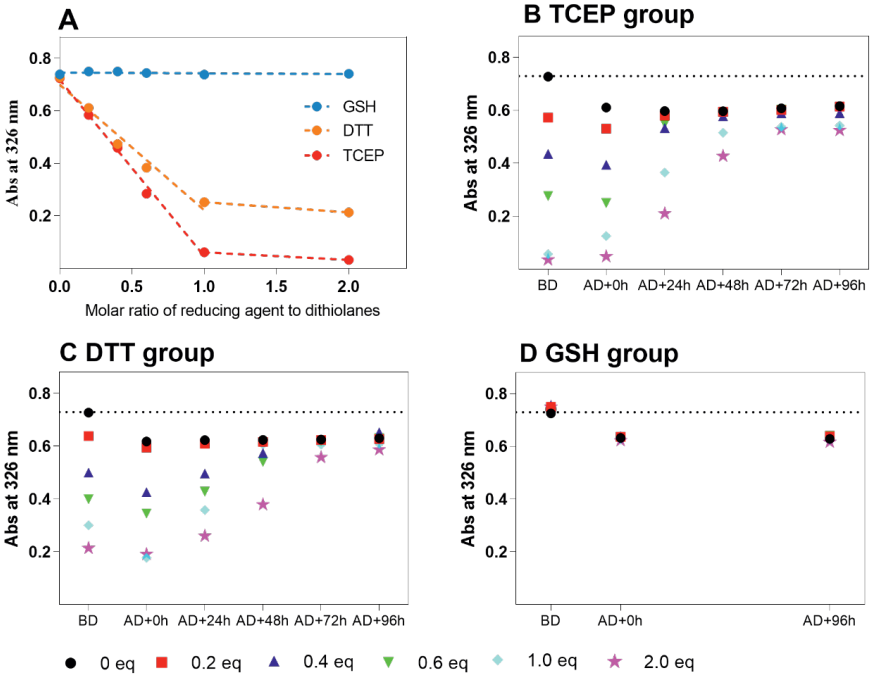


**Figure 7.** (A) The response of dithiolanes in micellar dispersions consisting of p($CL_{18}$-$DTC_{7.5}$)-PEG (**Entry 14**, table 1) on different reducing agents as a function of the absorbance (Abs) of micellar dispersions in PBS (pH 7.4) at 326 nm, recorded upon incubation at 37 °C for 1 h after addition of various amount of TCEP (red line), DTT (orange line) or GSH (blue line). (B-D) Absorbance (Abs) of p($CL_{18}$-$DTC_{7.5}$)-PEG (**Entry 14**, table 1) micellar dispersions at 326 nm in time before and after dialysis; micellar dispersions at polymer concentrations of 4 mg/mL in PBS/DMF (9/1 v/v) were incubated with different reducing agent: TCEP (B); DTT (C); GSH (D), respectively at various amounts (shown by the different symbols) for 7 h at 37 ℃ and then dialyzed against PBS for 12 h while the absorbance of these micellar dispersions was recorded before dialysis (BD), directly after dialysis (presented as "AD+0h") and at different timepoints after dialysis.

*3.4 Effect of the monomer sequence on the dynamic crosslinking properties of micelles*

Three different copolymers synthesized by MSA-catalyzed ROP (see section 3.1) that had similar chain lengths of hydrophobic blocks (9 units of CL and ~4 units of DTC) but differed in order of CL and DTC units in the hydrophobic blocks, *i.e.*, random p($CL_9$-$DTC_{3.9}$)-PEG (**Entry 2**, Table 1) or blocky p($CL_{9.1}$-*b*-$DTC_{4.1}$)-PEG (**Entry 5**, table 1) and p($DTC_{3.8}$-*b*-$CL_9$)-PEG) (**Entry 6**, table 1), were used to investigate whether the different CL and DTC sequences in the hydrophobic blocks of the copolymers have an effect on the dynamic properties of dithiolane-based crosslinking. These micelles showed the same changes in absorbance at 326 nm as observed above with the p($CL_{18}$-$DTC_{7.5}$)-PEG micelles, *i.e.,* a decreasing absorbance upon exposure to TCEP or DTT (before dialysis) and increasing during aging after dialysis, as can be seen from **Figures S8-S10** (supporting information). However, the rate of five-member dithiolanes recovery after dialysis was faster than that observed for p($CL_{18}$-$DTC_{7.5}$)-PEG micelles with random monomer order in the hydrophobic block. In summary, the equilibrium between the reformed five-member dithiolanes and new crosslinks is more rapidly reached but is not shifted by shorter chain lengths of the hydrophobic polyester/carbonate block and is independent of CL and DTC order in the hydrophobic blocks of the p(CL-*co*-DTC)-PEG block copolymers.

*3.5 Effect of nature of dithiolane unit on the dynamic crosslinking properties of micelles*

The preference to reform intramolecular disulfide bonds (*i.e.,* five-member dithiolane rings) rather than new intermolecular disulfide bonds in p(CL-*co*-DTC)-PEG-based micelles as shown above, may be influenced by the distance between the pendant sulfur groups and the backbone of the polymer chains, *i.e.,* the nature of dithiolane units in the polymer chains. To verify this hypothesis, random p($CL_9$-$DdeTC_{3.1}$)-PEG (**Entry 15**, table 1) containing ethylene glycol diester as a flexible spacer between the dithiolane groups and backbone of the polymer chains was used to prepare micellar dispersions with/without TCEP or DTT at a polymer concentration of 10 mg/mL.

In line with DTC-based micelles described in sections 3.3 and 3.4, addition of TCEP to the micellar dispersions triggered the reduction of disulfide bonds in DdeTC units within 1 h in a different extent and dependent on the TCEP concentration (**Figure S11A** and **C**, supporting information), but reduction by DTT took longer (5 h: **Figure S11B**). The absorbance at 328 nm of p($CL_9$-$DdeTC_{3.1}$)-PEG micelles without being preincubated with RA did not decrease during and after dialysis (**Figure 8A** and **B**, black dots). In line with this, GPC profiles of these p($CL_9$-$DdeTC_{3.1}$)-PEG micellar dispersions (not pre-incubated with a RA and after dissolution in DMF) obtained before, directly after dialysis and 96 h aging after dialysis were identical to that of the original p($CL_9$-$DdeTC_{3.1}$)-PEG block copolymer (**Figure S12**, red *vs* gray dotted lines, supporting information), demonstrating that spontaneous crosslinking of the micelles by disulfide exchange did not occur during dialysis, as opposed to the DTC-containing

micelles. In addition, DLS measurements demonstrate that both non-crosslinked control $pCL_9$-PEG and $p(CL_9$-$DdeTC_{3.1})$-PEG micelles fully dissolved in DMF, indeed suggesting that no disulfide crosslinked network was present in the micelles.
It was observed that for DdeTC-containing micelles preincubated with either TCEP or DTT, the reduced absorbance at 328 nm upon incubation with the RA gradually reversed towards the starting values over the course of 48 h after dialysis (**Figure 8**, red, blue and green dots). Considering the experimental error, the equilibrium values (~0.83) were close to those observed in micellar dispersions without being pre-incubated with a RA (~0.87), indicating that the majority of free thiols in reduced $p(CL_9$-$DdeTC_{3.1})$-PEG micelles returned to its original five-member dithiolane rings upon oxidation during aging. In line with this, GPC curves from these micelles obtained 96 h after dialysis (**Figure S12C**, solid lines, supporting information), showed only a small shoulder in the chromatogram at about 11 min, corresponding to the crosslinked micelles. Overall, these results suggest that the ability to crosslink micelles containing dithiolanes of DdeTC units was much lower than that of DTC (0% *vs* ~20% in the case of spontaneous crosslinking and *<5% vs* ~20% in the case of induction by a RA). In other words, inserting a flexible spacer between dithiolanes and backbone of the polymer chains does, unexpectedly, not favor the crosslinking capacity of dithiolanes in micelles. This could be ascribed to a slightly different ring tension between DTC and DdeTC or electronic induction effects caused by the different substitution pattern on the dithiolane ring. [67-69] In addition, these observations are inconsistent with those reported in previous studies, in which it was shown that pDdeTC-PEG-pDdeTC triblock copolymers self-assembled in water into bridged flower-like micelles which in turn efficiently crosslinked through ring-opening polymerizations of the dithiolanes initiated by the addition of a thiol.[37,40,42] The studies mentioned and ours differ in experimental setup and composition of the copolymers used. In order to exclude the possible impact of the former on the result, we repeated the same method as reported in [42] (described in Figure **S13**, supporting information), *i.e.,* direct hydration of the polymer followed by ring-opening polymerization of the dithiolanes initiated by 3,6-dioxa-1,8-octanedithiol and finally thiol capping by maleimide, using $p(CL_9$-$DdeTC_{3.1})$-PEG (**Entry 15**, table 1) and $pDdeTC_5$-PEG (**Entry 16**, table 1) at polymer concentrations of 10 and 20 mg/mL, respectively. As indicated by the decrease of the absorbance of DdeTC units at 328 nm in Figure **S13A** and **B** (supporting information), 3,6-dioxa-1,8-octanedithiol was able to reduce the dithiolanes in $p(CL_9$-$DdeTC_{3.1})$-PEG dispersions to some extent within 1 h (Figure **S13A**, red dots, supporting information) while reduction of $pDdeTC_5$-PEG dispersions took 3 h (**Figure S13B**, red dots, supporting information). It is noted that the absorbance of the dithiolanes in these micelles could not be measured after being capped by maleimide due to the interference of maleimide absorbance with that of DdeTC. However, both reduced dispersions, regardless of being capped with maleimide or not, showed the same GPC curves as the corresponding original $p(CL_9$-$DdeTC_{3.1})$-

PEG and pDdeTC$_5$-PEG polymers (**Figure S13C** and **D**, supporting information). Neither a peak nor a shoulder was observed at a retention time of 11 min, suggesting that under the same condition as reported previously,[42] The DdeTC-containing micelles were not able to be crosslinked through ring-opening polymerization of dithiolanes. The inconsistency between our and literature data might be ascribed to the slightly different polymer structures and compositions, even though such a big difference in crosslinking behavior between triblock pDdeTC$_4$-PEG(20kDa)-pDdeTC$_4$ and diblock pDdeTC$_5$-PEG(2kDa) with shorter PEG chains was unexpected.

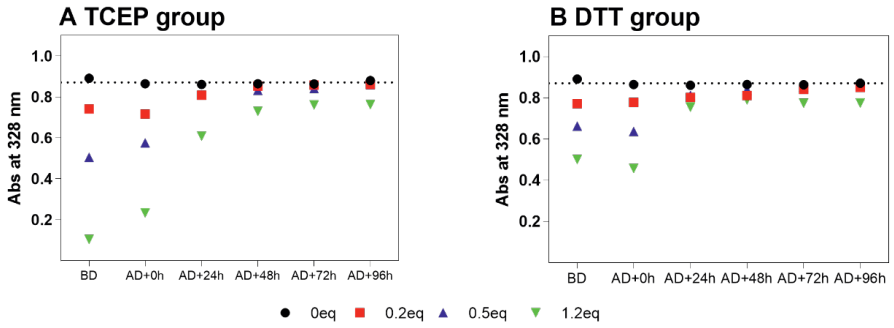


**Figure 8.** Absorbance (Abs) of DdeTC in micellar dispersions consisting of 10 mg/mL p(CL$_9$-DdeTC$_{3.1}$)-PEG (**Entry 15**, table 1) at 328 nm. Dispersions were incubated with 0–1.2 equivalents (shown by the different colors) of reducing agent TCEP (A) or DTT (B) for 7 h at 37 °C, dialyzed against PBS for 12 h and then aged for 96 h; the absorbance of the dispersions was recorded before dialysis ( "BD"), directly after dialysis ("AD+0h") and at different timepoints during aging after dialysis ("AD+Xh").

### *3.6 Reversibility of the crosslinking in micelles*

The reversibility of the crosslinking (or the reformed cyclic dithiolanes) in micelles that were aged for 96 h after TCEP reduction and subsequent dialysis (represented in red frame in the inset of **Figure 9**, denoted as 1st cycle), was investigated using p(CL$_{18}$-DTC$_{7.5}$)-PEG (**Entry 14**, table 1). The aged micelles were therefore re-incubated with TCEP for 7 h using various molar ratios to the dithiolanes (designated as 2nd cycle in **Figure 9**). As expected, for the p(CL$_{18}$-DTC$_{7.5}$)-PEG micelles not treated with TCEP in the second cycle, the absorbance of DTC at 326 nm did not change during the whole process of second time dialysis and aging, indicating that the crosslinked core of micelles remained intact with constant crosslinking density, which is further confirmed by the similar GPC traces of micelles obtained after first and second cycle of non-reducing conditions (supporting information **Figure S7**, red line, *vs* **Figure S14C**, black line, respectively). Upon addition of various amounts of TCEP in the second cycle, the absorbance of DTC in these micelles at 326 nm (at "BD" in **Figure 9**) showed a TCEP-concentration dependent decrease, which was consistent with that shown in the first cycle, meaning that the reformed dithiolane rings in the micelles in the first cycle were

reversibly cleaved under reductive conditions (TCEP), as expected.
Their absorbance values of the p($CL_{18}$-$DTC_{7.5}$)-PEG micelles treated with 0.2 equivalent TCEP and after dialysis, recovered within 24 h from 0.47 to the starting level of 0.6, which was comparable to the level observed for micelles incubated without TCEP (**Figure 9**, red *vs* black dots). Interestingly, when micelles had been incubated with TCEP ≥0.4 equivalents of TCEP, the absorbance values of micelles increased slowly during aging but did not reach the same plateau at 0.6 (see **Figure 9**). Also, Ellman's assay showed that the number of free thiols in those micelles obtained 96 h after dialysis in the second cycle was higher than that of the micelles from the first cycle (supporting information, **Figure S6**, pink *vs* blue dots). This suggests that the reduced dithiolane rings and/or crosslinking in micelles caused by relatively high amount of TCEP were not completely reversed to its original stage as shown in the first cycle under the same condition. DLS measurements show that the p($CL_{18}$-$DTC_{7.5}$)-PEG micelles pre-incubated without or with 0.2 equivalent TCEP in the second cycle, displayed constant and comparable size and derived count rate before dialysis, as well as directly after dialysis and 96 h aging after dialysis (**Figure S14A** and **B** in supporting information, red and black lines). However, micelles exposed ≥0.4 equivalent of TCEP in the second cycle, exhibited a significant decrease in size (from 23 to 10 nm) and the derived count rate (from 8000 to 2000) during and after dialysis (**Figure S14A** and **B**, blue, green, light green and pink lines). GPC chromatograms show that these p($CL_{18}$-$DTC_{7.5}$)-PEG micelles obtained after the second cycle (**Figure S14C**, blue, green, light green and pink lines, supporting information) displayed a decrease of the main peak at retention time of approximately 13 min, and appearance of a new peak at higher retention time (about 14.5 min), most likely attributed to hydrolyzed fragments of the p($CL_{18}$-$DTC_{7.5}$)-PEG diblock copolymer. In addition, the $^{1}$H-NMR spectrum of the p($CL_{18}$-$DTC_{7.5}$)-PEG micelles pre-exposed to 1 equivalent TCEP in the second cycle (**Figure S15** in supporting information) shows that the degree of polymerization of DTC and CL decreased from 7.5 to 1.4 and 18 to 11.5, respectively, suggesting that hydrolysis of polymers indeed occurred in the micelles. Thus, the incomplete reversibility of dithiolane ring formation and/or crosslinking in the case of the micelles pre-incubated with high amount of TCEP can be explained by the loss of DTC units. This accelerated hydrolysis is probably caused by the formation of cyclic 8-member carbonate between C=O (as the H-bond acceptor) in the backbone and the large amount of adjacent free sulfhydryls (as the H-bond donor) formed by a high amount of TCEP. This hydrolysis likely also occurred in the first cycle but to a lower extent than that observed in the second cycle due to the relatively shorter storage period of those micelles in PBS in the first circle as compared to the second cycle (4 and ~9 days respectively).

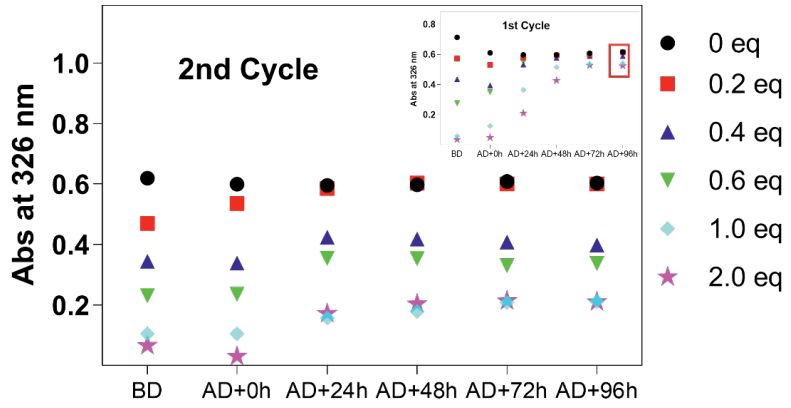


**Figure 9.** Absorbance (Abs) of micellar dispersions composed of p($CL_{18}$-$DTC_{7.5}$)-PEG (**Entry 14**, table 1) at 326 nm after a second exposure to various amounts (indicated by the different symbols) of TCEP for 7 h at 37 °C (presented as "BD"), after subsequent dialysis (presented as "AD+0h") and upon aging after dialysis for the indicated time points; micellar dispersions were used from the first cycle after 96 h of aging, as indicated by the red box in the insert copied from **Figure 7B**.

5

### *3.7 Decrosslinking of micelles*

As shown in previous sections, DTC-containing micelles, but not DdeTC-based micelles, spontaneously crosslinked during dialysis, to the same extent as with previous exposure to a RA. To evaluate the cleavage of the disulfide crosslinks in the former micelles in more detail, several spontaneously crosslinked p(CL-*co*-DTC)-PEG based micelles (**Entries 2**, **6**, **13** and **14**, table 2) were prepared by the nanoprecipitation method (and without exposure to RA), *i.e.,* by dropwise addition of the polymer solution in DMF to PBS (pH 7.4) at a volume ratio of 1:9 followed by dialysis against PBS for 12 h. GPC curves (**Figure S15** in supporting information) and the decrease of the absorbance of DTC at 326 nm before and after dialysis (**Table 2**) suggests that indeed crosslinked micelles were formed spontaneously after dialysis with about ~20% crosslinking density, as reported in sections 3.3 and 3.4. It is worth noting that micelles with higher DTC to CL comonomer ratio in the hydrophobic polyester/carbonate blocks (**Entry 13**, table 2) had similar crosslink density (*i.e.,* absorbance change) after dialysis as those with lower DTC to CL ratio (**Entries 2** and **14**, table 2), suggesting that the density of crosslinkable units was not a determinant factor for the final equilibrium ratio between intra- and inter-molecular disulfide bonds within the range of ratios studied here. In addition, as shown in **Table 2**, all prepared micelles had average diameters ranging from 17 to 21 nm with narrow PDIs in PBS.

**Table 2.** Characteristics of spontaneously crosslinked micelles prepared from different polymers at polymer concentrations of 4 mg/mL.

| Entry[a] | Polymers | Z-ave (nm)[b] | PDI | Absorbance change[c] |
|---|---|---|---|---|
| 2 | p($CL_9$-$DTC_{3.9}$)-PEG | 18±1 | 0.11±0.03 | 18±2% |
| 6 | p($DTC_{3.8}$-*b*-$CL_9$)-PEG | 18±1 | 0.10±0.05 | 18±2% |
| 9 | p$CL_9$-PEG | 17±1 | 0.15±0.06 | n.a.[d] |
| 13 | p($CL_9$-$DTC_{6.6}$)-PEG | 18±0 | 0.07±0.02 | 17±3% |
| 14 | p($CL_{18}$-$DTC_{7.5}$)-PEG | 22±2 | 0.09±0.02 | 20±2% |

[a] Entries in this table correspond to those listed in table 1.
[b] Z-average diameter of the micelles in PBS was measured by DLS after nanoprecipitation and dialysis (n=3).
[c] Relative decrease in absorbance at λ=326 nm.
[d] = not applicable.

The non-crosslinked control p$CL_9$-PEG micelles dissolved in DMF, resulting in loss of scattering intensity by DLS (result not shown). In contrast, when incubated with DMF, the size of spontaneously pre-crosslinked p(CL-*co*-DTC)-PEG based micelles (**Entries 2**, **6**, **13** and **14**, table 2) increased from approximately 20 nm to around 30-90 nm depending on molecular weight (*i.e.,* the chain lengths of hydrophobic blocks), while the PDIs were <0.3 (**Figure 10A** and **B**, blue vs black columns). In addition, derived count rates of these micelles decreased to some extent (**Figure 10C**, blue vs black columns). These observations suggest that DTC-containing micelles were indeed stabilized, *i.e.,* did not disassemble completely but swelled when dispersed in DMF, due to the existence of core-cross linkages in the micelles. The decreased count rates could be explained by either the decreased refractive index increment (dn/dc) resulting from swelling of the micelles or the micelles partly dissociated in DMF, most likely due to the dynamic and labile disulfide bonds and relatively low crosslinking density in the core of micelles. Interestingly, when incubated with TCEP in PBS, followed by addition of an excess of DMF, spontaneously pre-crosslinked p(CL-*co*-DTC)-PEG micelles did dissolve, as indicated by negligible derived count rates measured by DLS. These data suggest that indeed the disulfide crosslinks formed by dithiolanes in the core of micelles were reversibly destroyed in the presence of a reducing agent (*i.e.,* TCEP), leading to complete dissociation of micelles in DMF.

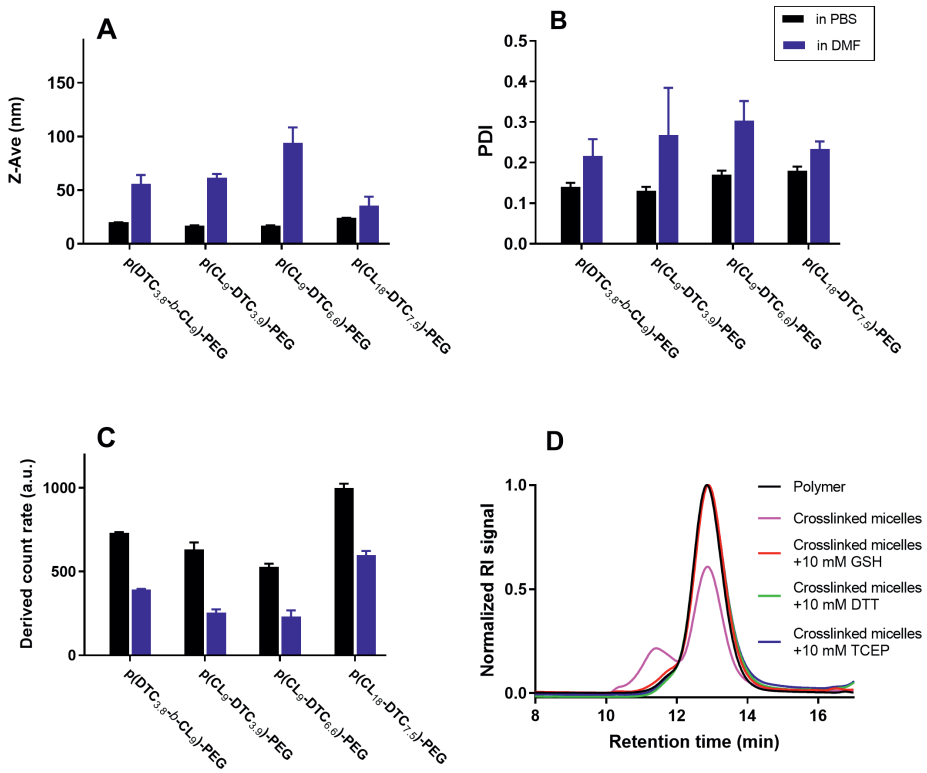


**Figure 10.** (A-C) Size (A), polydispersity index (PDI) (B), and derived count rate (C) of spontaneously crosslinked micellar dispersions composed of p(CL-*co*-DTC)-PEG based polymers (Entries 2, 6, 13 and 14, table 2) determined by DLS, after dilution in DMF or PBS; (D) GPC chromatograms of p($CL_{18}$-$DTC_{7.5}$)-PEG micelles with refractive index (RI) detection; spontaneously crosslinked micelles (pink line) were incubated with TCEP (blue line), DTT (green line) or GSH (red line) at final concentrations of 10 mM, for 7 h at 37 °C, and then freeze-dried. p($CL_{18}$-$DTC_{7.5}$)-PEG polymer directly dissolved in DMF was used as a control (black line).

In addition, the de-crosslinking potential of dithiolane crosslinked p($CL_{18}$-$DTC_{7.5}$)-PEG micelles triggered by different reducing agents (TCEP, DTT and GSH, respectively) was evaluated by GPC analysis. The GPC chromatograms of crosslinked p($CL_{18}$-$DTC_{7.5}$)-PEG micelles (**Entry 15**, table 2) obtained after incubation with 10 mM DTT, TCEP or GSH at 37 °C (**Figure 10D**, red, blue and green lines) were identical to the starting p($CL_{18}$-$DTC_{7.5}$)-PEG block copolymer (**Figure 10D**, black line), suggesting that the crosslinked micelles were fully reduced (*i.e.,* de-crosslinked) in the reductive environment at physiological temperature and redox potential (10 mM GSH is equal to the intracellular concentration [24]). In other words, all these three reducing agents, including the physiological GSH, were capable of cleaving the linear disulfide crosslinking present in the core of micelles. This is surprising, since the reducing ability of GSH was too weak to reduce the disulfide bonds present in the cyclic dithiolanes

(see section 3.3) but apparently sufficient to break the crosslinks, which suggests that the cyclic dithiolanes are more stable than the newly formed linear disulfide bonds in micelles after dialysis. This also explains to some extent why free thiols produced by reduction of dithiolanes tend to reform five-member dithiolanes during dialysis and aging rather than forming or keeping the crosslinks.

## 4. Conclusion

Poly(ε-caprolactone)-based polymeric micelles that are under investigation for drug delivery applications, can be made self-crosslinkable by introducing dithiolane rings directly connected to the backbone. On the other hand, introduction of a linker unit between the dithiolane and the backbone prevents crosslinking probably because of a different ring strain and/or electronic substituent effects. This crosslinking of micelles by disulfide exchange occurs spontaneously when the organic solvent (DMF) is removed during dialysis after nanoprecipitation and is independent of the monomer sequence (*i.e.,* random or blocky) in the hydrophobic blocks or CL/DTC ratio of the block copolymers or addition of reducing agents. Regarding the synthesis of the copolymers, we have shown that different catalyst types, *i.e.,* acidic (DPP or MSA), basic (TBD) or metallic ($Sn(Oct)_2$) catalyst, have a pronounced influence on the monomer sequence of the resulting copolymers as a consequence of the different polymerization rates of CL and DTC monomers and occurrence of transesterification reactions. Therefore, this study also provides a helpful perspective in selecting the right catalyst, which should have a suitable balance between reactivity and well controlled polymerization behavior. In addition, the dithiolane crosslinked micelles showed reduction-responsive behavior (*e.g.,* dissociation in the presence of 10 mM GSH), verifying their suitability for *in vivo* drug delivery applications.

## References


1. Cameron, D. J. A.; Shaver, M. P. Aliphatic polyester polymer stars: synthesis, properties and applications in biomedicine and nanotechnology. *Chemical Society Reviews* **2011,** *40*, 1761-1776.
2. Seyednejad, H.; Ghassemi, A.; Nostrum, C.; Vermonden, T.; Hennink, W. Functional aliphatic polyesters for biomedical and pharmaceutical applications. *J. Control. Release* **2011,** *152*, 168-176.
3. Gaucher, G.; Marchessault, R. H.; Leroux, J.-C. Polyester-based micelles and nanoparticles for the parenteral delivery of taxanes. *J. Control. Release* **2010,** *143*, 2-12.
4. BaoLin, G.; Ma, P. X. Synthetic biodegradable functional polymers for tissue engineering: a brief review. *Sci. China Chem.* **2014,** *57*, 490-500.
5. Vasir, J. K.; Labhasetwar, V. Biodegradable nanoparticles for cytosolic delivery of therapeutics. *Adv. Drug Deliv. Rev.* **2007,** *59*, 718-728.
6. Kamber, N. E.; Jeong, W.; Waymouth, R. M.; Pratt, R. C.; Lohmeijer, B. G. G.; Hedrick, J. L. Organocatalytic Ring-Opening Polymerization. *Chemical Reviews* **2007,** *107*, 5813-5840.
7. Albertsson, A.-C.; Varma, I. K. Recent Developments in Ring Opening Polymerization of Lactones for Biomedical Applications. *Biomacromolecules* **2003,** *4*, 1466-1486.
8. Dove, A. P. Organic Catalysis for Ring-Opening Polymerization. *ACS Macro Letters* **2012,** *1*, 1409-1412.
9. Couffin, A.; Delcroix, D.; Martín-Vaca, B.; Bourissou, D.; Navarro, C. Mild and efficient preparation of block and gradient copolymers by methanesulfonic acid catalyzed ring-opening polymerization of caprolactone and trimethylene carbonate. *Macromolecules* **2013,** *46*, 4354-4360.
10. Zaremski, M. Y.; Kalugin, D. I.; Golubev, V. B. Gradient copolymers: Synthesis, structure, and properties. *Polymer Science Series A* **2009,** *51*, 103-122.
11. Coulembier, O.; Lemaur, V.; Josse, T.; Minoia, A.; Cornil, J.; Dubois, P. Synthesis of poly(l-lactide) and gradient copolymers from al-lactide/trimethylene carbonate eutectic melt. *Chem. Sci.* **2012,** *3*, 723-726.
12. Ana Paula Pego, Z. Z., Pieter J. Dijkstra, Dirk W. Grijpma, Jan Feijen. Influence of catalyst and polymerization conditions on the properties of 1,3 - trimethylene carbonate and ε-caprolactone copolymers. *Macromolecular Chemistry and Physics* **2003,** *204*, 747-754.
13. Wei, J.; Meng, H.; Guo, B.; Zhong, Z.; Meng, F. Organocatalytic ring-opening copolymerization of trimethylene carbonate and dithiolane trimethylene carbonate: impact of organocatalysts on copolymerization kinetics and copolymer microstructures. *Biomacromolecules* **2018,** *19*, 2294-2301.
14. Fang, J.; Nakamura, H.; Maeda, H. The EPR effect: Unique features of tumor blood vessels for drug delivery, factors involved, and limitations and augmentation of the effect. *Adv. Drug Deliv. Rev.* **2011,** *63*, 136-151.
15. Danhier, F.; Feron, O.; Preat, V. To exploit the tumor microenvironment: Passive and active tumor targeting of nanocarriers for anti-cancer drug delivery. *J. Control. Release* **2010,** *148*, 135-146.
16. Deng, C.; Jiang, Y.; Cheng, R.; Meng, F.; Zhong, Z. Biodegradable polymeric micelles for targeted and controlled anticancer drug delivery: Promises, progress and prospects. *Nano Today* **2012,** *7*, 467-480.
17. Jain, R. K.; Stylianopoulos, T. Delivering nanomedicine to solid tumors. *Nat. Rev. Clin. Oncol.* **2010,** *7*, 653-664.

18. Tan, C.; Wang, Y.; Fan, W. Exploring polymeric micelles for improved delivery of anticancer agents: recent developments in preclinical studies. *Pharmaceutics* **2013,** *5*, 201-219.
19. Chauhan, V. P.; Jain, R. K. Strategies for advancing cancer nanomedicine. *Nature Materials* **2013,** *12*, 958-962.
20. Wicki, A.; Witzigmann, D.; Balasubramanian, V.; Huwyler, J. Nanomedicine in cancer therapy: challenges, opportunities, and clinical applications. *J. Control. Release* **2015,** *200*, 138-157.
21. Peer, D.; Karp, J. M.; Hong, S.; Farokhzad, O. C.; Margalit, R.; Langer, R. Nanocarriers as an emerging platform for cancer therapy. *Nature Nanotechnology* **2007,** *2*, 751-760.
22. Bae, Y. H.; Yin, H. Stability issues of polymeric micelles. *J Control Release* **2008,** *131*, 2-4.
23. Ron, N.; Cordia, J.; Yang, A.; Ci, S.; Nguyen, P.; Hughs, M.; Desai, N. Comparison of physicochemical characteristics and stability of three novel formulations of paclitaxel: Abraxane, Nanoxel, and Genexol PM. *Cancer Research* **2008,** *68*, 5622.
24. Meng, F.; Hennink, W. E.; Zhong, Z. Reduction-sensitive polymers and bioconjugates for biomedical applications. *Biomaterials* **2009,** *30*, 2180-2198.
25. Biswas, D.; An, S. Y.; Li, Y.; Wang, X.; Oh, J. K. Intracellular delivery of colloidally stable core-cross-linked triblock copolymer micelles with glutathione-responsive enhanced drug release for cancer therapy. *Mol. Pharmaceutics* **2017,** *14*, 2518-2528.
26. Brülisauer, L.; Gauthier, M. A.; Leroux, J.-C. Disulfide-containing parenteral delivery systems and their redox-biological fate. *J. Control. Release* **2014,** *195*, 147-154.
27. Andrzej Sadownik, J. S., and Steven L. Regen. Polymerized liposomes formed under extremely mild conditions *J. Am. Chem. Soc.* **1986,** *108*, 7789-7791.
28. Li, Y. L.; Zhu, L.; Liu, Z.; Cheng, R.; Meng, F.; Cui, J. H.; Ji, S. J.; Zhong, Z. Reversibly stabilized multifunctional dextran nanoparticles efficiently deliver doxorubicin into the nuclei of cancer cells. *Angew Chem. Int. Ed. Engl.* **2009,** *48*, 9914-9918.
29. Zou, Y.; Fang, Y.; Meng, H.; Meng, F.; Deng, C.; Zhang, J.; Zhong, Z. Self-crosslinkable and intracellularly decrosslinkable biodegradable micellar nanoparticles: A robust, simple and multifunctional nanoplatform for high-efficiency targeted cancer chemotherapy. *J. Control. Release* **2016,** *244*, 326-335.
30. Yang, W.; Zou, Y.; Meng, F.; Zhang, J.; Cheng, R.; Deng, C.; Zhong, Z. Efficient and Targeted Suppression of Human Lung Tumor Xenografts in Mice with Methotrexate Sodium Encapsulated in All-Function-in-One Chimeric Polymersomes. *Adv. Mater.* **2016,** *28*, 8234-8239.
31. Zhu, Y.; Zhang, J.; Meng, F.; Deng, C.; Cheng, R.; Feijen, J.; Zhong, Z. cRGD/TAT dual-ligand reversibly cross-linked micelles loaded with docetaxel penetrate deeply into tumor tissue and show high antitumor efficacy in vivo. *ACS Appl Mater Interfaces* **2017,** *9*, 35651-35663.
32. Zou, Y.; Meng, F.; Deng, C.; Zhong, Z. Robust, tumor-homing and redox-sensitive polymersomal doxorubicin: A superior alternative to Doxil and Caelyx? *J. Control. Release* **2016,** *239*, 149-158.
33. Zou, Y.; Zheng, M.; Yang, W.; Meng, F.; Miyata, K.; Kim, H. J.; Kataoka, K.; Zhong, Z. Virus-mimicking chimaeric polymersomes boost targeted cancer siRNA therapy *in vivo*. *Adv. Mater.* **2017,** *29*, 1-8.

34. Yang, W.; Xia, Y.; Fang, Y.; Meng, F.; Zhang, J.; Cheng, R.; Deng, C.; Zhong, Z. Selective cell penetrating peptide-functionalized polymersomes mediate efficient and targeted delivery of methotrexate disodium to human lung cancer *in vivo*. *Adv. Healthc Mater.* **2018,** *7*, 1-8.
35. Zhang, N.; Xia, Y.; Zou, Y.; Yang, W.; Zhang, J.; Zhong, Z.; Meng, F. ATN-161 Peptide Functionalized Reversibly Cross-Linked Polymersomes Mediate Targeted Doxorubicin Delivery into Melanoma-Bearing C57BL/6 Mice. *Mol. Pharmaceutics* **2017,** *14*, 2538-2547.
36. Fang, Y.; Yang, W.; Cheng, L.; Meng, F.; Zhang, J.; Zhong, Z. EGFR-targeted multifunctional polymersomal doxorubicin induces selective and potent suppression of orthotopic human liver cancer in vivo. *Acta Biomaterialia* **2017,** *64*, 323-333.
37. Barcan, G. A.; Zhang, X.; Waymouth, R. M. Structurally dynamic hydrogels derived from 1,2-dithiolanes. *J. Am. Chem. Soc.* **2015,** *137*, 5650-5653.
38. Andrzej Sadownik, J. S., and Steven L. Regen. Polymerized liposomes formed under extremely mild conditions. *J. Am. Chem. Soc.* **1986,** *108*, 7789-7791.
39. Bang, E. K.; Gasparini, G.; Molinard, G.; Roux, A.; Sakai, N.; Matile, S. Substrate-initiated synthesis of cell-penetrating poly(disulfide)s. *J. Am. Chem. Soc.* **2013,** *135*, 2088-2091.
40. Margulis, K.; Zhang, X.; Joubert, L. M.; Bruening, K.; Tassone, C. J.; Zare, R. N.; Waymouth, R. M. Formation of Polymeric Nanocubes by Self-Assembly and Crystallization of Dithiolane-Containing Triblock Copolymers. *Angew. Chem. Int. Ed. Engl.* **2017,** *56*, 16357-16362.
41. Wei, R.; Cheng, L.; Zheng, M.; Cheng, R.; Meng, F.; Deng, C.; Zhong, Z. Reduction-responsive disassemblable core-cross-linked micelles based on poly(ethylene glycol)-*b*-poly(N-2-hydroxypropyl methacrylamide)-lipoic acid conjugates for triggered intracellular anticancer drug release. *Biomacromolecules* **2012,** *13*, 2429-2438.
42. Zhang, X.; Waymouth, R. M. 1,2-dithiolane-derived dynamic, covalent Materials: Cooperative self-assembly and reversible cross-linking. *J. Am. Chem. Soc.* **2017,** *139*, 3822-3833.
43. Zhong, Y.; Zhang, J.; Cheng, R.; Deng, C.; Meng, F.; Xie, F.; Zhong, Z. Reversibly crosslinked hyaluronic acid nanoparticles for active targeting and intelligent delivery of doxorubicin to drug resistant CD44+ human breast tumor xenografts. *J. Control. Release* **2015,** *205*, 144-154.
44. Pratt, R. C.; Nederberg, F.; Waymouth, R. M.; Hedrick, J. L. Tagging alcohols with cyclic carbonate: a versatile equivalent of (meth)acrylate for ring-opening polymerization. *Chem. Commun.* **2008**, 114-116.
45. Delcroix, D.; Martín-Vaca, B.; Bourissou, D.; Navarro, C. Ring-opening polymerization of trimethylene carbonate catalyzed by methanesulfonic acid: Activated monomer versus active chain end mechanisms. *Macromolecules* **2010,** *43*, 8828-8835.
46. Lohmeijer, B. G. G.; Pratt, R. C.; Leibfarth, F.; Logan, J. W.; Long, D. A.; Dove, A. P.; Nederberg, F.; Choi, J.; Wade, C.; Waymouth, R. M.; Hedrick, J. L. Guanidine and Amidine Organocatalysts for Ring-Opening Polymerization of Cyclic Esters. *Macromolecules* **2006,** *39*, 8574-8583.
47. Bagheri, M.; Bresseleers, J.; Varela-Moreira, A.; Sandre, O.; Meeuwissen, S. A.; Schiffelers, R. M.; Metselaar, J. M.; van Nostrum, C. F.; van Hest, J. C. M.; Hennink, W. E. Effect of formulation and processing parameters on the size of mPEG-*b*-p(HPMA-Bz) polymeric micelles. *Langmuir* **2018,** *34*, 15495-15506.

48. Delcroix, D.; Couffin, A.; Susperregui, N.; Navarro, C.; Maron, L.; Martin-Vaca, B.; Bourissou, D. Phosphoric and phosphoramidic acids as bifunctional catalysts for the ring-opening polymerization of ε-caprolactone: a combined experimental and theoretical study. *Polymer Chemistry* **2011,** *2*, 2249-2256.
49. Susperregui, N.; Delcroix, D.; Martin-Vaca, B.; Bourissou, D.; Maron, L. Ring-opening polymerization of epsilon-caprolactone catalyzed by sulfonic acids: computational evidence for bifunctional activation. *J. Org. Chem* **2010,** *75*, 6581-6587.
50. Bordwell, F. G. Equilibrium acidities in dimethyl sulfoxide solution. *Acc. Chem. Res.* **1988,** *21*, 456-463.
51. Pratt, R. C.; Lohmeijer, B. G.; Long, D. A.; Waymouth, R. M.; Hedrick, J. L. Triazabicyclodecene: a simple bifunctional organocatalyst for acyl transfer and ring-opening polymerization of cyclic esters. *J. Am. Chem. Soc.* **2006,** *128*, 4556-4557.
52. Albertson, A.-C.; Eklund, M. Synthesis of copolymers of 1,3-dioxan-2-one and oxepan-2-one using coordination catalysts. *J. Polym. Sci., Part A: Polym. Chem. Sci.* **1993,** *32*, 265-279.
53. Krzysztof Matyjaszewski, M. J. Z., Stephen V. Arehart, Dorota Greszta and Tadeusz Pakula. Gradient copolymers by atom transfer radical copolymerization. *J. Phys. Org. Chem.* **2000,** *13*, 775–786.
54. Kamber, N. E. J., W.; Waymouth, R. M. Organocatalytic ring-opening polymerization. *Chem. Rev.* **2007,** *107*, 5813-5840.
55. Odian, G. Principles of polymerization. *Wiley-interscience: Hoboken, NJ,* **2004**, P 545-568.
56. A. Schindler, Y. M. H., C. G. Pitt. Aliphatic polyesters. III. molecular weight and molecular weight distribution in alcohol-Initiated polymerizations of ε-caprolactone. *J. Polym. Sci., Polym. Chem. Ed.* **1982,** *20*, 319-327.
57. Loontjens, C. A. M.; Vermonden, T.; Leemhuis, M.; van Steenbergen, M. J.; van Nostrum, C. F.; Hennink, W. E. Synthesis and characterization of random and triblock copolymers of ε-caprolactone and (Benzylated)hydroxymethyl glycolide. *Macromolecules* **2007,** *40*, 7208-7216.
58. Clément, B.; Grignard, B.; Koole, L.; Jérôme, C.; Lecomte, P. Metal-free strategies for the synthesis of functional and well-defined polyphosphoesters. *Macromolecules* **2012,** *45*, 4476-4486.
59. Ling, J.; Zhu, W.; Shen, Z. Controlling ring-opening copolymerization of ε-caprolactone with trimethylene carbonate by scandium tris(2,6-di-tert-butyl-4-methylphenolate). *Macromolecules* **2004,** *37*, 758-763.
60. Yang, L.-Q.; Yang, D.; Guan, Y.-M.; Li, J.-X.; Li, M. Random copolymers based on trimethylene carbonate and ε-caprolactone for implant applications: Synthesis and properties. *Journal of Applied Polymer Science* **2012,** *124*, 3714-3720.
61. Pastusiak, M.; Dobrzynski, P.; Kasperczyk, J.; Smola, A.; Janeczek, H. Synthesis of biodegradable high molecular weight polycarbonates from 1,3-trimethylene carbonate and 2,2-dimethyltrimethylene carbonate. *Journal of Applied Polymer Science* **2014,** *131*, 1-10.
62. Wennink, J. W. H.; Liu, Y.; Makinen, P. I.; Setaro, F.; de la Escosura, A.; Bourajjaj, M.; Lappalainen, J. P.; Holappa, L. P.; van den Dikkenberg, J. B.; Al Fartousi, M.; Trohopoulos, P. N.; Yla-Herttuala, S.; Torres, T.; Hennink, W. E.; van Nostrum, C. F. Macrophage selective photodynamic therapy by meta-tetra(hydroxyphenyl)chlorin loaded polymeric micelles: A possible treatment for cardiovascular diseases. *Eur. J. Pharm. Sci.* **2017,** *107*, 112-125.

63. Carstens, M. G.; Bevernage, J. J. L.; van Nostrum, C. F.; van Steenbergen, M. J.; Flesch, F. M.; Verrijk, R.; de Leede, L. G. J.; Crommelin, D. J. A.; Hennink, W. E. Small oligomeric micelles based on end group modified mPEG–oligocaprolactone with monodisperse hydrophobic blocks. *Macromolecules* **2007,** *40*, 116-122.

64. Iyer, K. S.; Klee, W. A. Direct spectrophotometric measurement of the rate of reduction of disulfide bonds. The reactivity of the disulfide bonds of bovine -lactalbumin. *The Journal of biological chemistry* **1973,** *248*, 707-710.

65. Han, J. C.; Han, G. Y. A procedure for quantitative determination of Tris(2-carboxyethyl) phosphine, an odorless reducing agent more stable and effective than dithiothreitol. *Analytical Biochemistry* **1994,** *220*, 5-10.

66. Meng, H.; Zou, Y.; Zhong, P.; Meng, F.; Zhang, J.; Cheng, R.; Zhong, Z. A smart nano-prodrug platform with reactive drug loading, superb stability, and fast responsive drug release for targeted cancer therapy. *Macromol Biosci* **2017,** *17*, 1-8.

67. Gasparini, G.; Sargsyan, G.; Bang, E. K.; Sakai, N.; Matile, S. Ring tension applied to thiol-mediated cellular uptake. *Angew. Chem. Int. Ed. Engl.* **2015,** *54*, 7328-7331.

68. Carmine, A.; Domoto, Y.; Sakai, N.; Matile, S. Comparison of lipoic and asparagusic acid for surface-initiated disulfide-exchange polymerization. *Chemistry* **2013,** *19*, 11558-11563.

69. A. Burns, G. M. W. Predicting the stability of cyclic disulfides by molecular modeling: "effective concentrationsin" thiol-disulfide interchange and the design of strongly reducing dithiols. *J. Am. Chem. Soc.* **1990,** *112*, 6296–6303.

## Supporting information

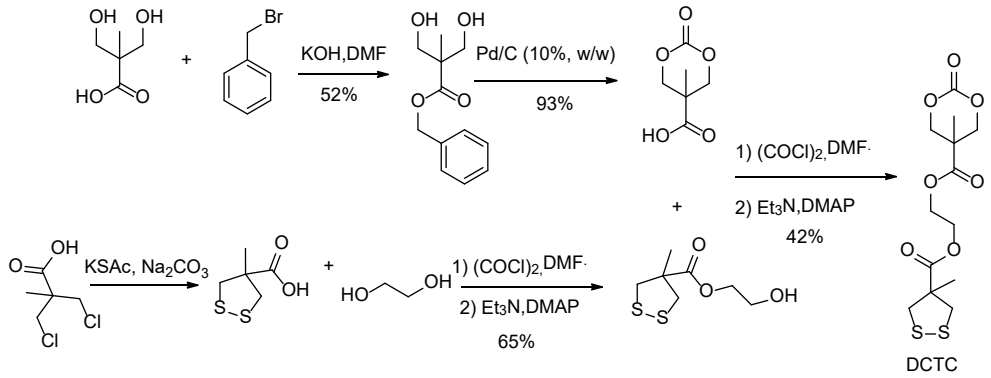


**Scheme S1.** Synthesis of DdeTC monomer according to previous reports.[1-3]

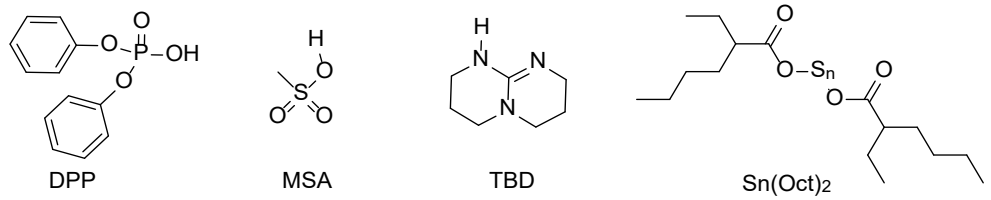


**Figure S1.** Structures of different catalysts used in this study.

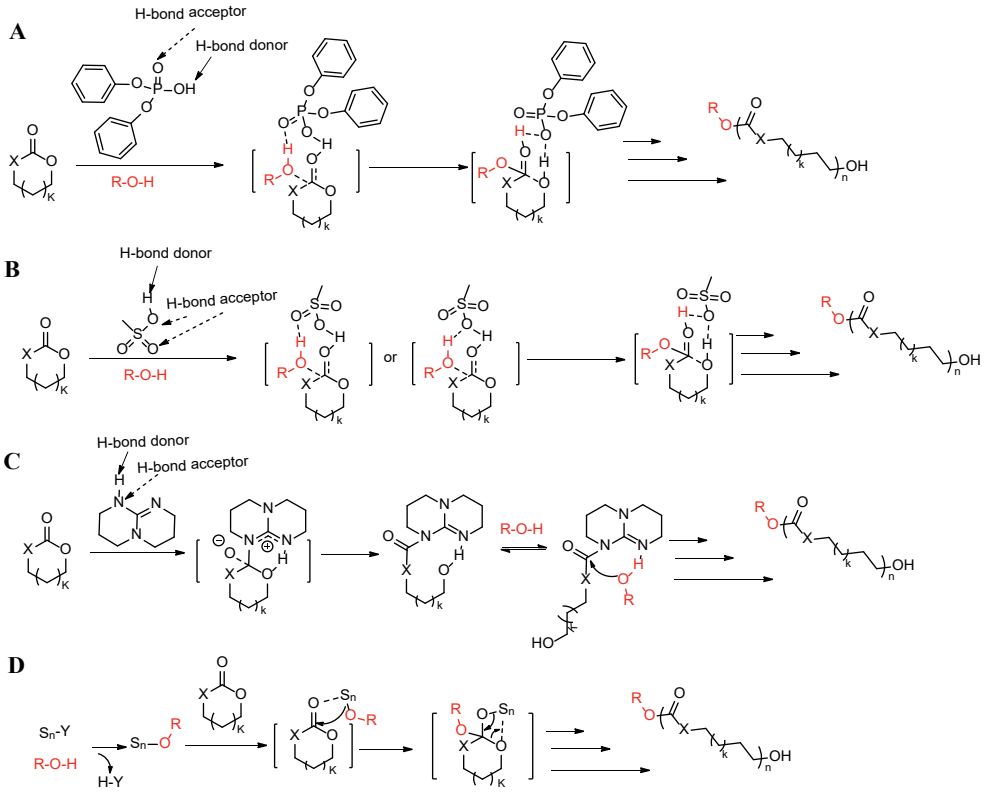


**Scheme S2**. Mechanisms for the ring opening polymerization of a cyclic ester or carbonate by different catalysts as proposed in the literature: ε-caprolactone (X=$CH_2$, k=2) and trimethylene carbonate (X=O, k=1) catalyzed by DPP (A) [4], MSA (B) [5], TBD (C) [6] and (D) [7]. Sn-Y in (D) represents $Sn(Oct)_2$.

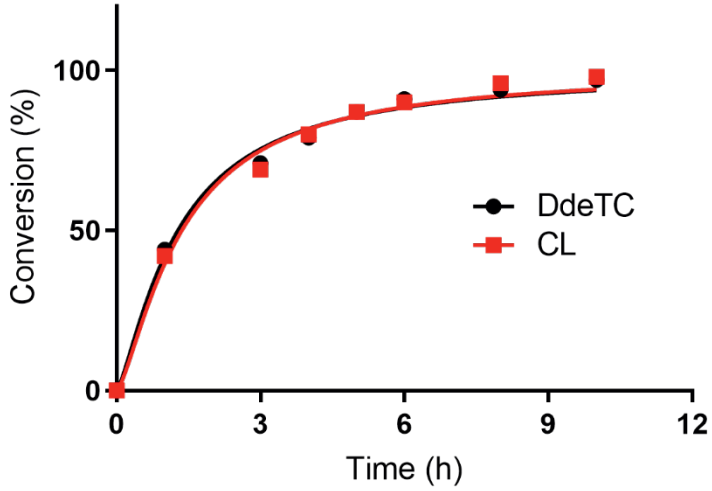


**Figure S2.** Conversion of CL (red squares) and DdeTC (black dots) during simultaneous copolymerization using MSA as catalyst with CL/DdeTC/initiator molar ratio of 9/4/1 (Entry 15, table 1), as determined by $^1$H-NMR.

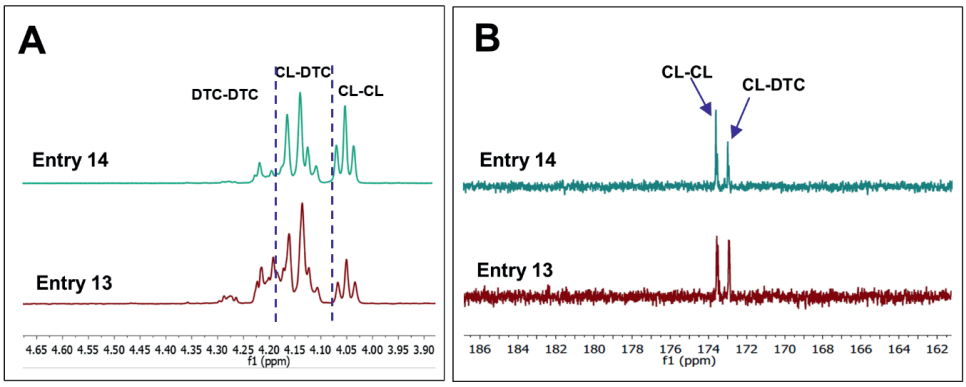


**Figure S3.** $^{1}$H (A) and $^{13}$C (B) -NMR spectra of p($CL_9$-$DTC_{6.6}$)-PEG (Entry 13) and p($CL_{18}$-$DTC_{7.5}$)-PEG (Entry 14) copolymers obtained by simultaneous polymerization of CL and DTC at a CL/DTC/mPEG-OH feed molar ratio of 9/8/1 and 18/8/1, respectively, using MSA as catalyst. $^{1}$H-NMR spectra (600MHz, $CDCl_3$) show the region of methylene protons linked to oxy-carbonyl group (C***H*****$_2$**OCO) while $^{13}$C-NMR spectra (150 MHz, $CDCl_3$) display a region of the caprolactone-carbonyl carbons. All the entries presented in the legend correspond to the same entries in table 1.

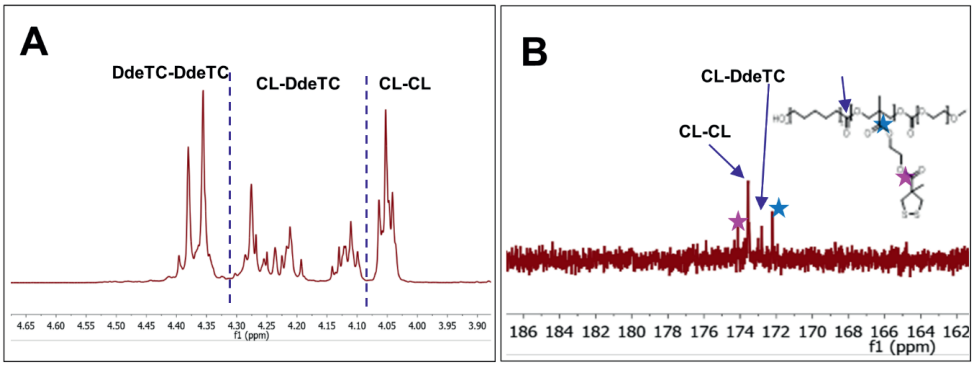


**Figure S4.** $^{1}$H (A) and $^{13}$C (B) -NMR spectra of p($CL_9$-$DdeTC_{3.1}$)-PEG (Entry 15, table 1) copolymer obtained with MSA as catalyst, at a CL/DdeTC/initiator feed molar ratio of 9/4/1. $^{1}$H-NMR spectrum (600MHz, $CDCl_3$) shows the region of methylene protons linked to oxy-carbonyl group (C***H*****$_2$**OCO) while $^{13}$C-NMR spectrum (150 MHz, $CDCl_3$) displays the region of the caprolactone-carbonyl carbons. Peaks labeled by stars in (B) are assigned to the carbonyl carbons in the side chain of the copolymer while peaks pointed by arrows in (B) are assigned to the carbonyl carbons in the backbone of the copolymer and used to distinguish different diads in the backbone of the copolymer.

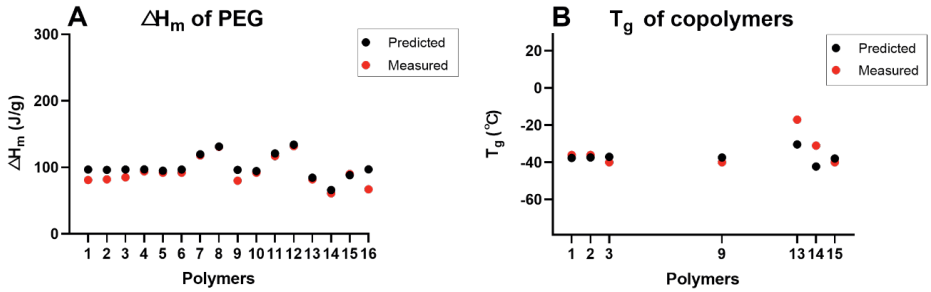


**Figure S5**. (A) Measured $\Delta H_m$'s of PEG in the synthesized block copolymers (red dots), corrected for the weight fraction of PEG of the block copolymer. The predicted $\Delta H_m$'s (black dots) were obtained by using mPEG-OH (182 J/g, Entry 17, table 1 and the weight fraction of PEG in the block copolymers) as the reference. (B) Measured $T_g$'s of the synthesized p(CL-*co*-DTC)-PEG and p(CL-*co*-DdeTC)-PEG copolymers (red dots) with random distribution of CL and DTC or DdeTC. Predicted $T_g$'s (black dots) were calculated based on the FOX equation in which $T_g$ of –60 °C for high molecular weight $PCL_{80}$ [8] and $T_g$'s of –6.3 and -17 °C for pDTC and pDdeTC (obtained from pDTC-PEG and pDdeTC-PEG, Entries 8 and 16, table 1), respectively, were used as references for the predictions. The numbers of the polymers on x-axis correspond to the same entries in table 1.



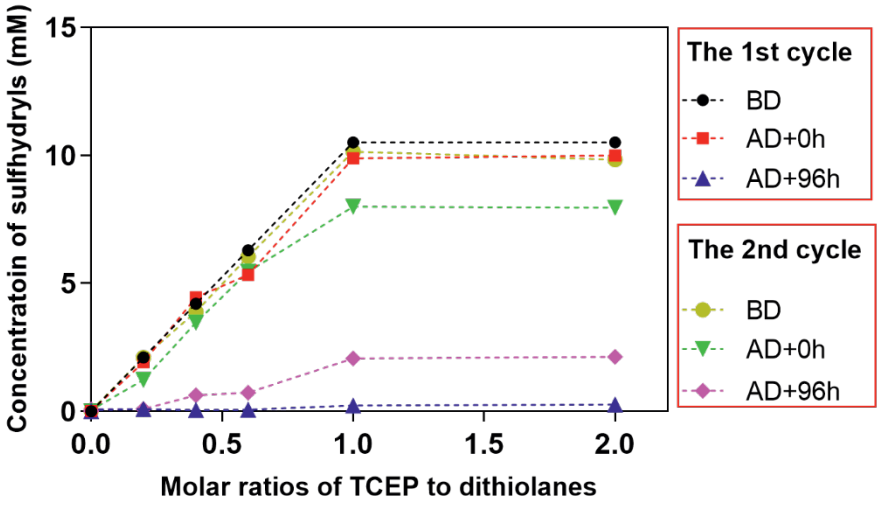


**Figure S6.** The concentrations of sulfhydryls (-SH) present in p($CL_{18}$-$DTC_{7.5}$)-PEG micellar dispersions as determined by Ellman's assay, after incubation with 0 to 2 equivalent TCEP relative to dithiolanes for 7 h at 37 °C (indicated by "BD" in the legend), after removal of the corresponding amount of TCEP by dialysis (indicated by "AD+0h" in the legend) and 96 h after dialysis (indicated by "AD+96h" in the legend). In the legend, the first cycle represents micellar dispersions that were freshly prepared, while in the second cycle micellar dispersions were used that were collected from the first cycle at "AD+96h" timepoint. Polymer concentrations were 4 mg/mL, corresponding to ~5 mM of dithiolanes (*i.e.,* ~10 mM of sulfhydryls when the dithiolanes are completely reduced).

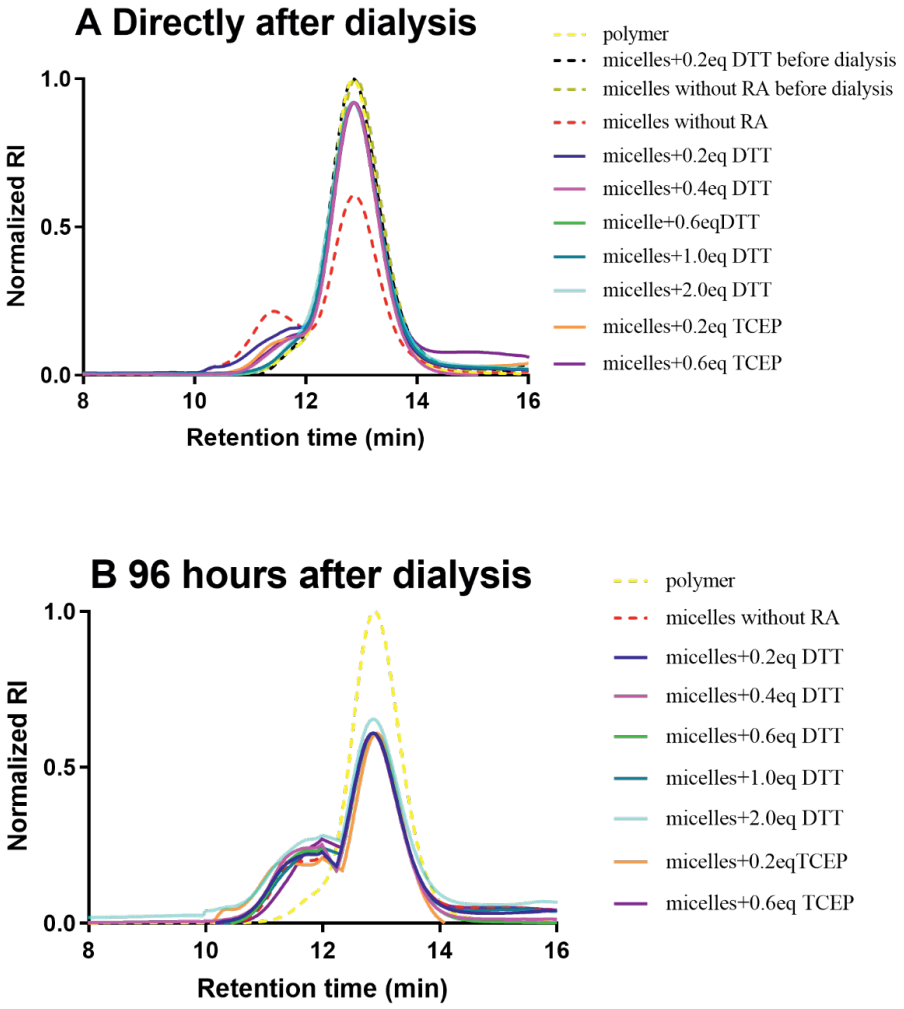


**Figure S7.** GPC chromatograms of p($CL_{18}$-$DTC_{7.5}$)-PEG micellar dispersions recorded by refractive index (RI) detector; micellar dispersions were first incubated with reducing agent (RA), *i.e.,* TCEP or DTT at various equivalent ratios (eq) to dithiolanes for 7 h at 37 °C, followed by dialysis while the micellar samples were collected right after dialysis (A) and 96 h after dialysis (B). In the legend, "polymer" represents P($CL_{18}$-$DTC_{7.5}$)-PEG copolymer as synthesized and immediately dissolved in DMF as a control, while "micelles without RA before dialysis" and "micelles+0.2 eq DTT before dialysis" in the legend of figure (A) were representative micellar samples prepared by nanoprecipitation and collected before dialysis. All the micellar samples were lyophilized and then dissolved in DMF for GPC analysis. The RI signals of samples were normalized to the RI signal of the polymer.

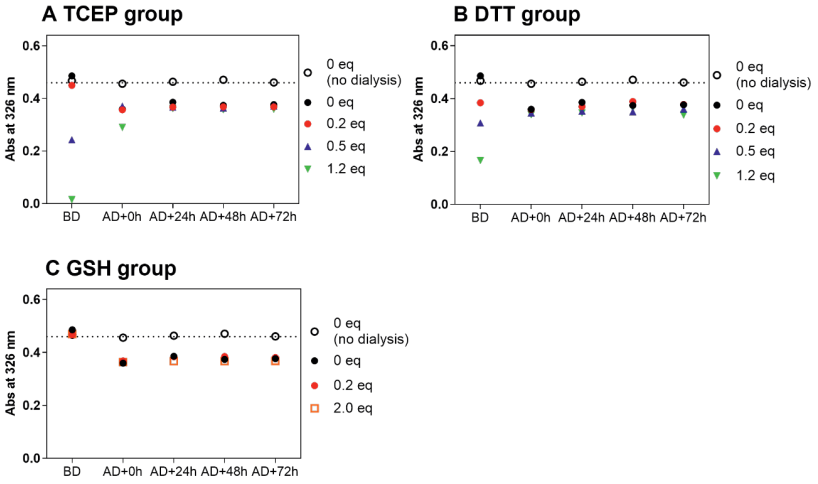


**Figure S8.** Absorbance (Abs) of p($CL_9$-$DTC_{3.9}$)-PEG (**Entry 2**, table 1) micellar dispersions at 326 nm in time before and after dialysis; micellar dispersions at polymer concentrations of 4 mg/mL in PBS/DMF (9/1 v/v) were incubated with different reducing agent: TCEP (A); DTT (B); GSH (C), respectively at various amounts (shown by the different symbols) for 7 h at 37 °C and then dialyzed against PBS for 12 h while the absorbance of these micellar dispersions was recorded before dialysis (BD), directly after dialysis (presented as "AD+0h") and at different timepoints after dialysis. "0 eq (no dialysis) " represents control micelles kept in PBS/DMF (9/1 v/v) without being preincubated with any reducing agent and not dialyzed.



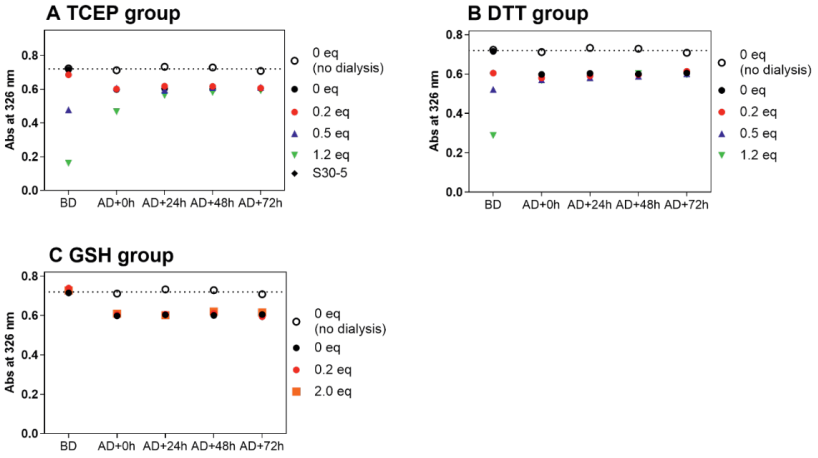


**Figure S9.** Absorbance (Abs) of p($CL_{9.1}$-*b*-$DTC_{4.1}$)-PEG (**Entry 5**, table 1) micellar dispersions at 326 nm in time before and after dialysis; micellar dispersions at polymer concentrations of 4 mg/mL in PBS/DMF (9/1 v/v) were incubated with different reducing agent: TCEP (A); DTT (B); GSH (C), respectively at various amounts (shown by the different symbols) for 7 h at 37 °C and then dialyzed against PBS for 12 h while the absorbance of these micellar dispersions was recorded before dialysis (BD), directly after dialysis (presented as "AD+0h") and at different timepoints after dialysis. "0 eq (no dialysis) " represents control micelles kept in PBS/DMF (9/1 v/v) without being preincubated with any reducing agent and not dialyzed.

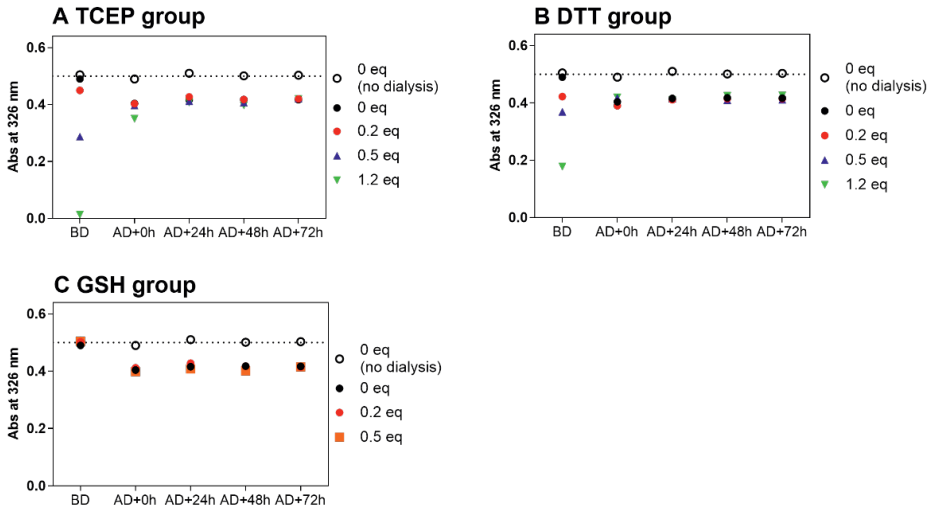


**Figure S10.** Absorbance (Abs) of p(DTC$_{3.8}$-*b*-CL$_9$)-PEG (**Entry 6**, table 1) micellar dispersions at 326 nm in time before and after dialysis; micellar dispersions at polymer concentrations of 4 mg/mL in PBS/DMF (9/1 v/v) were incubated with different reducing agent: TCEP (A); DTT (B); GSH (C), respectively at various amounts (shown by the different symbols) for 7 h at 37 °C and then dialyzed against PBS for 12 h while the absorbance of these micellar dispersions was recorded before dialysis (BD), directly after dialysis (presented as "AD+0h") and at different timepoints after dialysis. "0 eq (no dialysis) " represents control micelles kept in PBS/DMF (9/1 v/v) without being preincubated with any reducing agent and not dialyzed.

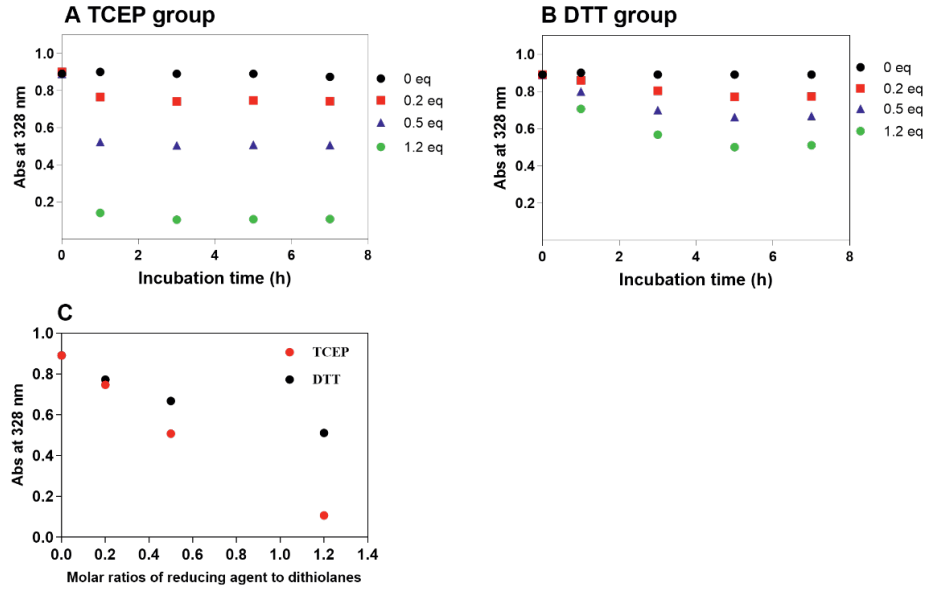


**Figure S11.** (A-B) Absorbance (Abs) of DdeTC at 328 nm in micellar dispersions consisting of P(CL$_9$-DdeTC$_{3.1}$)-PEG (**Entry 15**, table 1) during incubation with various amounts of TCEP (A) or DTT (B) at 37 °C. The legend indicates equivalent ratios (eq) of corresponding reducing agent to dithiolanes in the micellar dispersions. (C) Absorbance (Abs) of DdeTC recorded after 7 h, as a function of molar ratios of reducing agent to dithiolanes.

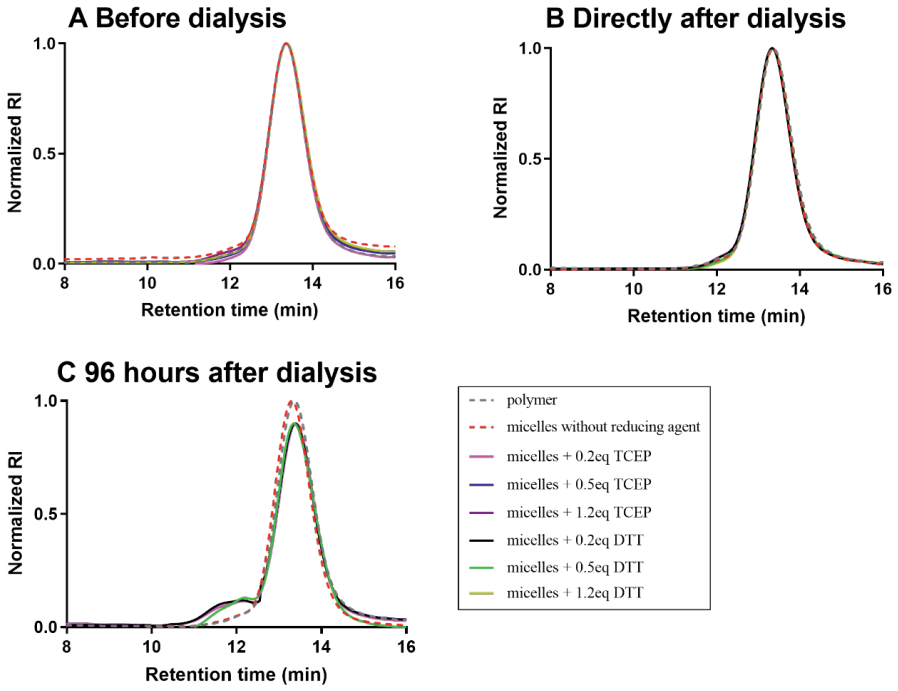


**Figure S12.** GPC chromatograms of micellar dispersions consisting of p($CL_9$-Dde$TC_{3.1}$)-PEG (Entry 5, table 1) recorded by refractive index (RI) detector; micellar dispersions were collected after 7 h incubation with TCEP or DTT at various equivalent ratios (eq) of reducing agent to dithiolanes at 37 °C (A, *i.e.,* before dialysis), directly after subsequent dialysis (B) and upon 96 h aging after dialysis (C), respectively. In the legend, "polymer" represents p($CL_9$-Dde$TC_{3.1}$)-PEG copolymer as synthesized and directly dissolved in DMF as a control. All the micellar samples were lyophilized and then dissolved in DMF for GPC analysis. The RI signals of samples were normalized to the RI signal of the polymer.

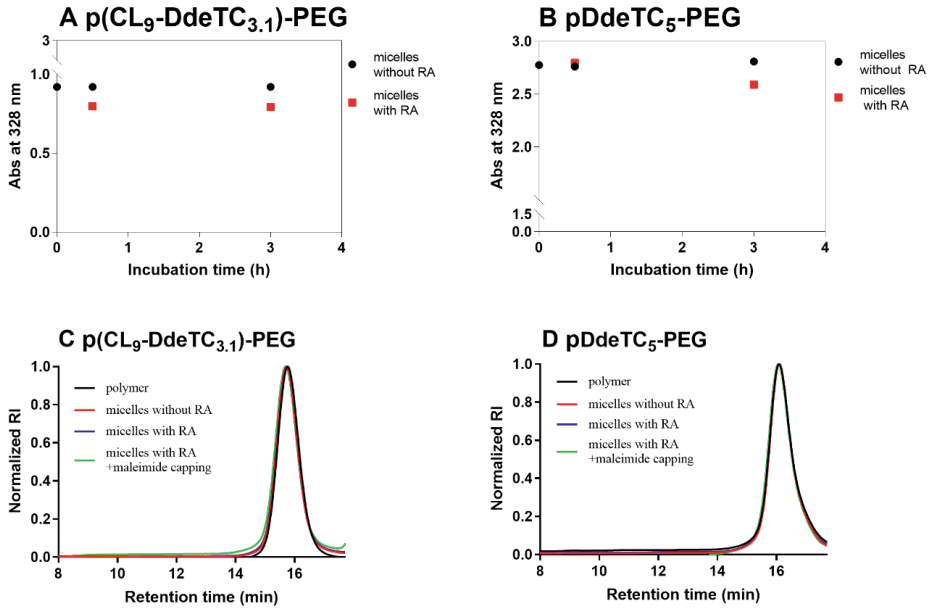


**Figure S13.** (A-B) Absorbance (Abs) and (C-D) GPC chromatograms of micellar dispersions composed of p($CL_9$-Dde$TC_{3.1}$)-PEG (A, C) (Entry 15, table 1) and pDde$TC_5$-PEG (B, D) (Entry 16, table 1), recorded at 328 nm and by refractive index (RI) detector, respectively. Dispersions were incubated with/without 3,6-dioxa-1,8-octanedithiol (0.2 equiv. relative to dithiolanes), presented as "micelles with RA" and "micelles without RA" in the legend. Detailed method is described below. The absorbance of the resulting dispersions was recorded after 30 min and 3 h incubation. For GPC analysis, dispersions were used with/without exposure to 3,6-dioxa-1,8-octanedithiol for 3 h and with/without subsequent maleimide capping (*i.e.,* "micelles with RA+maleimide capping" in the legend of (C, D)). As controls, the synthesized polymers used for preparation of the micelles were dissolved in DMF and presented as "polymer" in the legend of (C, D). All micellar samples were lyophilized and then dissolved in DMF for GPC. The RI signals of samples were normalized to the RI signal of the polymer.

***Method:*** Micelles dispersions were prepared as described previously.[3] Briefly, 3,6-dioxa-1,8-octanedithiol (0.2 equiv. relative to dithiolanes) was added to a dispersion of copolymers in water (10 mg/mL of p($CL_9$-Dde$TC_{3.1}$)-PEG or 20 mg/mL of pDde$TC_5$-PEG), followed by vortexing and equilibration in the dark for 30 min and 3 h. For the maleimide capping, half of the above dispersions were transferred into another vial to which maleimide (5 equiv. relative to thiol) was added, followed by vortexing until all maleimide dissolved. The absorbance of the resulting dispersions at 328 nm during equilibration was recorded using a Shimadzu UV-2450 spectrophotometer (Shimadzu, Japan). In addition, samples collected from the above mentioned micellar dispersions were freeze-dried and then re-dissolved in DMF at 5 mg/mL for GPC analysis as described in section 2.4.

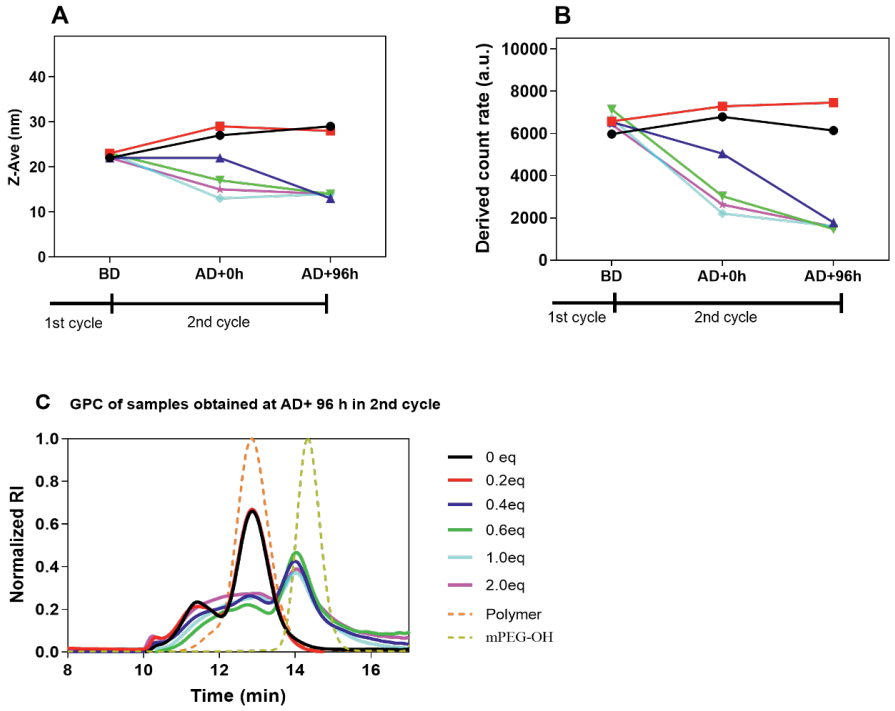


**Figure S14.** Size (A) and derived count rate (B) of micellar dispersions composed of p($CL_{18}$-$DTC_{7.5}$)-PEG (Entry 14, table 1) as determined by DLS in the second cycle after re-incubation with indicated equivalents of TCEP for 7 h at 37 °C (presented as "BD"), after subsequent dialysis (presented as "AD+0 h"), and 96 h after dialysis (presented as "AD+96 h"); micellar dispersions were collected from the first cycle (*i.e.,* freshly prepared micellar dispersions incubated with various amounts of TCEP for 7 h at 37 °C, followed by dialysis and 96 h aging after dialysis). (C) GPC curves of p($CL_{18}$-$DTC_{7.5}$)-PEG micellar dispersions obtained at the above mentioned "AD+96h" timepoint in the second cycle. All micellar samples were lyophilized and then dissolved in DMF for GPC analysis, while the synthesized polymers dissolved in DMF were used as a control. The RI signals of samples were normalized to the RI signal of the polymer.

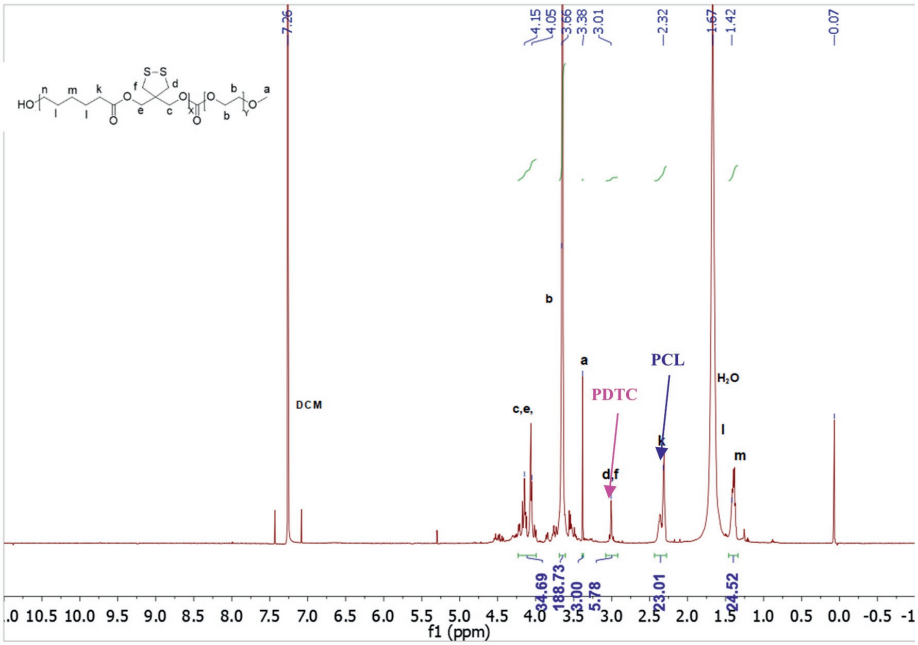


**Figure S15.** $^{1}$H-NMR spectrum (600 MHz, $CDCl_3$) of lyophilized micellar dispersion composed of p($CL_{18}$-$DTC_{7.5}$)-PEG (Entry 14, table 1) from the second cycle of exposure to TCEP, *i.e.*, micellar dispersion were twice incubated with 1 equivalent TCEP relative to dithiolanes for 7 h at 37 ℃, dialyzed and aged for 96 h.

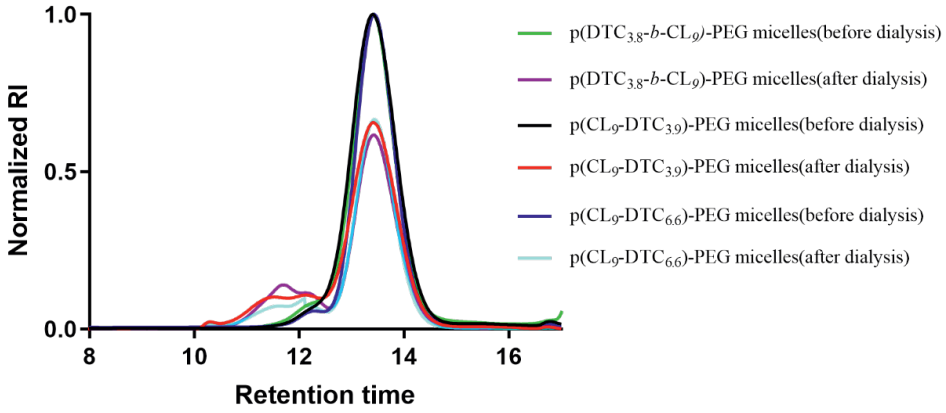


**Figure S16.** GPC chromatograms (using refractive index (RI) detection) of micelles composed of p($DTC_{3.8}$-*b*-$CL_9$)-PEG (Entry 6, table 2), p($CL_9$-$DTC_{3.9}$)-PEG (Entry 2, table 2), or p($CL_9$-$DTC_{6.6}$)-PEG (Entry 13, table 2) before and after dialysis; micellar dispersions were prepared by dropwise addition of polymer solution in DMF to PBS (pH 7.4) at a volume ratio of 1:9, followed by dialysis against PBS for 12 h. Micellar dispersions before and after dialysis were collected and lyophilized, followed by dissolution in DMF for GPC analysis.

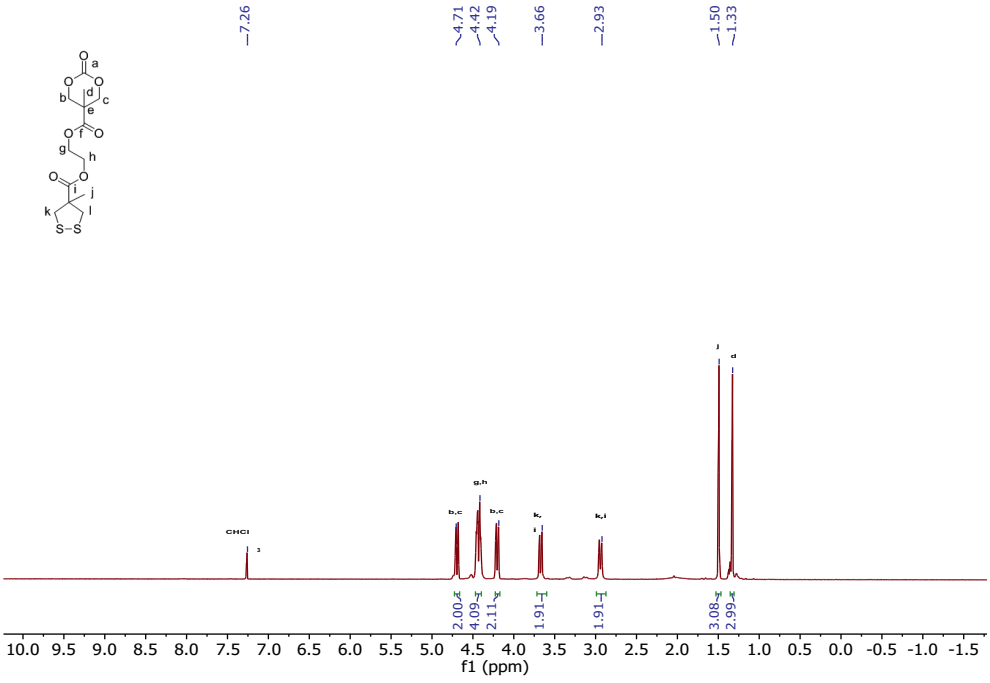


**Figure S17.** $^{1}$H-NMR spectrum (600 MHz, $CDCl_3$) of DdeTC.

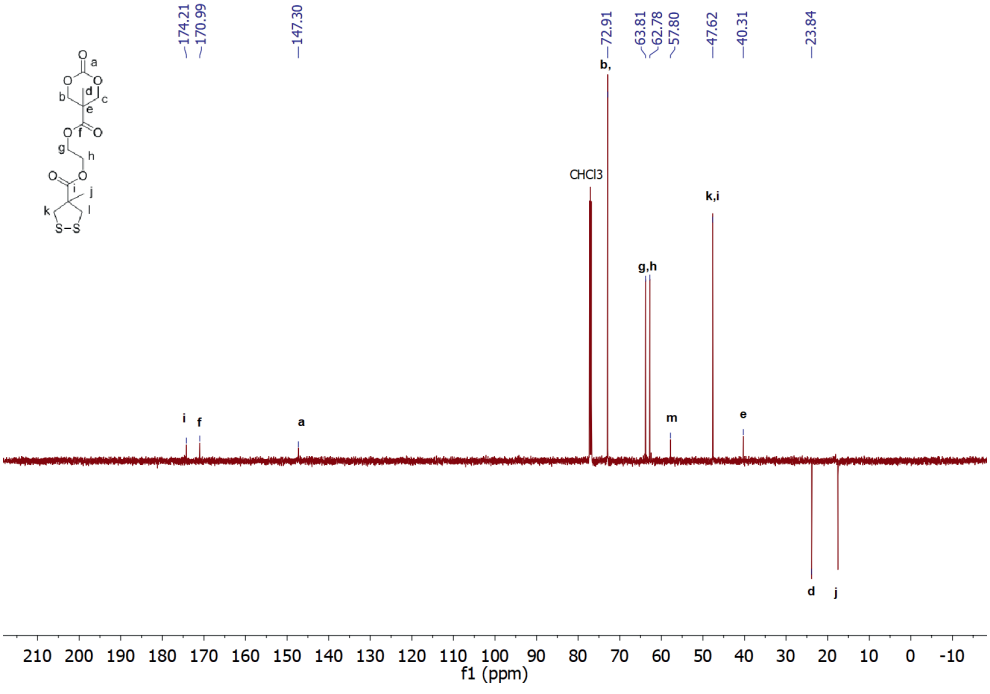


**Figure S18.** $^{13}$C-NMR spectrum (150 MHz, $CDCl_3$) of DdeTC monomer.

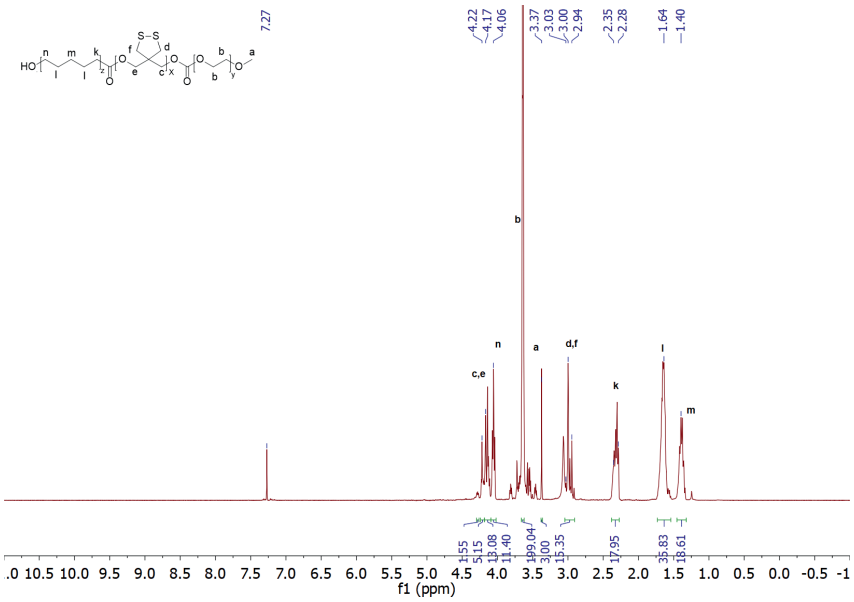


**Figure S19.** $^{1}$H-NMR spectrm (600 MHz, $CDCl_3$) of p($CL_9$-$DTC_{3.8}$)-PEG block copolymer synthesized by ROP and catalyzed by DPP (Entry 1, table 1). $^{1}$H-NMR (600 MHz, $CDCl_3$): δ 4.29–4.00 (m, COO***CH***$_2$C***CH***$_2$OCO, ***CH***$_2$OH), 3.63 (m, PEG protons), 3.37 (s, ***CH***$_3$O), 2.97 (m, C***CH***$_2$SS***CH***$_2$C), 2.32 (m, $CH_2CH_2$***CH***$_2$COO), 1.64 (m, $CH_2$***CH***$_2CH_2$***CH***$_2CH_2$), 1.40 (m, $CH_2CH_2$***CH***$_2CH_2CH_2$).

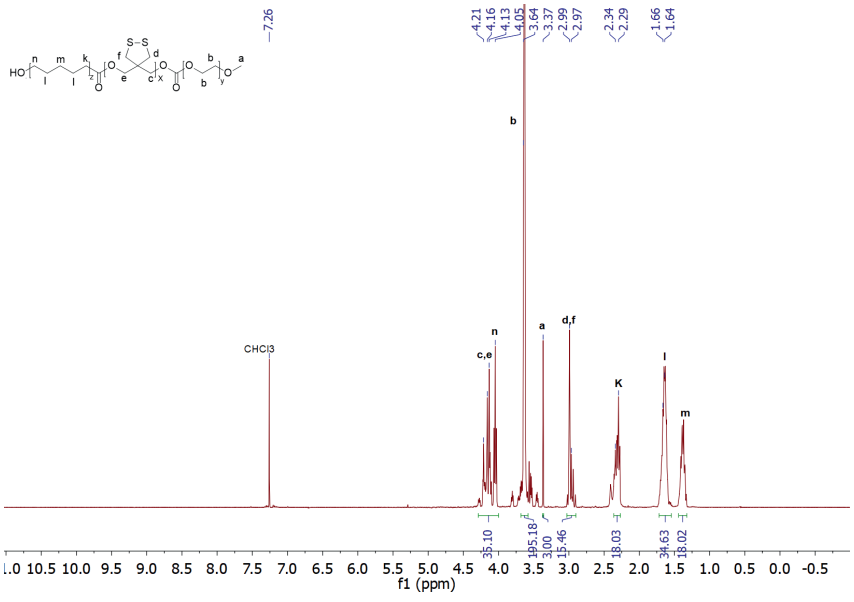


**Figure S20**. $^{1}$H-NMR spectrum (600 MHz, $CDCl_3$) of p($CL_9$-$DTC_{3.9}$)-PEG block copolymer synthesized by ROP catalyzed by MSA (Entry 2, table 1). $^{1}$H-NMR (600 MHz, $CDCl_3$): δ 4.29–4.00 (m, COO***CH***$_2$C***CH***$_2$OCO, ***CH***$_2$OH), 3.63 (m, PEG protons), 3.37 (s, ***CH***$_3$O), 2.97 (m, C***CH***$_2$SS***CH***$_2$C), 2.32 (m, $CH_2CH_2$***CH***$_2$COO), 1.65 (m, $CH_2$***CH***$_2CH_2$***CH***$_2CH_2$), 1.39 (m, $CH_2CH_2$***CH***$_2CH_2CH_2$).

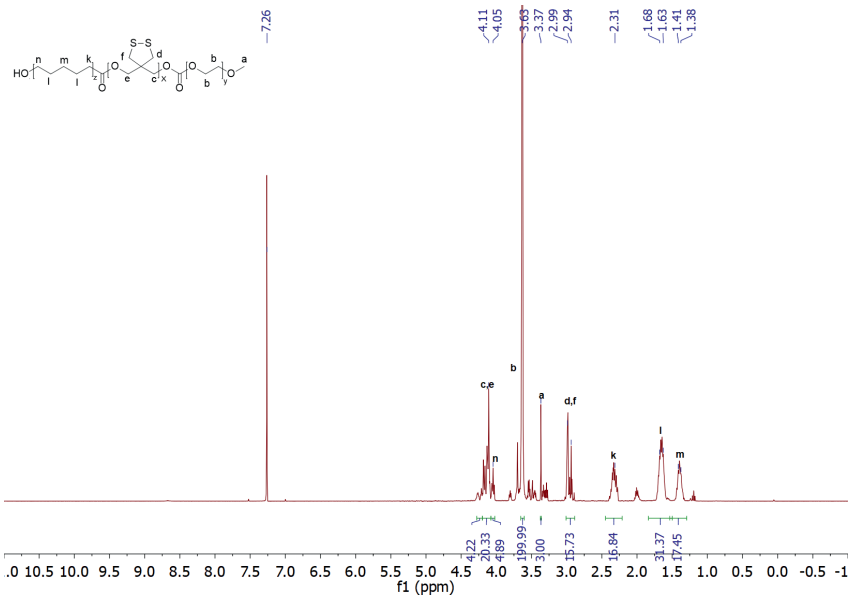


**Figure S21**. $^{1}$H-NMR spectrum (600 MHz, $CDCl_3$) of p($CL_{8.4}$-$DTC_{3.9}$)-PEG block copolymer synthesized by ROP catalyzed by TBD (Entry 3, table 1). $^{1}$H-NMR (600 MHz, $CDCl_3$): δ 4.29–4.00 (m, COO***CH*****$_2$**C***CH*****$_2$**OCO, ***CH*****$_2$**OH), 3.63 (m, PEG protons), 3.37 (s, ***CH*****$_3$**O), 2.97 (m, C***CH*****$_2$**SS***CH*****$_2$**C), 2.31 (m, $CH_2CH_2$***CH*****$_2$**COO), 1.65 (m, $CH_2$***CH*****$_2$**$CH_2$***CH*****$_2$**$CH_2$), 1.38 (m, $CH_2CH_2$***CH*****$_2$**$CH_2CH_2$).

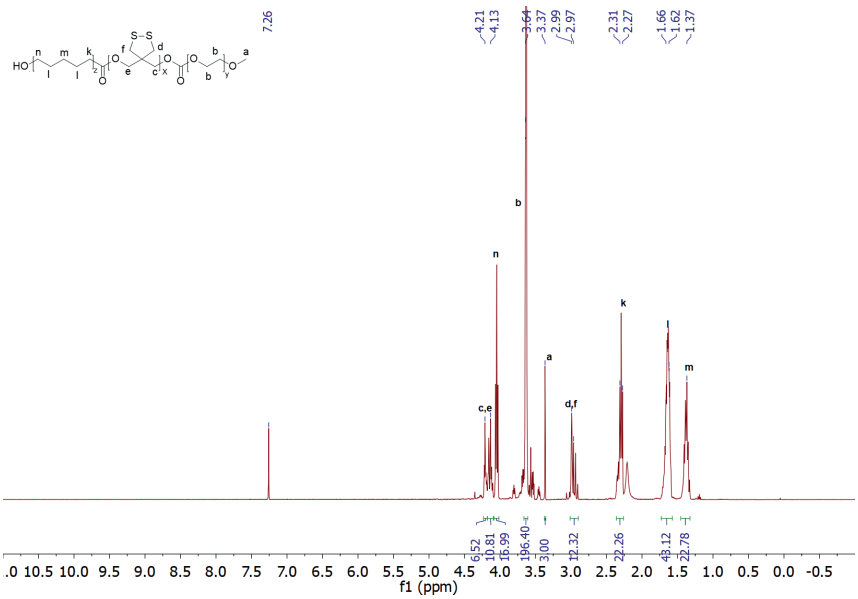


**Figure S22.** $^{1}$H-NMR spectrum (600 MHz, $CDCl_3$) of p($CL_{10.1}$-$DTC_{3.1}$)-PEG block copolymer synthesized by ROP catalyzed by $Sn(Oct)_2$ (Entry 4, table 1). $^{1}$H-NMR (600 MHz, $CDCl_3$): δ 4.29–4.00 (m, COO***CH*****$_2$**C***CH*****$_2$**OCO, ***CH*****$_2$**OH), 3.63 (m, PEG protons), 3.37 (s, ***CH*****$_3$**O), 2.97 (m, C***CH*****$_2$**SS***CH*****$_2$**C), 2.31 (m, $CH_2CH_2$***CH*****$_2$**COO), 1.66 (m, $CH_2$***CH*****$_2$**$CH_2$***CH*****$_2$**$CH_2$), 1.37 (m, $CH_2CH_2$***CH*****$_2$**$CH_2CH_2$).

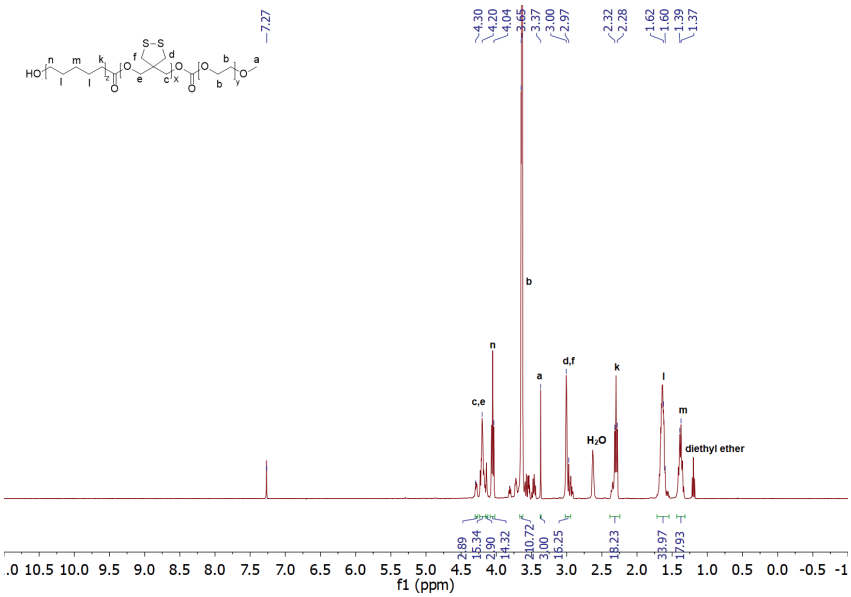


**Figure S23**. $^1$H-NMR spectrum (600 MHz, $CDCl_3$) of p($CL_{9.1}$-*b*-$DTC_{4.1}$)-PEG block copolymer synthesized by ROP catalyzed by MSA (Entry 5, Table 1). $^1$H-NMR (600 MHz, $CDCl_3$): δ 4.29–4.00 (m, COO***CH***$_2$C***CH***$_2$OCO, ***CH***$_2$OH), 3.63 (m, PEG protons), 3.37 (s, ***CH***$_3$O), 2.97 (m, C***CH***$_2$SS***CH***$_2$C), 2.29 (m, $CH_2CH_2$***CH***$_2$COO), 1.62 (m, $CH_2$***CH***$_2CH_2$***CH***$_2CH_2$), 1.39 (m, $CH_2CH_2$***CH***$_2CH_2CH_2$).

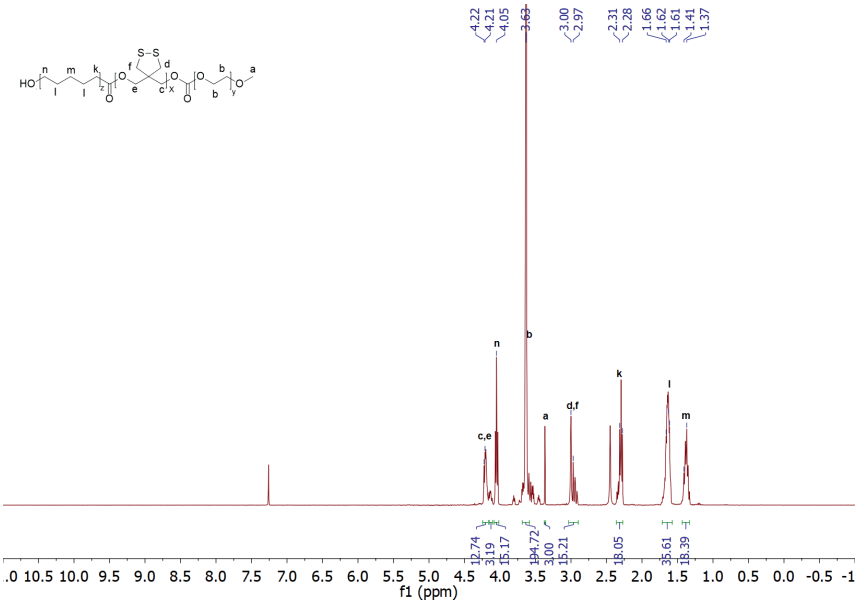


**Figure S24**. $^1$H-NMR spectrum (600 MHz, $CDCl_3$) of p($DTC_{3.8}$-*b*-$CL_9$)-PEG block copolymer synthesized by ROP catalyzed by MSA (Entry 6, table 1). $^1$H-NMR (600 MHz, $CDCl_3$): δ 4.29–4.00 (m, COO***CH***$_2$C***CH***$_2$OCO, ***CH***$_2$OH), 3.63 (m, PEG protons), 3.37 (s, ***CH***$_3$O), 2.97 (m, C***CH***$_2$SS***CH***$_2$C), 2.29 (m, $CH_2CH_2$***CH***$_2$COO), 1.65 (m, $CH_2$***CH***$_2CH_2$***CH***$_2CH_2$), 1.39 (m, $CH_2CH_2$***CH***$_2CH_2CH_2$).

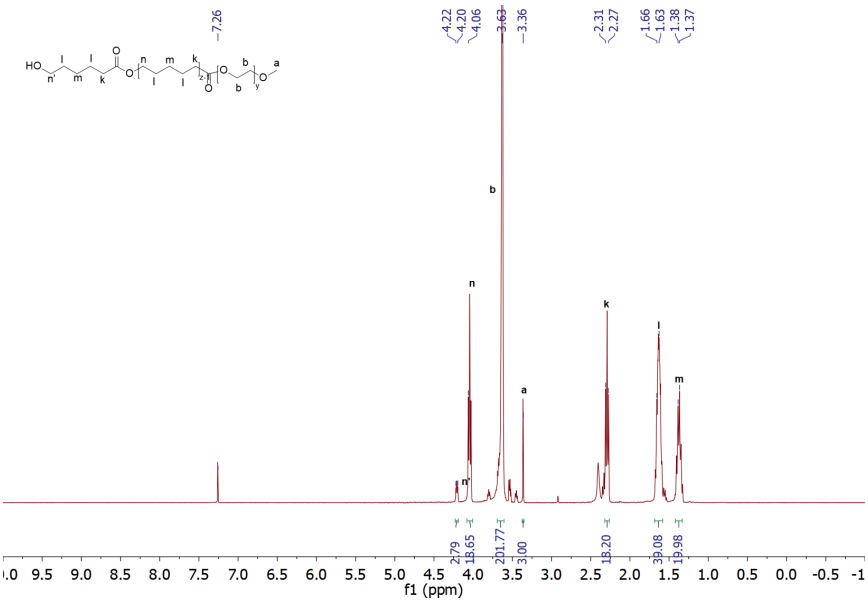


**Figure S25**. $^1$H-NMR spectrum (600 MHz, $CDCl_3$) of $pCL_{9.1}$-PEG block copolymer synthesized by ROP catalyzed by MSA (Entry 7, table 1). $^1$H-NMR (600 MHz, $CDCl_3$): δ 4.29–4.00 (m, COO***CH*****$_2$**, $CH_2$***CH*****$_2$**OH), 3.64 (m, PEG protons), 3.37 (s, ***CH*****$_3$**O), 2.29 (m, $CH_2CH_2$***CH*****$_2$**COO), 1.66 (m, $CH_2$***CH*****$_2$**$CH_2$***CH*****$_2$**$CH_2$), 1.38 (m, $CH_2CH_2$***CH*****$_2$**$CH_2CH_2$).

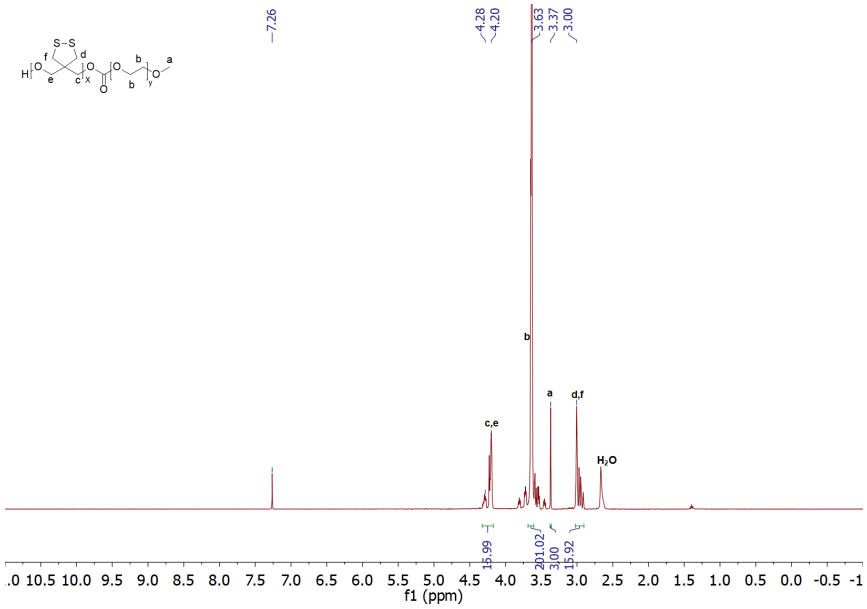


**Figure S26**. $^1$H-NMR spectrum (600 MHz, $CDCl_3$) of $pDTC_4$-PEG block copolymer synthesized by ROP catalyzed by MSA (Entry 8, table 1). $^1$H-NMR (600 MHz, $CDCl_3$): δ 4.29–4.00 (m, COO***CH*****$_2$**C***CH*****$_2$**OCO, ***CH*****$_2$**OH), 3.63 (m, PEG protons), 3.37 (s, ***CH*****$_3$**O), 3.00 (m, C***CH*****$_2$**SS***CH*****$_2$**C).

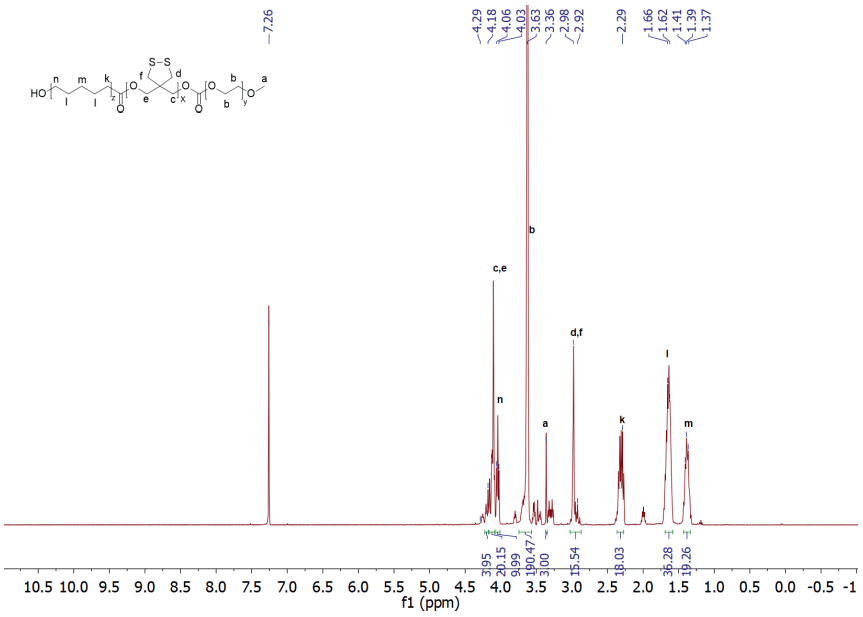


**Figure S27**. $^{1}$H-NMR spectrum (600 MHz, $CDCl_3$) of p($CL_9$-$DTC_{3.9}$)-PEG block copolymer synthesized by ROP catalyzed by TBD (Entry 9, table 1). $^{1}$H-NMR (600 MHz, $CDCl_3$): δ 4.29–4.00 (m, COO***CH*****$_2$**C***CH*****$_2$**OCO, ***CH*****$_2$**OH), 3.63 (m, PEG protons), 3.37 (s, ***CH*****$_3$**O), 2.97 (m, C***CH*****$_2$**SS***CH*****$_2$**C), 2.29 (m, $CH_2CH_2$***CH*****$_2$**COO), 1.65 (m, $CH_2$***CH*****$_2$**$CH_2$***CH*****$_2$**$CH_2$), 1.39 (m, $CH_2CH_2$***CH*****$_2$**$CH_2CH_2$).

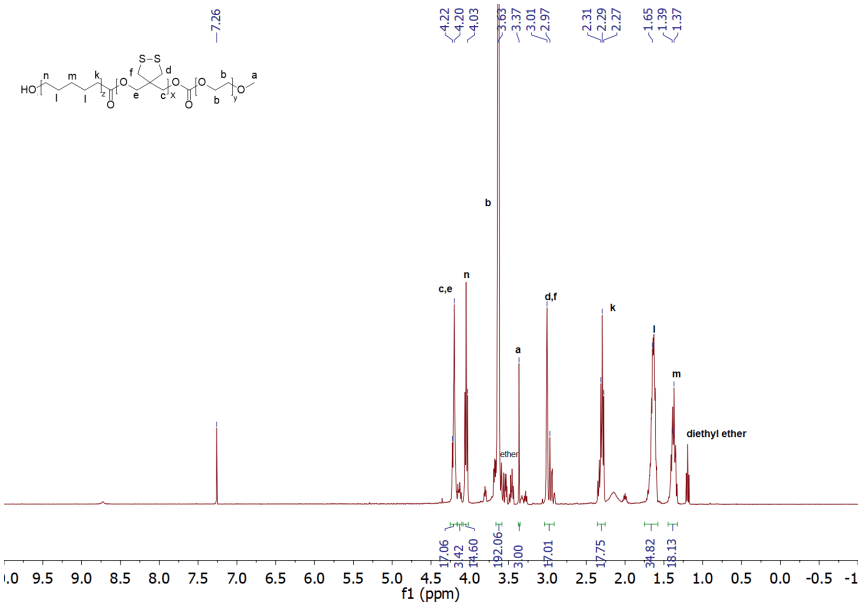


**Figure S28**. $^{1}$H-NMR spectrum (600 MHz, $CDCl_3$) of p($DTC_{4.3}$-*b*-$CL_{8.9}$)-PEG block copolymer synthesized by ROP catalyzed by TBD (Entry 10, table 1). $^{1}$H-NMR (600 MHz, $CDCl_3$): δ 4.29–4.00 (m, COO***CH*****$_2$**C***CH*****$_2$**OCO, ***CH*****$_2$**OH), 3.63 (m, PEG protons), 3.37 (s, ***CH*****$_3$**O), 2.97 (m, C***CH*****$_2$**SS***CH*****$_2$**C), 2.29 (m, $CH_2CH_2$***CH*****$_2$**COO), 1.65 (m, $CH_2$***CH*****$_2$**$CH_2$***CH*****$_2$**$CH_2$), 1.39 (m, $CH_2CH_2$***CH*****$_2$**$CH_2CH_2$).

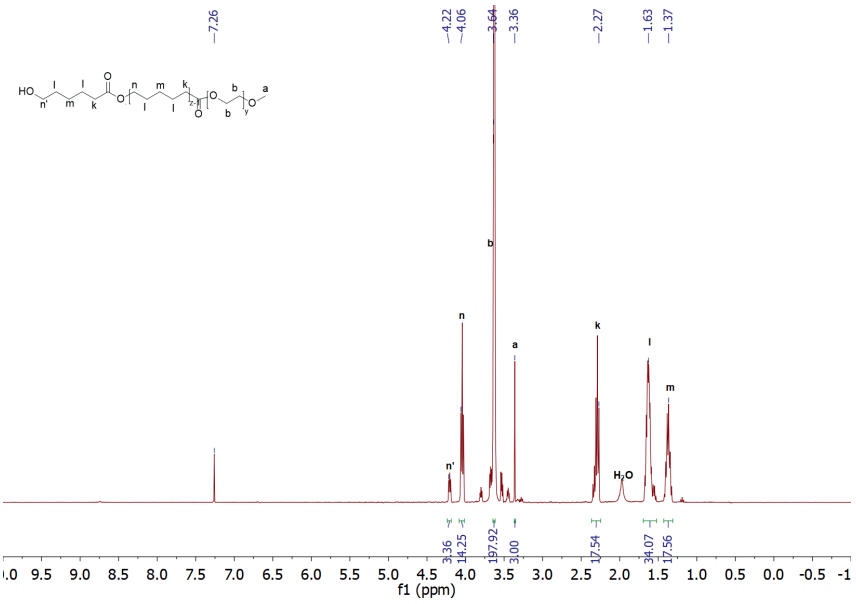


**Figure S29**. $^1$H-NMR spectrum (600 MHz, $CDCl_3$) of $pCL_{8.8}$-PEG block copolymer synthesized by ROP catalyzed by TBD (Entry 11, table 1). $^1$H-NMR (600 MHz, $CDCl_3$): δ 4.29–4.00 (m, COO***CH*****$_2$**C***CH*****$_2$**OCO, ***CH*****$_2$**OH), 3.64 (m, PEG protons), 3.37 (s, ***CH*****$_3$**O), 2.29 (m, $CH_2CH_2$***CH*****$_2$**COO), 1.63 (m, $CH_2$***CH*****$_2$**$CH_2$***CH*****$_2$**$CH_2$), 1.39 (m, $CH_2CH_2$***CH*****$_2$**$CH_2CH_2$).

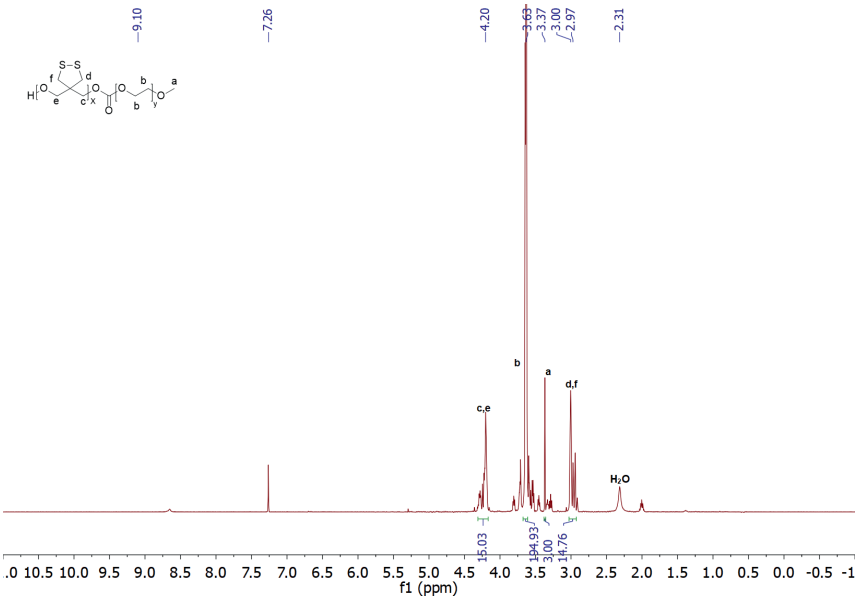


**Figure S30**. $^1$H-NMR spectrum (600 MHz, $CDCl_3$) of $pDTC_{3.7}$-PEG block copolymer synthesized by ROP catalyzed by TBD (Entry 12, table 1). $^1$H-NMR (600 MHz, $CDCl_3$): δ 4.29–4.00 (m, COO***CH*****$_2$**C***CH*****$_2$**OCO, ***CH*****$_2$**OH), 3.63 (m, PEG protons), 3.37 (s, ***CH*****$_3$**O), 3.00 (m, C***CH*****$_2$**SS***CH*****$_2$**C).

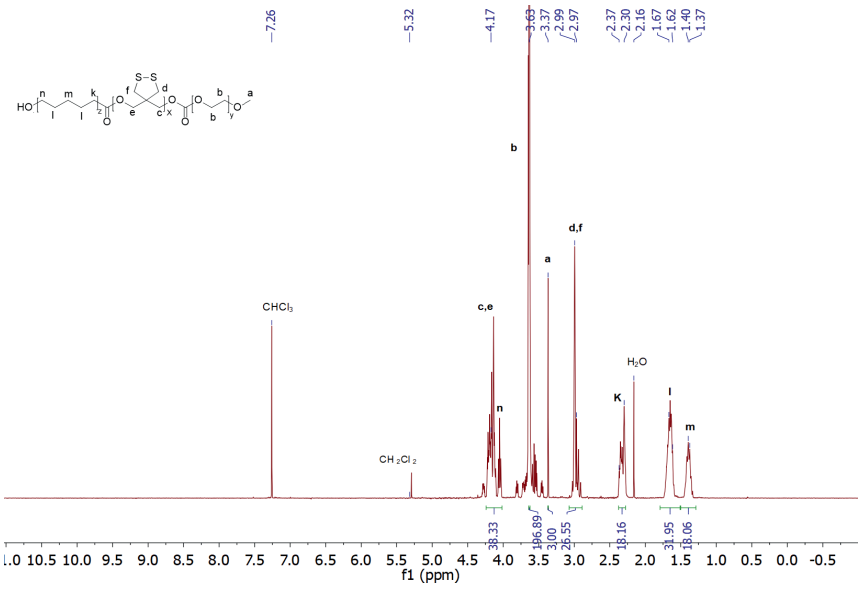


**Figure S31**. $^1$H-NMR spectrum (600 MHz, $CDCl_3$) of p($CL_9$-$DTC_{6.6}$)-PEG block copolymer synthesized by ROP catalyzed by MSA (Entry 13, table 1). $^1$H-NMR (600 MHz, $CDCl_3$): ): δ 4.29–4.00 (m, COO***CH*****$_2$**C***CH*****$_2$**OCO, ***CH*****$_2$**OH), 3.63 (m, PEG protons), 3.37 (s, ***CH*****$_3$**O), 2.97 (m, C***CH*****$_2$**SS***CH*****$_2$**C), 2.31 (m, $CH_2CH_2$***CH*****$_2$**COO), 1.66 (m, $CH_2$***CH*****$_2$**$CH_2$***CH*****$_2$**$CH_2$), 1.37 (m, $CH_2CH_2$***CH*****$_2$**$CH_2CH_2$).

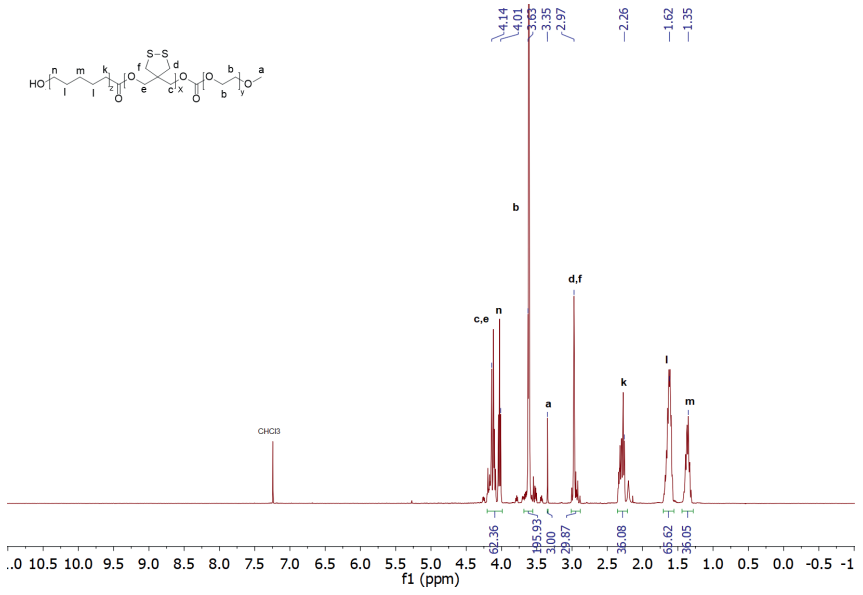


**Figure S32**. $^1$H-NMR spectrum (600 MHz, $CDCl_3$) of p($CL_{18}$-$DTC_{7.5}$)-PEG block copolymer synthesized by ROP catalyzed by MSA (Entry 14, table 1). $^1$H-NMR (600 MHz, $CDCl_3$): ): δ 4.29–4.00 (m, COO***CH*****$_2$**C***CH*****$_2$**OCO, ***CH*****$_2$**OH), 3.63 (m, PEG protons), 3.37 (s, ***CH*****$_3$**O), 2.97 (m, C***CH*****$_2$**SS***CH*****$_2$**C), 2.31 (m, $CH_2CH_2$***CH*****$_2$**COO), 1.66 (m, $CH_2$***CH*****$_2$**$CH_2$***CH*****$_2$**$CH_2$), 1.37 (m, $CH_2CH_2$***CH*****$_2$**$CH_2CH_2$).

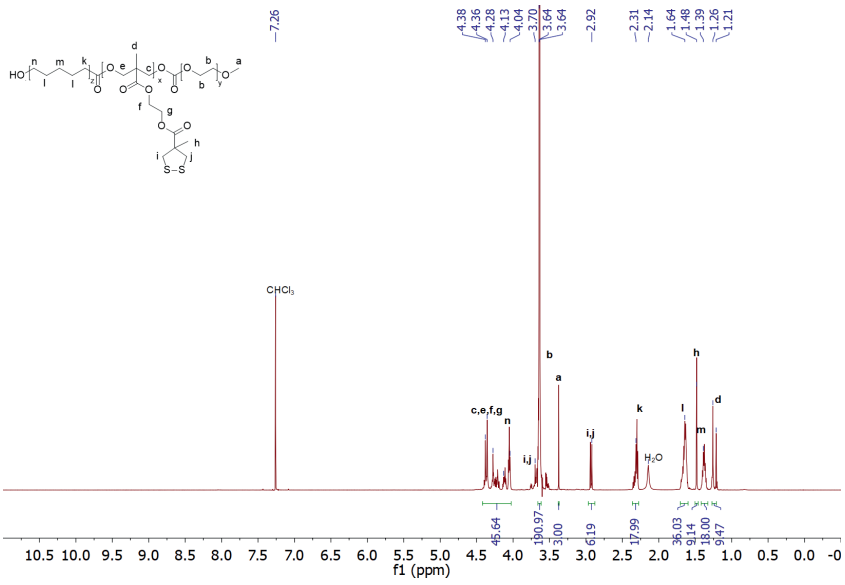


**Figure S33**. $^{1}$H-NMR spectrum (600 MHz, $CDCl_3$) of p($CL_9$-DdeT$C_{3.1}$)-PEG block copolymer synthesized by ROP catalyzed by MSA (Entry 15, table 1).$^{1}$H-NMR (600 MHz, $CDCl_3$): δ 4.42–4.13 (m, COO***CH***$_2$C***CH***$_2$OCO, COO***CH***$_2$***CH***$_2$COO), 4.04 (m, COC$H_2$C$H_2$C$H_2$C$H_2$***CH***$_2$OH), 3.70 (m, C***CH***$_2$SS***CH***$_2$C), 3.64 (m, PEG protons), 3.37 (s, 3H, ***CH***$_3$O), 2.92 (m, C***CH***$_2$SS***CH***$_2$C), 2.31 (m, C$H_2$C$H_2$***CH***$_2$COO), 1.64 (m, C$H_2$***CH***$_2$C$H_2$***CH***$_2$C$H_2$), 1.48 (s, SC$H_2$C***CH***$_3$), 1.39 (m, C$H_2$C$H_2$***CH***$_2$C$H_2$C$H_2$), 1.26-1.21 (m, OC$H_2$C***CH***$_3$).

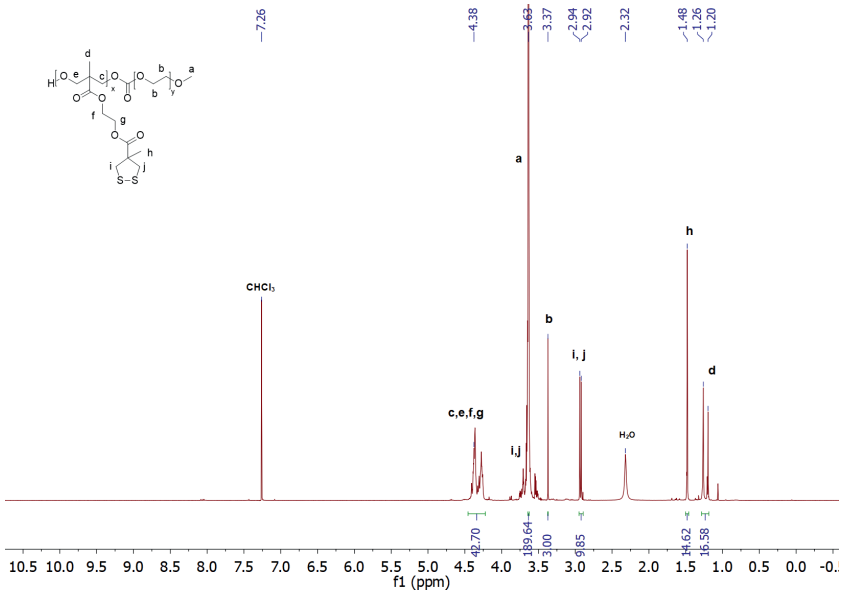


**Figure S34**. $^{1}$H-NMR spectrum (600 MHz, $CDCl_3$) of pDdeT$C_5$-PEG block copolymer synthesized by ROP catalyzed by MSA (Entry 16, table 1). **$^{1}$H**-NMR (600 MHz, $CDCl_3$): δ 4.42–4.13 (m, COO***CH***$_2$C***CH***$_2$OCO, COO***CH***$_2$***CH***$_2$COO), 3.70 (m, C***CH***$_2$SS***CH***$_2$C), 3.63 (m, PEG protons), 3.37 (s, 3H, ***CH***$_3$O), 2.92 (m, C***CH***$_2$SS***CH***$_2$C), 1.48 (s, SC$H_2$C***CH***$_3$CC$H_2$S), 1.26-1.21 (m, OC$H_2$C***CH***$_3$CC$H_2$O).

## References


1. Barcan, G. A.; Zhang, X.; Waymouth, R. M. Structurally dynamic hydrogels derived from 1,2-dithiolanes. *J. Am. Chem. Soc.* **2015,** *137*, 5650-5653.
2. Pratt, R. C.; Nederberg, F.; Waymouth, R. M.; Hedrick, J. L. Tagging alcohols with cyclic carbonate: a versatile equivalent of (meth)acrylate for ring-opening polymerization. *Chem. Commun.* **2008**, 114-116.
3. Zhang, X.; Waymouth, R. M. 1,2-dithiolane-derived dynamic, covalent Materials: Cooperative self-assembly and reversible cross-linking. *J. Am. Chem. Soc.* **2017,** *139*, 3822-3833.
4. Delcroix, D.; Couffin, A.; Susperregui, N.; Navarro, C.; Maron, L.; Martin-Vaca, B.; Bourissou, D. Phosphoric and phosphoramidic acids as bifunctional catalysts for the ring-opening polymerization of ε-caprolactone: a combined experimental and theoretical study. *Polymer Chemistry* **2011,** *2*, 2249-2256.
5. Susperregui, N.; Delcroix, D.; Martin-Vaca, B.; Bourissou, D.; Maron, L. Ring-opening polymerization of epsilon-caprolactone catalyzed by sulfonic acids: computational evidence for bifunctional activation. *J. Org. Chem.* **2010,** *75*, 6581-6587.
6. Pratt, R. C.; Lohmeijer, B. G.; Long, D. A.; Waymouth, R. M.; Hedrick, J. L. Triazabicyclodecene: a simple bifunctional organocatalyst for acyl transfer and ring-opening polymerization of cyclic esters. *J. Am. Chem. Soc.* **2006,** *128*, 4556-4557.
7. Kamber, N. E. J., W.; Waymouth, R. M. Organocatalytic ring-opening polymerization. *Chem. Rev.* **2007,** *107*, 5813-5840.
8. Couffin, A.; Delcroix, D.; Martín-Vaca, B.; Bourissou, D.; Navarro, C. Mild and efficient preparation of block and gradient copolymers by methanesulfonic acid catalyzed ring-opening polymerization of caprolactone and trimethylene carbonate. *Macromolecules* **2013,** *46*, 4354-4360.

# 6

# Chapter 6

## Correlation between *In Vitro* Stability and Pharmacokinetics of Poly(ε-caprolactone)-based Micelles Loaded with a Photosensitizer

Yanna Liu [1], Marcel H.A.M. Fens [1], Robin Bruno Capomaccio [2], Dora Mehn [2], Luca Scrivano [1], Robbert J. Kok [1], Sabrina Oliveira [1,3], Wim E. Hennink [1], and Cornelus F. van Nostrum [1*]

[1] Department of Pharmaceutics, Utrecht Institute for Pharmaceutical Sciences, Utrecht University, Utrecht, the Netherlands.
[2] European Commission, Joint Research Centre, Ispra, Italy.
[3] Division of Cell Biology, Department of Biology, Utrecht University, Utrecht, the Netherlands.

*Submitted for publication*

## Abstract

Polymeric micelles are extensively investigated as drug delivery systems for hydrophobic drugs including photosensitizers (PSs). In order to benefit from micelles as targeted delivery systems for PS, rather than only solubilizers, the stability and cargo retention of the (PS-loaded) micelles should be properly assessed in biologically relevant media to get insights into the essential parameters predicting their *in vivo* performance (*i.e.,* pharmacokinetics). In the present study, asymmetric flow field-flow fractionation (AF4) was used to investigate the *in vitro* stability in human plasma of empty and meta-tetra(hydroxyphenyl)chlorin (mTHPC)-loaded dithiolane-crosslinked micelles based on poly(ε-caprolactone)-*co*-poly(1,2-dithiolane-carbonate)-*b*-poly(ethylene glycol) (p(CL-*co*-DTC)-PEG) and non-crosslinked micelles composed of poly(ε-caprolactone)-*b*-poly(ethylene glycol) (pCL-PEG). AF4 allows separation of the micelles from plasma proteins, which showed that small non-crosslinked $pCL_9$-PEG (17 nm) and $pCL_{15}$-PEG (22 nm) micelles had lower stability in plasma than $pCL_{23}$-PEG micelles with larger sizes (43 nm) and higher degree of crystallinity of pCL, and had also lower stability than covalently crosslinked $p(CL_9\text{-}DTC_{3.9})$-PEG and $p(CL_{18}\text{-}DTC_{7.5})$-PEG micelles with similar small sizes (~20 nm). In addition, PS (re)distribution to specific plasma proteins is observed, giving strong indications for the (in)stability of PS loaded micelles in plasma. Nevertheless, fluorescence spectroscopy in human plasma showed that the retention of mTHPC in non-crosslinked but semi-crystalline $pCL_{23}$-PEG micelles (>8 h) was much longer than that in covalently crosslinked $p(CL_{18}\text{-}DTC_{7.5})$-PEG micelles (~4 h). In line with this, *in vivo* circulation kinetics showed that $pCL_{23}$-PEG micelles loaded with mTHPC had significantly longer half-life values (t½-β of micelles and mTHPC was 14 and 18 h, respectively) than covalently crosslinked $p(CL_{18}\text{-}DTC_{7.5})$-PEG micelles (t½-β of both micelles and mTHPC was ~2 h). As a consequence, long circulating $pCL_{23}$-PEG micelles resulted in significantly higher tumor accumulation of both the micelles and loaded mTHPC as compared to short circulating $p(CL_{18}\text{-}DTC_{7.5})$-PEG micelles. These *in vivo* data were in good agreement with the *in vitro* stability studies.

In conclusion, the present study points out that AF4 and fluorescence spectroscopy are excellent tools to evaluate the (in)stability of nanoparticles in biological media and thus predict the (in)stability of drug loaded nanoparticles after *i.v.* administration, which is favorable to screen promising delivery systems with reduced experimental time and costs and without excessive use of animals.

## 1. Introduction

Photosensitizers (PSs) are harmless compounds which are activated by absorbed light to the excited state, following by release of its energy to dissolved oxygen to yield singlet oxygen species, which in turn cause cell death [1,2]. This process is exploited in so-called photodynamic therapy (PDT), a modality that has been clinically approved for treatment of different types of cancer [3,4]. However, some properties of PSs need optimization to fully benefit from the anti-cancer efficacy by PDT. For instance, m-tetra(hydroxyphenyl) chlorin (mTHPC) is a clinically approved second generation PS [5-7]. However, its very hydrophobic character (log P of ~9 [8]) encounters obstacles similar to that of many other PSs and (extremely) hydrophobic chemotherapeutic drugs, such as extremely low-aqueous solubility, aggregation in aqueous media and limited tumor specificity [4,9,10].
Polymeric micelles have the capacity to accommodate hydrophobic PS to yield nanomedicines facilitating its administration and increase accumulation of the PS at targeted tissues via passive targeting *(i.e.* enhanced permeability and retention (EPR) effect) and/or active targeting strategies [4,11-13]. Indeed, as demonstrated in our previous publications [14,15], mTHPC can be solubilized in poly(ε-caprolactone)-*b*-poly(ethylene glycol) (pCL-PEG) based polymeric micelles. In order to benefit from micelles as targeted delivery systems for PS, polymeric micelles must have sufficient stability and simultaneously good cargo retention in the circulation [16-18]. However, rapid release of this PS in the circulation after *i.v.* administration of the mTHPC loaded micelles was observed in our previous studies [14,19]. This can be likely ascribed to interactions of the micelle forming block copolymer unimers and/or loaded PS with blood constituents among which plasma proteins [20-26]. Therefore, advanced *in vitro* methods are necessary to get mechanistic insights into the stability of drug loaded nanocarriers in biologically relevant media simultaneously avoiding the use of *in vivo* animal models. Indeed, there are currently some research methods available to explore the stability of drug-loaded polymeric micelles in well-defined and simple media, for example, dialysis [27,28] and particle size analysis [29,30]. However, these methods cannot give a clear indication of the stability of nanomedicines in complex biological media such as blood. An attractive technology, and hardly exploited for this purpose, is asymmetrical flow field-flow fractionation (AF4), which allows high resolution separation of particles and plasma proteins based on size differences under physiologically relevant conditions [31].
In the present study, the *in vitro* and *in vivo* stability of mTHPC-loaded dithiolane-crosslinked micelles based on poly(ε-caprolactone)-*co*-poly(1,2-dithiolane-carbonate)-*b*-poly(ethylene glycol) (p(CL-*co*-DTC)-PEG) was investigated. In **Chapter 5** of this thesis, it was shown that p(CL-*co*-DTC)-PEG micelles crosslink spontaneously by disulfide-exchange between dithiolanes in the core of the micelles. Here, the *in vitro* release of mTHPC from these covalently crosslinked p(CL-*co*-DTC)-PEG micelles and the *in vitro* stability of these micelles in human plasma was evaluated by fluorescence

spectroscopy and AF4, respectively, and compared with non (covalently)-crosslinked pCL-PEG based micelles. To validate the *in vitro* findings, the *in vivo* pharmacokinetics including circulation kinetics and tumor accumulation of the crosslinked micelles as well as the loaded mTHPC were studied in A431 tumor-bearing mice and compared with free mTHPC and non (covalently)-crosslinked pCL-PEG based micelles loaded with the same PS.

## 2. Materials and Methods

### *2.1 Materials*

Benzyl-poly(ε-caprolactone)-*b*-poly(ethylene glycol) (pCL-PEG) block copolymers with different chain lengths of CL (molecular weight of PEG was 2 kDa) (measured by $^{1}$H NMR; Supplementary **Scheme S1A**) were synthesized and characterized as described in our previous publication [15]. Poly(ε-caprolactone)-*co*-poly(1,2-dithiolane-carbonate)-*b*-poly(ethylene glycol) (p(CL-*co*-DTC)-PEG) block copolymers with a random or blocky distribution of CL and DTC in polyester/carbonate blocks (*i.e.,* random p(CL-DTC)-PEG and blocky p(CL-*b*-DTC)-PEG) were synthesized by simultaneous and sequential copolymerization of CL and DTC using methoxy-poly(ethylene glycol) (mPEG-OH, 2 kDa) as initiator (**Scheme S1B**, supporting information), respectively, and the monomer sequences in the resulting block copolymers were confirmed by $^{1}$H/$^{13}$C-NMR analysis, as described in **Chapter 5** of this thesis. The characteristics of the synthesized block copolymers are summarized in **Table S1** (Supporting information) (also presented in [15] and **Chapter 5** of this thesis). p(CL-*co*-DTC) oligomers were synthesized as described in section S1 of the supporting information. Phosphate buffered saline (PBS, pH 7.4, containing 11.9 mM phosphates, 137 mM sodium chloride and 2.7 mM potassium chloride) was obtained from Fischer Bioreagents (Bleiswijk, the Netherlands). Standard regenerated cellulose dialysis tubing (Spectra/Por®6) with molecular weight cutoff (MWCO) of 1 kDa was purchased from Spectrumlabs (Rancho Dominguez, Califonia, USA). Maleimide functionalized cyanine7 fluorescent dye (Cy7-maleimide) was ordered from Lumiprobe Corporation (Hannover, Germany). 1,4-Dithiothreitol (DTT) was a product of Sigma Aldrich (Zwijndrecht, the Netherlands). m-Tetra(hydroxyphenyl) chlorin (mTHPC) was obtained from Molekula (Munich, Germany). All other solvents and reagents were obtained from Biosolve (Valkenswaard, the Netherlands).

### *2.2 Synthesis and characterization of Cy7-labeled p(CL-co-DTC)-PEG*

Cy7-labeled p($CL_{18}$-$DTC_{7.5}$)-PEG block copolymer was synthesized as previously reported [15] (**Scheme S2**, supporting information). The successful coupling of Cy7 to the polymer and complete removal of unreacted Cy7 was demonstrated by GPC analysis, with which the amount of Cy7 in the copolymer was quantified using UV/Vis

detection at 755.5 nm, showing 17% coupling efficiency as reported previously [15]. On average, one polymer chain carried 0.17 Cy7 molecule.

### *2.3 Preparation and characterization of empty and mTHPC loaded micelles*

Non (covalently)-crosslinked micelles consisting of 10 mg/mL pCL-PEG without and with 0.5wt% and 5wt% mTHPC loadings were prepared using a film hydration method, as described previously [14,15]. Covalently crosslinked micelles based on different dithiolane containing p(CL-*co*-DTC)-PEG block copolymers (4 mg/mL polymer) were prepared by a nanoprecipitation method, as previously reported [15,19]. Briefly, for empty micelles, 4 mg copolymer was dissolved in 100 µL of DMF (40 mg/mL), while for mTHPC loaded crosslinked p(CL-*co*-DTC)-PEG micelles (different loadings), a certain volume of mTHPC solution in DMF (5 mg/mL, volume depending on the aimed wt% loading), was added to the weighted polymer, followed by addition of a certain volume of DMF to obtain a final polymer concentration of 40 mg/mL. Subsequently, the resulting copolymer/mTHPC solution was added dropwise to PBS, at 1/9 volume ratio. Homogenous micellar dispersions were formed after gentle shaking and subsequently dialyzing the obtained dispersion using a dialysis tubing (MWCO =1 kDa) against PBS at room temperature for 12 h.

The Z-average hydrodynamic diameter ($Z_{ave}$) and polydispersity index (PDI) of the formed micelles were determined by dynamic light scattering (DLS) using a ZetaSizer Nano S (Malvern). The loading capacity (LC) and loading efficiency (LE) of mTHPC were determined by UV-Vis analysis and calculated using following equations as previously reported [14].

$$LE\ (\%) = \frac{mTHPC\ loaded\ (mg)}{mTHPC\ in\ the\ feed\ (mg)} x100\%$$

$$LC\ (\%) = \frac{mTHPC\ loaded\ (mg)}{polymer\ \ used\ (mg) + mTHPC\ loaded\ (mg)} x100\%$$

### *2.4 In vitro stability studies*

#### *2.4.1 In vitro release of mTHPC from micelles as studied by fluorescence spectroscopy*

The *in vitro* release of mTHPC from (de)crosslinked p(CL-*co*-DTC)-PEG micelles (10wt% mTHPC loading, prepared in PBS as described in section 2.3) was studied in human plasma (from Seralab, UK) at 37 °C by monitoring the change of fluorescence intensity of mTHPC, as previously reported [14]. Free mTHPC (*i.e.,* mTHPC in a solution of ethanol/propylene glycol (40/60, w/w)) was used as reference. In short, to 960 µL of mTHPC loaded crosslinked micelles in PBS (4 mg/mL polymer) were pre-incubated with 80 µL of 20 mg/mL DTT solution in PBS (final DTT concentration was 10 mM) to reduce disulfide bonds in the core of the micelles or with 80 µL PBS at 37°C for 12 h. Subsequently, the pretreated micelles as well as free mTHPC were added

to human plasma or PBS (as control) at a volume ratio of 1/9. During incubation with plasma at 37 °C, samples were taken at different time points (5 min, and 0.5, 1, 1.5, 2, 3, 5, 8 h) and placed in a 384-well plate to record the fluorescence intensity using a Jasco FP8300 spectrofluorometer (Japan) at 655 nm after excitation at 420 nm.

### *2.4.2 Stability of empty and mTHPC loaded micelles as studied by AF4*

Asymmetric flow field-flow fractionation (AF4) was used to investigate the *in vitro* stability of empty micelles in human plasma as well as the release of mTHPC from micelles in a solution of human serum albumin (HSA) or human plasma (both from Sigma Aldrich, Darmstadt, Germany). For this purpose, covalently crosslinked p(CL-*co*-DTC)-PEG micelles with random monomer order in the hydrophobic block (4 mg/mL polymer) and non (covalently)-crosslinked pCL-PEG micelles (10 mg/mL polymer) without and with mTHPC loadings (5wt% and 0.5wt%) were prepared in PBS as described in section 2.3. In detail, empty micelles were mixed with human plasma or PBS at a volume ratio of 7/3. To study release, mTHPC loaded micelles were incubated either with HSA solution in PBS (final HSA concentration was 45 mg/mL) or human plasma at a volume ratio of 7/3, while free mTHPC (*i.e.,* mTHPC in a solution of ethanol/propylene glycol (40/60, w/w)) at mTHPC concentrations of 0.5 and 0.05 mg/mL (corresponding to the amounts that were present in 5wt% and 0.5wt% mTHPC loadings in micelles) was employed as reference. During incubation at 37 °C, samples were taken at predetermined time points ranging from 0 to 24 h and analyzed by AF4.
AF4 measurements were performed using an AF2000 separation system (Postnova Analytics, Landsberg, Germany) equipped with PN1130 isocratic pumps, degasser and different detectors, namely a refractive index (RI, PN3150) detector, a fluorescence (PN3412) detector and a DLS (Zetasizer Nano ZS, Malvern Instruments, Herrenberg, Germany) detector, respectively. The separation channel consisted of a spacer with 350 µm thickness, deltoid shaped channel profile and 27 cm channel length, and a regenerated cellulose membrane with a cut-off of 10 kDa from Postnova Analytics (Landsberg, Germany). PBS was used as a mobile phase.
A 50 µL of sample was injected into the system during the focusing step with an injection flow rate of 0.2 mL/min, and a focus flow rate of 3 mL/min over 4 min. Next, in the fractionation step, after a transition time of 1 min, the cross-flow was kept constant at 2.7 mL/min for 7 min and then decreased exponentially in 20 min to 0.1 mL/min. The crossflow was kept constant at 0.1 mL/min for 15 min and at 0.00 mL/min for another 4 min to ensure complete sample elution. Samples were eluted with a flow rate of 0.5 mL/min. Detailed flow rates in each step are presented in **Table S2** (supporting information). The detection of the eluted and fractionated protein components and (mTHPC loaded) micelles was performed sequentially by RI, fluorescence at $\lambda_{em}$ 650 nm with $\lambda_{ex}$ 420 nm (for mTHPC) and DLS. The AF2000 control unit software was used for data acquisition and processing.

### *2.5 In vivo studies of free mTHPC and Cy7 labeled micelles loaded with mTHPC in A431 tumor-bearing mice*

For the *in vivo* studies, mTHPC (0.6 wt% loading) in dithiolane crosslinked p($CL_{18}$-$DTC_{7.5}$)-PEG micelles with random monomer order in the hydrophobic block and non (covalently)-crosslinked $pCL_{23}$-PEG micelles were prepared in PBS as described in section 2.3, except that the micelles were labeled by mixing the corresponding non-labeled polymers with Cy7-labeled p($CL_{18}$-$DTC_{7.5}$)-PEG (synthesis is described in section 2.2) (at a ratio of 98.5% to 1.5% w/w) before preparation of the micelles. mTHPC injection solution was prepared by 1:1 dilution of a 120 μg/mL mTHPC stock solution in solvent (*i.e.,* ethanol/propylene glycol, 40/60 w/w) with PBS (final mTHPC concentration was 60 μg/mL, equal to the concentration of injected micellar samples with 0.6% mTHPC loading).

The animal experiments were approved by the local Utrecht animal ethics welfare committee and national regulatory authorities. Female Balb/c nude mice, weighing 20-28 g were purchased from Envigo (Horst, the Netherlands). Mice were housed in ventilated cages at 25 °C and 55% humidity under natural light/dark conditions. Food and water were provided *ad libitum* during the entire study. Mice were inoculated with $1x10^6$ A431 cells suspended in 100 μL PBS subcutaneously into the right flank. When the tumors reached a size of 100-300 $mm^3$, mice were included in the studies. Tumors were measured using a digital caliper. The tumor volume V (in $mm^3$) was calculated using the equation $V = (\pi/6)LS^2$ where L is the largest and S is the smallest superficial diameter [17].



#### *2.5.1 Circulation kinetics*

Two groups of tumor-bearing mice (n = 3-6 per group) were intravenously (*i.v.*) injected via the tail vein with free mTHPC dissolved in ethanol/propylene glycol/PBS (20/30/50, v/v/v) or mTHPC loaded Cy7-labeled p($CL_{18}$-$DTC_{7.5}$)-PEG micelles, respectively, at injection doses of 300 μg mTHPC/kg, corresponding to a dose of ~6 μg mTHPC per individual mouse.

Blood samples were collected in tubes with EDTA-anticoagulant via submandibular puncture (~60 μL) at 1 min (100% injection control), and at 1 and 2 h, and via cardiac puncture (~200 μL) after 4 and 24 h, post injection. For the latter, mice were killed through cervical dislocation while under deep isoflurane anesthesia. The collected blood samples were centrifuged at 1000 ×g for 15 min at 4 °C. The plasma supernatant was collected, extracted using acetonitrile/DMSO (4/1, v/v) and analyzed by high-performance liquid chromatography (HPLC) and a LI-COR Odyssey imaging system to quantify the amount of mTHPC and Cy7 labeled polymer, respectively, as described in [15,19]. Pharmacokinetic parameters were determined by non-compartmental analysis with the PKSolver add-in for Microsoft Excel [32].

*2.5.2 Biodistribution in tumor bearing mice*

Mice were sacrificed 4 and 24 h (3-6 animals per group) after *i.v.* administration of the formulations including free mTHPC and mTHPC loaded Cy7-labeled covalently crosslinked p($CL_{18}$-$DTC_{7.5}$)-PEG and non (covalently)-crosslinked p$CL_{23}$-PEG micelles. Tumors were excised and then stored at -80 °C until further processing for quantification. Tumors from three untreated animals were used as controls.

To quantify the content of mTHPC and Cy7 labeled micelles in the tumors, the excised tumor samples were treated as described previously [19]. In short, to weighted tumor samples, an equal volume of RIPA lysis buffer (v/w) was added. The mixture was homogenized at a speed of 6000/s for 60 s and the homogenate was subsequently aliquoted.

To determine the mTHPC concentration in the samples, an aliquot of the homogenate was vortex-mixed with acetonitrile/DMSO (4/1 v/v) at a volume ratio of 1 to 4 for 1 min. After centrifugation at 15,000 ×g for 10 min, 50 µL of the obtained supernatant was injected to the HPLC system consisting of a Waters X Select CSH C18 3.5 µm 4.6 x 150 mm column coupled with a fluorescence detector set at $\lambda_{ex}$ 420 nm, $\lambda_{em}$ 650 nm to analyze mTHPC concentration in the samples as described previously [19]. To determine the concentration of Cy7 labeled micelles, another aliquot of the homogenate was vortex-mixed with RIPA lysis buffer (1/2, v/v) for 1 min. The fluorescence of Cy7 in the mixture (20 µL) was detected at the 800 nm channel (*i.e.* $\lambda_{ex}$ 785 nm and $\lambda_{em}$ 820 nm), using a LI-COR Odyssey scanner imaging system as reported previously [19].

*2.6 Statistical analysis*

Statistical analysis was done by GraphPad Prism 8.3.0 software. Statistical significance of biodistribution among different mTHPC formulations was determined by two-way analysis of variance (ANOVA). A value of $p < 0.05$ was considered significant. Statistical significance is depicted as * $p < 0.05$, ** $p < 0.01$, *** $p < 0.001$.

## 3. Results and Discussion

*3.1 Preparation and characterization of polymeric micelles*

Spontaneously crosslinked micelles based on dithiolane based on p(CL-*co*-DTC)-PEG at a polymer concentration of 4 mg/mL were prepared by a previously reported nanoprecipitation method [15,19] while non (covalently)-crosslinked micelles consisting of 10 mg/mL pCL-PEG were prepared by a film hydration method [14,15]. Different block copolymers were chosen for the preparation of crosslinked micelles, which differed in the sequence of CL and DTC (*i.e.*, blocky or random) and/or chain lengths of the hydrophobic block (Table S1, supporting information). As reported in **Chapter 5** of this thesis and summarized in Figure S1 (supporting information), the

covalently crosslinked p(CL-*co*-DTC)-PEG micelles (**Figure 1A**) have hydrodynamic diameters that slightly increased from 17 to 22 nm with increasing chain length of the hydrophobic block from ~12 to ~25 monomeric units, independent of the monomer sequence (*i.e.,* blocky or random distribution of CL and DTC in the polymer chain). In contrast, for non (covalently)-crosslinked pCL-PEG micelles, the increase in sizes was more significant (from 17 to 43 nm), with increasing CL chain length from 9 to 23 units (**Figure 1A)** [15], which can probably be explained by the more condensed p(CL-*co*-DTC)-PEG micellar core caused by crosslinking compared to the non (covalently)-crosslinked pCL-PEG micelles. The different micelles were able to efficiently load mTHPC (~80%) in the micellar core at mTHPC feed concentration of ~0.5 mg/mL, which is in line with our previously published data [14,15].

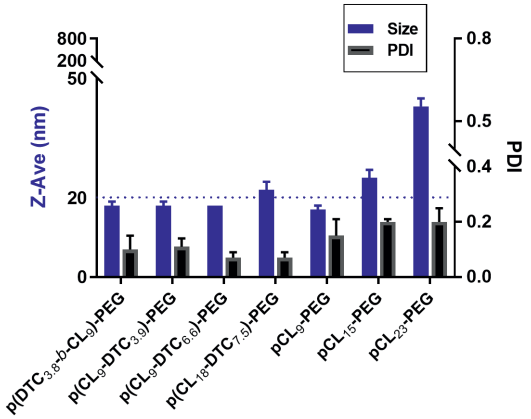


**Figure 1.** (A) Hydrodynamic diameter ($Z_{ave}$, blue columns) and polydispersity index (PDI, black columns) of polymeric micelles consisting of p(CL-*co*-DTC)-PEG (4 mg/mL) or pCL-PEG (10 mg/mL), according to DLS measurements, as presented in [15]. Average ± SD of 3 independently prepared samples are reported. The loading efficiency of mTHPC in the different micelles was ~80 % for both an initial feed of 10 wt and 5 wt%, respectively.

### *3.2 In vitro stability studies*

#### *3.2.1 In vitro release of mTHPC from micelles in human plasma as studied by fluorescence spectroscopy*

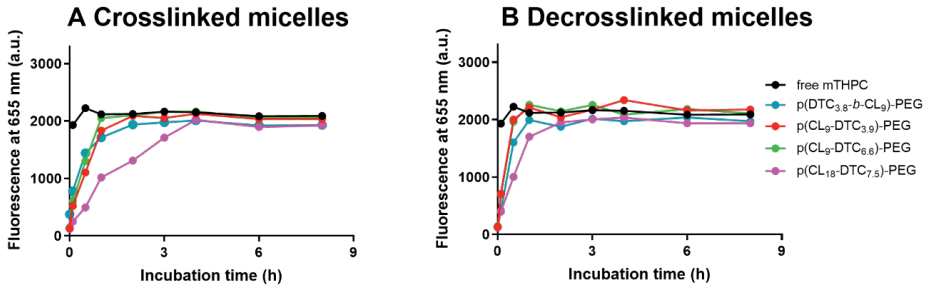


**Figure 2.** Fluorescence intensity ($\lambda_{ex}$ 420 nm, $\lambda_{em}$ 655 nm) of free mTHPC and mTHPC-loaded (10 wt%) (de)crosslinked p(CL-*co*-DTC)-PEG micelles as a function of time at 37 °C in human plasma; free mTHPC and micelles were 10× diluted with human plasma to obtain final polymer and mTHPC concentrations of 0.4 mg/mL and 32 mg/mL, respectively. The fluorescence intensities of the corresponding mTHPC loaded micelles diluted with PBS were used as 0 h timepoint. Decrosslinked micelles were prepared by incubation of the crosslinked counterparts with DTT (10 mM in PBS, to reduce the disulfide bonds) for 12 h at 37 °C.

The *in vitro* release of mTHPC from the crosslinked p(CL-*co*-DTC)-PEG micelles was investigated in human plasma over time at 37 °C (**Figure 2**) by making use of the quenched state when mTHPC is aggregating in the core of the micelles and fluorescence dequenching, which occurs after its release from the micelles [14]. To explain, when mTHPC releases from the micelles, fluorescence intensity increases resulting from a combination of fluorescent mTHPC when it is released and simultaneous less fluorescence quenching of retained PS in the core of the micelles. Similar as observed in our previous study [14], when free mTHPC (dissolved in a mixture of ethanol and propylene glycol) was added to PBS, severe precipitation occurred and hardly any fluorescence was detected (**Figure S1A**, black line, supporting information). Upon 10× dilution of micelles in PBS, the fluorescence of mTHPC when loaded in the micelles was quite low and constant over 8 h at 37 °C due to the afore-mentioned fluorescence quenching (**Figure S1A**, supporting information). Upon 10× dilution in plasma, free mTHPC showed fluorescence at a value of ~2,100 a.u. (**Figure 2**, black lines), indicating the capability of plasma proteins to solubilize mTHPC. For mTHPC loaded in crosslinked micelles consisting of p(CL-*co*-DTC)-PEG with relatively short chain lengths of the hydrophobic blocks (9 units of CL and 4 to 7 units of DTC) (**Figure 2A**, red, green and cyan lines), substantial increase of fluorescence was observed during the first 1 h incubation with plasma. This figure also shows that the fluorescence intensities leveled off at ~2,100 a.u., identical to that observed from free mTHPC (black line), suggesting complete and rapid release of mTHPC from these micelles in plasma. This

was observed regardless of the monomer sequence and the DTC content in the polymer chains, and was consistent with our previous studies on non (covalently)-crosslinked $pCL_9$-PEG and $pCL_{17.6}$-PEG based micelles having similar short hydrophobic pCL blocks [14,19]. However, for the crosslinked $p(CL_{18}\text{-}DTC_{7.5})$-PEG micelles containing longer hydrophobic block (**Figure 2A**, pink line, ~25 units of CL and DTC in total), quantitative release of mTHPC from the micelles took 4 h, suggesting better mTHPC retention in these micelles. In our previous study, we also demonstrated that increasing the pCL hydrophobic block from 9 to 23 units resulted in better retention of mTHPC (0.5 and 8 h, respectively) [15]. Therefore, as compared to micelles with shorter hydrophobic blocks (**Figure 2A**, red, green and cyan lines), this slower release of mTHPC from $p(CL_{18}\text{-}DTC_{7.5})$-PEG micelles (**Figure 2A**, pink line) can be explained by the chemical crosslinking and/or the increased hydrophobic interactions, both responsible for stabilization of micelles [33,34]. Interestingly, despite more or less similar chain lengths of the core-forming hydrophobic blocks, the slower release of mTHPC from the non (covalently)-crosslinked $pCL_{23}$-PEG micelles as compared to the covalently crosslinked ones (8 *vs* 4 h) might be ascribed to the physical state of the core-forming hydrophobic blocks at 37 °C, as a result of the different melting points of $pCL_{23}$ and $p(CL_{18}\text{-}DTC_{7.5})$ hydrophobic blocks ($T_m$: 45 *vs* 20 °C with $\Delta H_m$: 88 *vs* 21 J/g, **Table S3** in supporting information). In other words, the semi-crystalline state with crystallites acting as physical crosslinks in the core-forming hydrophobic pCL block in the $pCL_{23}$-PEG micelles may confer greater PS retention by decreasing its rate of diffusion [34-36] as compared to the liquid state of the core of $p(CL_{18}\text{-}DTC_{7.5})$-PEG micelles at 37 °C.
After reduction by DTT of the disulfide bonds present in the core of the p(CL-*co*-DTC)-PEG based micelles (*i.e.,* decrosslinking) and subsequent incubation in plasma, faster increase in the fluorescence intensity of mTHPC was observed (**Figure 1B**) compared to the micelles before decrosslinking (**Figure 1A**), *i.e.,* the plateau fluorescence reached within 1 h. This observation demonstrates that a faster release of mTHPC from micelles can be triggered by reversible reduction of disulfide bonds present in the micellar core resulting in decrosslinking of the micelles.

### *3.2.2 Stability of empty and mTHPC loaded micelles as studied by AF4*

#### *3.2.2.1 Stability of empty micelles in human plasma*

AF4 as a fractionation technique provides opportunities to isolate particles and proteins from complex mixtures based on their hydrodynamic sizes [31]. Therefore, this technique was performed to assess whether micellar disassembly resulting from protein-micelle interactions plays a role in the mTHPC release profiles shown in section 3.2.1. To this end, empty covalently crosslinked $p(CL_9\text{-}DTC_{3.9})$-PEG and $p(CL_{18}\text{-}DTC_{7.5})$-PEG micelles and non (covalently)-crosslinked pCL-PEG micelles that showed different retention characteristics of mTHPC in the presence of plasma (as discussed in section 3.2.1) were incubated with plasma at 37 °C and subsequently fractionated and analyzed

using AF4.

Fractograms obtained by refractive index (RI) detection of the empty micelles in PBS at 37 °C did not change upon 24 h incubation, regardless of being covalently crosslinked or not and of their initial sizes (**Figure S2**, supporting information). In line with this, the size distribution of these micelles as measured by in-line DLS did not change over 24 h in PBS (**Figure S3**, supporting information), demonstrating excellent stability of the micelles in PBS. **Figure 3** clearly shows that the different micelles incubated with plasma displayed two well-separated main peaks, namely one at retention time of ~10 min, representing human serum albumin (as verified by overlaying the fractograms with that of human plasma, *e.g.,* **Figure 3A**, blue *vs* black line) and another at retention times ranging from approximately 20 to 30 min, corresponding to micelles (as evidenced by the fractograms of micelles in PBS, **Figure S2**, supporting information). In-line DLS measurements of the micelles in plasma (**Figure S4**, supporting information) showed an increase in particle size with increasing retention time, as expected, which did not significantly change over the course of the 24 h incubation time. However, it is clear (**Figure 2A** and **B**) that the peak corresponding to both non-(covalently)-crosslinked $pCL_9$-PEG and $pCL_{15}$-PEG micelles with relatively small sizes (<25 nm) shifted to higher retention times and thus increased in size with increasing incubation time, suggesting a certain degree of instability of the micelles. Probably, the observed release of mTHPC from the $pCL_9$-PEG and $pCL_{17.6}$-PEG micelles in plasma as described in our previous publications [14,19] is related to the instability of these micelles as shown by the AF4 data. Interestingly, shifts of the micellar peaks were not observed for the covalently crosslinked $p(CL_9\text{-}DTC_{3.9})$-PEG and $p(CL_{18}\text{-}DTC_{7.5})$-PEG micelles with similar relatively small sizes (<25 nm) (**Figure 3D** and **E**), as well as for the physically crosslinked $pCL_{23}$-PEG micelles (**Figure 3C**) with a larger size (43 nm), suggesting that these micelles were stable in this medium.

From the above data, it is noted that covalently crosslinked $p(CL_9\text{-}DTC_{3.9})$-PEG micelles (**Figure 3D**) showed superior stability in plasma as compared to the non (covalently)-crosslinked $pCL_9$-PEG micelles (**Figure 3A**) of similar size (18 *vs* 17 nm), and $pCL_{15}$-PEG micelles (**Figure 3B**) which have comparable chain lengths of the hydrophobic segment but slightly differed in size (~18 *vs* ~24 nm, **Figure 1A**). This indicates that indeed chemical-crosslinking improves the stability of small micelles in plasma. Likewise, covalently crosslinked $p(CL_{18}\text{-}DTC_{7.5})$-PEG micelles (**Figure 3E**) had better stability as compared to non (covalently)-crosslinked $pCL_{15}$-PEG micelles (**Figure 3B**) having comparable sizes (22 *vs* 24 nm). On the other hand, non (covalently)-crosslinked $pCL_{23}$-PEG micelles (**Figure 3C**) displayed similar high stability when compared to $p(CL_{18}\text{-}DTC_{7.5})$-PEG micelles (**Figure 3E**), which have similar chain lengths of the core-forming block but different sizes (43 *vs* 22 nm). As discussed in section 3.2.1, this is probably attributed to physical crosslinks resulting from the crystallization of pCL blocks in the core of the $pCL_{23}$-PEG micelles (so

these micelles are referred to physically crosslinked $pCL_{23}$-PEG micelles from here). In fact, according to the obtained AF4 results for the non (covalently)-crosslinked pCL-PEG micelles, the stability of these micelles improved by increasing the chain length of hydrophobic pCL block from 9 to 23 units (**Figure 3A** and **B** *vs* **C**).

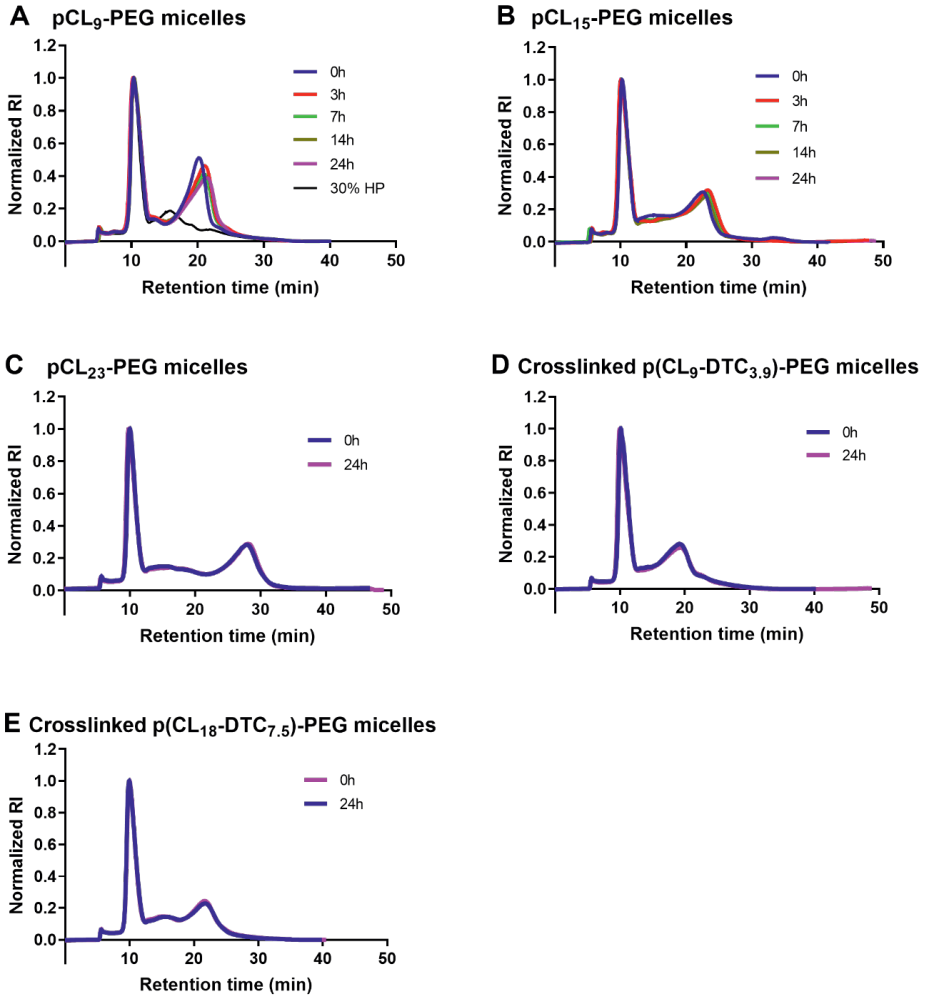


**Figure 3.** AF4 fractograms of micelles using refractive index (RI) detection. The micelles were incubated for 24 hours with human plasma (HP) at 37 °C: non (covalently)-crosslinked micelles composed of $pCL_9$-PEG (A), $pCL_{15}$-PEG (B) and $pCL_{23}$-PEG (C) and dithiolane crosslinked micelles consisting of $p(CL_9\text{-}DTC_{3.9})$-PEG (D) and $p(CL_{18}\text{-}DTC_{7.5})$-PEG (E) were incubated with plasma at a volume ratio of 7/3 for 24 h. After being mixed with plasma, the final polymer concentrations of non (covalently)-crosslinked pCL-PEG and crosslinked p(CL-*co*-DTC)-PEG based micelles were 7.0 and 2.8 mg/mL, respectively. A sample of human plasma (donated as 30% HP in (A)) was used to assign the peaks of plasma components. The signals were normalized to the highest signals.

*3.2.2.2 Release of mTHPC from micelles in buffer with human serum albumin and human plasma as studied by AF4*

Besides protein-polymer interactions, favorable interactions of the loaded cargo with plasma proteins can also lead to its premature release from the micelles, even when the nanoparticles are stable in plasma [37-39]. Previous studies showed high binding affinity of mTHPC for plasma (lipo)proteins leading to mTHPC redistribution from intact liposomes to lipoproteins [22,24-26]. Indeed, we also observed that even though the empty micelles are stable in plasma for 24 h according to the AF4 data (**Figure 3D** and **E**), mTHPC was quantitatively released from covalently crosslinked p($CL_9$-$DTC_{3.9}$)-PEG and p($CL_{18}$-$DTC_{7.5}$)-PEG micelles in 1 and 4 h, respectively (**Figure 2A**, red and pink lines). To investigate this further, mTHPC loaded in stable micelles (*i.e.,* covalently crosslinked p($CL_9$-$DTC_{3.9}$)-PEG and p($CL_{18}$-$DTC_{7.5}$)-PEG micelles or physically crosslinked p$CL_{23}$-PEG micelles) with different mTHPC loadings, were incubated with human serum albumin (HSA) or human plasma for 16 hours at 37 °C. RI detection was used to record fractograms of plasma components and micelles, while mTHPC was also detected making use of its inherent fluorescence intensity through a fluorescence detector coupled to the AF4.

By comparing the RI fractograms of HSA (**Figure 4A**, red line) and plasma (**Figure 4B**, green line), it can be concluded that the peak of plasma at approximate 10 min represents the most abundant component, *i.e.,* albumin, whereas the broad peak at approximate 20 and 30 min corresponds to low- and high-density lipoproteins, respectively. Importantly, it is obvious from **Figure 4B** (purple lines) that free mTHPC preferably binds to lipoproteins, particularly low-density lipoproteins which is in agreement with previous studies [26,40], while it just slightly binds to albumin in the absence of lipoproteins (**Figure 4A**, blue lines).

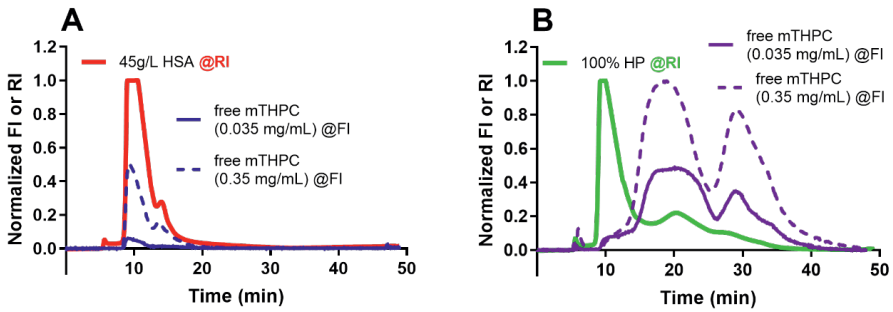


**Figure 4.** Fractograms of free mTHPC in PBS with 45 g/L human serum albumin (A) and 100% human plasma (B) obtained by refractive index (RI) (A, red line and B, green line) and fluorescence intensity (FI) ($\lambda_{ex}$ 420 nm, $\lambda_{em}$ 650 nm) (A, blue lines and B, purple lines); free mTHPC was added at a final concentration of 0.035 and 0.35 mg/mL, respectively. The signals were normalized to the highest signals.

For mTHPC-loaded $pCL_{23}$-PEG micelles, fractograms obtained by RI detection show that the peak of the micelles (retention time of ~30 min.) kept constant upon 16 h incubation regardless of the medium (HSA or plasma) (0.5 wt% loading, **Figure 5A**, **B** and 5 wt% loading, **Figure 6A**, **B**), which is in line with the stability results of the corresponding empty micelles (**Figure 3C**). The fractograms obtained by recording the intrinsic fluorescence of mTHPC show (**Figure 5C** and **D**) that for $pCL_{23}$-PEG micelles with 0.5 wt% mTHPC loading, no detectable release of mTHPC from micelles was observed with 0.5 wt% loading after 7 h incubation with either 30 or 60% plasma. It suggests good mTHPC retention in $pCL_{23}$-PEG micelles, which is in good agreement with the release profile based on the quenching of mTHPC fluorescence reported in our previous study [15]. On the other hand, for $pCL_{23}$-PEG micelles with 5 wt% mTHPC loading, upon incubation with 30% plasma, a small fluorescence peak at approximately 15 min in the fractogram (**Figure 6C**) was observed after 3 h and remained constant till 16 h, suggesting that initially a small fraction (< 5%) of mTHPC was released and subsequently bound to with lipoproteins probably as a result of overloading of the core of the micelles with mTHPC. In contrast, the release of mTHPC in HSA was negligible (**Figure 6D**), which demonstrates that the release of this PS from $pCL_{23}$-PEG micelles is medium dependent and emphasizes the high affinity of the PS for lipoproteins and not for albumin.

The release of mTHPC from covalently crosslinked p(CL-*co*-DTC)-PEG micelles could not be evaluated by AF4 because released mTHPC that bound to lipoproteins has the same retention time of the micelles (~17 min).



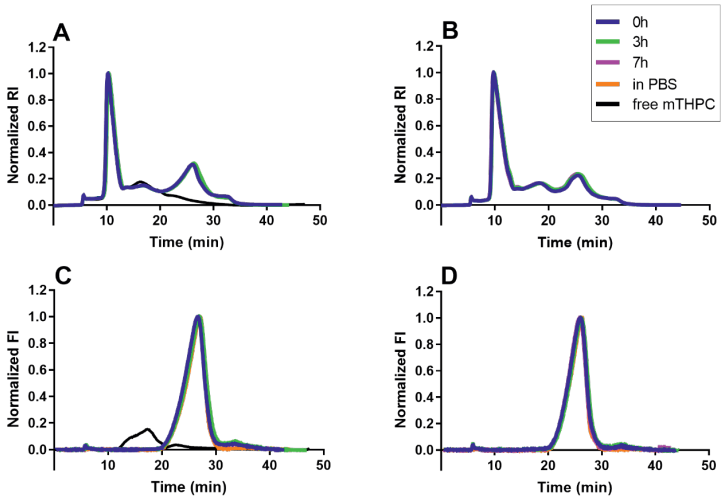


**Figure 5.** Fractograms of mTHPC-loaded (0.5 wt%) $pCL_{23}$-PEG micelles incubated for 7 h with human plasma (HP) at 37 °C and at PBS/plasma volume ratios of 7/3 (A, C) and 4/6 (B, D), respectively, obtained by refractive index (RI) (A, B) and fluorescence intensity (FI) ($\lambda_{ex}$ 420 nm, $\lambda_{em}$ 650 nm) (C, D). After being mixed with plasma, the final polymer concentrations were 7 (A, C) and 4 (B, D) mg/mL, respectively. As a control, free mTHPC at a final concentration of 0.035 mg/mL was added to plasma (black line), corresponding with the concentrations obtained from micelles with 0.5 wt% mTHPC loadings. The signals were normalized to the highest signals.

Overall, the results of AF4 analysis indicate that this technique is a powerful analytical tool to evaluate the stability of PS loaded micelles in biological media, *e.g.,* blood plasma. It can separate the micelles and different plasma proteins without disrupting or disturbing nanoparticle-protein complex, which is necessary for analysis of possible interactions between proteins and particles but challenging using conventional separation methods, *e.g.,* size exclusion chromatography or ultracentrifugation. In addition, PS (re) distribution to specific plasma proteins is observed, giving strong indications for the (in) stability of PS loaded micelles in plasma. This information is important to explain or even predict micelles' behavior *in vivo* and importantly, provides a valuable reference to take effective measures to prevent possible and unwanted premature cargo release in the circulation.

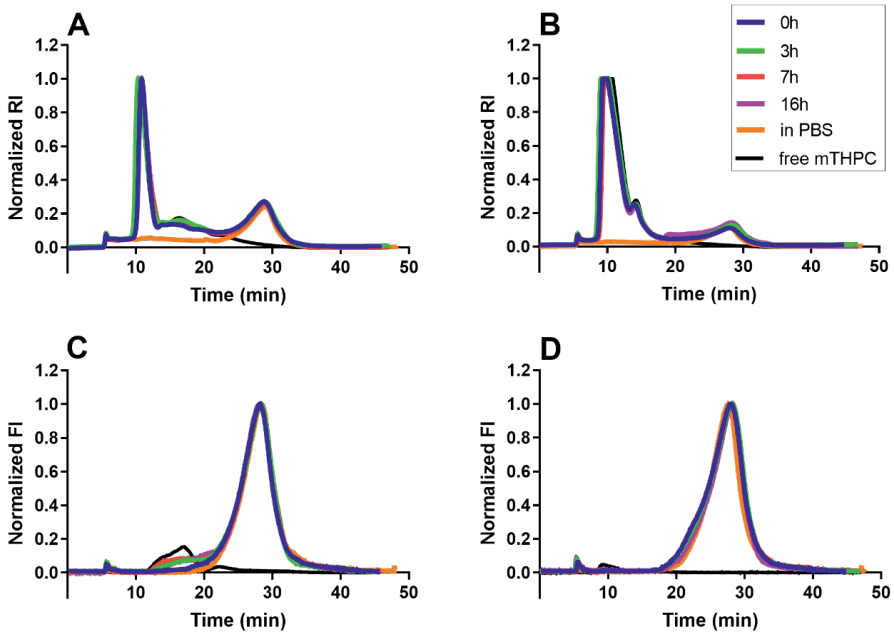


**Figure 6.** Fractograms of mTHPC-loaded (5 wt%) $pCL_{23}$-PEG micelles incubated at 37 °C for 16 h with plasma (7/3, v/v) (A, C) or 45 g/L HSA (B, D), obtained by refractive index (RI) (A, B) and fluorescence intensity detection (FI) ($\lambda_{ex}$ 420 nm, $\lambda_{em}$ 650 nm) (C, D). After being mixed with plasma or HSA (solution in PBS), the final polymer concentrations of the different micelles were 7.0 mg/mL. As a control, free mTHPC at a final concentration of 0.035 mg/ml was added to plasma and HSA, corresponding to the same concentration of mTHPC in 0.5%wt loading in the micelles. The signals were normalized to the highest signals (RI or FI).

### *3.3 Circulation kinetics and biodistribution of free mTHPC and Cy7-labeled micelles loaded with mTHPC*

In our previous study, we showed and discussed the pharmacokinetics of mTHPC-loaded Cy7-labeled physically crosslinked $pCL_{23}$-PEG micelles to and *i.v.* injection of free mTHPC as control [15]. In the present study, the pharmacokinetic data of Cy7-labeled dithiolane crosslinked $p(CL_{18}\text{-}DTC_{7.5})$-PEG micelles loaded with mTHPC and injected in A431 tumor-bearing mice are reported and discussed, and compared with free mTHPC. Micelles based on $p(CL_{18}\text{-}DTC_{7.5})$-PEG were selected because of the high *in vitro* stability of these empty micelles in plasma (**Figure 3E**) and relatively slow release of mTHPC (see **Figure 2A**, pink line). It is noted that no (short term) side effects were observed in mice that received mTHPC loaded crosslinked $p(CL_{18}\text{-}DTC_{7.5})$-PEG micelles during or after their administration, similar to other pCL-PEG based micelles [15,19].

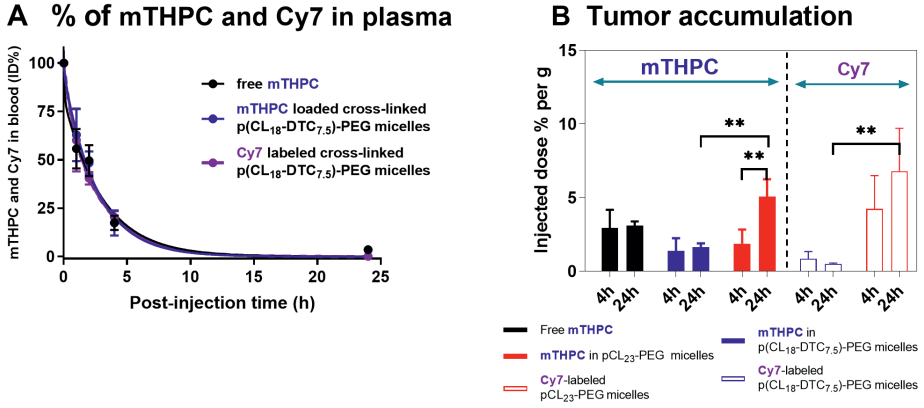


**Figure 7**. (A) Circulation kinetics of free mTHPC and mTHPC-loaded (0.6 wt%) Cy7-labeled covalently crosslinked $p(CL_{18}\text{-}DTC_{7.5})$-PEG micelles, showing mTHPC levels (black and blue lines) and Cy7 level (purple line) (B) Biodistribution of free mTHPC and mTHPC loaded (0.6 wt%) Cy7-labeled $p(CL_{18}\text{-}DTC_{7.5})$-PEG and $pCL_{23}$-PEG micelles in tumors of mice 4 and 24 h post administration. Data are reported as % of injected doses (ID) upon tail vein administration in A431 tumor-bearing Balb/c mice (300 μg mTHPC/kg, *i.e.* ~6 μg mTHPC/mouse). Data are presented as mean ± SD, n= 3-5.

As indicated in **Figure 7A**, the plasma concentration curves of mTHPC after administration of either free mTHPC or the micellar formulation (black and blue lines) were comparable, which is similar to the Cy7 labeled micelles (purple line). It is shown that ~45% of the injected dose (ID) of mTHPC and Cy7 was rapidly cleared in the initial α-elimination phase (first 1 h). Non-compartmental analysis of the mTHPC and Cy7 curves was used to determine pharmacokinetic parameters including terminal

half-lives (t½-β), area under the curves (AUCs), distribution volumes and clearances (**Table 1**). Pharmacokinetic parameters calculated from mTHPC analysis (**Table 1**, top part) were tightly associated with those derived from Cy7 analysis (**Table 1**, bottom part). Unexpectedly, it is difficult to conclude whether these parameters of mTHPC calculated for the micellar formulation reflect (released) free mTHPC or that remaining associated with the micelles because of coincidently similar data observed for free mTHPC and Cy7. However, combined with the *in vitro* release study (**Figure 2A**, pink line), premature release of mTHPC from micelles most likely occurred in the circulation, which was observed in various liposomal mTHPC formulations and other mTHPC loaded micelles [14,15,41].

Interestingly, the circulation kinetics of $pCL_{23}$-PEG micelles and mTHPC loaded in those physically crosslinked micelles as well as the corresponding pharmacokinetic parameters presented in [15], were significantly superior as compared to the covalently crosslinked $p(CL_{18}\text{-}DTC_{7.5})$-PEG micelles (**Table 1**). For instance, we demonstrated that after *i.v.* injection, this PS loaded in $pCL_{23}$-PEG micelles displayed markedly prolonged blood circulation time (t½-β:14 h), compared to free mTHPC, which is due to the long circulating $pCL_{23}$-PEG micelles (t½-β:18 h) (Table 1). These results are very well in line with the *in vitro* stability presented in section 3.2 (**Figures 4** and **5**) and our previous publication [15], which both showed sufficient mTHPC retention in $pCL_{23}$-PEG micelles during 8 h in human plasma and again indicates that physical crosslinks resulting from the crystallization of pCL blocks in $pCL_{23}$-PEG micelles confer greater PS retention compared to covalently crosslinks in $p(CL_{18}\text{-}DTC_{7.5})$-PEG micelles.

**Table 1.** Pharmacokinetic parameters of mTHPC in different formulations and the corresponding (Cy7 labeled) micelles.

| Detection | Formulations | Half-life (h) | | AUC (h*%) | Volume of distribution (mL/kg) | Clearance (mL/kg/h) |
|---|---|---|---|---|---|---|
| | | Phase α[a] | Phase β | | | |
| **mTHPC** | Free mTHPC | <0.5 | 2.1 | 442 | 120 | 13.2 |
| | mTHPC in $p(CL_{18}\text{-}DTC_{7.5})$-PEG micelles | <0.5 | 2.1 | 441 | 116 | 13.2 |
| | mTHPC in $pCL_{23}$-PEG micelles | 0.7[b] | 14.1[b] | 928[b] | 88[c] | 4.6[c] |
| **Cy7** | $p(CL_{18}\text{-}DTC_{7.5})$-PEG micelles | <0.5 | 2.1 | 397 | 60 | 14.7 |
| | $pCL_{23}$-PEG micelles | 0.5[b] | 18.1[b] | 739[b] | 125[c] | 4.9[c] |

[a]Initial phase half-lives (t½-α) were estimated from plasma disappearance rates during the first hour after administration while half-lives of the terminal phase (t½-β) were calculated from non-compartmental analysis. Distribution volumes and clearances were calculated assuming a standard plasma volume of 58.5 mL/kg [14].

[b]was reported in [15] while [c]was calculated from the plasma concentration curves reported in reference [15].

Finally, the biodistribution of mTHPC loaded in covalently crosslinked p($CL_{18}$-$DTC_{7.5}$)-PEG (that showed short circulation time and poor PS retention) and physically crosslinked p$CL_{23}$-PEG micelles (that had prolonged circulation time and good PS retention (**Table 1**)) was investigated and compared with free mTHPC in tumor-bearing mice.

Tumors were excised from mice that were sacrificed at 4 and 24 h post *i.v.* injection of the formulations, and tumor accumulation of Cy7-labeled micelles was quantified by fluorescence intensity measurements (**Figure 7B**, open bars). It was shown that Cy7 levels from covalently crosslinked p($CL_{18}$-$DTC_{7.5}$)-PEG micelles in tumors were quite low (<1% ID/g) and remained constant at 24 h (**Figure 7B**, open blue bars). Interestingly, tumor accumulation of physically crosslinked p$CL_{23}$-PEG micelles was much higher than that of covalently crosslinked p($CL_{18}$-$DTC_{7.5}$)-PEG micelles (5% *vs* <1% ID/g) at 4 h and importantly, progressively increased to ~8% upon 24 h after administration (**Figure 7B**, open red bars), which led to a significant difference with crosslinked p($CL_{18}$-$DTC_{7.5}$)-PEG micelles. This result demonstrates that long circulating micelles are indeed favorable for EPR-mediated tumor accumulation [16,18,42].

**Figure 7B** (solid bars on the left side) displays the biodistribution in tumors of mTHPC that was injected in free form and as covalently crosslinked p($CL_{18}$-$DTC_{7.5}$)-PEG or physically crosslinked p$CL_{23}$-PEG formulations. For free mTHPC and mTHPC loaded in covalently crosslinked p($CL_{18}$-$DTC_{7.5}$)-PEG micelles, the mTHPC accumulation in the tumors was similar for 4 and 24 h (~2-3% ID/g) (**Figure 7B**, solid black and blue bars). These mTHPC levels were higher than Cy7 levels (**Figure 7B**, open blue bar), suggesting that mTHPC was not retained with the host micelles, *i.e.,* mTHPC was rapidly released from the micelles, in line with the *in vitro* release study (**Figure 2A**, pink line). However, when loaded in physically crosslinked p$CL_{23}$-PEG micelles, the tumor accumulation of mTHPC increased progressively in time (1.8 at 4 h to 5% ID/g at 24 h) (**Figure 7B**, solid red bar). Despite relatively lower mTHPC level as compared to Cy7 level at each timepoint, this upward trend was correlated well with the Cy7 accumulation in the tumor demonstrating the ability of long circulating polymeric micelles to facilitate PS targeting to tumors via the EPR effect [16,18,42].



## 4. Conclusion

In the present study, we demonstrated that AF4 is a powerful analytical technique for the separation and characterization of (drug loaded) nanoparticles and its stability in complex biological media *e.g.,* human plasma. PS (re)distribution to lipoproteins was observed, giving strong indications for the (in)stability of the drug-loaded micelles in plasma. With this tool, the (in)stability of drug loaded nanoparticles after *i.v.* administration could be predicted, which is favorable to screen promising delivery systems with reduced

experimental time and costs and without excessive use of animals.

**Acknowledgement**

The research leading to these results resulted from access to the Nanobiotechnology Laboratory under the Framework for open access to the Joint Research Centre Research Infrastructures of the European Commission. Y. Liu is supported by a PhD scholarship from China Scholarship Council (CSC).

## References


1. Meulemans, J.; Delaere, P.; Vander Poorten, V. Photodynamic therapy in head and neck cancer: Indications, outcomes, and future prospects. *Curr Opin Otolaryngol Head Neck Surg* **2019,** *27*, 136-141.
2. van Driel, P.; Boonstra, M. C.; Slooter, M. D.; Heukers, R.; Stammes, M. A.; Snoeks, T. J. A.; de Bruijn, H. S.; van Diest, P. J.; Vahrmeijer, A. L.; van Bergen En Henegouwen, P. M. P.; van de Velde, C. J. H.; Lowik, C.; Robinson, D. J.; Oliveira, S. EGFR targeted nanobody-photosensitizer conjugates for photodynamic therapy in a pre-clinical model of head and neck cancer. *J. Control. Release* **2016,** *229*, 93-105.
3. van Straten, D.; Mashayekhi, V.; de Bruijn, H. S.; Oliveira, S.; Robinson, D. J. Oncologic photodynamic therapy: basic principles, current clinical status and future directions. *Cancers* **2017,** *9*, 1-54.
4. Yakavets, I.; Millard, M.; Zorin, V.; Lassalle, H. P.; Bezdetnaya, L. Current state of the nanoscale delivery systems for temoporfin-based photodynamic therapy: Advanced delivery strategies. *J. Control. Release* **2019,** *304*, 268-287.
5. Baskaran, R.; Lee, J.; Yang, S. G. Clinical development of photodynamic agents and therapeutic applications. *Biomater. Res.* **2018,** *22*, 1-8.
6. Biel, M. A. M. D. Photodynamic therapy of head and neck cancer-what's old and what's new. In handbook of photodynamic therapy: updates on recent applications of porphyrin-based compounds. *World Scientific* **2016**, pp 439-458.
7. Hopper, C. Photodynamic therapy: a clinical reality in the treatment of cancer. *The Lancet. Oncology* **2000,** *1*, 212-219.
8. Chen, M.; Liu, X.; Fahr, A. Skin penetration and deposition of carboxyfluorescein and temoporfin from different lipid vesicular systems: In vitro study with finite and infinite dosage application. *International journal of pharmaceutics* **2011,** *408*, 223-234.
9. Redmond, R. W.; Land, E. J.; Truscott, T. G. Aggregation effects on the photophysical properties of porphyrins in relation to mechanisms involved in photodynamic therapy. *Advances in experimental medicine and biology* **1985,** *193*, 293-302.
10. Triesscheijn, M.; Ruevekamp, M.; Out, R.; Van Berkel, T. J.; Schellens, J.; Baas, P.; Stewart, F. A. The pharmacokinetic behavior of the photosensitizer meso-tetra-hydroxyphenyl-chlorin in mice and men. *Cancer chemotherapy and pharmacology* **2007,** *60*, 113-122.
11. Lammers, T.; Kiessling, F.; Hennink, W. E.; Storm, G. Drug targeting to tumors: principles, pitfalls and (pre-) clinical progress. *J. Control. Release* **2012,** *161*, 175-187.
12. Wang, A. Z.; Langer, R.; Farokhzad, O. C. Nanoparticle delivery of cancer drugs. *Annu. Rev. Med.* **2012,** *63*, 185-198.
13. Maeda, H.; Wu, J.; Sawa, T.; Matsumura, Y.; Hori, K. Tumor vascular permeability and the EPR effect in macromolecular therapeutics: a review. *J. Control. Release* **2000,** *65*, 271-284.
14. Wennink, J. W. H.; Liu, Y.; Makinen, P. I.; Setaro, F.; de la Escosura, A.; Bourajjaj, M.; Lappalainen, J. P.; Holappa, L. P.; van den Dikkenberg, J. B.; Al Fartousi, M.; Trohopoulos, P. N.; Yla-Herttuala, S.; Torres, T.; Hennink, W. E.; van Nostrum, C. F. Macrophage selective photodynamic therapy by meta-tetra(hydroxyphenyl)chlorin loaded polymeric micelles: A possible treatment for cardiovascular diseases. *Eur. J. Pharm. Sci.* **2017,** *107*, 112-125.

15. Liu, Y.; Scrivano, L.; Peterson, J. D.; Fens, M. H. A. M.; Beltrán Hernández, I.; Mesquita, B.; Sastre Torano, J.; Hennink, W. E.; van Nostrum, C. F.; Oliveira, S. EGFR targeted nanobody functionalized polymeric micelles loaded with mTHPC for selective photodynamic therapy. *Molecular pharmaceutics* **2020,** *17*, 1276–1292.
16. Kwon, I. K.; Lee, S. C.; Han, B.; Park, K. Analysis on the current status of targeted drug delivery to tumors. *J. Control. Release* **2012,** *164*, 108-114.
17. Shi, Y.; van der Meel, R.; Theek, B.; Oude Blenke, E.; Pieters, E. H.; Fens, M. H.; Ehling, J.; Schiffelers, R. M.; Storm, G.; van Nostrum, C. F.; Lammers, T.; Hennink, W. E. Complete regression of xenograft tumors upon targeted delivery of paclitaxel via π-π stacking stabilized polymeric micelles. *ACS Nano* **2015,** *9*, 3740-3752.
18. Bertrand, N.; Leroux, J.-C. The journey of a drug-carrier in the body: An anatomo-physiological perspective. *J. Control. Release* **2012,** *161*, 152-163.
19. Liu, Y.; Fens, M. H. A. M.; Lou, B.; van Kronenburg, N. C. H.; Maas-Bakker, R. F. M.; Kok, R. J.; Oliveira, S.; Hennink, W. E.; van Nostrum, C. F. π-π-Stacked poly(ε-caprolactone)-b-poly(ethylene glycol) micelles loaded with a photosensitizer for photodynamic therapy. *Pharmaceutics* **2020,** *12*, 338-363.
20. Liu, B.; Thayumanavan, S. Importance of evaluating dynamic encapsulation stability of amphiphilic assemblies in serum. *Biomacromolecules* **2017,** *18*, 4163-4170.
21. Talelli, M.; Barz, M.; Rijcken, C. J. F.; Kiessling, F.; Hennink, W. E.; Lammers, T. Core-crosslinked polymeric micelles: Principles, preparation, biomedical applications and clinical translation. *Nano Today* **2015,** *10*, 93-117.
22. Sasnouski, S.; Zorin, V.; Khludeyev, I.; D'Hallewin, M. A.; Guillemin, F.; Bezdetnaya, L. Investigation of Foscan interactions with plasma proteins. *Biochimica et biophysica acta* **2005,** *1725*, 394-402.
23. Talelli, M.; Barz, M.; Rijcken, C. J.; Kiessling, F.; Hennink, W. E.; Lammers, T. Core-crosslinked polymeric micelles: Principles, preparation, biomedical applications and clinical translation. *Nano Today* **2015,** *10*, 93-117.
24. Polo, L.; Valduga, G.; Jori, G.; Reddi, E. Low-density lipoprotein receptors in the uptake of tumour photosensitizers by human and rat transformed fibroblasts. *The international journal of biochemistry & cell biology* **2002,** *34*, 10-23.
25. Chowdhary, R. K.; Sharif, I.; Chansarkar, N.; Dolphin, D.; Ratkay, L.; Delaney, S.; Meadows, H. Correlation of photosensitizer delivery to lipoproteins and efficacy in tumor and arthritis mouse models; comparison of lipid-based and Pluronic P123 formulations. *Journal of pharmacy & pharmaceutical sciences* **2003,** *6*, 198-204.
26. Reshetov, V.; Zorin, V.; Siupa, A.; D'Hallewin, M. A.; Guillemin, F.; Bezdetnaya, L. Interaction of liposomal formulations of meta-tetra(hydroxyphenyl)chlorin (temoporfin) with serum proteins: protein binding and liposome destruction. *Photochemistry and photobiology* **2012,** *88*, 1256-1264.
27. Shi, H.; Leonhard, W. N.; Sijbrandi, N. J.; van Steenbergen, M. J.; Fens, M.; van de Dikkenberg, J. B.; Torano, J. S.; Peters, D. J. M.; Hennink, W. E.; Kok, R. J. Folate-dactolisib conjugates for targeting tubular cells in polycystic kidneys. *J. Control. Release* **2019,** *293*, 113-125.

28. Abouelmagd, S. A.; Sun, B.; Chang, A. C.; Ku, Y. J.; Yeo, Y. Release kinetics study of poorly water-soluble drugs from nanoparticles: are we doing it right? *Mol. Pharmaceutics* **2015,** *12*, 997-1003.
29. Owen, S. C.; Chan, D. P. Y.; Shoichet, M. S. Polymeric micelle stability. *Nano Today* **2012,** *7*, 53-65.
30. Lin, W.-J.; Juang, L.-W.; Lin, C.-C. Stability and release performance of a series of pegylated copolymeric micelles. *Pharmaceutical Research* **2003,** *20*, 668-673.
31. Wagner, M.; Holzschuh, S.; Traeger, A.; Fahr, A.; Schubert, U. S. Asymmetric flow field-flow fractionation in the field of nanomedicine. *Analytical Chemistry* **2014,** *86*, 5201-5210.
32. Zhang, Y.; Huo, M.; Zhou, J.; Xie, S. PKSolver: An add-in program for pharmacokinetic and pharmacodynamic data analysis in Microsoft Excel. *Comput Methods Programs Biomed* **2010,** *99*, 306-314.
33. O'Reilly, R. K.; Hawker, C. J.; Wooley, K. L. Cross-linked block copolymer micelles: functional nanostructures of great potential and versatility. *Chemical Society reviews* **2006,** *35*, 1068-1083.
34. Gaucher, G.; Dufresne, M. H.; Sant, V. P.; Kang, N.; Maysinger, D.; Leroux, J. C. Block copolymer micelles: Preparation, characterization and application in drug delivery. *J Control. Release* **2005,** *109*, 169-188.
35. Glavas, L.; Olsen, P.; Odelius, K.; Albertsson, A. C. Achieving micelle control through core crystallinity. *Biomacromolecules* **2013,** *14*, 4150-4156.
36. Zhang, J.; Wang, L.-Q.; Wang, H.; Tu, K. Micellization Phenomena of Amphiphilic Block Copolymers Based on Methoxy Poly(ethylene glycol) and Either Crystalline or Amorphous Poly(caprolactone-b-lactide). *Biomacromolecules* **2006,** *7*, 2492-2500.
37. Bastiat, G.; Pritz, C. O.; Roider, C.; Fouchet, F.; Lignieres, E.; Jesacher, A.; Glueckert, R.; Ritsch-Marte, M.; Schrott-Fischer, A.; Saulnier, P.; Benoit, J. P. A new tool to ensure the fluorescent dye labeling stability of nanocarriers: a real challenge for fluorescence imaging. *J. Control. Release* **2013,** *170*, 334-342.
38. Rijcken, C. Tuneable & degradable polymeric micelles for drug delivery: from synthesis to feasibility in vivo. *Doctoral dissertation; Utrecht University, Utrecht,* **2007**, pp 239-260.
39. Soga, O. Biodegradable thermosensitive polymers: synthesis, characterization and drug delivery applications. *Doctoral dissertation; Utrecht University, Utrecht,* **2006**, pp 87-102.
40. Michael-Titus, A. T.; Whelpton, R.; Yaqub, Z. Binding of temoporfin to the lipoprotein fractions of human serum. *British journal of clinical pharmacology* **1995,** *40*, 594-597.
41. Decker, C.; Schubert, H.; May, S.; Fahr, A. Pharmacokinetics of temoporfin-loaded liposome formulations: correlation of liposome and temoporfin blood concentration. *J. Control. Release* **2013,** *166*, 277-285.
42. Kamaly, N.; Xiao, Z.; Valencia, P. M.; Radovic-Moreno, A. F.; Farokhzad, O. C. Targeted polymeric therapeutic nanoparticles: design, development and clinical translation. *Chemical Society reviews* **2012,** *41*, 2971-3010.

## Supporting information

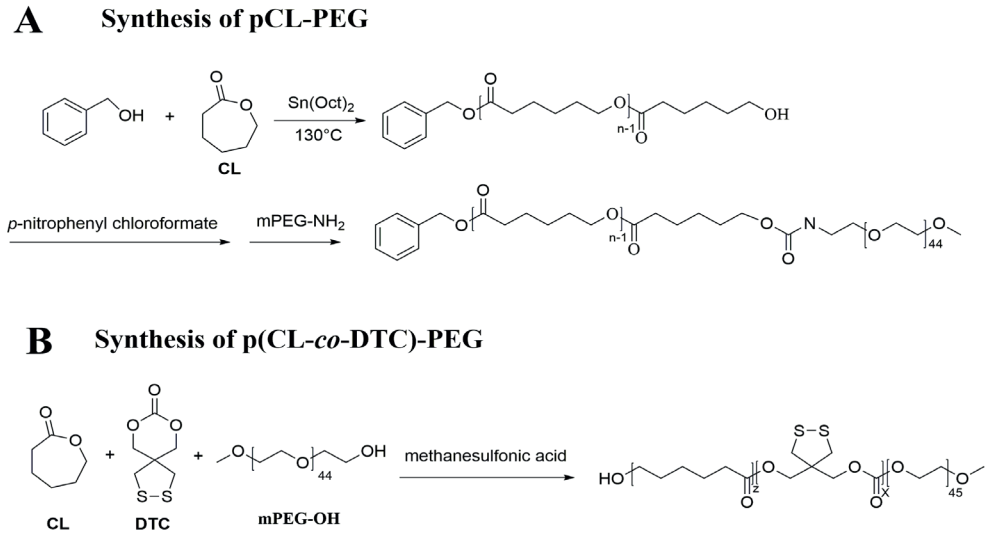


**Scheme S1**. Synthesis route of pCL-PEG (A) and p(CL-*co*-DTC)-PEG (B). (Details are presented in [1] and **Chapter 5** of this thesis, respectively).

**Table S1.** Characteristics of pCL-PEG and p(CL-*co*-DTC)-PEG (PEG molecular weight was 2 kDa) based block copolymers (as presented in [1] and **Chapter 5** of this thesis).

| Polymers | Actual $M_n$ ($^1$H-NMR) | $M_w$ (GPC) | $M_n$ (GPC) | $M_w/M_n$ (GPC) |
|---|---|---|---|---|
| $pCL_9$-PEG | 3.1 | 2.7 | 2.5 | 1.06 |
| $pCL_{15}$-PEG | 3.8 | 3.3 | 3.0 | 1.09 |
| $pCL_{23}$-PEG | 4.7 | 3.7 | 3.2 | 1.16 |
| $p(DTC_{3.8}$-*b*-$CL_9)$-PEG[a] | 4.0 | 2.7 | 2.6 | 1.05 |
| $p(CL_9$-$DTC_{3.9})$-PEG[b] | 4.0 | 2.9 | 2.7 | 1.07 |
| $p(CL_9$-$DTC_{6.6})$-PEG[b] | 4.5 | 3.0 | 2.9 | 1.07 |
| $p(CL_{18}$-$DTC_{7.5})$-PEG[b] | 5.7 | 4.0 | 3.6 | 1.11 |

[a] Copolymer with blocky sequence of CL and DTC.
[b] Copolymers with a random distribution of CL and DTC in the copolymers.

### *S1 Synthesis of* pCL and p(CL-*co*-DTC) oligomers

Benzyl-poly(ε-caprolactone) (pCL) oligomers were building blocks for the final pCL-

PEG block copolymers (**Scheme S1A**, initiation step) (synthesis is presented in [1]). Benzyl-poly(ε-caprolactone-*co*-dithiolane substituted trimethylene carbonate) (p(CL-*co*-DTC)) oligomers were synthesized following the same procedure as that used for synthesis p($CL_9$-$DTC_{3.9}$)-PEG and p($CL_{18}$-$DTC_{7.5}$)-PEG (**Scheme S1B**) except using benzyl alcohol rather than PEG-OH as an initiator, as described in **Chapter 5** of this thesis. In short, CL and DTC were simultaneously copolymerized in dichloromethane at 37 °C for 10 h using benzyl alcohol as the initiator and methanesulfonic acid as catalyst at ε-CL/DTC/initiator/catalyst molar ratios of 9/4/1/1.3 and 18/8/1/1.3, respectively. The final p(CL-*co*-DTC oligomers were obtained after precipitation in cold diethyl ether (-20 °C) and characterized as described in **Chapter 5** of this thesis. Thermal properties of the resulting pCL and p(CL-*co*-DTC) oligomers were measured using differential scanning calorimetry (DSC), TA Instruments, calibrated with indium, as described in [2].

**Table S2**. Flow rates of different steps.

| | **Going-in flow rate (mg/mL)** | | **Going-in flow rate (mg/mL)** | |
|---|---|---|---|---|
| | Tip flow | Focus flow | Cross flow | Detector flow |
| Injection step | 0.2 | 3.0 | 2.7 | 0.5 |
| Separation step, start | 3.2 | 0.0 | 2.7 | 0.5 |
| Separation step, end | 0.6 | 0.0 | 0.1 | 0.5 |
| Final step | 0.5 | 0.0 | 0.0 | 0.5 |

**Table S3.** Thermal properties of pCL and p(CL-*co*-DTC) oligomers.

| **Polymer** | **DSC** | | |
|---|---|---|---|
| | $T_m$ (°C) | $T_g$ (°C) | $\Delta H_m$ (J/g) |
| **$pCL_9$** | 26 | -63 | 88 |
| **$pCL_{15}$** | 39 | -64 | 88 |
| **$pCL_{23}$** | 45 | -64 | 86 |
| **p($CL_9$-$DTC_4$)** | 13 | -60 | 6 |
| **p($CL_{18}$-$DTC_7$)** | 20 | -54 | 21 |

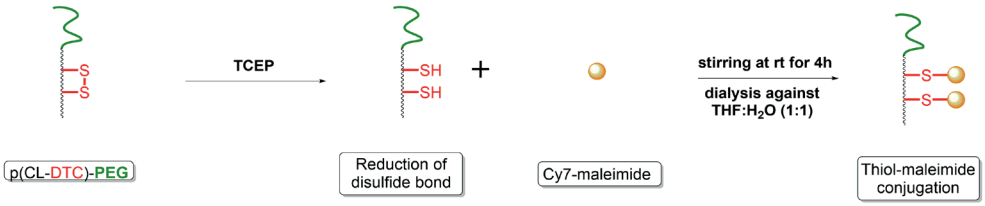


**Scheme S2.** Schematic diagram of coupling of Cy7 to p($CL_{18}$-$DTC_{7.5}$)-PEG block copolymer through thiol-maleimide reaction (Details are presented in [1]).

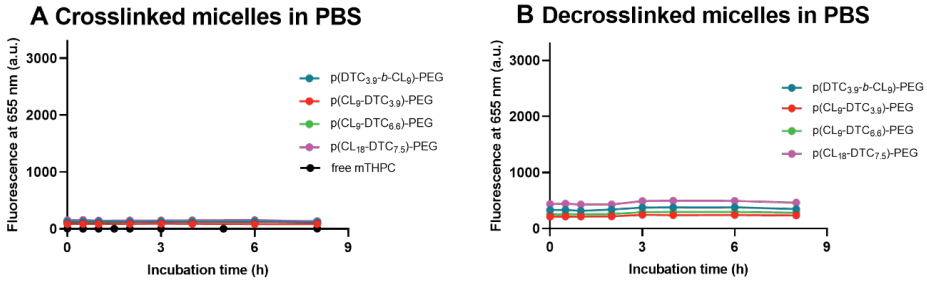


**Figure S1.** Fluorescence intensity ($\lambda_{ex}$ 420 nm, $\lambda_{em}$ 655 nm) of mTHPC-loaded (10 wt%) covalently cross-linked p(CL-*co*-DTC)-PEG micelles (4 mg/mL) as a function of time at 37 °C in PBS; free mTHPC and micelles were diluted 10× in PBS to obtain final polymer and mTHPC concentrations of 0.4 mg/mL and 32 mg/mL, respectively. Decrosslinked micelles were prepared by incubation of the micelles with DTT (to reduce the disulfide bonds) for 12 h at 37 °C.

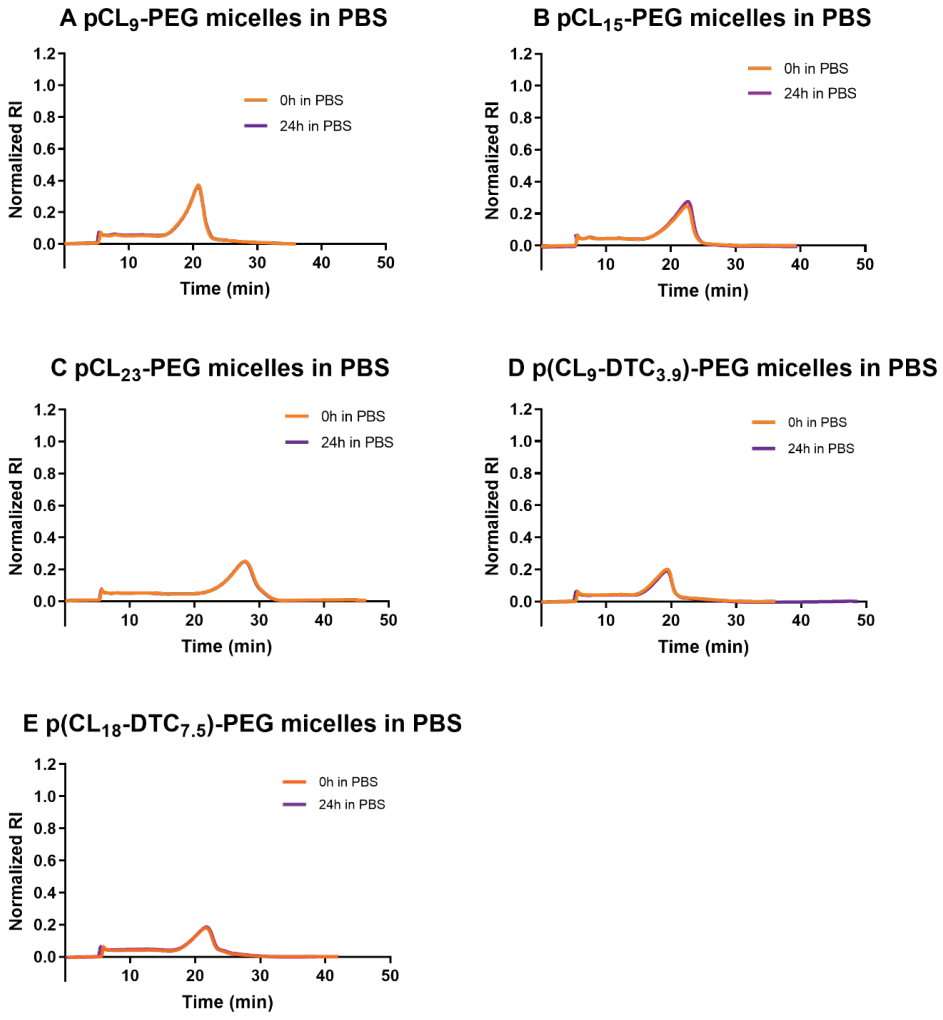


**Figure S2.** Refractive index (RI) of micelles after fractionation by AF4 as a function of incubation time in PBS; empty non (covalently)-crosslinked micelles composed of $pCL_9$-PEG (A), $pCL_{15}$-PEG (B) and $pCL_{23}$-PEG (C) and dithiolane crosslinked micelles consisting of $p(CL_9\text{-}DTC_{3.9})$-PEG (D) and $p(CL_{18}\text{-}DTC_{7.5})$-PEG (E) in PBS were further diluted with PBS at a volume ratio of 7/3 to obtain final polymer concentrations of 7.0 and 2.8 mg/mL, respectively, and incubated for 24 h at 37 °C.

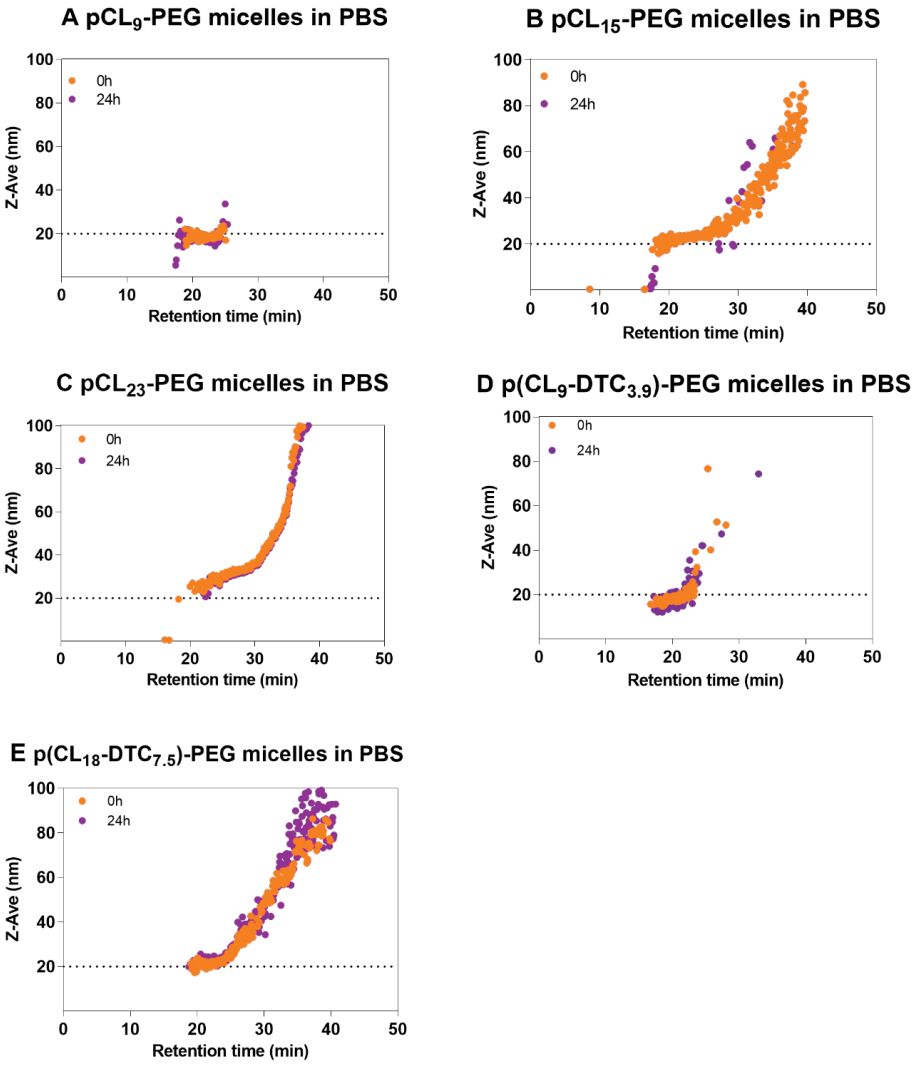


**Figure S3.** Distribution of hydrodynamic diameter ($Z_{ave}$) of micelles after fractionation by AF4, measured by in-line DLS; non (covalently)-crosslinked micelles based $pCL_9$-PEG (A), $pCL_{15}$-PEG (B) and $pCL_{23}$-PEG (C) and dithiolane cross-linked micelles consisting of $p(CL_9\text{-}DTC_{3.9})$-PEG (D) and $p(CL_{18}\text{-}DTC_{7.5})$-PEG (E) in PBS were further diluted with PBS at a volume ratio of 7/3 to obtain final polymer concentrations of 7.0 and 2.8 mg/mL, respectively, and incubated over a period of 24 h at 37 °C.

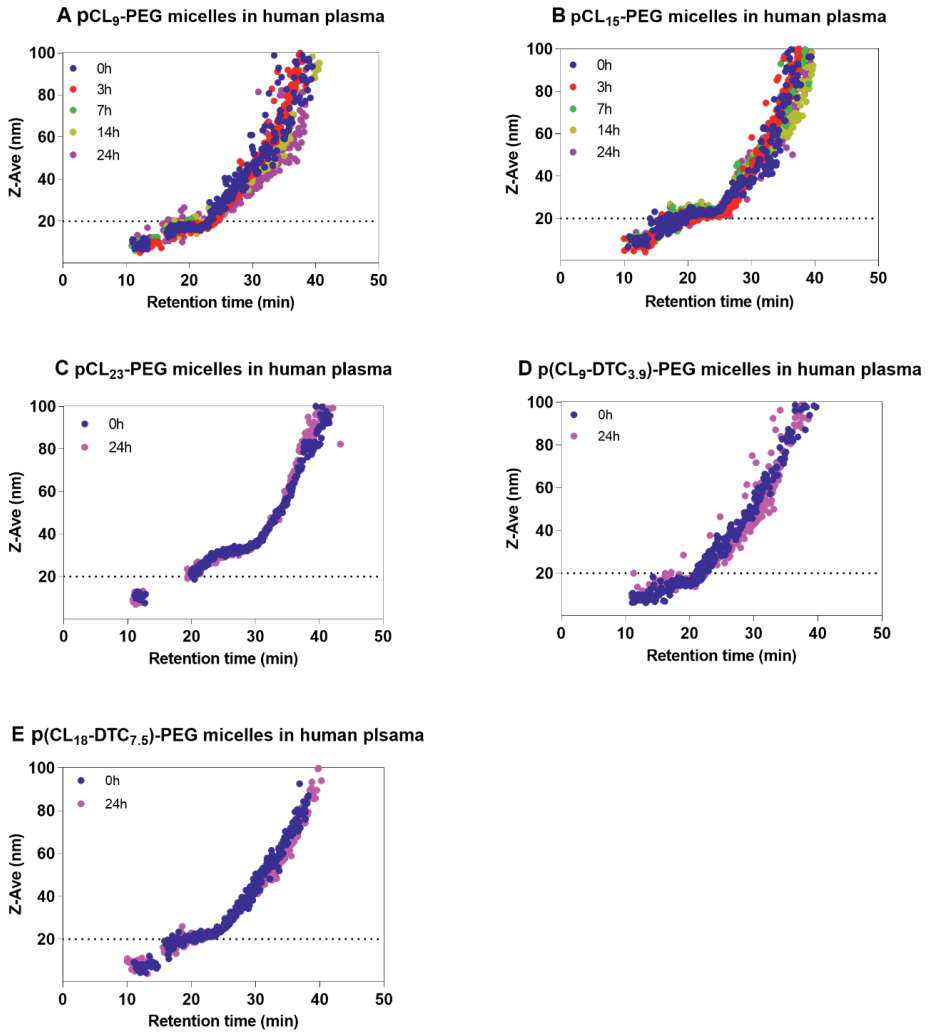


**Figure S4.** Distribution of hydrodynamic diameter ($Z_{ave}$) of micelles after fractionation by AF4, measured by in-line DLS; non (covalently)-crosslinked micelles based $pCL_9$-PEG (A), $pCL_{15}$-PEG (B) and $pCL_{23}$-PEG (C) and dithiolane crosslinked micelles consisting of $p(CL_9\text{-}DTC_{3.9})$-PEG (D) and $p(CL_{18}\text{-}DTC_{7.5})$-PEG (E) in PBS were diluted with human plasma at a volume ratio of 7/3 to obtain final polymer concentrations of 7.0 and 2.8 mg/mL, respectively and incubated over a period of 24 h at 37 °C.

## Reference

1. Liu, Y.; Scrivano, L.; Peterson, J. D.; Fens, M. H. A. M.; Beltrán Hernández, I.; Mesquita, B.; Sastre Torano, J.; Hennink, W. E.; van Nostrum, C. F.; Oliveira, S. EGFR targeted nanobody functionalized polymeric micelles loaded with mTHPC for selective photodynamic therapy. *Mol. Pharmaceutics* **2020,** *17*, 1276–1292.
2. Liu, Y.; Fens, M. H. A. M.; Lou, B.; van Kronenburg, N. C. H.; Maas-Bakker, R. F. M.; Kok, R. J.; Oliveira, S.; Hennink, W. E.; van Nostrum, C. F. π-π-Stacked poly(ε-caprolactone)-b-poly(ethylene glycol) micelles loaded with a photosensitizer for photodynamic therapy. *Pharmaceutics* **2020,** *12*, 338.

# 7

# Chapter 7

## Summary and Perspectives

## 1. Summary

m-Tetra(hydroxyphenyl)chlorin (mTHPC) is one of the most potent second generation photosensitizers (PSs), clinically used for photodynamic therapy (PDT) of head and neck squamous cell carcinomas. However, the very hydrophobic character of mTHPC encounters problems similar to that of many other PSs and chemotherapeutic drugs, such as low-water solubility, aggregation in aqueous media, and limited tumor specificity. These lead to difficulties of formulation and administration, suboptimal PDT efficacy, and off-target effects, such as skin sensitivity. Nanoparticulate drug delivery systems for mTHPC provide opportunities to tackle these drawbacks, by their capacity to encapsulate hydrophobic PS to yield aqueous dispersions facilitating its administration and increase accumulation of the PS at targeted tissues via passive targeting (*i.e.* enhanced permeability and retention (EPR) effect) and/or active targeting strategies.[1-4] It has been demonstrated that the combination of PSs with nano-sized delivery platforms enables delivery of PS to the target tissues, thus improving the PDT effectiveness.[4] Among different drug delivery systems, polymeric micelles, composed of a hydrophilic stealth corona (most commonly based on PEG) for ensuring long circulation and colloidal stability, and a hydrophobic core for accommodating hydrophobic drugs, are suitable and attractive systems for delivery of mTHPC. Over the past decades, polymeric micelles have been extensively investigated for solubilisation and delivery of hydrophobic chemotherapeutic drugs.[5-8] Apart from the high number of academic publications on this topic, encouragingly, several micellar formulations have entered clinical trials.[6,9,10] In this thesis, different polymeric micelles based on poly(ε-caprolactone)-*b*-poly(ethylene glycol) (PCL-PEG) block copolymers were prepared to load mTHPC with the aim to develop suitable micellar systems for targeted delivery of mTHPC. The stability of polymeric micelles and the retention of mTHPC in the micelles are essential for improved pharmacokinetics, selective biodistribution and consequently effective PDT. Therefore, this thesis reports on studies of *in vitro* stability, *in vivo* circulation kinetics, and biodistribution of different micellar mTHPC formulations. Further emphasis is given on the synthesis and characterization of a variety of amphiphilic block copolymers based on PEG (as hydrophilic block) and PCL (as hydrophobic blocks). To modulate and tailor the properties of the hydrophobic block, CL is copolymerized with carbonates functionalized by aromatic groups (**Chapter 4**) and crosslinkable dithiolanes (**Chapters 5** and **6**), respectively, to design π-π stacked and core crosslinked micelles with the aim to improve the stability of the micelles in the circulation and the retention of mTHPC in the core of the micelles.

In **Chapter 1**, a general introduction of PDT and PSs including mTHPC is given. Subsequently, mTHPC's current commercial formulations, namely Foscan®, Foslip®, and FosPEG®, and their limitations are briefly reviewed. In addition, this chapter also provides a short introduction of polymeric micelles for targeted delivery of mTHPC.

Finally, the aim of this thesis is outlined.

Selective elimination of macrophages by PDT is a new and promising therapeutic modality for the reduction of atherosclerotic plaques. In **Chapter 2**, mTHPC was encapsulated in polymeric micelles based on benzyl-poly(ε-caprolactone)-*b*-methoxy poly(ethylene glycol) (Bz-PCL-PEG) with high efficiency and capacity, aiming at macrophage selective PDT. mTHPC-loaded micelles' photo-cytotoxicity is induced by the degradation of the PCL block of Bz-PCL-PEG micelles by lipases. In accordance with their higher lipase activity, RAW264.7 macrophages degrade the micelles faster and thus activate the PS earlier than C166 endothelial cells, consequently creating a window for selective killing of RAW264.7 macrophages, which model the macrophages located in atherosclerotic plaques. However, we observed release of mTHPC from the micelles incubated with blood plasma for 30 minutes, which explains that the observed *in vivo* pharmacokinetics of mTHPC as micellar formulation was similar to that of free mTHPC. Therefore, translation from *in vitro* to *in vivo* of the beneficial selective macrophage photocytotoxicity resulting from formulating PS in Bz-PCL-PEG micelles was not possible. Nevertheless, we observed accumulation of mTHPC in atherosclerotic lesions of mice aorta which is probably the result of binding to lipoproteins upon release from the micelles.

The premature mTHPC release from the micelles observed in **Chapter 2**, makes our following research dedicated to improving the stability of mTHPC-loaded Bz-PCL-PEG based micelles and thus the mTHPC retention in micelles by different strategies. In **Chapter 3**, we synthesized the benzyl-poly(ε-caprolactone)-*b*-methoxy-poly(ethylene glycol) (Bz-$PCL_n$-PEG) based block copolymers, with the same structure as the polymer mentioned in **Chapter 2**, but with varying chain lengths of $PCL_n$ (n=9, 15, 23). Polymeric micelles with three different diameters (17, 24 and 45 nm) based on Bz-$PCL_n$-PEG (n=9, 15 or 23) were prepared with different mTHPC loadings. We hypothesized that the core of the micelles can be stabilized by increasing the hydrophobic interactions (*i.e.* the chain length of hydrophobic block). To favor uptake of the micelles by cancer cells that over-express the epidermal growth factor receptor (EGFR), the micelles were decorated with an EGFR targeted nanobody (named EGa1). It was shown that EGa1 conjugated micelles were internalized upon specific binding with the EGFR receptor over-expressed on the surface of A431 cells, resulting in enhanced cellular uptake, as compared to EGFR low expressing HeLa cells. In line with this, mTHPC-loaded in EGa1-conjugated $PCL_{23}$-PEG micelles showed selective PDT against A431 cells, compared to HeLa cells. Finally, an *in vivo* pharmacokinetic study showed that after *i.v.* injection, mTHPC loaded in the $PCL_{23}$-PEG micelles displayed a significant increase in half-lives in the circulation, as compared to that of free mTHPC ($t_{½}$-α: ~1 *vs* <0.3 while $t_{½}$-β: 14 *vs* 2 h), independently of the presence of EGa1, due to the prolonged circulating time of the micelles ($t_{½}$-β:18 h). Thus, this chapter demonstrated that increasing the hydrophobic interactions resulting from increased hydrophobic blocks (*i.e.* PCL in this case) can lead

to the excellent stability of the prepared micelles and consequently, prolonged retention of mTHPC in the circulation. In addition, this chapter indicates that conjugation of EGa1 nanobody to the surface of $PCL_{23}$-PEG micelles has potential to significantly improve the selectivity and efficacy of PDT to EGFR over-expressing tumors.

It was previously reported by our group that incorporation of aromatic rings in the hydrophobic core of polymeric micelles can stabilize them due to π-π stacking interactions.[11,12] Inspired by that, in **Chapter 4**, a pendant aromatic rings containing monomer (*i.e.* a benzyl-functionalized trimethylene carbonate (TMC-Bz)) was incorporated in the hydrophobic block of the poly(ε-caprolactone)-*b*-poly(ethylene glycol) (PCL-PEG) polymer chains. For comparison, PCL-PEG block copolymers with unmodified hydroxide and Bz modified end groups were also synthesized. We showed that incorporation of aromatic rings in PCL-PEG based copolymers, regardless of their positions and the amounts in the polymer chains, yielded smaller micelles (18-30 nm) with better colloidal stability in PBS, than micelles without aromatic groups. The *in vivo* circulation time of micelles containing multiple pendant aromatic groups was longer than that of micelles with a single terminal aromatic group ($t_{1/2}$-α: ~0.7 and $t_{1/2}$-β: 2.9 h for the former *vs* $t_{1/2}$: <0.3 h for the latter) while partitioning of the encapsulated photosensitizer (mTHPC) between micelles and human plasma *in vitro* was indeed favored for micelles that contained the pendant aromatic groups. However, the increased stability was not sufficient to fully retain mTHPC in the micelles upon injection in the circulation, as indicated by similar biodistribution patterns of micellar mTHPC compared to free mTHPC, and unequal biodistribution patterns of mTHPC and the host micelles. This chapter again points that targeted delivery of PS mediated by EPR effect would not be possible due to a rapid release of mTHPC from the micellar formulations.

In many studies, chemical crosslinking has shown to be effective to stabilize polymeric micelles.[13-16] Therefore, the research in **Chapter 5** and **6** was focused on the preparation of stable micelles, by introducing disulfide units (*i.e.* dithiolane rings) as crosslinkable moieties, which can form dynamic and reversible crosslinks in the micellar core. In **Chapter 5**, we introduced pendant dithiolane rings as crosslinkable moieties in poly(ε-caprolactone)-*b*-poly(ethylene glycol) (PCL-PEG) block copolymers by ring opening copolymerization of CL and dithiolane-substituted cyclic carbonates, with or without a flexible diester linker between the dithiolane ring and the cyclic carbonate unit using different catalysts. The type of catalyst was shown to have a profound influence on the monomer sequence, as a consequence of the different monomer reactivities and occurrence of transesterification reactions. Interestingly, we demonstrated that self-crosslinkable copolymers were obtained with the dithiolane units connected closely to the polymer backbone, whereas the presence of a linker unit between the dithiolane and the backbone prevented self-crosslinking. The obtained amphiphilic PEGylated block copolymers formed micelles by nanoprecipitation in aqueous environment and

crosslinked spontaneously by disulfide-exchange during subsequent dialysis, independent of the monomer sequence, comonomer ratio, or the presence of reducing agents. The dithiolane crosslinked micelles showed reduction-responsive dissociation in the presence of 10 mM glutathione. Importantly, we also evaluated the intracellular dissociation kinetics upon reduction of two representative dithiolane crosslinked micelles explored in this chapter, based on poly(ε-caprolactone)-*co*-poly(1,2-dithiolane-carbonate)-*b*-poly(ethylene glycol) (*i.e.* P($CL_9$-$DTC_{3.9}$)-PEG and P($CL_{18}$-$DTC_{7.5}$)-PEG). For this, micelles were dually labeled with Cy3/Cy5, which is a known pair for Förster resonance energy transfer (FRET),[17] allowing for the intracellular dissociation of the micelles to be observed as a reduction of FRET fluorescence over time. The representative confocal microscopy images (**Figure 1A** and **B**) show that the fluorescence intensities in living A431 and HeLa cells pretreated with crosslinked P($CL_9$-$DTC_{3.9}$)-PEG and P($CL_{18}$-$DTC_{7.5}$)-PEG micelles exhibited a significant decrease after 1 and 1.5 h, giving clear proof of intracellular dissociation of both micelles (unpublished data). In line with this, the quantified fluorescence intensity from the images (**Figure 1C**) indicates that FRET fluorescent of both micelles showed a time-dependent decrease in both A431 and HeLa cells, reflecting the time-dependent micellar dissociation.

In **Chapter 6**, studies were carried out to evaluate *in vitro* and *in vivo* stability of mTHPC-loaded dithiolane-crosslinked micelles based on poly(ε-caprolactone)-*co*-poly(1,2-dithiolane-carbonate)-*b*-poly(ethylene glycol) (P(CL-*co*-DTC)-PEG) which were explored in **Chapter 5** of this thesis and compared with PCL-PEG based micelles that were explored in **Chapter 3** of this thesis. We demonstrated that asymmetric flow field-flow fractionation (AF4) is an excellent technique to evaluate the stability of nanoparticles in biological media and thus predict the stability of drug loaded nanoparticles after *i.v.* administration. AF4 analysis showed that small non-crosslinked $PCL_9$-PEG (17 nm) and $PCL_{15}$-PEG (22 nm) micelles have lower stability in plasma than physically (due to crystallinity PCL) crosslinked $PCL_{23}$-PEG micelles with larger sizes (43 nm) and chemically crosslinked P($CL_9$-$DTC_{3.9}$)-PEG and P($CL_{18}$-$DTC_{7.5}$)-PEG micelles with similar small sizes (~20 nm). AF4 also showed that PS (re)distribution to different plasma proteins was observed, demonstrating that the PS was not retained in the hydrophobic core of the micelles. Importantly, *in vivo* circulation kinetics show that chemically crosslinked P($CL_{18}$-$DTC_{7.5}$)-PEG micelles and the loaded mTHPC had significantly shorter half-life values ($t_{1/2}$-β of both micelles and mTHPC: ~2 h) as compared to physically crosslinked $PCL_{23}$-PEG micelles and the loaded PS ($t_{1/2}$-β of micelles and mTHPC:14 and 18 h, respectively) observed in **Chapter 3** of this thesis. In line with this, long circulating $PCL_{23}$-PEG micelles resulted in significantly higher tumor accumulation of both the micelles and its loaded mTHPC, as compared to short circulating crosslinked P($CL_{18}$-$DTC_{7.5}$)-PEG micelles. These *in vivo* data were in great agreement with the *in vitro* stability studies, which showed that in plasma, despite excellent *in vitro* stability of both micelles as observed by AF4, the retention of

mTHPC in $PCL_{23}$-PEG micelles (>8 h) was much longer than that in $P(CL_{18}$-$DTC_{7.5})$-PEG micelles (~4 h) as observed using fluorescence microscopy.

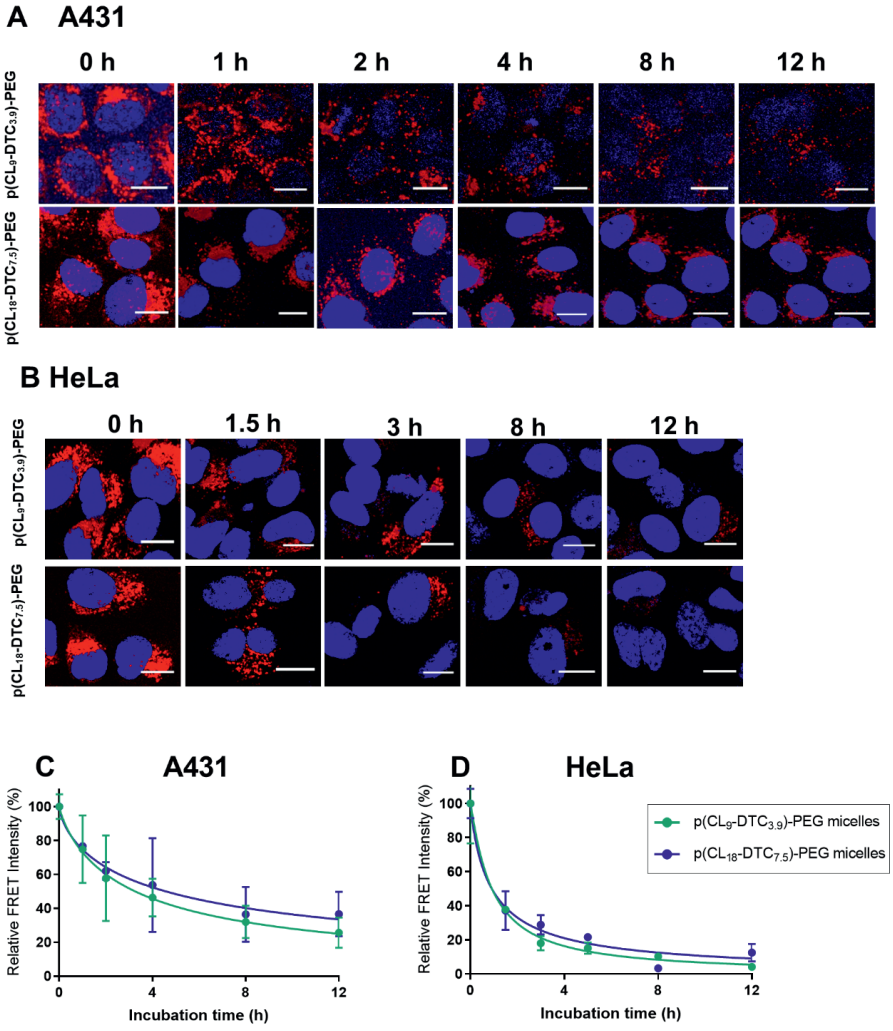


**Figure 1**. (A-B) Representative confocal fluorescence microscopic images of A431 and HeLa cells incubated with dithiolane crosslinked $P(CL_9$-$DTC_{3.9})$-PEG and $P(CL_{18}$-$DTC_{7.5})$-PEG micelles dually labeled with Cy3 and Cy5. A431 (A) and HeLa (B) cells were incubated with micelles (2 mg/mL) for 4 and 5 h at 37℃, respectively, followed by washes to remove non-internalized micelles. Subsequently, cells were continuously cultured at 37 °C, and the emission fluorescence at 676 nm recorded upon excitation at 488 nm (*i.e.* FRET signal) up to 12 h post removal of the formulations. Cell nuclei were stained in blue with Hoechst, while the FRET fluorescence of Cy3/Cy5-labeled micelles is presented in red. Scale bars indicate 15 μm. (C) Quantification of FRET fluorescence intensity of Cy3/Cy5-labeled micelles ($\lambda_{ex}$ 488 nm, $\lambda_{em}$ 676 nm, 2 mg/mL polymer) of A431 and HeLa cells, post removal of micellar formulations. The quantified fluorescence intensity was normalized by the intensity of Cy3/Cy5-labeled micelles directly after 4 and 5 h incubation with A431 and HeLa cells, respectively, in each group and by the number of cells.

## 2. Perspectives

This thesis focuses on investigating the preparation of stable polymeric micelles with smaller sizes (below 60 nm) for delivery of a clinically used PS (mTHPC). Their small sizes make them suitable to extravasate the bloodstream, accumulate at and retain in tumors through the EPR effect (passive targeting), and subsequently penetrate into the interior of the tumor, being crucial factors for anti-tumoral efficacy of nanomedicines. [18-20] However, these small sizes can compromise the stability of micelles in the circulation leading to premature drug release, as shown in **Chapter 2**. This chapter shows that the PCL-PEG based micelles with 16 nm are not stable in biological fluids, which was further substantiated using asymmetric flow field-flow fractionation (AF4) as reported and discussed in **Chapter 6** of this thesis, thus leading to the premature and unwanted mTHPC release in the bloodstream. Therefore, different strategies were here exploited to enhance the micellar stability and thus the cargo retention in the core of these small micelles. These included the increase in physical interactions between polymer chains and/or loaded PS, by either increasing the chain length of the micellar core-forming hydrophobic block (**Chapter 3**) or incorporating multiple π-π stacking monomers in PCL-PEG based copolymers (**Chapter 4**), as well as the use of reversibly chemical core-crosslinking (**Chapter 6**).

As demonstrated in **Chapter 3**, increasing the hydrophobic interactions by increasing the molecular weight of the hydrophobic blocks (*i.e.* PCL in this case) leads to the excellent stability of the prepared micelles. This, in turn, resulted in significantly prolonged retention of mTHPC in the circulation, compared to free mTHPC. These promising results encourage further research of this system for targeted PS delivery in the future. For instance, the PDT efficacy studies should be carried out using different tumor models to further prove the efficacy of the mTHPC loaded micelles with long circulation behavior and also to verify the added value of using the nanobody for targeting cancer cells as compared to the non-targeted formulation.

**Chapter 4** shows that despite the improved circulation time of micelles with multiple pendant aromatic groups (~50 mol%) by strong π-π stacking, premature release of mTHPC from these micelles *in vivo* was still observed, leading to the loss of the beneficial effect of targeted delivery of PS via micelles mediated by EPR effect. In other words, the investigated polymeric micelles only act as a solubilizer rather than a true carrier. In line with our findings, it was previously reported that paclitaxel (PTX) loaded in thermosensitive micelles containing aromatic HPMAm-Bz monomers (~30 mol%) exhibited similar pharmacokinetic profile as loaded in micelles without aromatic groups and compared with free PTX, despite the significantly improved *in vitro* stability and drug retention by π-π stacking [21-23]. Shi *et al* demonstrated in the later study that by increasing aromatic repeating units (*i.e.* HPMAm-Bz) to 100 mol%, the prepared mPEG-*b*-p(HPMAm-Bz) micelles displayed prolonged blood circulation kinetics and,

importantly, efficient PTX retention in the micelles, thus resulting in high tumor accumulation of PTX and substantially improved anti-tumor efficacy.[11] Therefore, to make these π-π stacked micelles based on P(CL/TMC-Bz)-PEG stably incorporate mTHPC (*i.e.* become a true carrier), we propose to further increase the content of pendant aromatic rings (TMC-Bz) in the polymer chains, and/or to increase the total chain length of hydrophobic blocks.

Disulfide containing dithiolane rings are interesting moieties to crosslink and thus stabilize the core of polymeric micelles due to their reversible nature. As shown in **Chapter 5**, dithiolane units directly connected to the polymer backbone can spontaneously rearrange, when they come in close proximity and thus form crosslinks between the polymer chains. As a result, the micelles are not only stabilized, but also become responsive to the reducing environment inside a cell, and thus allow triggered release of the cargo, as indicated in **Figure 1**. However, the dithiolane derived crosslinking in the micelles was not very effective as the dithiolanes are too stable, resulting in only a small portion of rearrangement (≤20%). In line with low crosslinking capacity derived from dithiolane, the *in vivo* studies in **Chapter 6** showed that the dithiolane crosslinked micelles had short circulating time in the bloodstream and importantly, poor mTHPC retention within the micelles, as indicated by lower tumor accumulation of the micelles as compared to the loaded mTHPC and the free PS. This insufficient mTHPC retention requires further optimization. Therefore, to further improve the *in vivo* behavior of these micelles, a proposed strategy for future research is to increase the crosslinking density of the micellar core by introducing different kinds of disulfide or (protected) thiol groups. Notably, the dissociation of polymeric micelles can be prevented by chemical crosslinking [13,24,25] but this approach does not necessarily improve the cargo retention in the micelles. For instance, it was reported that even by using stable core-crosslinked micelles based on mPEG-*b*-p((HEMAm-Lac) with long circulation time in the bloodstream, physically loaded PTX exhibited an elimination time similar as that of free PTX, which is ascribed to a low PTX retention in those micelles.[23,26] To improve drug retention in the core of polymeric micelles, chemical conjugation of drug molecules has been shown to be an effective method.[27-29] Therefore, to stably incorporate PS in the particles and thus achieve targeted drug delivery, it is proposed to attach the PS to the polymer chains via *e.g.* a (reducible) disulfide bond or pH sensitive hydrazine bond. The reversibly covalent bonds or linkers would be preferably selected for coupling PS with polymer, which can be broken in the cells and release the PS. However, it should be noted that chemical modification of PS molecules and their conjugation to polymeric micelles can be technically challenging, as their photochemical properties can be affected.

It is worth mentioning that polymeric micelles are in general attractive candidates for encapsulation of hydrophobic drugs in their hydrophobic core. On the one hand, polymer micelles can be used to solubilize hydrophobic drugs in aqueous media and enable the parenteral administration of drugs without the use of organic cosolvents.

These non-organic solvent containing excipients can avoid drug precipitation at the injection site and pain upon bolus administration. More importantly, due to the good biocompatibility of many currently used amphiphilic polymers such as PCL-PEG,[5,30-32] polymeric micelles are safe solubilization agents for hydrophobic drugs. This is in contrast to some other types of solubility enhancers, *e.g.* Cremophor EL for PTX, which can cause hypersensitivity reactions.[33,34] On the other hand, in an ideal situation, besides being solubilizers, polymeric micelles can act as drug delivery systems for targeted delivery of micelle-loaded drugs exploiting the EPR effect, and even the receptor-mediated uptake for more selective therapy. However, this can only be accomplished by polymeric micelles with sufficient stability in the circulation and simultaneously good drug retention. Therefore, the systems explored in **Chapters 2**, **4** and **6** can be used as safe solubilizers while the polymeric micelles shown in **Chapter 3** can be considered as safe solubilizers/delivery systems of mTHPC or other hydrophobic compounds. Particularly, the micelles based on $PCL_{23}$-PEG as a relative 'simple' polymer showed high stability in plasma and excellent circulation kinetics and retention of mTHPC, likely because of physical crosslinking of the core due to crystallization of the PCL blocks. These micelles also showed relatively high tumor accumulation of both the micelles and the loaded PS after *i.v.* administration. These polymeric micelles have the following advantages, beneficial to clinical translation: 1) simple synthesis procedures favoring large-scale manufacturing; 2) biocompatible; 3) high drug loading efficiency; 4) non-organic solvents used, facilitating its administration and reducing pain and discomfort during administration; and 5) cost-effective for industrial exploration and commercialization.

## 3. Conclusion

The research presented in this thesis explores the possibility of preparation of stable PCL-PEG based polymeric micelles with small sizes as targeted delivery systems of mTHPC for PDT. We focused on the stabilization of small micelles exploiting chemical (disulfide crosslinking) and physical crosslinking (crystallization or π-π stacking), thus improving the retention of PS *in vivo* by tailoring the compositions and architectures of amphiphilic block copolymers using different strategies. The results of the pharmacokinetics, including circulation kinetics and biodistribution of these different stabilized micelles and their loaded mTHPC, provide important scientific insights for the further rational development of the polymeric micelles as nanocarriers for targeted drug delivery.

## References


1. Lammers, T.; Kiessling, F.; Hennink, W. E.; Storm, G. Drug targeting to tumors: principles, pitfalls and (pre-) clinical progress. *J. Control. Release* **2012,** *161*, 175-187.
2. Wang, A. Z.; Langer, R.; Farokhzad, O. C. Nanoparticle delivery of cancer drugs. *Annu Rev Med* **2012,** *63*, 185-198.
3. Maeda, H.; Wu, J.; Sawa, T.; Matsumura, Y.; Hori, K. Tumor vascular permeability and the EPR effect in macromolecular therapeutics: a review. *J. Control. Release* **2000,** *65*, 271-284.
4. Yakavets, I.; Millard, M.; Zorin, V.; Lassalle, H. P.; Bezdetnaya, L. Current state of the nanoscale delivery systems for temoporfin-based photodynamic therapy: Advanced delivery strategies. *J. Control. Release* **2019,** *304*, 268-287.
5. Deng, C.; Jiang, Y.; Cheng, R.; Meng, F.; Zhong, Z. Biodegradable polymeric micelles for targeted and controlled anticancer drug delivery: Promises, progress and prospects. *Nano Today* **2012,** *7*, 467-480.
6. Varela-Moreira, A.; Shi, Y.; Fens, M. H. A. M.; Lammers, T.; Hennink, W. E.; Schiffelers, R. M. Clinical application of polymeric micelles for the treatment of cancer. *Materials Chemistry Frontiers* **2017,** *1*, 1485-1501.
7. Cabral, H.; Kataoka, K. Progress of drug-loaded polymeric micelles into clinical studies. *J. Control. Release* **2014,** *190*, 465-476.
8. Houdaihed, L.; Evans, J. C.; Allen, C. Overcoming the road blocks: advancement of block copolymer micelles for cancer therapy in the clinic. *Mol. Pharmaceutics* **2017,** *14*, 2503-2517.
9. Cabral, H.; Kataoka, K. Progress of drug-loaded polymeric micelles into clinical studies. *J. Control. Release* **2014,** *190*, 465-476.
10. Gong, J.; Chen, M.; Zheng, Y.; Wang, S.; Wang, Y. Polymeric micelles drug delivery system in oncology. *J. Control. Release* **2012,** *159*, 312-323.
11. Shi, Y.; van der Meel, R.; Theek, B.; Oude Blenke, E.; Pieters, E. H.; Fens, M. H.; Ehling, J.; Schiffelers, R. M.; Storm, G.; van Nostrum, C. F.; Lammers, T.; Hennink, W. E. Complete regression of xenograft tumors upon targeted delivery of paclitaxel via π-π stacking stabilized polymeric micelles. *ACS Nano* **2015,** *9*, 3740-3752.
12. Shi, Y.; Elkhabaz, A.; Yengej, F. A.; van den Dikkenberg, J.; Hennink, W. E.; van Nostrum, C. F. π-π Stacking induced enhanced molecular solubilization, singlet oxygen production, and retention of a photosensitizer loaded in thermosensitive polymeric micelles. *Advanced healthcare materials* **2014,** *3*, 2023-2031.
13. van Nostrum, C. F. Covalently cross-linked amphiphilic block copolymer micelles. *Soft Matter* **2011,** *7*, 3246-3259.
14. Meng, F.; Hennink, W. E.; Zhong, Z. Reduction-sensitive polymers and bioconjugates for biomedical applications. *Biomaterials* **2009,** *30*, 2180-2198.
15. Biswas, D.; An, S. Y.; Li, Y.; Wang, X.; Oh, J. K. Intracellular delivery of colloidally stable core-cross-linked triblock copolymer micelles with glutathione-responsive enhanced drug release for cancer therapy. *Mol. Pharmaceutics* **2017,** *14*, 2518-2528.

16. Tan, C.; Wang, Y.; Fan, W. Exploring polymeric micelles for improved delivery of anticancer agents: recent developments in preclinical studies. *Pharmaceutics* **2013,** *5*, 201-219.
17. Roy, R.; Hohng, S.; Ha, T. A practical guide to single-molecule FRET. *Nat. Methods* **2008,** *5*, 507-516.
18. Cabral, H.; Matsumoto, Y.; Mizuno, K.; Chen, Q.; Murakami, M.; Kimura, M.; Terada, Y.; Kano, M. R.; Miyazono, K.; Uesaka, M.; Nishiyama, N.; Kataoka, K. Accumulation of sub-100 nm polymeric micelles in poorly permeable tumours depends on size. *Nat. Nanotechnol* **2011,** *6*, 815-823.
19. Danhier, F.; Feron, O.; Preat, V. To exploit the tumor microenvironment: Passive and active tumor targeting of nanocarriers for anti-cancer drug delivery. *J. Control. Release* **2010,** *148*, 135-146.
20. Jain, R. K.; Stylianopoulos, T. Delivering nanomedicine to solid tumors. *Nat. Rev. Clin. Oncol.* **2010,** *7*, 653-664.
21. Shi, Y.; van Steenbergen, M. J.; Teunissen, E. A.; Novo, L.; Gradmann, S.; Baldus, M.; van Nostrum, C. F.; Hennink, W. E. π-π stacking increases the stability and loading capacity of thermosensitive polymeric micelles for chemotherapeutic drugs. *Biomacromolecules* **2013,** *14*, 1826-1837.
22. Kim, S. C.; Kim, D. W.; Shim, Y. H.; Bang, J. S.; Oh, H. S.; Wan Kim, S.; Seo, M. H. In vivo evaluation of polymeric micellar paclitaxel formulation: toxicity and efficacy. *J. Control. Release* **2001,** *72*, 191-202.
23. Rijcken, C. J. Tuneable & degradable polymeric micelles for drug delivery: from synthesis to feasibility *in vivo*. *Doctoral dissertation; Utrecht University, Utrecht,* **2007**.
24. O'Reilly, R. K.; Hawker, C. J.; Wooley, K. L. Cross-linked block copolymer micelles: functional nanostructures of great potential and versatility. *Chemical Society reviews* **2006,** *35*, 1068-1083.
25. Read, E. S.; Armes, S. P. Recent advances in shell cross-linked micelles. *Chem. Commun.* **2007**, 3021-3035.
26. Letchford, K.; Burt, H. M. Copolymer micelles and nanospheres with different in vitro stability demonstrate similar paclitaxel pharmacokinetics. *Mol. Pharmaceutics* **2012,** *9*, 248-260.
27. Bae, Y.; Nishiyama, N.; Fukushima, S.; Koyama, H.; Yasuhiro, M.; Kataoka, K. Preparation and biological characterization of polymeric micelle drug carriers with intracellular pH-triggered drug release property: tumor permeability, controlled subcellular drug distribution, and enhanced in vivo antitumor efficacy. *Bioconjug. Chem.* **2005,** *16*, 122-130.
28. Bae, Y.; Nishiyama, N.; Kataoka, K. In Vivo Antitumor Activity of the Folate-Conjugated pH-Sensitive Polymeric Micelle Selectively Releasing Adriamycin in the Intracellular Acidic Compartments. *Bioconjug. Chem.* **2007,** *18*, 1131-1139.
29. Talelli, M.; Iman, M.; Varkouhi, A. K.; Rijcken, C. J.; Schiffelers, R. M.; Etrych, T.; Ulbrich, K.; van Nostrum, C. F.; Lammers, T.; Storm, G.; Hennink, W. E. Core-crosslinked polymeric micelles with controlled release of covalently entrapped doxorubicin. *Biomaterials* **2010,** *31*, 7797-7804.
30. Bao, G.; Ma, P. X. Synthetic biodegradable functional polymers for tissue engineering: a brief review. *Sci. China Chem* **2014,** *57*, 490-500.
31. Vasir, J. K.; Labhasetwar, V. Biodegradable nanoparticles for cytosolic delivery of therapeutics. *Adv. Drug Deliv. Rev.* **2007,** *59*, 718-728.
32. Peer, D.; Karp, J. M.; Hong, S.; Farokhzad, O. C.; Margalit, R.; Langer, R. Nanocarriers as an emerging platform for cancer therapy. *Nature Nanotechnology* **2007,** *2*, 751-760.

33. Spencer, C. M.; Faulds, D. Paclitaxel. A review of its pharmacodynamic and pharmacokinetic properties and therapeutic potential in the treatment of cancer. *Drugs* **1994,** *48*, 794-847.
34. Weiss, R. B.; Donehower, R. C.; Wiernik, P. H.; Ohnuma, T.; Gralla, R. J.; Trump, D. L.; Baker, J. R., Jr.; Van Echo, D. A.; Von Hoff, D. D.; Leyland-Jones, B. Hypersensitivity reactions from taxol. *Journal of clinical oncology* **1990,** *8*, 1263-1268.

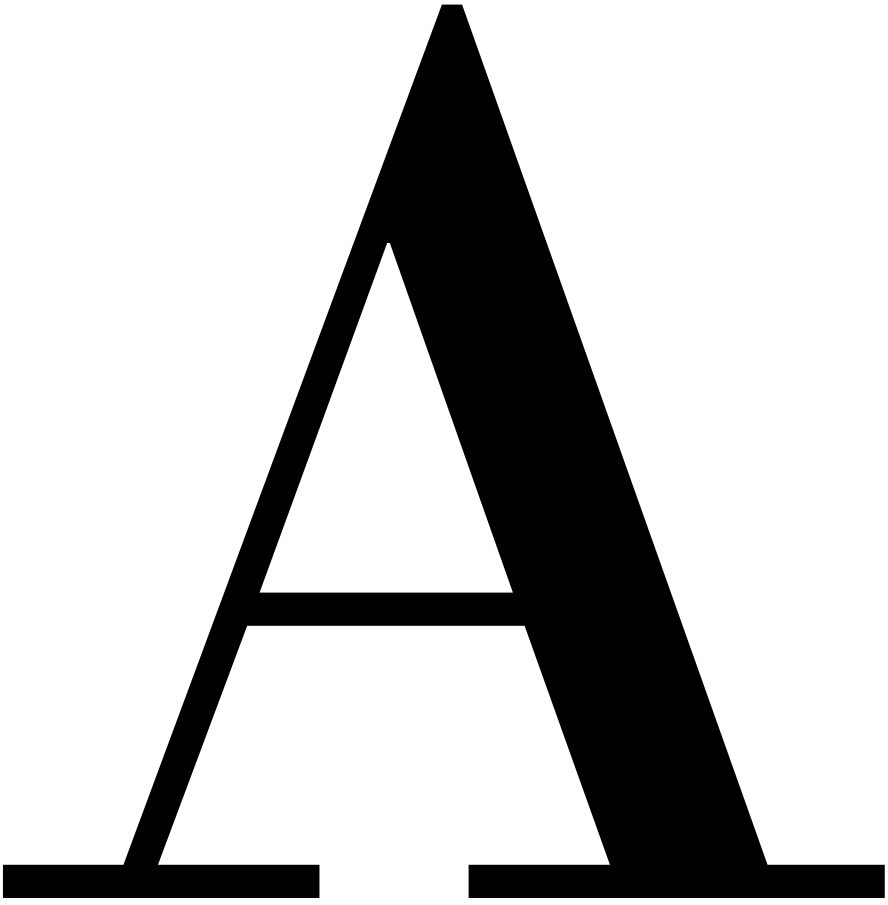

# Appendices

Nederlandse Samenvatting
Acknowledgements
Curriculum Vitae
List of Publications

## Nederlandse Samenvatting

m-Tetra(hydroxyphenyl)chlorin (mTHPC) is een van de meest potente tweede generatie fotosensibilisatoren (PSs) en wordt klinisch toegepast voor fotodynamische therapie (PDT) in hoofd- en halsplaveiselcelcarcinoom. Desalniettemin, veroorzaakt het zeer hydrofobe karakter van mTHPC verschillende problemen op die vergelijkbaar zijn met veel andere PSs en chemotherapeutische middelen, zoals lage wateroplosbaarheid, aggregatie in waterige media, en gelimiteerde tumor specificiteit. Deze eigenschappen zorgen voor formulering en administratie moeilijkheden, suboptimale PDT-werkzaamheid, en off-target effecten, zoals huidgevoeligheid. Het ontwikkelen van een geneesmiddelafgiftesysteem gebruikmakend van nanodeeltjes voor mTHPC biedt kansen om deze nadelen aan te pakken, door middel van hun capaciteit om hydrofobe PS in te kapselen, leidend tot waterige dispersies die vervolgens een rol spelen in het faciliteren van de toediening en verhoogde accumulatie van de PS in doelweefsels via passieve 'targeting' (dat wil zeggen een verbeterde permeabiliteit en retentie (EPR) effect) en/of actieve 'targeting' strategieën. Het is aangetoond dat PSs in combinatie met nano-afleverplatformen de mogelijkheid geven tot afgifte van PS aan doelweefsels, resulterend in toename van PDT effectiviteit. Polymere micellen, bestaande uit een hydrofiele 'stealth' corona (meestal gebaseerd op PEG) die verantwoordelijk is voor een lange circulatie en goede colloïdale stabiliteit, en een hydrofobe kern geschikt voor het accommoderen van hydrofobe geneesmiddelen, zijn geschikte en aantrekkelijke afgiftesystemen voor mTHPC. In de afgelopen decennia is veel onderzoek verricht naar polymere micellen voor de verbetering van de oplosbaarheid en afgifte van hydrofobe chemotherapeutische middelen. Afgezien van het hoge aantal academische publicaties omtrent dit onderwerp, is ook het aantal micellaire formuleringen in klinische trials een bemoedigend gegeven. In dit proefschrift zijn verschillende polymere micellen vervaardigd op basis van poly(ε-caprolacton)-*b*-poly(ethyleen glycol) (PCL-*b*-PEG) blokcopolymeren voor de belading van mTHPC met als doel om geschikte micellaire systemen te ontwikkelen voor de doelgerichte afgifte van mTHPC. De stabiliteit van polymere micellen en de retentie van mTHPC in de micellen zijn essentieel voor verbeterde farmacokinetiek, selectieve biodistributie en zodoende effectieve PDT. Om die reden, wordt in dit proefschrift verslag gedaan van studies met betrekking tot *in vitro* stabiliteit, *in vivo* circulatiekinetiek, en biodistributie van verschillende micellaire mTHPC formuleringen. Verdere nadruk wordt besteed aan de synthese en karakterisering van een verscheidenheid aan amfifiele blokcopolymeren op basis van PEG (als hydrofiel blok) en PCL (als hydrofoob blok). Voor de modulatie en aanpassing van hydrofobe blokeigenschappen, is copolymerisatie van CL met aromatisch gefunctionaliseerde carbonaten (**Hoofdstuk 4**) en vernetbare dithiolanen (**Hoofdstuk 5** en **6**), respectievelijk, toegepast voor het ontwerp van π-π stapeling en vernetting in de micelkernen met als doel om de stabiliteit van micellen in de circulatie en de retentie van mTHPC in de micelkernen te verbeteren. **Hoofdstuk 1**

biedt een algemeen overzicht over PDT en PSs, inclusief mTHPC. Vervolgens, worden de actuele commerciële formuleringen van mTHPC (Foscan®, Foslip®, en FosPEG®) alsmede hun beperkingen kort beschreven. Daarnaast verstrekt dit hoofdstuk een korte introductie over polymere micellen voor gerichte afgifte van mTHPC. Tenslotte wordt in dit hoofdstuk het doel van dit proefschrift beschreven.

Selectieve eliminering van macrofagen door PDT is een nieuwe en veelbelovende therapeutische modaliteit om afname van atherosclerotische plaques te bewerkstelligen. In **Hoofdstuk 2**, werd mTHPC met hoge efficiëntie en capaciteit ingekapseld in polymere micellen die gebaseerd zijn op benzyl-poly(ε-caprolacton)-*b*-methoxy poly(ethyleen glycol) (Bz-PCL-PEG), met macrofaag-selectieve PDT als doel. De fototoxiciteit van mTHPC-beladen micellen is geïnduceerd door de degradatie van de PCL-blokken in Bz-PCL-PEG-micellen door lipases. Op basis van hun hogere lipase-activiteit, zijn RAW264.7 macrofagen instaat om de micellen sneller te degraderen en dit leidt vervolgens tot eerdere PS-activatie in vergelijking met C166 endotheelcellen, waardoor een mogelijkheid wordt gecreëerd voor het selectief doden van RAW264.7 macrofagen, die homoloog zijn aan macrofagen gelokaliseerd in atherosclerotische plaques. Afgifte van mTHPC vanuit micellen werd waargenomen vanuit micellen die gedurende 30 minuten geïncubeerd werden met bloedplasma en dit verklaart dat de waargenomen *in vivo* farmacokinetiek van mTHPC als micellaire formulering vergelijkbaar was met mTHPC in vrije vorm. Daarom was de translatie van *in vitro* naar *in vivo* niet mogelijk voor de gunstige selectieve macrofaag fototoxiciteit voortvloeiend uit het formuleren van PS in Bz-PCL-PEG-micellen. Desondanks, werd accumulatie van mTHPC waargenomen in atherosclerotische laesies van muisaorta's wat waarschijnlijk een gevolg is van lipoproteïne binding na afgifte uit de micellen.

De vroegtijdige afgifte van mTHPC vanuit micellen beschreven in **Hoofdstuk 2**, zorgt ervoor dat ons vervolgonderzoek zich richt op de verbetering van de stabiliteit van mTHPC-beladen Bz-PCL-PEG gebaseerde micellen evenals de mTHPC retentie in micellen via verschillende strategieën. In **Hoofdstuk 3**, zijn benzyl-poly(ε-caprolacton)-*b*-methoxy-poly(ethyleen glycol) (Bz-$PCL_n$-PEG) gebaseerde blokcopolymeren gesynthetiseerd, met dezelfde chemische structuur als de genoemde polymeren in **Hoofdstuk 2**, maar dan met variërende $PCL_n$ ketenlengtes (n = 9, 15 of 23). Polymere micellen met drie verschillende diameters (17, 24 en 45 nm) gebaseerd op Bz-$PCL_n$-PEG (n = 9, 15 of 23) werden vervaardigd met verschillende mTHPC beladingen. Er werd verondersteld dat de micelkernen gestabiliseerd konden worden door toenemende hydrofobe interacties (*d.w.z.* de ketenlengte van het hydrofobe blok). Om de opname van micellen door kankercellen met overexpressie van de epidermale groeifactorreceptor (EGFR) te bevorderen, werden de micellen gedecoreerd met een EGFR-gerichte 'nanobody' (EGa1). Internalisatie van de EGa1-geconjugeerde micellen werd aangetoond na specifieke binding met de EGFR-receptor met overexpressie en aanwezig op het oppervlak van A431 cellen, resulterend in verbeterde cellulaire

opname, in vergelijking met HeLa cellen met een lage EGFR-expressie. In lijn met deze vinding, toonde mTHPC beladen in EGa1-geconjugeerde $PCL_{23}$-PEG-micellen selectieve PDT tegen A431 cellen, in vergelijking met HeLa cellen. Ten slotte, een *in vivo* farmacokinetiek studie toonde aan dat na *iv* injectie, mTHPC beladen $PCL_{23}$-PEG-micellen een significante toename vertoonden in half-waarde tijd in de circulatie, vergeleken met die van mTHPC in vrije vorm ($t_{1/2}$-α: ~1 *vs* <0.3 terwijl $t_{1/2}$-β: 14 *vs* 2 h), onafhankelijk van de aanwezigheid van EGa1, veroorzaakt door de lange circulatietijd van de micellen ($t_{1/2}$-β:18 h). Dit hoofdstuk demonstreert dus dat toename van hydrofobe interacties door toenemende hydrofobe blokken (*d.w.z.* PCL in dit geval) kan leiden tot uitstekende stabiliteit van de vervaardigde micellen, met langdurige mTHPC retentie in de circulatie als gevolg. Daarenboven wordt in dit hoofdstuk aangetoond dat de conjugatie van EGa1 'nanobodies' aan het oppervlak van $PCL_{23}$-PEG-micellen de potentie heeft tot een significante verbetering in PDT-selectiviteit en werkzaamheid voor cellen met EGFR overexpressie.

In eerder onderzoek uitgevoerd door onze groep, is aangetoond dat de inbouw van aromatische ringen in de hydrofobe kern van polymere micellen kan zorgen voor stabilisatie door π-π stapeling interacties. In **Hoofdstuk 4**, wordt hieruit inspiratie gehaald door een monomeer met aromatische zijgroepen (namelijk benzyl-gefunctionaliseerd trimethyleen carbonaat (TMC-Bz)) te introduceren in het hydrofobe blok van de poly(ε-caprolacton)-*b*-poly(ethyleen glycol) (PCL-PEG) polymeerketens. Voor vergelijking werden PCL-PEG-blokcopolymeren met niet Bz gemodificeerde eindgroepen ook gesynthetiseerd. We hebben laten zien dat, ongeacht de posities en hoeveelheden in de polymeerketens, de inbouw van aromatische ringen in PCL-PEG gebaseerde copolymeren resulteerde in kleinere micellen (18–30 nm) met betere colloïde stabiliteit in PBS dan micellen zonder aromatische groepen. De *in vivo* circulatietijd van micellen die meerdere aromatische zijgroepen bevatten was langer dan die van micellen met een enkele terminale aromatische groep ($t_{1/2}$-α: ~0.7 en $t_{1/2}$-β: 2.9 h voor de eerstgenoemde *vs* $t_{1/2}$: <0.3 h voor de laatstgenoemde), terwijl de verdeling van de ingekapselde fotosensibilisator (mTHPC) over de micellen en humaan plasma *in vitro* inderdaad werd begunstigd voor micellen die aromatische zijgroepen bevatten. Desondanks was de toegenomen stabiliteit niet voldoende om mTHPC volledig vast te houden in de micellen na injectie in de bloedcirculatie, zoals aangetoond door de waargenomen vergelijkbare biodistributie patronen van micellaire mTHPC in vergelijking met mTHPC in vrije vorm, maar ongelijkmatige biodistributiepatronen van mTHPC en de gastmicellen. Dit hoofdstuk toont nogmaals aan dat doelgerichte afgifte van PS gemedieerd door het EPR effect niet mogelijk zou zijn vanwege een snelle afgifte van mTHPC uit de micellaire formuleringen.

In meerdere studies is aangetoond dat chemische koppeling een effectieve methode is om polymere micellen te stabiliseren. Daarom is het onderzoek in **Hoofdstuk 5** en **6** gericht op de vervaarding van stabiele micellen door introductie van disulfide eenheden

(*d.w.z.* dithiolaan ringen) als vernetbare groepen, die dynamische en reversibele crosslinks kunnen vormen in de micelkern. In **Hoofdstuk 5**, introduceren we dithiolaan ringen als vernetbare groepen in poly(ε-caprolacton)-*b*-poly(ethyleen glycol) (PCL-PEG) blokcopolymeren door ringopeningspolymerisatie van CL en dithiolaan gesubstitueerde cyclische carbonaten, met of zonder een flexibele diesterlinker tussen de dithiolaanring en de cyclische carbonaateenheid gebruikmakend van verschillende katalysatoren. Het is aangetoond dat het type katalysator een belangrijke invloed heeft op de monomeersequentie, vanwege de verschillende monomeerreactiviteiten en transesterificatiereacties. Belangwekkend, wij hebben aangetoond dat vernetbare copolymeren verkregen worden door dithiolaan eenheden direct te verbinden met de polymeerruggengraat, terwijl introductie van een linkereenheid tussen de dithiolaan en de ruggengraat onverwachts vernetting tegenging. Het vernettten van micellen door disulfide uitwisseling gebeurde spontaan tijdens dialyse van gePEGyleerde blokcopolymeren na nanoprecipitatie, en was onafhankelijk van de monomeersequentie, comonomeerverhouding of toevoeging van reducerendere reagentia. De dithiolaan vernetbare micellen lieten redox-reactieve dissociatie zien in aanwezigheid van 10 mM glutathion, wat deze micellen karakteriseert als veelbelovende afgiftesystemen van farmaca voor belading afgifte na intracellulaire 'triggers'.

In **Hoofdstuk 6**, werd onderzoek uitgevoerd betreffende de *in vitro* en *in vivo* stabiliteit van mTHPC-beladen dithiolaan en vernette micellen gebaseerd op poly(ε-caprolacton)-*co*-poly(1,2-dithiolaan-carbonaat)-*b*-poly(ethyleen glycol) (P(CL-*co*-DTC)-PEG) die in **Hoofdstuk 5** van dit proefschrift onderzocht zijn en vergeleken met PCL-PEG gebaseerde micellen die beschreven zijn in **Hoofdstuk 3** van dit proefschrift. We hebben aangetoond dat asymmetrische 'flow field flow fractionation' (AF4) een uitstekende techniek is voor de evaluatie van de stabiliteit van nanodeeltjes in biologische media en dus de stabiliteit van farmaca beladen nanodeeltjes kunnen voorspellen na *i.v.* toediening. PS (her)distributie naar verschillende plasma eiwitten werd geobserveerd, wat een sterke indicatie is voor de (in)stabiliteit van de farmaca beladen micellen in plasma. Onze resultaten van de AF4 analyse tonen aan dat kleine niet-vernette $pCL_9$-PEG (17 nm) en $pCL_{15}$-PEG (22 nm) micellen een lagere stabiliteit hebben in vergelijking met de fysisch vernette $pCL_{23}$-PEG micellen door de kristalliniteit van pCL met grotere afmetingen (43 nm) en chemisch vernette $p(CL_9\text{-}DTC_{3.9})$-PEG and $p(CL_{18}\text{-}DTC_{7.5})$-PEG micellen met vergelijkbare kleinere afmetingen (< 25 nm). Het is belangrijk om op te merken dat *in vivo* circulatiekinetiek laat zien dat chemisch vernette $P(CL_{18}\text{-}DTC_{7.5})$-PEG micellen en beladen met mTHPC significant lagere halfwaardes hadden (t½-β van zowel de micellen als mTHPC was ~2 h) in vergelijking met de fysisch vernette en PS beladen $PCL_{23}$-PEG micellen (t½-β van micellen en mTHPC was 14 en 18 h, respectievelijk) zoals waargenomen in **Hoofdstuk 3** van dit proefschrift. In lijn met deze waarneming, zorgde lang circulerende $PCL_{23}$-PEG micellen voor significant hogere tumoraccumulatie van zowel de micellen als de beladen mTHPC, in vergelijking met

de kort circulerende vernette P($CL_{18}$-$DTC_{7.5}$)-PEG micellen. Deze *in vivo* data zijn in goede overeenstemming met de *in vitro* stabiliteitstudies, die lieten zien dat in plasma, ondanks uitstekende *in vitro* stabiliteit van beide micellen zoals geobserveerd met AF4, de retentie van mTHPC in $PCL_{23}$-PEG micellen (>8 h) vele malen langer was dan die in P($CL_{18}$-$DTC_{7.5}$)-PEG micellen (~4 h) zoals waargenomen met fluorescentiemicroscopie. Samenvattend, het onderzoek gepresenteerd in dit proefschrift exploreert de mogelijkheden van de vervaardiging van stabiele PCL-PEG gebaseerde polymere micellen met kleine afmetingen als doelgericht afgiftesystemen van mTHPC voor PDT. We legde de nadruk op de stabilisering van kleine micellen door het gebruik van chemische (disulfide vernetting) en fysische vernetting (kristallisatie of π-π 'stacking'), leidend tot verbetering van PS-retentie *in vivo* door op maat gemaakte composities en architecturen van amfifiele blokcopolymeren gebruikmakend van verschillende strategieën. De resultaten van de farmacokinetiekstudies, inclusief circulatiekinetiek en biodistributie van deze verschillende gestabiliseerde micellen beladen mTHPC, verschaffen belangrijke wetenschappelijke inzichten voor de verdere rationele ontwikkeling van polymere micellen als nanodeeltjes voor doelgerichte geneesmiddelafgifte.

## Acknowledgements

I started my journey at Utrecht University on 5th Oct 2015, which is full of lessons and challenges especially at the beginning; I cannot talk in English, I did not know what lab journal is, I did not know how to write scientific reports…. Over the past 4 years' learning, I have made tremendous improvements in many aspects, thanks to all people I have met and all things I have experienced during this journey. This journey is approaching the end now and it is time to express my sincere gratitude to all those people who become part of my journey.

First of all, I would like to express my greatest gratitude to my promotor/supervisor Prof. **Wim** Hennink. I could not accomplish this fruitful thesis without your endless support, inspiration and help. I am impressed by your knowledge, vision, hardworking and responsibility. Your constructive input and tough questions from our monthly discussions made me think about my research deeper and more critical. Your attention to the smallest details and pursuit of facts have made me have a deeper understanding and respect for scientific research. I often received your detailed and timely comments on my manuscripts after midnight and you checked every manuscript/chapter over and over again until you were satisfied with it, no matter how busy you were. Even though you have extremely busy schedules, you still took the time to check my Dutch summary. Words can hardly express my gratitude to all you have done to me. As a scientist, you are knowledgeable, critical, serious, respectful but to be honest, not easy to tackle. However, I also saw your other side during our borrels, poker games and other Biopharmacy group's activities. You are a funny and friendly guy. You like to make jokes, drink beers, make fun of your students, say "Yes, Yes, Yes"…. It is my greatest honor to be your student and I am proud of that. Your attitude towards scientific research and work has a profound effect on mine towards the educational work that I may be engaged in in the future.

Secondly, I would like to thank my copromotor/daily supervisor Dr. **Rene** van Nostrum. Your mild personality did make me less nervous when dealing with Wim. You are so smart that you were the only person who got most of my key information from my talk with my broken English at the very early stage of my Ph.D.. You are so open-minded in research that you gave me some extent of flexibility to try my new ideas, explore different research directions and learn new technology. You are so supportive whenever I need it. When my writing skills needed a lot of improvements, you made many changes to my manuscript to show me the way how to write out scientifically. I really appreciate such a precious learning opportunity you offered me and all your help and understanding.

I also would like to thank my copromotor Dr. **Sabrina** Oliveira for your supervision, motivation and input during my research. Your trust, support and warm encouragement especially during the hard times, are invaluable to me. Also, thanks for all your nice suggestions and efforts to improve my manuscripts.

Special thanks to Dr. **Robbert** Jan Kok, who showed me how to analyze and scientifically present pharmacokinetic data and also gave a lot of helpful comments on improving the manuscript of Chapter 4. I also would like to thank Dr. **Marcel** H.A.M. Fens who helped me to successfully apply and conduct animal studies. Without your help and efforts, I could not have done these animal studies perfectly. Thanks to your thoughtful and comprehensive experimental settings of animal studies, all the obtained data were able to be published.

I would like to also acknowledge my students. **Julia** Denise Peterson, my first student from Drug Innovation Program, explored the experiment conditions of conjugation micelles with EGa1 nanobody. **Luca** Scrivano, a visiting Ph.D. student from Italy I collaborated with, continued with Julia's project and did further studies. Both of you made great contributions to Chapter 3 of this thesis. **Kevin** Dickie, a master student also from Drug Innovation Program, worked with evaluation of stability and intracellular degradation kinetics of polymeric micelles using FRET. Due to the deadline limit of completing this thesis, only part of your work is presented in this thesis (Chapter 7). My special thanks to **Kevin** also because you have done a perfect job to help me prepare the Dutch summary of my thesis. **Huibin** Zhou was a bachelor student from College of Pharmaceutical Sciences (CPS), who focused on optimization and *in vitro* evaluation of polymeric micelles loaded with novel photosensitizers. It is my pleasure to collaborate with you all, such talented people and I am grateful for all your contributions to my Ph.D. project.

Our lab could not function in such an orderly and normal manner without hard work and dedication from our lovely technicians. Therefore, I would like to express my gratitude to them. **Mies**. your laboratory knowledge and skills about polymer synthesis, characterization and related equipment are impressive. Even though you are busy, you always took the time to help me with your patience whenever I needed it. I have gained tremendous knowledge due to your teaching. The atmosphere is full of laughter and fun when you are around. Your encouragement calmed me down when I was nervous about my presentation at the conference. When I made mistakes in the lab, you showed your understanding instead of blaming me. I am so grateful for all of these. **Joep**, I am impressed by your knowledge about cell culture. Whatever questions about cell culture I asked, you always can answer me with clear indications. Also, under your supervision, our cell culture lab is always clean and well-organized and cells hardly get infected. Thank you for all your commitment. **Roel**, thank you for taking the time to help me process the animal samples. Thank **Nicky** for your help with animal studies. Thank **Ebel** for your help with application of animal study. Thank **Louis** for your help with Zeta potential. Thank **Feiko** for your help. Thank our beautiful secretary **Barbara** de Jong-van Amstel for your arrangement of meetings with my supervisors, for your cake and also for your help with all the administrative work required for my Ph.D..

Besides, I would like to thank **Bo** Lou, who gave me a lot of suggestions and inputs

on how to continue and expand my project. You always leave your work behind and gave my problems a priority whenever I came to you. I am grateful for that. **Haili** Shi, my dearest friend, we have witnessed most of the hard times of each other experienced during our Ph.D. period; struggle, confusion, frustration, pressures, disappointment, *etc*. Fortunately, we shared all these feelings and we trusted, supported, encouraged and motivated each other. Finally, both of us have overcome these hard times and ushered in the dawn. All your spiritual and physical support, sharing, listening and company meant a lot to me and all of these are invaluable to me. **Xiangjie** Su, my little fairy, after Haili left, you sit opposite to me and we made a new group and spent most of our time together; we supported each other, we ride home together, traveled together, had lunch together, we discussed our research together, we also shared a lot of our own stories, *etc*. All of these are precious memories to me. Besides, we also talked about our fancy dreams. I knew that your dream is to become a novelist and you promised that I will be the heroine of your novel, who is loved by everyone including "my prince charming". I am looking forward to seeing your dream come true.

I also would like to express my gratitude to **Xinlei** Fan, who is the first Chinese I met in the Netherlands. You helped me rent a room to stay without any deposit in Zeist when I was still in China and picked up me at the Utrecht central station at the first time I have arrived at the Netherlands, which meant a lot to me, especially at the time when I was first abroad.

I would like to thank my two close friends **Jing** Li and **Donglong** Fu. We were the only three Chinese, who started our Ph.D. research in 2015 at David de Wied building. We used to hang out a lot, shared a lot of our experiences and difficulties, made fun of each other, traveled together, made dinners together. I have enjoyed the time being with you guys and all those are precious memories to me.

I would also like to thank my friend and schoolmate **Xiaobing** Zhang. Although both of us studied at the same faculty of Shandong university, we were only say-hello acquaintances and did not know each other well at that time due to our different majors. We became close friends after we made our first trip together in Europe. We shared a lot of opinions in respect of our research, career and life. You let me stay with you when I was stuck at the Schipol airport due to my prevention from boarding, which is my worst experience I have ever had in Europe. Your accompany and help warmed my heart and comforted me.

I would also like to express my gratitude to my dear colleagues and friends in our Department of Pharmaceutics. To my dear friend, **Aida** Moreira. We are the only two Ph.D. students who sit in the non-popular office area (the left side of the office area) at the moment we met, which gave us chance to talk to each other more often and get to know each other well. Thank you for your Portuguese dinner, lunch breaks, all chattings and great moments we had together. Special thanks to my dear friend **Gina** ("Portuguese queen") and my first deskmate **Salma**. Thank you for integrating me into your group at

the beginning of my Ph.D., which gave me the chance to know your cultures, to enjoy your traditional food, shared our values about marriage, career, *etc*, and also to practice my English. It's been so great to get to know you and all of these experiences we have had together are precious to me. To **Sjaak** Jong, the youngest Ph,D. of our group. You started your Ph.D. almost the same day as me. You were the first person who was willing to talk to me and bring me soup at the very early stage of my Ph.D., at which I knew nobody and my English was really bad. Talking to you gave me a chance to practice my English. Thank **Sjaak** for your kindness and help during my Ph.D. period. **Mahsa**, due to the project about AF4 in JRC, Italy, and the CRS conference, we had a chance to spend quite a lot of time together; we traveled together, we watched Bull-fighting together, we enjoyed delicious Italian food together, we caught up flight together… We do have different personalities: you like to stick to your plan but I am more flexible and casual. However, we managed to get well along with each other and enjoyed our time together. Thanks for your company and all the memorable moments we had together. Special thanks to **Bárbara**, who performed singlet oxygen measurement for me. Thank **Blessing** for all the funny conversations we had and also for the midnight-overtime party that only belongs to both of us. Besides, thank **Laura**, **Lies**, **Lucía**, **Thijs**, **Karina**, **Andhyk**, **Yvonne**, **Jeffrey**, **Carl**, **Neda**, **Negar**, **Mathew, Marzieh**, **Alexandra**, **Charis**, **Koichi**, **Marko**, **Kung**, **Erik**, **Ada**, **Danny**, *etc* for all the good time we have spent together in the lab and all the fun we had made during various activities in our group.

I would like to thank our UIPS Chinese community, **Weiluan** Chen, **Dandan** Li, **Yinan** Chen, **Bo** Lou, **Feilong** Sun, **Haili** Shi, **Linglei** Jiang. Thanks for organizing great dinner parties and also for all your shared tips and experiences about how to deal with challenges and supervisors during my Ph.D. period. Moreover, thank our UIPS other Chinese community members, **Jerry** Chun Yin Lau**, Yong** Guo, **Xiangjie** Su, **Boning** Qiu, **Mengshan** Liu, and **Yan** Wang for helping each other. I would also like to thank our Running team (**Wenjing** Lu, **Haili** Shi, **Yong** Guo, **Fuqiang** Chang, **Samia**) for running together and importantly, motivating each other to keep healthy. Besides, I would also like to thank many other Chinese friends I met in Utrecht, **Fang** Liu, **Yuru** Wang, **Han** Zhou, **Hong** Zhang, **WeiXuan**, **Guangyun** Yu, **Jing** Chen, **Liling** Shan, **Xin** Yang, **Jie** Shi, **Jianming** Chen, **Xinwei** Ye, **Minglong** Liu, **Lifeng** Sun, **YanYan** Liu, **Yulong** Zhao, **Yumao** Zhang, **Jie** Zhang, **Xingxiu** Pan ….. It is my great pleasure to meet all of you abroad and thanks for being part of my journey.

I would like to particularly thank **Aida** and **Xiangjie** for accepting to be my paranymphs. Many thanks for the efforts you will put to organize my Ph.D. promotion.

It would not have been possible to continue my education abroad without the financial support from **CSC**. I am grateful for the opportunity they gave me to pursue my Ph.D. abroad.

Last but not the least, I would like to express my sincere gratitude to **my parents**. You are so open-minded in terms of education and you did your best to let me get a good

education because you believe "knowledge changes life", which is in fact true. Because of education, I have the opportunity to go abroad to experience different lifestyles, explore different parts of the world and meet people with various cultures and backgrounds, which broadened my horizons and enriched my knowledge. Thank my parents for being so open-minded and supportive. I cannot have gone this far without your understanding and support. I would also like to thank my young brother **Menglin** Liu, who took responsibility for accompanying and caring for my parents when I was abroad. Also, I would like to thank my **relatives** who offered help to my parents when I was not around. Besides, special thanks to my aunt **Guiqin** Wang for your suggestions, input and contributions in terms of the layout and cover design of this thesis.

In June 2020, it is my turn to defense my Ph.D., which will be one of the most important experiences in my entire life. This so-called "academic wedding" represents a perfect ending of my schooling career and also a fresh start of my new character and career. Four years of Ph.D. study are full of different moments: happiness, sadness, frustration, helplessness, loneness, crying… After gone through all of these, I have become the better version of myself. I am proud of myself being who I am now. Therefore, I would also like to thank myself for being hardworking, perseverance and never giving up to make this happen. Life is like a box of chocolates, you never know what you are going to get. This journey is approaching the end and I am looking forward to opening my next box.

Yanna Liu
April 2020, Zhaoyuan

## Curriculum vitae

Yanna Liu was born on November 1st, 1988 in Zhaoyuan City, Shandong Province, China. After obtained her Bachelor's degree at Binzhou Medical College, China, in 2012, she started her Master's study at the School of Pharmaceutical Sciences, Shandong University, China, and did her major in Medicinal Chemistry under the supervision of Prof. Zhaopeng Liu. Her master project was mainly focused on design, synthesis, and biological evaluation of 1-methyl-1,4-dihydroindeno[1,2-c]pyrazole analogues as potential anticancer agents targeting tubulin colchicine binding site, resulting in two first-author publications and one patent. After earning her Master's degree in 2015, she started as a Ph.D. candidate in the Drug Innovation program at the Department of Pharmaceutics, Utrecht University, the Netherlands, under the supervision of Prof. Wim E. Hennink, Dr. C.F. van Nostrum and Dr. S. Oliveira. The results of her work are presented in this Ph.D. thesis entitled "Polymeric micelles loaded with mTHPC for photodynamic therapy: from synthesis to *in vitro* and *in vivo* evaluation".

## List of publications

### Publications in this thesis:

Jos W.H. Wennink*, **Yanna Liu*** **(Co-first author)**, Petri I. Mäkinen, Francesca Setaro, Andrès de la Escosura, Meriem Bourajjaj, Jari P. Lappalainen, Lari P. Holappa, Joep B. van den Dikkenberg, Mina al Fartousi, Panagiotis N. Trohopoulos, Seppo Ylä-Herttuala, Tomas Torres, Wim E. Hennink, Cornelus F. van Nostrum. Macrophage selective photodynamic therapy by meta-tetra(hydroxyphenyl)chlorin loaded polymeric micelles: a possible treatment for cardiovascular diseases. *European Journal of Pharmaceutical Sciences* **2017**, 107, 112-125.

**Yanna Liu,** Luca Scrivano, Julia Denise Peterson, Marcel H. A. M. Fens, Irati Beltrán Hernández, Bárbara Mesquita, Javier Sastre Toraño, Wim E. Hennink, Cornelus F. van Nostrum, Sabrina Oliveira. EGFR targeted nanobody functionalized polymeric micelles loaded with mTHPC for selective photodynamic therapy. *Molecular Pharmaceutics* **2020***,* 17, 1276–1292.

**Yanna Liu,** Marcel H.A.M. Fens, Bo Lou, Nicky C.H. van Kronenburg, Roel F.M. Maas-Bakker, Robbert J. Kok, Sabrina Oliveira, Wim E. Hennink, Cornelus F. van Nostrum. π-π-Stacked poly(ε-caprolactone)-*b*-poly(ethylene glycol) micelles loaded with a photosensitizer for photodynamic therapy. *Pharmaceutics* **2020**, 12 (4), 338.

**Yanna Liu**, Mies J. van Steenbergen, Sabrina Oliveira, Wim E. Hennink, Cornelus F. van Nostrum. Dithiolane crosslinked poly(ε-caprolactone)-based micelles: impact of monomer sequence, nature of monomer and reducing agent on the dynamic crosslinking properties. *Macromolecules* **2020**, 53 (16), 7009–7024.

**Yanna Liu**, Marcel H.A.M. Fens, Robin Bruno Capomaccio, Dora Mehn, Luca Scrivano, Sabrina Oliveira, Wim E. Hennink, Cornelus F. van Nostrum. Correlation between *in vitro* stability and pharmacokinetics of poly(ε-caprolactone)-based micelles loaded with a photosensitizer. Submitted for publication.

### Other publications:

**Yanna Liu,** Jingjing Wang, Yating Ji, Guodong Zhao, Longqian Tang, Chengmei Zhang, Xiuli Guo, Zhaopeng Liu. Design, synthesis, and biological evaluation of 1-methyl-1,4-dihydroindeno[1,2-*c*]pyrazole analogues as potential anticancer agents targeting tubulin colchicine binding site. *Journal of Medicinal Chemistry* **2016**, *59*, 5341–5355.

**Yanna Liu**, Renzhong Wan, Zhaopeng Liu. Recent developments of small molecule PI3K/mTOR dual inhibitors. *Mini-Reviews in Medicinal Chemistry* **2013**, 13, 2047-2059.

Yating Ji, **Yanna Liu**, Zhaopeng Liu. Tubulin colchicine binding site inhibitors as vascular disrupting agents in clinical developments. *Current Medicinal Chemistry* **2015**, 22, 1348-1360.

Haili Shi, Mies J. van Steenbergen, Bo Lou, **Yanna Liu**, Wim E. Hennink, Robbert J. Kok. Folate decorated polymeric micelles for targeted delivery of dactolisib to cancer cells. *International Journal of Pharmaceutics* **2020**, 582, 119305.